ENERGY TRANSFER, PHOTOSENSITIZATION AND SENSING WITH NOVEL BODIPY COMPOUNDS AND THEIR SUPRAMOLECULAR ASSEMBLIES

A DISSERTATION SUBMITTED TO
THE GRADUATE SCHOOL OF ENGINEERING AND SCIENCE
OF BILKENT UNIVERSITY
IN PARTIAL FULFILLMENT OF THE REQUIREMENTS FOR
THE DEGREE OF
DOCTOR OF PHILOSOPHY
IN
CHEMISTRY

By
NİSA YEŞİLGÜL

June 2017

ENERGY TRANSFER, PHOTOSENSITIZATION AND SENSING WITH NOVEL BODIPY COMPOUNDS AND THEIR SUPRAMOLECULAR ASSEMBLIES

By Nisa Yeşilgül

June 2017

We certify that we have read this dissertation and that in our opinion it is fully adequate, in scope and in quality, as a dissertation for the degree of Doctor of Philosophy.

Engin Umut Akkaya (Principal Advisor)

Dönüş Tuncel

Özgür Altan Bozdemir

Özdemir Doğan

Canan Ünaleroğlu

Approved for the Graduate School of Engineering and Science:

Ezhan Karaşan
Director of the Graduate School

ABSTRACT

ENERGY TRANSFER, PHOTOSENSITIZATION AND SENSING WITH NOVEL BODIPY COMPOUNDS AND THEIR SUPRAMOLECULAR ASSEMBLIES

Nisa Yeşilgül

Ph.D. in Department of Chemistry

Supervisor: Engin Umut Akkaya

June 2017

Fluorescent dyes have been used for decades in many applications due to their versatility, sensitivity and many other useful properties. Since their discovery in 1968, BODIPY dyes have come forward and have been used in many fields of research such as photodynamic therapy, anion/cation sensing, dye-sensitized solar cells. In this thesis, novel applications of fluorescent dyes, mainly based on BODIPY fluorophores are reported. In the first project, a photosensitizer derived from erythrosine attached to a luminol derivative is presented. The main purpose was to achieve photosensitization without requiring external excitation with light. In another project, we synthesized and characterized a series of heavy atom substituted BODIPY based photosensitizers. In a related study, the photophysical properties of a BODIPY based chemosensor substituted with benzo-21-crown-7 units were studied in the presence of various α,ω-diamino alkanes. Then, we designed a BODIPY based probe sensitive to bioreductive conditions known to be prevalent in hypoxic cancer cells. In the final chapter, we present a mechanically interlocked energy transfer cassette consisted of a distyryl-BODIPY acceptor and two donor units.

Keywords: Photodynamic therapy, photosensitizer, energy transfer cassette, chemiluminescence, BODIPY.

ÖZET

YENİ BODIPY BİLEŞİKLERİ VE SUPRAMOLEKÜLER TOPLULUKLARIYLA ENERJİ TRANSFERİ, FOTODUYARLAŞTIRMA VE ALGILAMA

Nisa Yeşilgül

Kimya Bölümü, Doktora

Tez Danışmanı: Engin Umut Akkaya

Haziran 2017

Floresant boyalar çeşitlilik, duyarlılık ve daha pekçok kullanışlı özelliklerinden dolayı yıllardır birçok çalışmada kullanılmaktadırlar. BODIPY boyaları 1968 yılında keşfedildiklerinden beri ön plana çıkmış ve fotodinamik terapi, anyon/katyon sensörü, boya esaslı güneş pilleri olarak birçok alanda kullanılmışlardır. Bu tezde BODIPY boyaları başta olmak üzere floresant boyaların yeni kullanımları çalışılmıştır. İlk projede, luminole bağlanmış eritrosin bazlı fotoduyarlaştırıcı tasarlanmıştır. Burdaki temel amaç dışarıdan ışık uygulanmasına ihtiyaç olmadan fotoduyarlaşma sağlanmasıdır. Sonraki projede ise ağır atom içeren BODIPY temelli fotoduyarlaştırıcılar sentezlenmiş ve karakterize edilmiştir. Başka bir çalışmada α,ω-diamino alkan varlığında benzo-21-crown-7 iliştirilmiş BODIPY temelli kemosensörlerin fotofiziksel özellikleri çalışılmıştır. Daha sonra kanserli hücrelerde yaygın olduğu bilinen biyo-indirgeyici koşullara duyarlı BODIPY temelli boya dizayn edilmistir. Son bölümde ise mekanik olarak birbirine bağlanmış, distiril-BODIPY akseptörü ve iki donör biriminden oluşan enerji hasadı birimi sentezlenmiştir.

Anahtar kelimeler: Fotodinamik terapi, fotoduyarlaştırıcı, enerji transfer birimi, kemilüminesans, BODIPY.

ACKNOWLEDGEMENT

First and foremost I would like to express my sincere thanks to my supervisor Prof. Engin Umut Akkaya for his support and advice throughout my graduate studies by providing an environment conducive to independent research, creativity and hard work. I will never forget his support throughout my life.

I also would like to thank all members of the Chemistry Department for providing a multidisciplinary research atmosphere and for joyful friendships.

I owe a special thanks to Bilal Kılıç for his everlasting help, support and friendship. I am sincerely grateful to Ruslan Guliyev and Bilal Uyar for their help and guidance they provided through all these years.

Thanks to all past and present members of Akkaya Group for their help, time and friendship during all these years. Esma Uçar, Ziya Köstereli, İlke Şimşek-Turan, Seylan Ayan, Deniz Yıldız, Yahya Ismaeli, Serdal Kaya, Cansu Kaya, Simay Aydonat, Abdurrahman Türksoy, Özge Pehlivan, Merve Canyurt, Beste Gündüz and rest of the SCL (Supramolecular Chemistry Laboratory) members. It has been a great pleasure for me to work with you.

This thesis is dedicated to my mother, without whom I would never be where I am today. I would like to thank my sister and my little nephew for all love and understanding. I want to express my gratitude to my friend and my second sister Özlem Seven for her endless support and friendship. I also owe gratitude to Melih Koca for the enedless help, love and support. There is no way to thank them for their love, care, trust and encouragement they have provided all these years for me.

LIST OF ABBREVIATIONS

AcOH	**:**	Acetic Acid
BODIPY	**:**	Boradiazaindacene
$CHCl_3$	**:**	Chloroform
DDQ	**:**	Dichlorodicyanoquinone
DMF	**:**	Dimethylformamide
DPBF	**:**	1,3-Diphenylisobenzofuran
ET	**:**	Energy Transfer
Et_3N	**:**	Triethylamine
FRET	**:**	Förster Resonance Energy Transfer
HEPES	**:**	4-(2-Hydroxyethyl)piperazine-1-ethanesulfonic acid
HOMO	**:**	Highest Occupied Molecular Orbital
ICT	**:**	Internal Charge Transfer
IFE	**:**	Inner Filter Effect
LUMO	**:**	Lowest Unoccupied Molecular Orbital
MALDI	**:**	Matrix-Assisted Laser Desorption/Ionization
MS	**:**	Mass Spectroscopy
NMR	**:**	Nuclear Magnetic Resonance
PET	**:**	Photoinduced Electron Transfer
TFA	**:**	Trifluoroacetic Acid
THF	**:**	Tetrahydrofuran
TLC	**:**	Thin Layer Chromotography
TOF	**:**	Time of Flight

TABLE OF CONTENTS

LIST OF FIGURES

LIST OF SCHEMES

LIST OF TABLES

CHAPTER 1

1. Introduction

1.1. Photodynamic Therapy

Photodynamic therapy, also called as photoirradiation therapy, phototherapy, photochemotherapy or PDT, is one of the promising methods for certain cancer types such as bladder cancer, head and neck cancer, gastrointestinal cancer, skin cancer, gynecological, cervical cancer or some cardiovascular diseases in consequence of its noninvasive approach [1], [2]. In this therapy, photosensitizing agents, also called as photosensitizers, are brought in locally or intravenously and these agents localized in cancer tissues [2]. After administration of a photosensitizer (PS), usually 1 to 3 days depending on type of the drug, it is activated by light of certain wavelength, preferentially by red or near infrared light.

An acceptable photosensitizer should be inactive or in other words 'harmless' without light. However, by applying a suitable light, photosensitizer gets activated and reactive oxygen species as singlet oxygen ($^1O_2$) are generated. Depending on the localization of photosensitizer, surrounding molecules such as DNA, proteins, lipids or tumor tissues can be damaged oxidatively [3], [4]. Therefore, selectivity of photosensitizer is an important issue such that when a phtotosensitizer is designed for the target tumor cells, it will be localized selectively, so when the light at therapeutic window is applied surrounding healthy tissues will not be photodamaged.

In a successful photodynamic therapy application, therefore, photosensitizer should have certain properties. Photosensitizer, photodynamic therapy agent, should absorb light at near-IR region, also known as therapeutic region. This is because light below this range cannot penetrate deeply cancer tissue and above this range, water in the body absorbs light [5]. Absorption maximum of a PDT agent is also important because it determines singlet oxygen generation efficiency as it will be mentioned later. Singlet oxygen is one of the key elements for a successful PDT application.

1.1.1. History of Photodynamic Therapy

Light was a widely used treatment in many diseases such as psoriasis, rickets or skin cancer by ancient nations as Egyptians, Chineses or Indians for thousands of years [6], [7]. However, photodynamic therapy is known for more than a hundred year [8]. In 1900, cytotoxic affect of acridine orange is observed with day light [8]. In 1903, Niels Finsen was awarded Nobel Prize for treatment of smallpox and cutaneous tuberculosis by phototherapy [9]. After mid 1900s, many successful studies with hematoporphyrin derivative (HPD) were reported [10]–[14]. Therefore, clinical trials of this drug were initiated in 1976 [1]. The first human trials were successful and a hematoporphyrin derivative was used for the treatment of recurrent bladder cancer. These cancer tissues were destroyed by necrosis by slowing down malignant tissue growth. Later 25 patients were treated by the same method successfully [15].

In later years, photodynamic therapy was used in different cancer types and different diseases as brain tumors, skin carcinoma, cholangioma, pancreatic carcinoma etc. [16]–[21]. In 1993, porfimer sodium was reported as the first approved photodynamic therapy agent (Figure 1) [22].

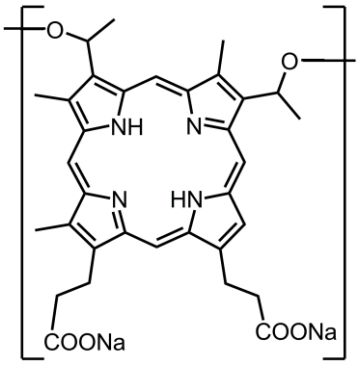

Figure 1: Chemical structure of the first approved photodynamic therapy agent [22].

1.1.2. Mechanism of Photodynamic Therapy

Generation of reactive oxygen species is the crucial step of photodyanmic theraphy application. When light at appropriate wavelength is applied, photosensitizer is

energetically activated (PS → $^1PS^*$) The formed excited singlet state is not stable and has a very short life time, which is in nanoseconds. Therefore, here, these short lifetime species may decay to its ground state so that fluorescence occurs or these species can go for a more stable triplet state by intersystem crossing (Figure 2).

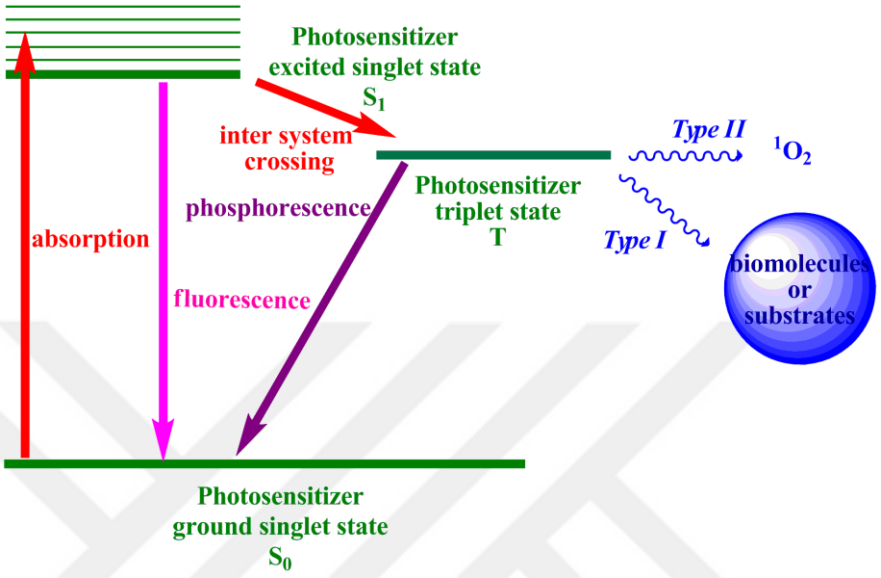

Figure 2: The modified Jablonski energy diagram.

The triplet state species has a lifetime in microseconds, longer than singlet state. In this state, generation of singlet oxygen is possible or electron falls back to its ground state so that delayed fluorescence, phosphorescence occurs. The former pathway is favored by attaching heavy halogens to photosensitizers (heavy atom effect). In this step, reactive oxygen species can form by two different mechanisms. In the type I reaction, triplet state phtosensitizer transfers its energy to surroundings as protons or electrons so that radicals or radical ions form. These radicals or radical ions react with oxygen, therefore, singlet oxygen species form. In type II reactions, triplet state phtosensitizer transfers its energy directly to surrounding oxygen molecules to yield reactive oxygen species (Figure 3).

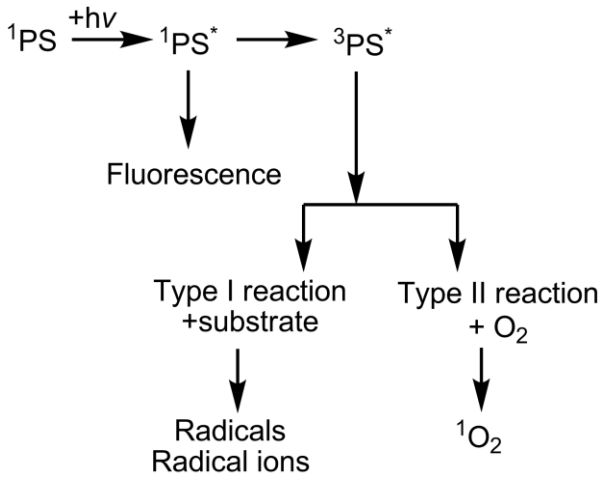

Figure 3: Type 1 and Type 2 reactions.

Reactive oxygen species have very short lifetimes and are highly reactive, therefore, only tissues where photosensitizers are localized, are treated with PDT. It should be noted that PDT efficiency decreases as the oxygen concentration in targeted tissue decreases [1].

The photodamage of photosensitizer results as apoptosis or necrosis in PDT applied tissues (Figure 4) [23]. Apoptosis is a programmed cell death and characterized by cell shrinkage [24]. Necrosis is an unnatural cell death and characterized by swelling of the cell. The cell deaths are the cytotoxic outcome in photodynamic application [25]. Other then cytotoxic drawback, PDT has some other minor results in human body as prolonged skin sensitization to the sunlight so that patients should avoid at least 1 to 4 weeks away from sunlight [26]. The efficiency of treatment can be affected by light wavelength, light doses, photosensitizer administration to body [27].

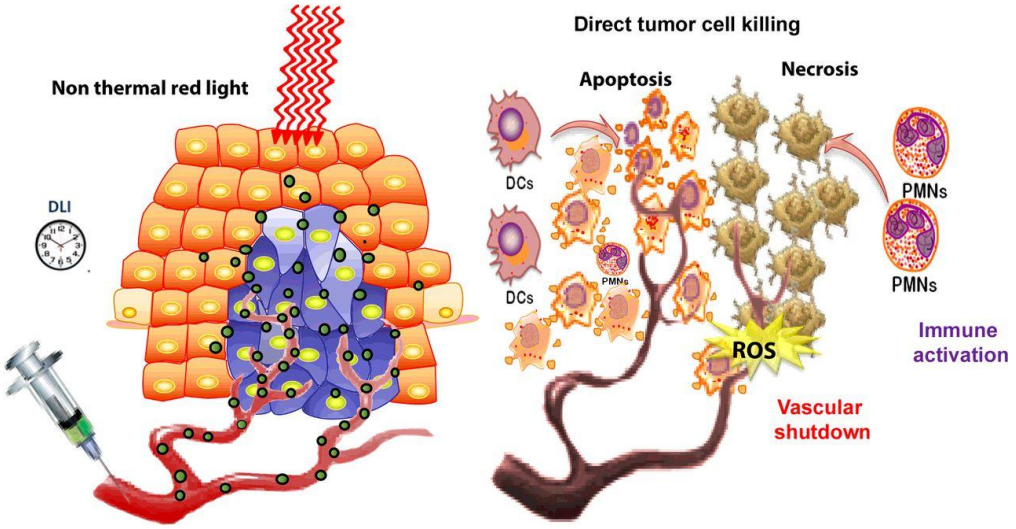

Figure 4: Mechanism of photodynamic therapy on a tumor. Reprinted with permission from reference [23]. Copyright 2015, Bioscience Reports.

1.1.3. Photodynamic Effect

In photodynamic therapy application, photosensitizers also can be mentioned as drugs in clinical applications, light and oxygen (or cytotoxic oxygen) are the basic elements. In order to generate a successful treatment, all these components of PDT should provide optimum standards. As reactive oxygen species form, they directly react with surrounding cellular components such as proteins, lipids, nucleic acids [28]. Therefore, formation of reactive singlet oxygen species triggers immediately cellular damage and vascular shutdown so that immune response system is activated by cellular destruction.

As it is mentioned, necrosis and apoptosis occur as cellular death by PDT. The type of cellular death is determined by the localization of drug and quantity of reactive singlet oxygen. In apoptosis, photosensitizers are generally located in mitochondria or endoplasmic reticulum. In necrosis, however, photosensitizers are generally located in lysosomes or in plasma membrane [29]. The targeted phtotosensitizers are preferable choices for succesfull PDT applications with minor side affects.

Besides targeting property of a photosensitizer, effective singlet oxygen generation capability is also a crucial step in photodynamic therapy applications. Spin orbit

coupling can be increased by spin forbidden transition from ground state oxgen ($^3O_2$) to excited state oxygen [30], [31].

$$H_{SO} = \frac{e^2 Z^4}{2a_o m^2 c^2 n^3} \; L.S$$

In the above formula, L is angular momentum number and S is spin operator and spin-orbit Hamiltonian term is shown with H_{SO}. Z is atomic number, a_o is Bohr's radius, m is mass of electron, c is speed of light, n is principle quantum number and e is electron charge.

As it can be found from spin orbit Hamiltonian formulation, H_{SO} is proportional to fourth power of atomic number. Therefore, when heavy atoms are fused in photosensitizer core, spin-orbit coupling increases so as spin-forbidden transition of singlet-triplet states.

In living organisms, there are many absorbing molecules, therefore, light penetration differs according to where it is applied. For instance, melanin collagens, hemoglabins absorb different regions of visible light or some aromatic compounds as aminoacids phenylalanin absorbs near visible light (Figure 5) [32]. Therefore, longwavelength light is the essential key for sufficient tissue penetration. However, it should be considered that above 900 nm, water absorbs the applied light. That's because the therapatic window, which is between nearly 650-900 nm, gives the best penetration depth in photodynamic theraphy applications. Thus, the use of photosensitizers in PDT application is done accordingly [33].

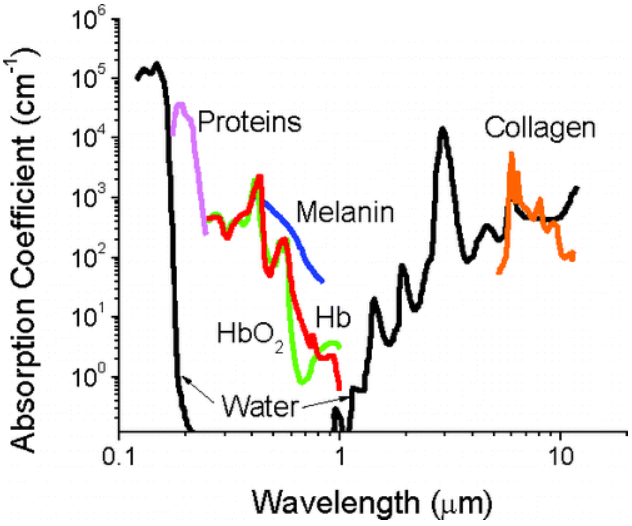

Figure 5: Therapeutic window of the body, absorbance of melanin, oxy-Hemoglobin (HbO_2) and water. Reprinted with permission from reference [34]. Copyright 2012, American Chemical Society.

Therefore, absorption maxima of a photosensitizer must be in the therapeutic window in order to generate effective reactive singlet oxygen species so that it can absorb the given light strongly.

1.1.4. Photosensitizers

As the key element of photodyanmic therapy application, there are extensive studies for generation of effective photosensitizers [35]. The first generation photosensitizers generally based on porphyrin [36]. For example, photofrin is a porphyrin based photosensitizer and does not have a good absorption at therapeutic window, has an absorption maxima at 630 nm. Therefore, light does not penetrate deeply and also painful edema is the side effect of this drug application [37].

Due to the drawbacks of photofrin, hematoporphyrin type of drugs and other drug types as synthetic chlorins, which have absorption maxima at therapeutic window, are more favorable (Figure 6) [36]. 5-Aminolaevulinic acid (5-ALA), which is a porphyrin precursor, is another clinically approved photosensitizer. It is used in skin cancer [38]. Sessler *et al.* reported new type of photosensitizers in 1988 [39]. Texaphyrins have common properties with porphyrin derivatives as high intensity colors. These dyes have an absorption maxima at near IR region.

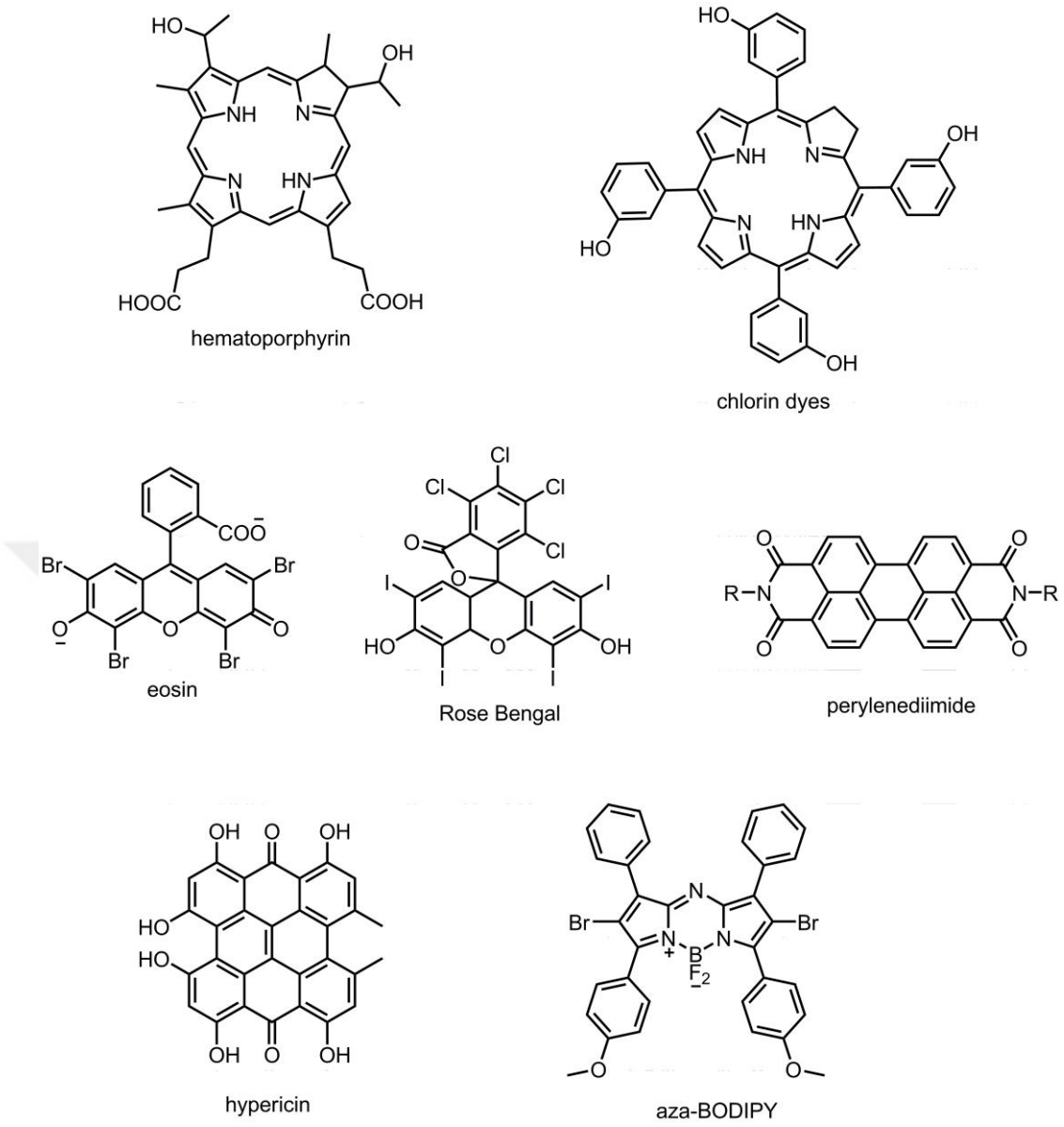

Figure 6: Selected examples of the recent photosensitizers from literature.

After the first clinical trials in 1976, photodynamic therapy is used in the treatment of many diseases [1]. Many approved phtosensitizers are used in clinical applications widely in cancer treatments (Table 1). Lung, bladder, neck and head, prostate, nonmelanoma cancer types are just a few of the examples [40]–[47]. Besides trials of some cardiovascular diseases are conducted and approval of new treatments are soon to be expected in the near future [48].

Table 1: Some approved photosensitizers and the diseases for which they are used for treatment [36].

Photosensitizer	Trade Name	Approval	Wavelength (nm)	Area of Use
Taloporfin Sodium	LS11	Phase I&II	664	Choroidal neovascularization, liver and colorectal metastasis
Motexafin Lutetium	MLu, Lutex, Lutrin	Phase I	732	Prostate, Atherosclerosis
Silicon pthalocyanine-4	PC-4	Phase I	672	Skin
mTHPC	Foscan	2001 EU	652	Head and neck, prostate, pancreas, esophagus, mesothelioma
Methyl aminolevulate-PpIX	Hexvix	2005 EU	405	Detection of Bladder tumors
Pd-bacteriopheophorbide	Tookad	Phase I	762	Prostate
Porfimer Sodium	Photofrin	1998 FDA	630	Lung, Barrett's esophagus

Boron dipyrromethene, BODIPY, dyes are attractive phtosenstizer agents with their high extinction coefficient and phtostabilities [49]. In 2005, a BODIPY derivative is synthesized as a photosensitizer. In this work, Nagano *et al*., show that haloganated BODIPY generates singlet oxygen species with intersystem crossing, **2** (Figure 7). In another work, heavy atoms are introduced to 3-, 5- and 2-, 6- positions of BODIPY core, **3**, **4** and **5** (Figure 7). As singlet oxygen generation efficiencies of BODIPY derivatives are compared, it is observed that BODIPY derivatives that are haloganated in 2-, 6- positons have high fluorescence and high singlet oxygen quantum yield. Also, It should be noted that these BODIPY derivatives are highly stable in light [50].

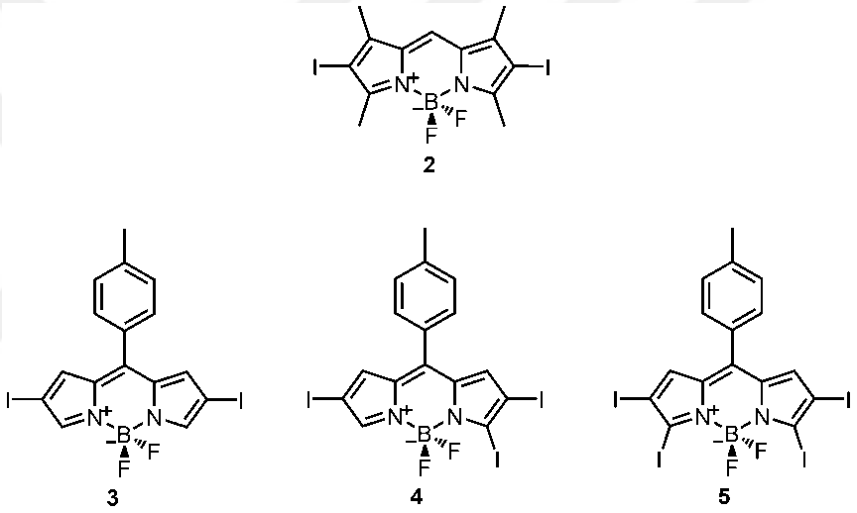

Figure 7: Halogenation of BODIPY core at different positions.

O'Shea *et al.* also reported a new class of BODIPY based photosensitizers [51]. These aza-BODIPY derivatives have a strong absorption at near-IR region, **6** and **7** (Figure 8). In figure 8, there are some examples of photosensitizers that can work in the therapeutic window of the body [52]–[54]. Akkaya *et al.* has published a nice example of a smart photosensitizer that takes into account cancer parameters, **9** [54]. In this article, the increased acidity amounts in cancer cells were used as one parameter for photosensitizer to work. The other parameter was the sodium concentration of the medium. In acidic medium, pyridine groups were protonated and bathochromic shift in absorbance was observed. Light at 660 nm was applied, only

protonated molecules show photodynamic work and by Na^+ binding photoinduced electron transfer, PET, was blocked. Therefore, a smart photosensitizer that works only in cancer cells that has low pH and high Na^+ concentration.

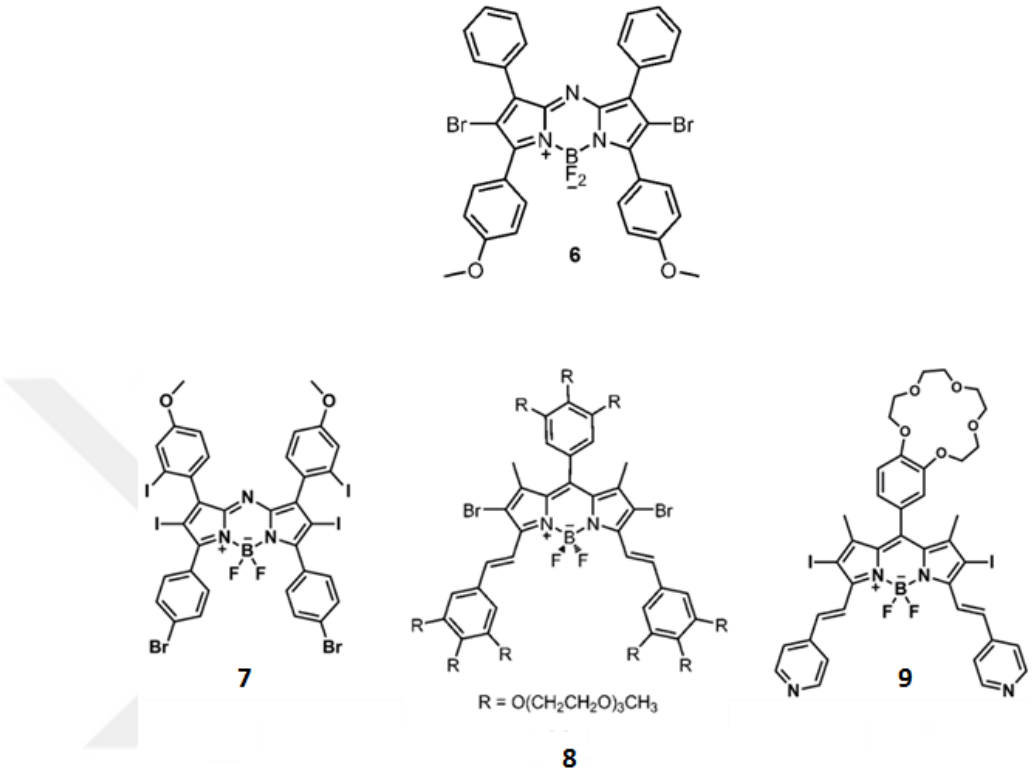

Figure 8: Literature examples of BODIPY based photosensitizers.

1.1.5. Chemiluminescence

As it is stated before, typical photosensitizers absorb at 600-800 nm so UV light to excite these molecules has some problems related to penetration depth of light [35], [55]–[58]. Therefore, photodynamic theraphy with these common photosensitizers are suitable only for tumors under skin with a ceratin depth interval (~1cm) or on skin. Also the method is not suitable for metastatic tumors, which are main reason of cancer deaths [55], [56]. Therefore, photosensitizers, which can be activated without any external light source, are important in photodynamic applications. In self illuminating photodynamic therapy system, nonradiative energy is transferred from suitable donors to acceptor molecules. The energy transfer porcess is either

chemiluminescent resonance energy transfer (CRET) or bioluminescent resonance energy transfer (BRET) [55], [58]–[64]. During the process, chemiluminescent or bioluminescent donors activate photosensitizer intracellulary without using any light source.

Chemiluminescence is the emission of light, which is formed as a result of a chemical reaction. When chemiluminescence occurs in living cells by enzyme catalyzation, it is called as bioluminescence [65]–[69]. Bioluminescence is a sub-type of chemiluminescence. Bacteria, insects and worms are some of the living organisms that bioluminescence can be observed [65], [66]. Many of the chemiluminescent substrates contain an oxygen-oxygen peroxide bond. The excited state products form by thermal activation in this case [65], [66], [70]. Dioxetanedione, R_1,R_2,R_3,R_4-dioxetane and R1,R2-dioxetanone (Figure 9) are the main groups for substrates that contain peroxide [65], [66], [70], [71]. The main criterion for peroxide containing substrates is whether they can provide enough energy for chemiexcitation of acceptor during the thermal process.

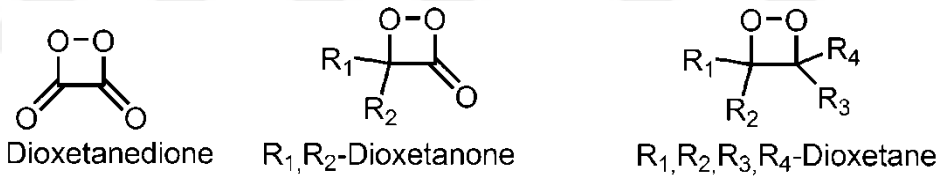

Figure 9: Peroxide containing chemiluminescent substrates.

Peroxide-containing bioluminescent and chemiluminescent substrates have three parts. A peoxide bond is one of these parts [65], [66], [70]. The peroxide bond breaking results with thermally activated ground state to excited state chemiexcitation. The other part is electron rich moity. This part arranges the electron or charge transfer for peroxide ring decomposition. The final part is ionazable groups that are responsible of arranging activation energy for thermal decomposition (Figure 10) [72]–[74].

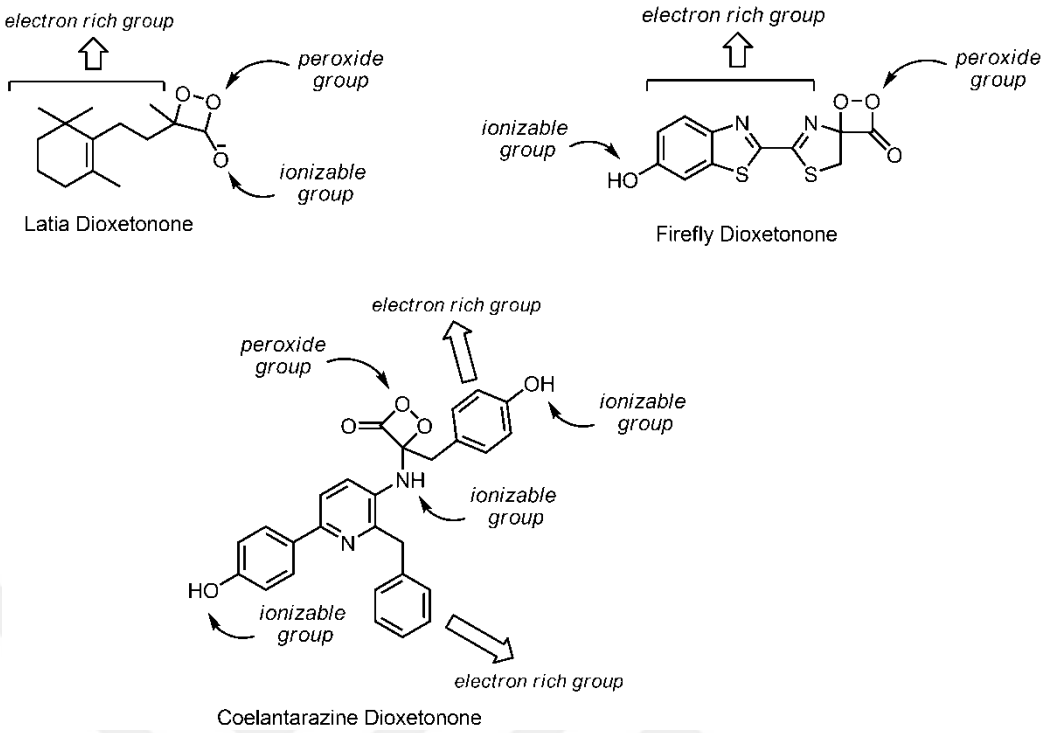

Figure 10: Peroxide-containing bioluminescent and chemiluminescent substrates.

1.1.6. Chemiluminescent and Photoluminescent Systems in Photodynamic Therapy

The oxidation of luminol is one of the many reactions that reasulted with emission of light [75], [76]. A basic solution and an oxidant catalyst as Fe^{2+}, Cu^{2+}, Co^{2+}, periodate ions or hydrogen peroxide is reaquired for the oxidation of luminol. As it is shown in figure 11, the interaction of luminol with hydroxide anions results with dianion formation. The resulted dianion reacts with oxygen and the oxidation product forms. Aminophthalte ion in excited state has an emission at max 425 nm and a blue chemiluminescence (Figure 11) [75], [77]. There are several examples of use of luminol derivatives in photodynamic therapy studies. For instance, Wang and coworkers study chemiluminescence of luminol in photodynamic theraphy [61]. In the study, oligo (*p*-phenylene vinylene) (OPV) as the photosensitizer absorbs chemiluminescence of luminol. Luminol, hydrogen peroxide and horseradish (HRP) were used to induce chemiluminescence. OPV has an absorption range of 350-550 nm and luminol has an emission maxima at 425 nm. Therefore, in this case spectral

overlap is also achieved chemiluminescence resonance energyu tarnsfer CRET or bioluminescence resonance energy tarnsfer BRET. CRET is also favorable by considering the fact that dianionic excited product of luminol chemilumescence and cationic OPV.

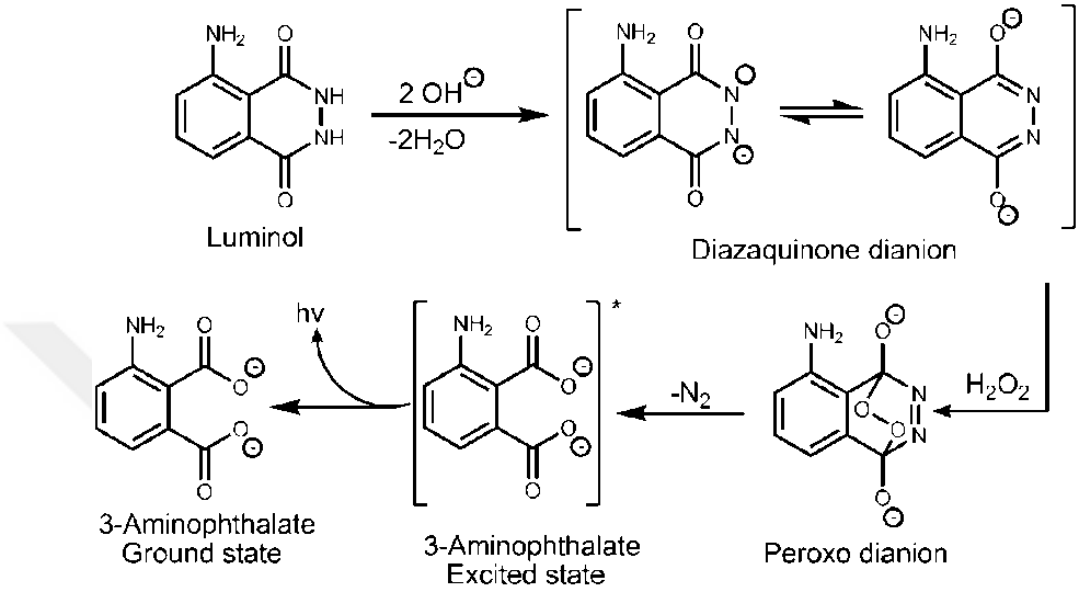

Figure 11: Chemiluminescence reaction mechanism of luminol.

Firer and coworkers injected luminol, hydrogen peroxide and as a catalyst Fe^{2+} to murine hybridoma cells in order to activate hematoprophyrin, which was used as photosensitizer (Figure 12) [55]. The results showed that luminol induces intracellular chemiluminescence and photodyanmic theraphy activation is induced cytotoxicity in %95 of cells.

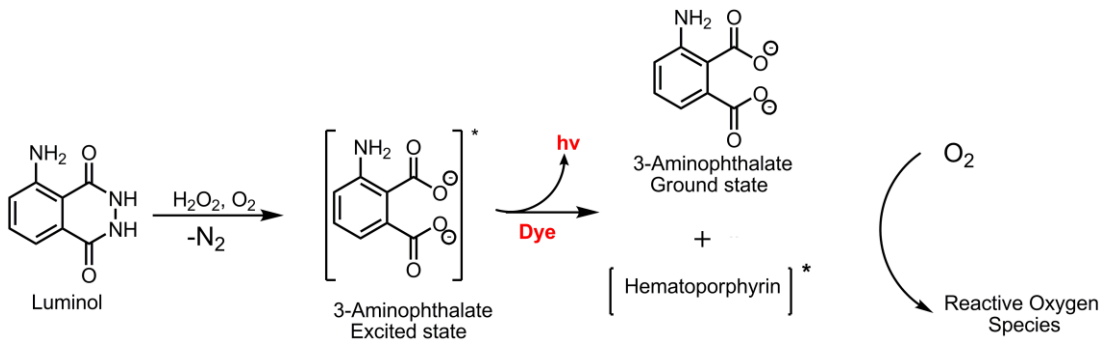

Figure 12: Excitation of a photosensitizer, hematoporphyrin, by luminol.

1.2. Energy Transfer (ET)

The design and synthesis of artificial energy light harvesting systems have been an attractive area in supramolecular studies since there are many inspiring examples of light-harvesting antenna systems [78]. There are two different types of energy transfer mechanism: Dexter and Förster energy transfers (Figure 13).

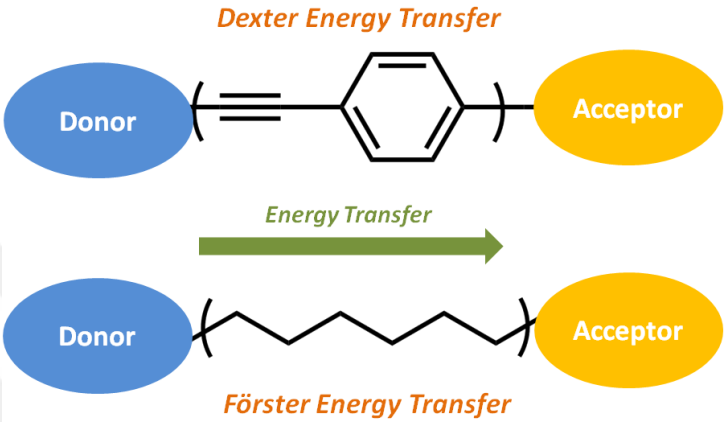

Figure 13: Schematic representation of Dexter and Förster type energy transfers.

1.2.1. Energy Transfer Mechanisms

Resonance energy transfer is a photophysical process that occurs between an electronically excited donor molecule and an acceptor molecule so that at the end, lifetime of donor molecule decreases. In supramolecular systems, energy transfer can be observed between two localized electronically excited states by radiationlessly. Non-radiative energy transfer can be explained by two different mechanisms, which are inductive resonance and exchange interaction. The inductive resonance mechanism also called as Förster type mechanism (Coulombic energy transfer) is a long range mechanism, on the other hand, exchange mechanism also called as Dexter type mechanism is significant only less than 10 Å distance between donor and acceptor molecules [79]. The orbital aspects of both energy transfer mechanisms are represented in figure 14.

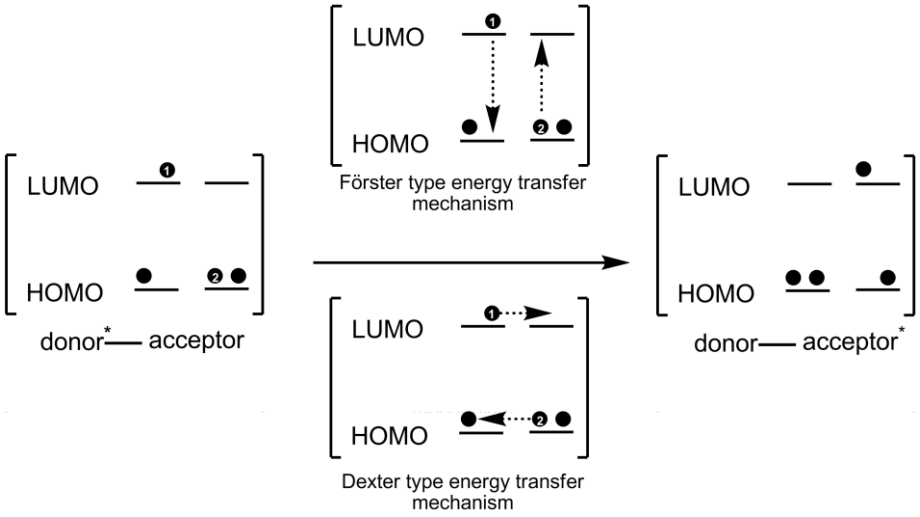

Figure 14: The coulombic and exchange energy transfer mechanisms.

1.2.1.1. Förster Type Energy Transfer

In an interaction of a donor molecule and an acceptor molecule, non-radiative energy transfer of excitation energy occurs and if the emission spectrum of donor molecule and the absorption spectrum of acceptor molecule overlaps, the energy transfer between donor and acceptor could be possible (Figure 15) [80], [81]. This type of energy transfer is called as Förster (resonance, inductive resonance, Coulombic or through space) Resonance Energy Transfer.

Förster Type energy transfer does not require a physical contact or interaction between donor molecule or acceptor molecule [82], [83]. However, for an effective energy transfer process, donor chromophore should be fluorescent. If the donor molecule is a fluorescent molecule, the energy transfer is called as fluorescence energy transfer (FRET). FRET requires that the energy gap between ground and excited states should be nearly equal for both donor and acceptor molecules. Therefore, in an interaction of a donor molecule and an acceptor molecule, non-radiative energy transfer of excitation energy occurs and if the emission spectrum of donor molecule and the absorption spectrum of acceptor molecule overlap, the energy transfer between donor and acceptor could be possible (Figure 15). The dipole-dipole term is the most important term in Förster theory.

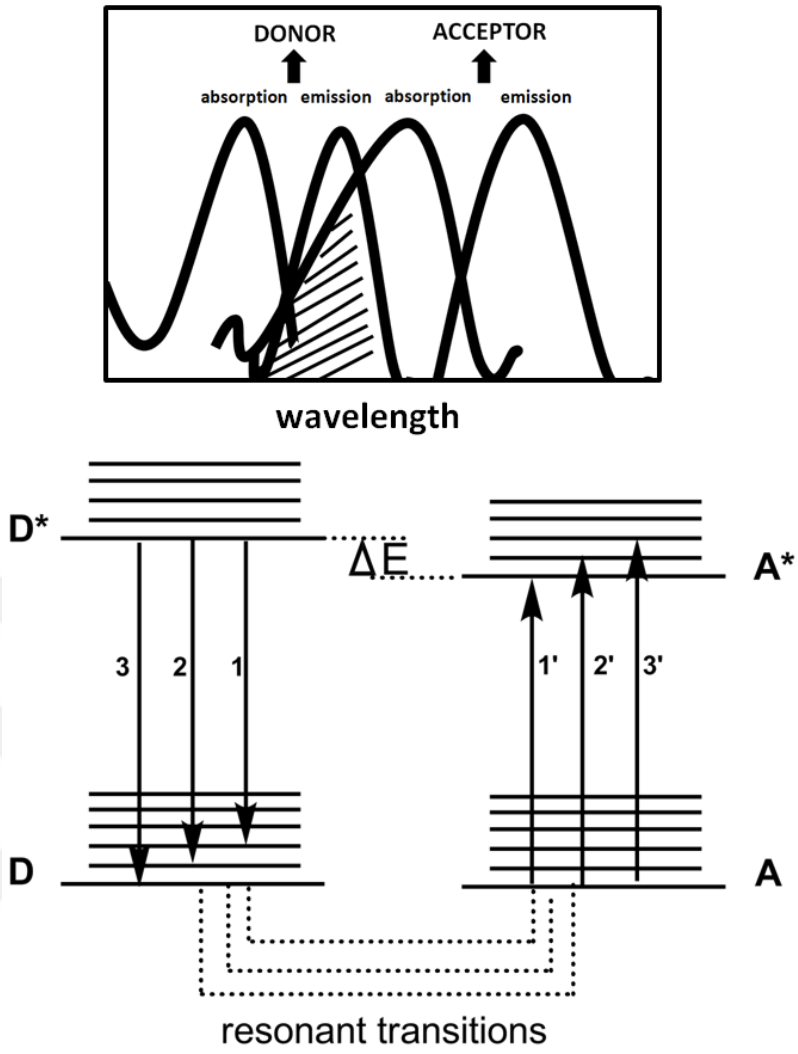

Figure 15: Energy level scheme for donor and acceptor molecules.

In the energy level scheme of donor and acceptor molecules, coupled transitions where vibrational relaxation is faster than energy transfer can be observed and the integral overlap between absorption of acceptor and the emission of donor is shown. The spectral overlap of donor and acceptor occurs when an electron in LUMO of donor molecule goes to its HOMO, energy is released so that an electron in HOMO of acceptor molecule goes to its LUMO.

In early 1920s, J. Perrin stated that if molecules can be separated by a sufficient distance, energy can be transferred from a donor molecule to an acceptor molecule

non-radiatively. Later on, Förster in 1946 showed that the energy transfer possible up to 10 nm and explained the energy transfer quantitatively where

$$k_F = k_{rad}(R_F/R)^6$$

k_{rad} is radiative rate, R_F is critical distance or Förster radius [84]. Förster radius is determined by the overlap of emission spectrum of donor and absorbance spectrum of acceptor molecules. R_F is generally in a range of 1-8 nm. Some literature R_F values are given in table 2 [85].

Table 2: Typical values of R_F, Förster radius.

Donor	**Acceptor**	**Typical Values of R_F (Å)**
Fluorescein	Tetramethylrhodamine	55
IAEDANS	Fluorescein	46
EDANS	Dabcyl	33
Fluorescein	Fluorescein	44
BODIPY FL	BODIPY FL	57
Fluorescein	QSY7 and QSY9 dyes	61

Two different methods can be used to calculate Förster Type Energy Transfer efficiency, which are steady state and time resolved [86]. In steady state approach, the amount of decrease in quantum yield of donor molecule is used. However, self absorption of emitted light by the same molecule or surrounded ones is a problem

which is called as inner filter effect. In order to avoid inner filter effect, dilute solutions should be used. FRET efficiency is formulated as:

$$\mathbf{E = 1 - \phi_{DA} / \phi_D}$$

Where, Φ_{DA} is quantum yield of donor in the presence of acceptor and Φ_D is quantum yield of donor in the absence of acceptor. FRET efficiency can be calculated with a different formulation in the same approach:

$$\mathbf{E = A_A (\lambda_D) / A_D (\lambda_D) * [I_{AD} (\lambda_A^{em}) / I_A (\lambda_A^{em}) - 1]}$$

In this formulation, A_A is absorbance value of acceptor at the maximum absorbance wavelength of donor and A_D is absorbance value of donor at the maximum absorbance wavelength of donor. I_{AD} is integrated emission area of acceptor in the presence of donor at λ_A^{em} and I_A refer to integrated emission area of acceptor in the absence of donor at λ_A^{em}.

In time resolved approach, time resolved emission data of donor and acceptor molecules is used. Since the inner filter effect is eliminated here, this method provides much more accurate data. FRET efficiency can be formulated as shown below, in the case of decay emission is a single exponential:

$$\mathbf{k_{FRET} = 1/\tau_{DA} - 1/\tau_D}$$

$$\mathbf{E = \tau_D k_{FRET} / (1+\tau_D k_{FRET})}$$

where τ_D refers to excited state lifetime of donor in the absence of acceptor and τ_{DA} refers to excited state lifetime of donor in the presence of acceptor.

In figure 16, there is a BODIPY based, Förster type energy transfer system shown [87]. The system consists of an acceptor, perylene diimide core, and four donors, four BODIPYs. The increased number of donors increases the extinction coefficient. The extinction coefficient of the molecule is 250000 M^{-1} cm^{-1} at the maximum

absorbance wavelength of donor molecules, at 526 nm. The critical Förster radius is determined to be 4.7 nm and with energy transfer efficiency of 99%.

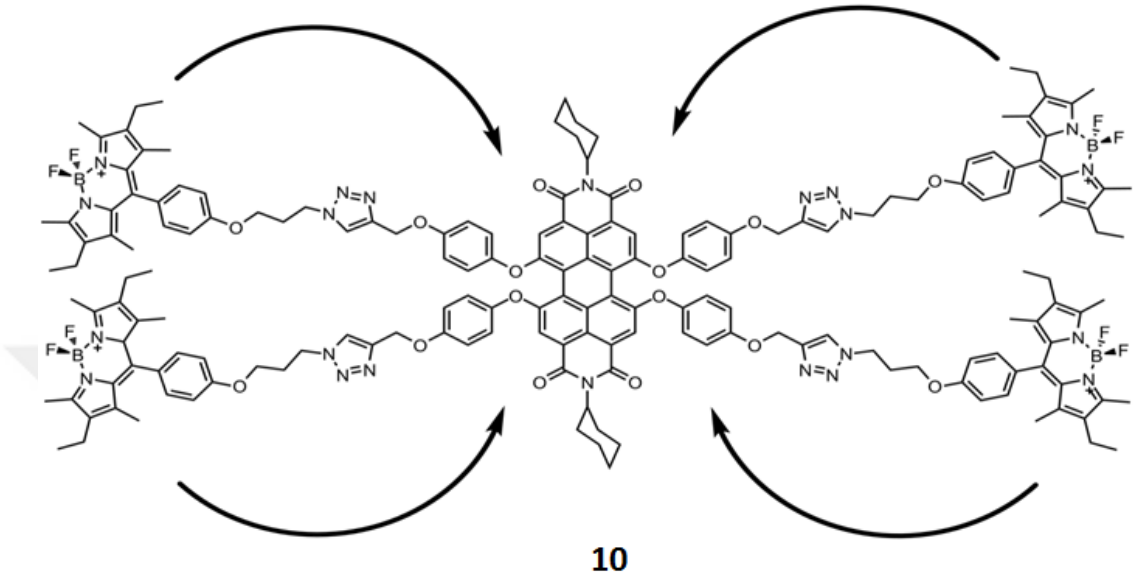

10

Figure 16: A BODIPY-based Förster type energy transfer system.

1.2.1.2. Dexter Type Energy Transfer

The interaction between highest occupied orbital of donor molecule and lowest unoccupied orbital of an acceptor molecule is called as Dexter type energy transfer or electron exchange type mechanism or through bond energy transfer [88]. The orbital interaction limits the distance between acceptor and donor so that maximum distance is generally 10 Å and the rate constant of Dexter type energy decreases exponentially with the distance to nuclei [79]. The rate constant is formulated as below:

$$k_{ET} = K\ J\ \exp(-2R_{DA} / L)$$

where K is orbital interaction, J represents the overlap integral between emission of donor molecule and absorption of acceptor molecule, R_{DA} is the donor acceptor separation and finally L is the van der Waals radii.

There are different molecular systems with this type of energy transfer. Two anthracene-BODIPY based systems **11** and **12** are shown in figure 17. The important point about the energy transfer system **12** is that it is much more efficient than **11** and when the molecule is excited at the maximum absorption of anthracene, energy transfer occurs very fast, which is about ~200 fs. Anthracene unit behaves as donor and BODIPY serves as acceptor in this system. It's because of the parallel alignment of S_1 transition dipole moment of donor and S_0 transition of acceptor units and due to the steric hindrance in **11**, conjugation is disturbed and energy transfer decreased [89]. The compound **13** is another example of a BODIPY based energy transfer cassette in which two donor units are attached to an acceptor unit with conjugated bridges. In this literature example, the decrease in through bond energy transfer with increased distance is observed [90].

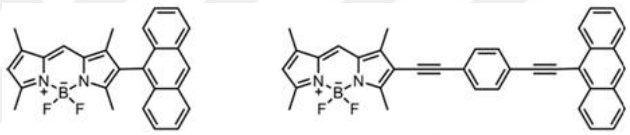

11 **12**

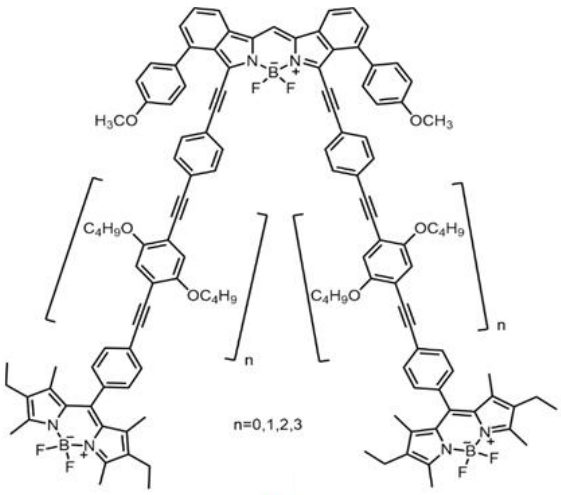

13

Figure 17: Through-bond energy transfer cassettes.

1.2.2. Energy Transfer and Molecular Machines

Rotaxanes and catenanes have been studied for development of mechanically bonded systems. Switches, molecular shuttles are a few examples of mechanically bonded molecular machines [91]–[97]. There are many attempts to construct rotaxanes in energy transfer systems. In these systems, chromophoric units can be placed in axle or wheel parts. Rotaxane systems are especially favorable in Förster energy transfer cassettes due to having a chance to place donor and acceptor components in close distances.

Brouwer and coworkers have published a study of [2]rotaxane system for Förster resonance energy transfer as the first known example of pillararene based rotaxane [98]. In the design of energy transfer cassette, wheel component constructed from pillar[5]arene and a dipyrene is attached to pillar[5]arene. As an axle, pyridinium is used and perylene unit is used as the stopper (Figure 18). In the mechanically interlocked rotaxane system, efficient Förster resonance energy transfer from wheel component to stopper component is proved.

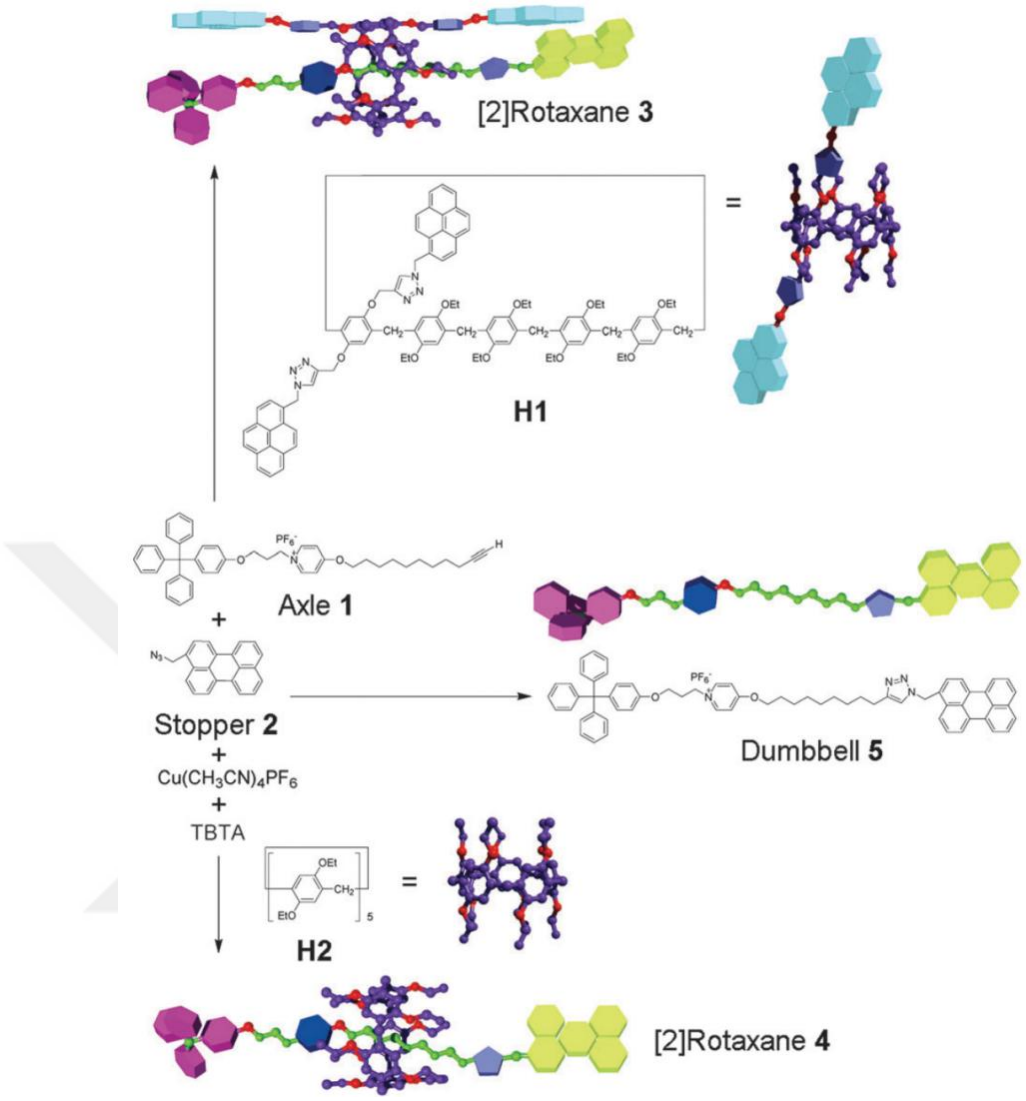

Figure 18: [2]rotaxane system for Förster resonance energy transfer. Reprinted with permission from [98]. Copyright 2013, Royal Society of Chemistry.

There is another example of Förster resonance energy transfer in a mechanically interlocked system (Figure 19) [99]. In the synthesized rotaxane system, Coumarine 2 is placed on the axle and served as the donor component and Coumarine 343 placed on the macrocycle and served as the acceptor. A schematic representation of rotaxane system shows that a macrocycle (red) is mechanically interlocked by a hydrogen bonding site (green) to an axle (black). Bulky group represented as yellow.

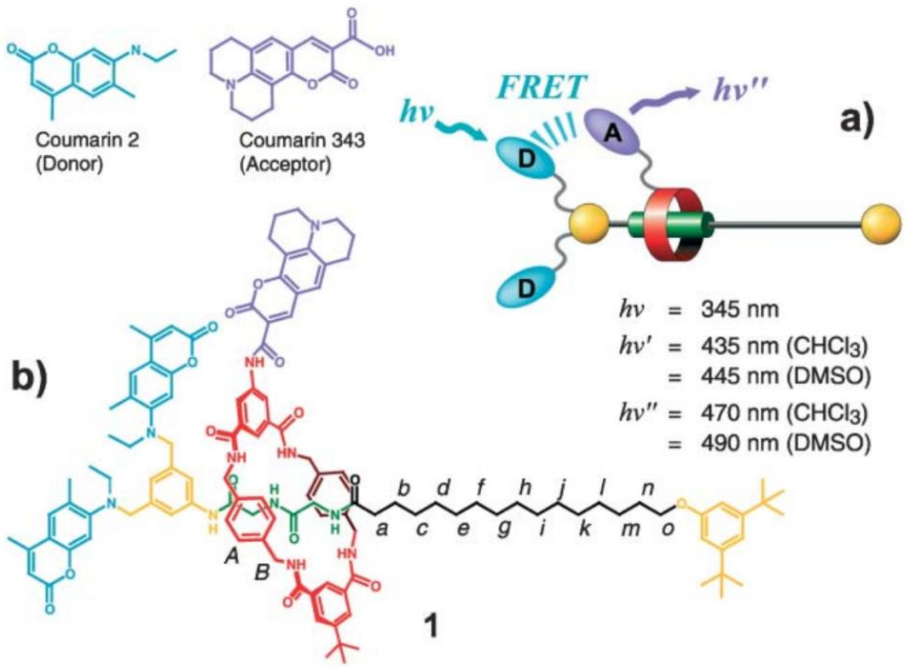

Figure 19: A mechanically interlocked rotaxane in Förster resonance energy transfer. Reprinted with permission from [99]. Copyright 2005, Royal Society of Chemistry.

1.3. Electron Transfer Processes

A fluorescent probe can be designed by the combination of a fluorophore to provide optical signal from a chemical input and a receptor to provide the sensitivity and selectivity towards the intended material [100]. In a fluorescent probe, receptor can be directly connected to fluorophore to from a conjugated system or there can be a spacer between the fluorophore and the receptor (Figure 20) [101].

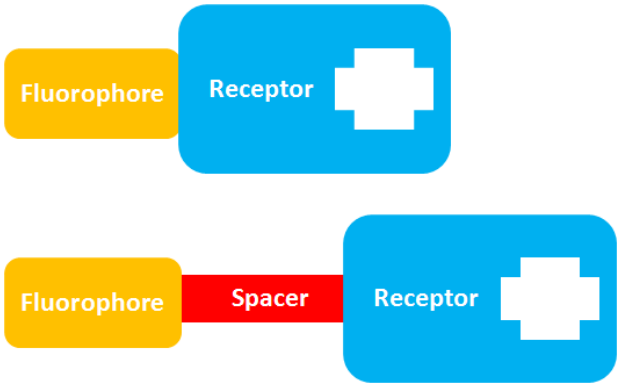

Figure 20: Schematic representations of fluorescent chemosensors.

1.3.1. Internal Charge Transfer (ICT)

In internal charge transfer (ICT) system, a receptor is directly attached to a fluorophore, as a result a conjugated fluorescent probe forms (Figure 21). When an analyte binds through the receptor, dipole moment changes causing intramolecular charge transfer from donor to acceptor. Therefore, a spectral shift in absorption and emission is observed.

The type of the ligand determines the character of the shift in absorption and emission spectrum according to the electronic character of the receptor and the analyte. When an electron donor group is attached to a fluorophore, a cation binding as an analyte will decrease electron density and the conjugation which means that cation binding destabilize the excited state so the energy gap between HOMO and LUMO levels increases. Thus, there will be a blue shift in absorbance and emission spectrum [102].

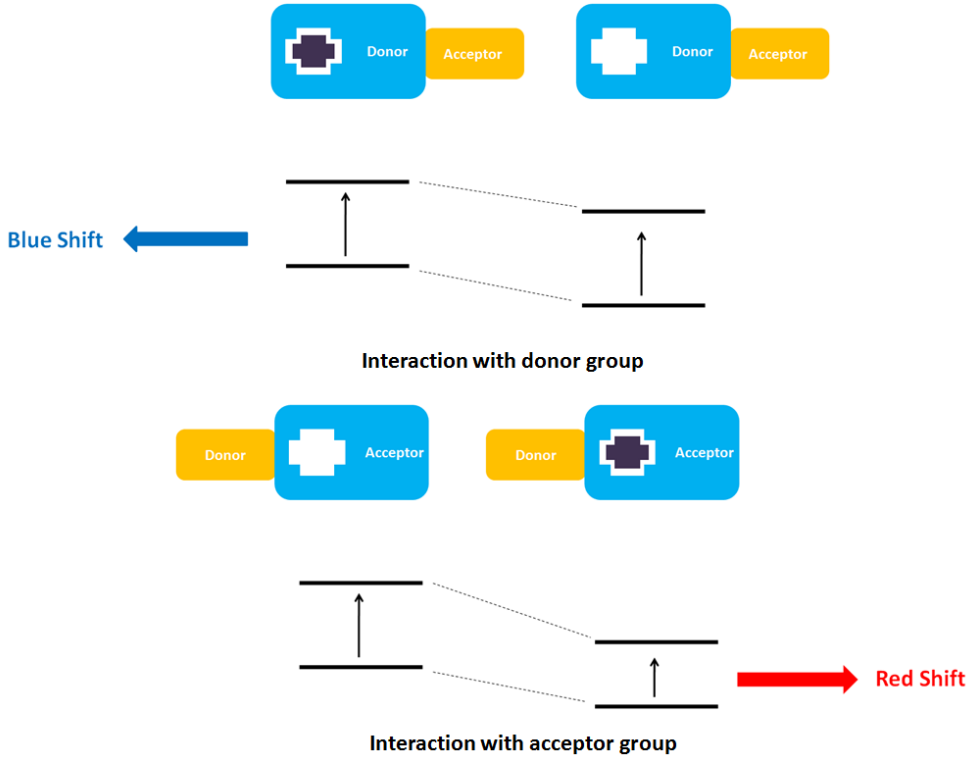

Figure 21: Red and blue shifts according to energy gap between HOMO and LUMO in ICT based chemosensors.

On the other hand, when an electron withdrawing group is attached to a fluorophore, a cation binding as an analyte will increase electron density and the conjugation which means that cation binding stabilize the excited state so the energy gap between HOMO and LUMO levels decreases. Thus, there will be a red shift in absorbance and emission spectrum [103]. In figure 22, there are examples for ICT based systems that show blue shift in case of metal ion binding [104], [105].

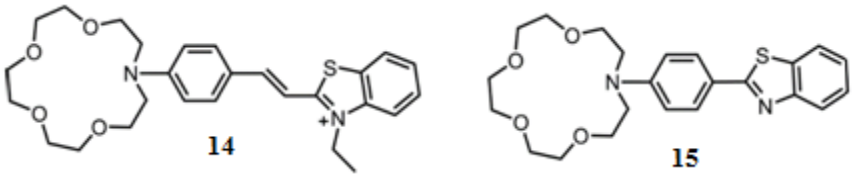

Figure 22: Examples for ICT based sensor which has crown ether as receptor.

1.3.2. Photoinduced Electron Transfer (PET)

In photoinduced electron transfer (PET) systems, the conjugation is prevented by placing a spacer between a fluorophore and receptor but electronic interaction can be still possible (Figure 23) [106]. The PET working mechanism starts with the absorption of photon by a fluorophore, therefore, electron is excited from highest occupied molecular orbital (HOMO) to lowest unoccupied molecular orbital (LUMO). After excitation an electron from the donor atom move to the HOMO of fluorophore. Since the HOMO level of fluorophore is fully occupied, the excited electron of fluorophore cannot return, as a result fluorescence is quenched.

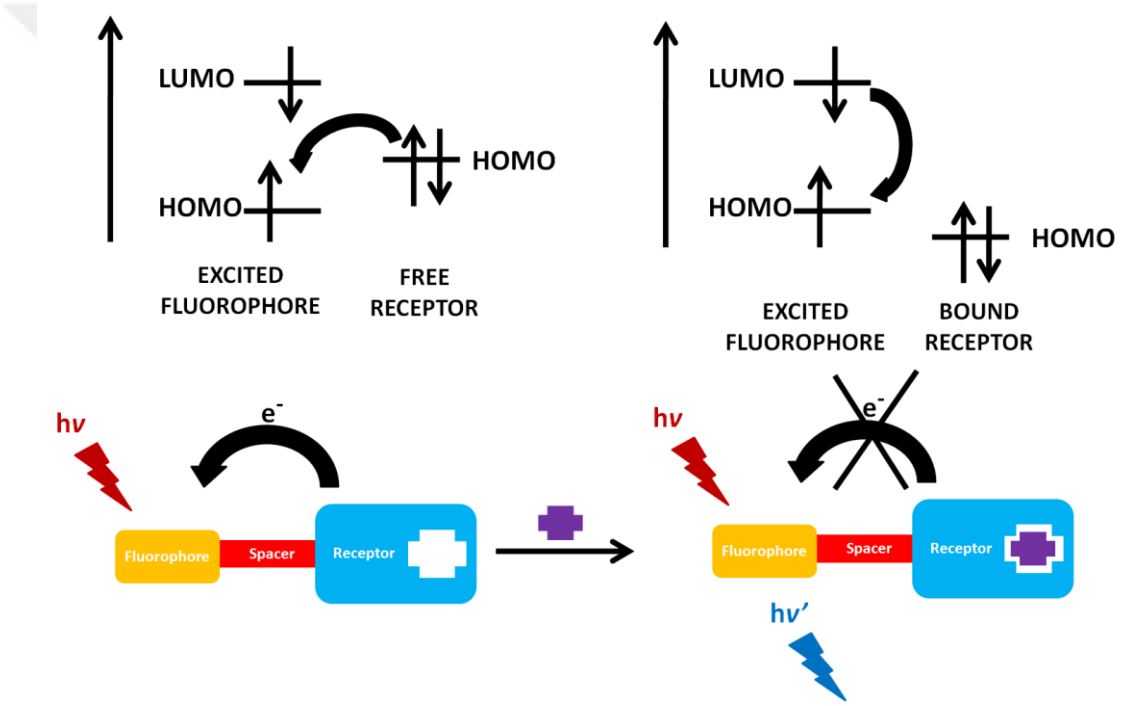

Figure 23: Schematic representation and mechanism of PET.

The figure 24 shows some literature examples for PET based chemosensors for different metal ions. In these examples, fluorescence is quenched by the binding of some alkali and transition metal ions [107].

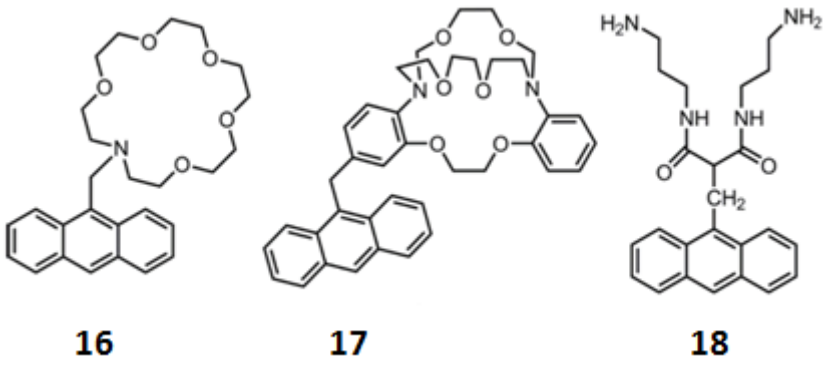

Figure 24: Example compounds for PET based chemosensors.

In figure 25, The PET based system consists of two pyrene moieties attached to a diazacrown ether. In the case of a cation binding, as it is expected, monomer to excimer ration changes and fluorescence increases due to decreased PET from the nitrogen atoms of diazacrown ether to pyrene groups. The monomer to excimer ratio strongly depends on the size of the binding cation and K^+ and Ba^{2+} shows the highest stability [108].

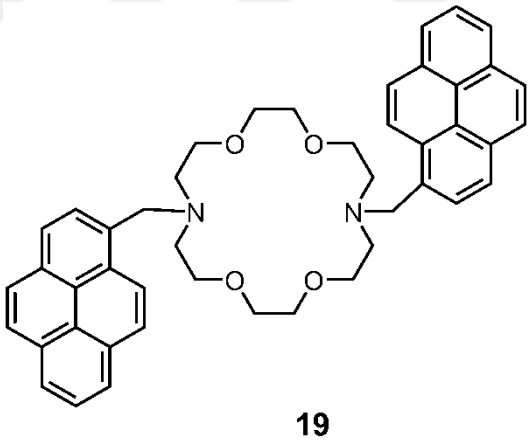

Figure 25: A PET sensor involving excimer formation.

1.4. Fluorescent Dyes

Fluorescent organic dyes, as it is mentioned before, have many applications. A wide variety of fluorescent dyes with emission in ultraviolet (UV), visible (VIS), infrared (IR) and near-infrared (NIR) regions can be observed in different applications. In

figure 26, there are fluorescent organic dyes with different emission wavelengths [109].

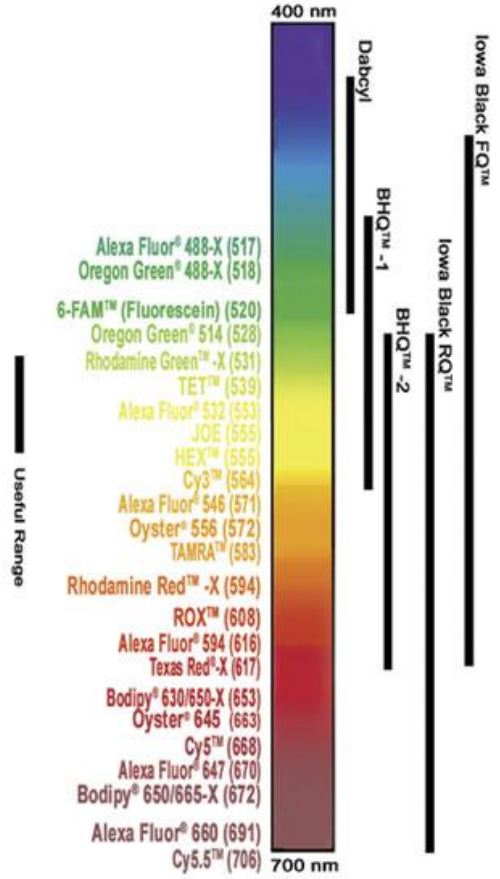

Figure 26: Common fluorescent dyes in visible region [109].

The UV region mainly contains coumarin, pyrene and naphthalene based dyes and the IR region contains BODIPY, fluorescein, cyanine and rhodamine dyes.

1.4.1. Fluorescein Dyes

Fluorescein dyes are also called as 2-(6-hydroxy- 3-oxo-xanthen-9-yl)benzoic acid synthesized first time in 1871 by Adolph Von Baeyer by the condensation of resorcinol and phthalic anhydride in the presence of a strong acid and a catalyst, sulfuric acid and zinc chloride, respectively [110]. Fluoerescein dye derivatives have many applications in biotechnology considering their high quantum yield and relatively good water solubility [111]. As in BODIPY dyes they have many literature

application examples as chemosensors, DNA attachments, laser applications and photosensitizers [112], [113]. The basic numbering of the xanthene core of Fluorescein dyes are shown in figure 27 .

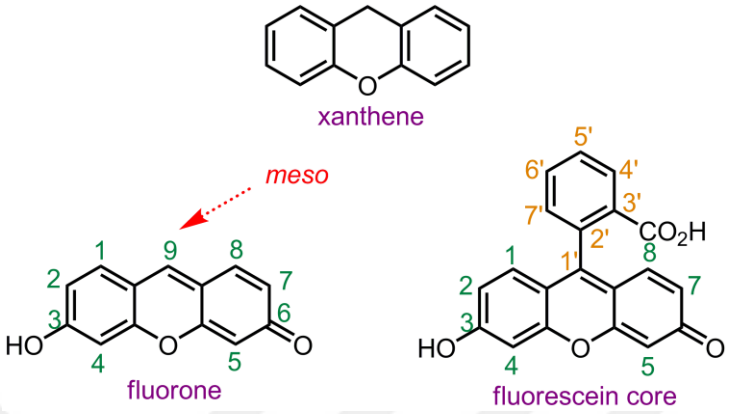

Figure 27: Basic numbering system of xanthenes dyes.

The properties of fluorescein dyes can be improved with different functionalization on the core. Halogenation, alkylation, sulfonation or other specific type of reactions can be used to improve absorption or emission wavelengths or quantum yields. In literature, there are many examples of fluorescein derivatives (Figure 28).

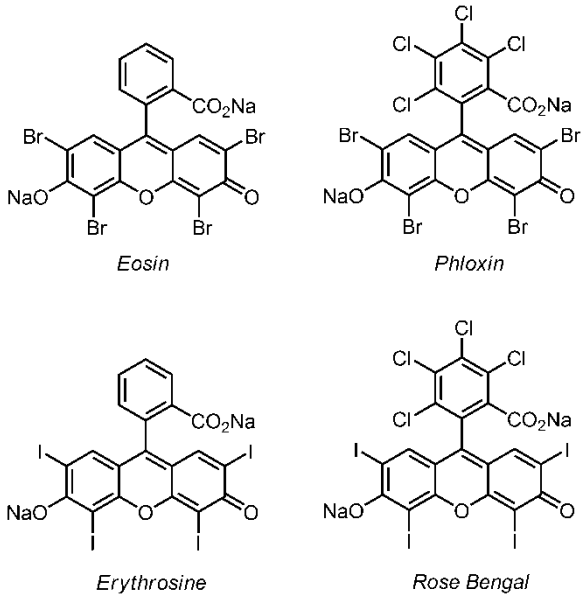

Figure 28: Named derivatives of fluorescein.

The synthesis of fluorescein dyes consists of a condensation of two equivalents of resorcinol and one equivalent of phthalic anhydride in the presence of a strong acid as sulfuric acid, later it was found that using zinc chloride as the catalyst increaes the yield.

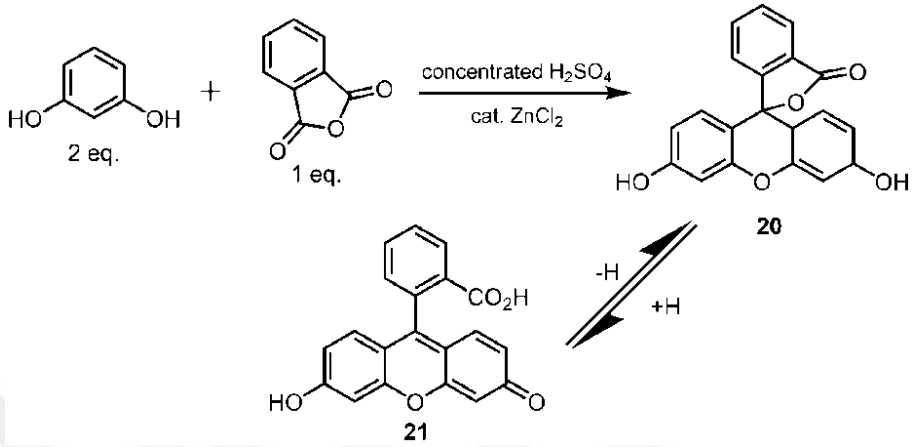

Scheme 1: Synthesis of Fluorescein.

Fluorescein has a lactone locked form in acidic conditions and going from neutral conditions to acidic conditions, the transformation from an open from to lactone form, fluorescein undergoes five different forms. The five different forms of fluorescin depending on pH can be seen in scheme 2.

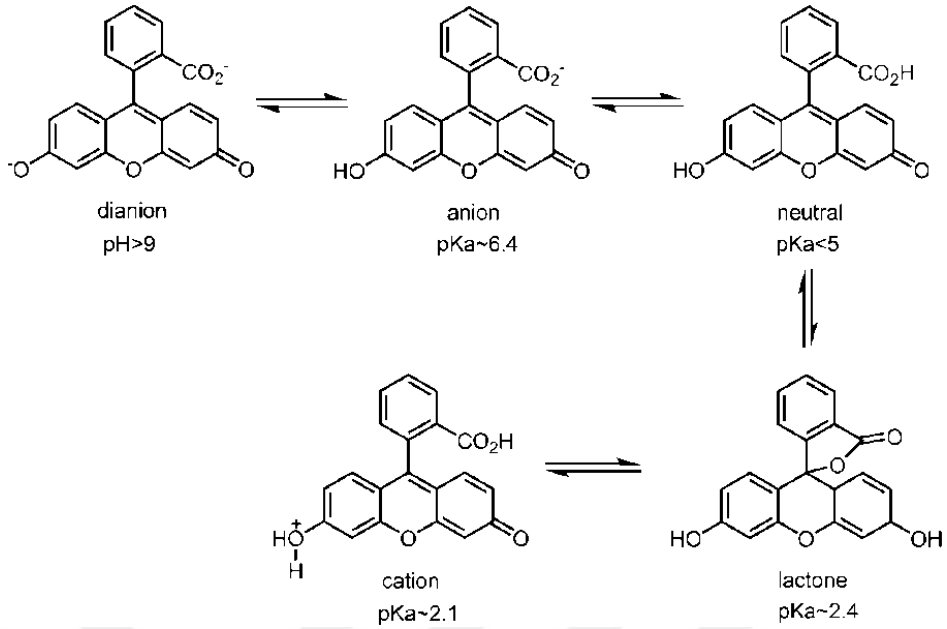

Scheme 2: pKa dependence of fluorescein [114].

The phenol and carboxylic groups on fluorescein core are almost ionized completely when pH is higher than 9. As pH get lowers (pKa~6.4), first the phenol group in dianion protonates and monoanion forms and as the acidification of monoanion (pKa<5.0), carboxyl group gets protonate and fluorescein in neutral form is produced. A fluorescein cation forms with further acidification (pKa~2.1). At pKa= 2.4, a colorless nonfluorescent lactone form of fluorescein is produced. The monoanion and the dianion forms of fluorescein are the only ones that are fluorescent and with quantum yields of 0.36 and 0.93, respectively (Table 3) [114].

Table 3: Quantum yields of pKa dependent structures of fluorescein in 1%DMSO–Tris buffer solution [114].

Species	Quantum yield
dianion (ring opened phenolate)	0.93
anion (ring opened phenol)	0.36
neutral forms	0.29
cation	09-1.0

In literature, there are many fluorescein derivative examples. In figure 29, there is a FRET system based on fluorescein dye. In this system, a bispyrene moiety works as donor unit and fluorescein serves as the acceptor unit. Highy efficiency of system is provided two crucial parts. Emission of pyrenyl excimer has an overlap with the absorption of fluorescein unit. Secondly, triggiring lactone to ring open form of fluorescein by the target. Therefore, a trun-on probe is produced [115].

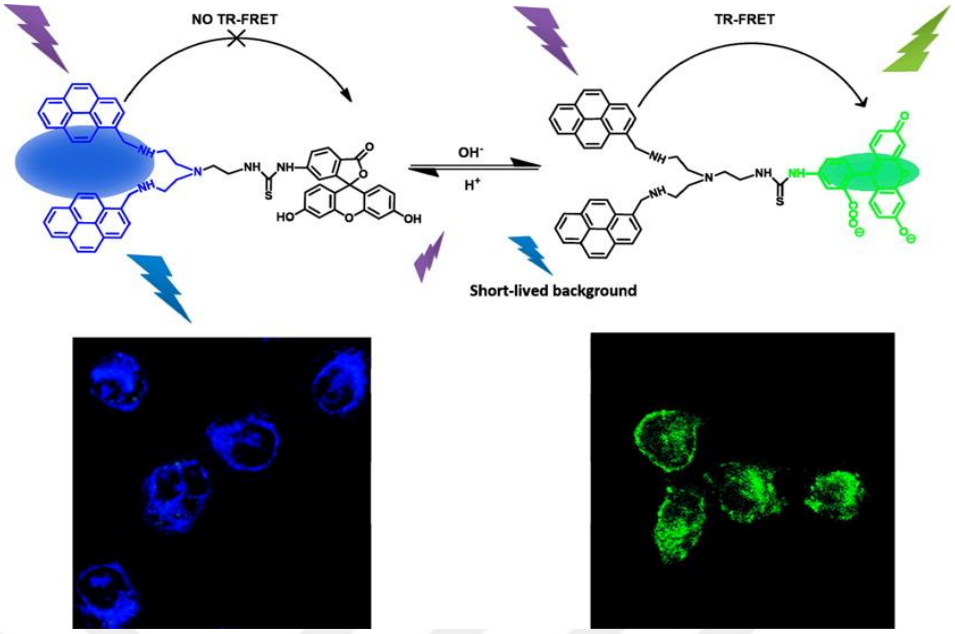

Figure 29: A literature examples of fluorescein based FRET system. Reprinted with permission from [115]. Copyright 2014 American Chemical Society.

1.4.2. BODIPY Dyes

4,4'-difluoro-4-bora-3a,4a-diaza-s-indacene is abbreviated as BODIPY and synthesized by Treibs and Kreuzer in 1968 first time. They have been used in many applications such as in energy transfer systems, PDT applications, in solar cell systems or in biological labeling [116], [117].

The BF_2 bridge in BODIPY dyes increases the planarity of dipyrrin so that BODIPY dyes have highly delocalized system (Figure 30). There are numerous distinctive properties of BODIPY dyes compared to other organic dyes. They have high fluorescent quantum yields and narrow emission bands in UV and also near-IR region. BODIPY dyes also have high thermal and photostabilities. Furthermore, their ease of solubility in organic solvents and ease of functionalization make them attractable in many applications as it is mentioned above. There are different examples of BODIPY derivatives with functionalization at different positions [49], [118]–[126].

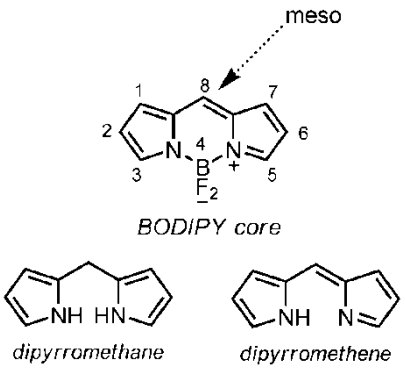

Figure 30: Molecular structures of BODIPY and its precursors.

In order to functionalize of 2-,6- positions, an electrophilic reaction such as sulfonation, halogenation is required (Figure 31a). It is because the 2- and 6- positions hold less positive charge (Figure 31b). Heavy atom, Br or I, introduction to 2- and 6- positions cause a significant red shift of absorption and emission maxima. This type of functionalization is favored by PDT applications due to intersystem crossing resulting with low fluorescence.

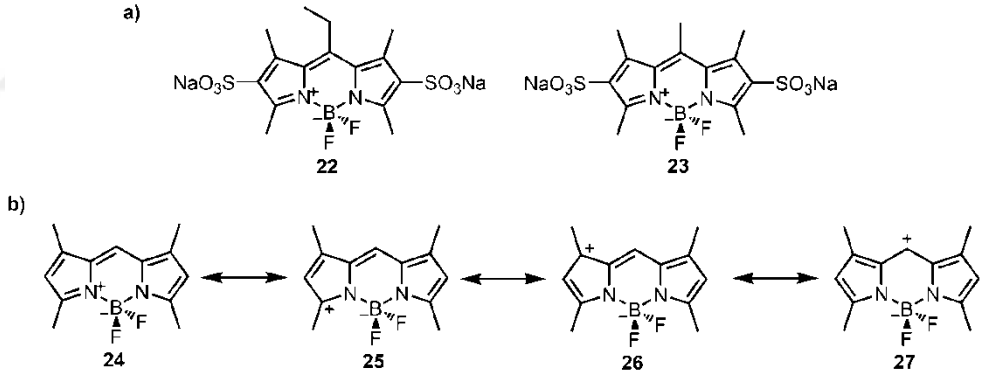

Figure 31: Sulfonated Bodipy derivatives in literature (Figure 31a). Available positions in electrophilic substation (Figure 31b).

In the case of the effect of functionalization position on absorption and emission bands, it can be stated that the substitution of aryl groups on the *meso* position has a minor effect (Figure 32). However, substitution on 1-, 7- positions increases the quantum yield according to unsubstituted ones [118]. It is because of free rotation of phenyl ring on meso position is prevented with 1-, 7- substitution.

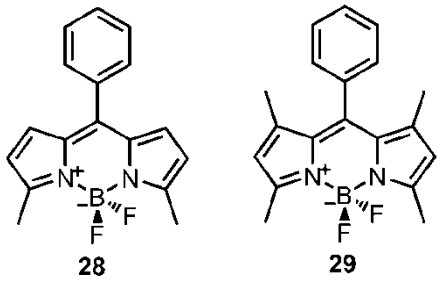

Figure 32: Two Bodipy derivatives from the literature. Quantum yields of compound **28** and **29**; 0.19 and 0.65 in MeOH, respectively.

BODIPY dyes with extended conjugation and dispersed emission maxima can be synthesized by the functionalization on 1-, 3-, 5- and 7- positions with different type of reactions such as transition metal catalyzed reactions (Suzuki, Sonagashira, Stille and Heck couplings). The substation on 3- and 5- positions give BODIPY derivatives with shifted emission and absorption maxima such as thioalkoxides or amino groups on these positions cause bathochromic shift (Figure 33). The acidic character of methyl groups on these positions gives a high yield with Knoevenagel reactions [127].

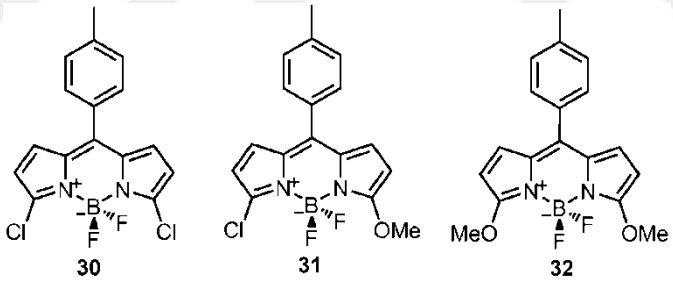

Figure 33: The substation on 3- and 5- positions on BODIPY core.

Knoevenagel condensation reaction is a nucleophilic addition of active hydrogen compound to a carbonyl compound. The reaction medium requires a basic environment and removal of water, Dean-Stark apparatus is used for this purpose. This method results with high results with substitution on 1-, 3-, 5- and 7- positions. Therefore, in one Knoevenagel reaction, mono-, di-, tri-, and tetrastyryl-Bodipy derivatives can be synthesized in an order [128]–[130].

In 2009, Akkaya et al synthesized the first tetra styryl derivative of BODIPY dye [131]. In this study, it's suggested that 1,7- positions of BODIPY core is as acidic as methyls at 3-, 5- positions. The acidic character of different positions can be observed by Mulliken-charge analysis on the core carbon atoms of tetramethyl-BODIPY (Figure 34).

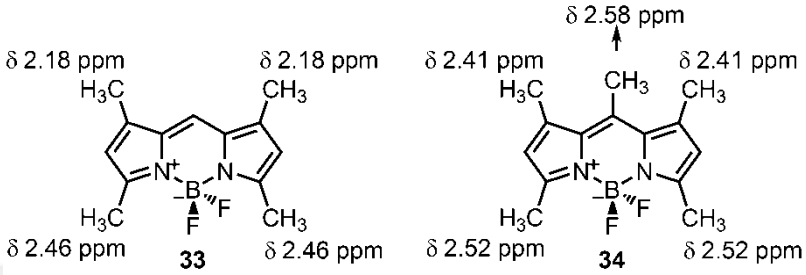

Figure 34: Tetramethyl- and pentamethyl Bodipy derivatives with ^{1}H NMR chemical shifts in $CDCl_3$.

In this study, bromine atoms in 2-, 6- positions and pyridine groups in tetrastyryl substitution were used (Figure 35).

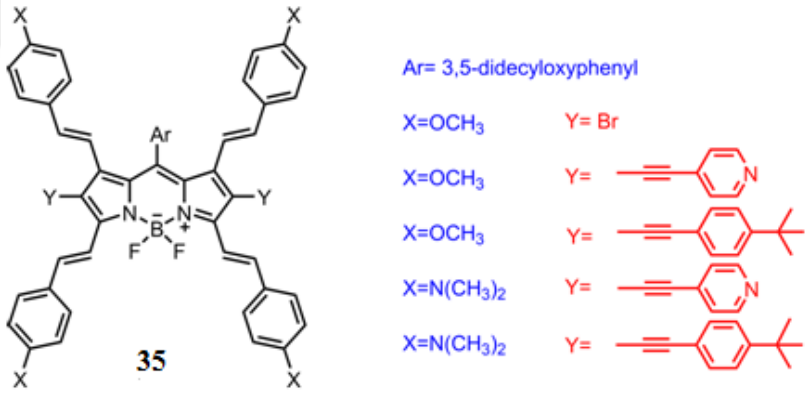

Figure 35: The synthesized tetra-styryl BODIPY derivatives [131].

After the mentioned article of tetrastyryl substitution, Ziessel *et.al.* synthesized different BODIPY derivatives bearing same and different aldehydes (Figure 36) [132]. The new tetrastyryl substituted BODIPY derivatives have absorption maxima at 720 nm and emission maxima at 800 nm. Ziessel *et.al.* also reported that methyls at 3-, 5- positions on BODIPY core are more reactive according to methyls at 1-, 7- positions in Knoevenagel condensation.

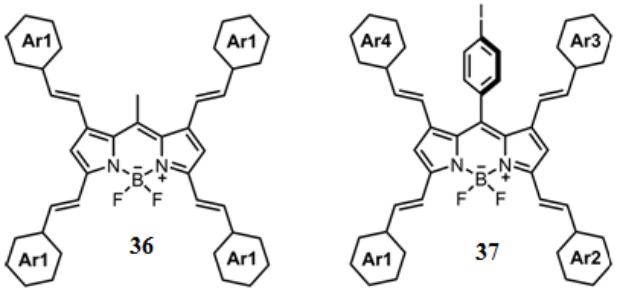

Figure 36: A schematic representation of tetra-styryl BODIPY derivatives.

In another study, Liu *et.al.* substituted 2, and 6, positions with formyl groups and they observed that 1, and 7- positions more attractive to go Knoevenagel reaction according to the 3, and 5, positions (Scheme 3) [133]. By this approach, different BODIPY derivatives, functionalized first by 1- and/or 7- positions and then allowing to functionalize on methyl groups at 3- and 5- positions.

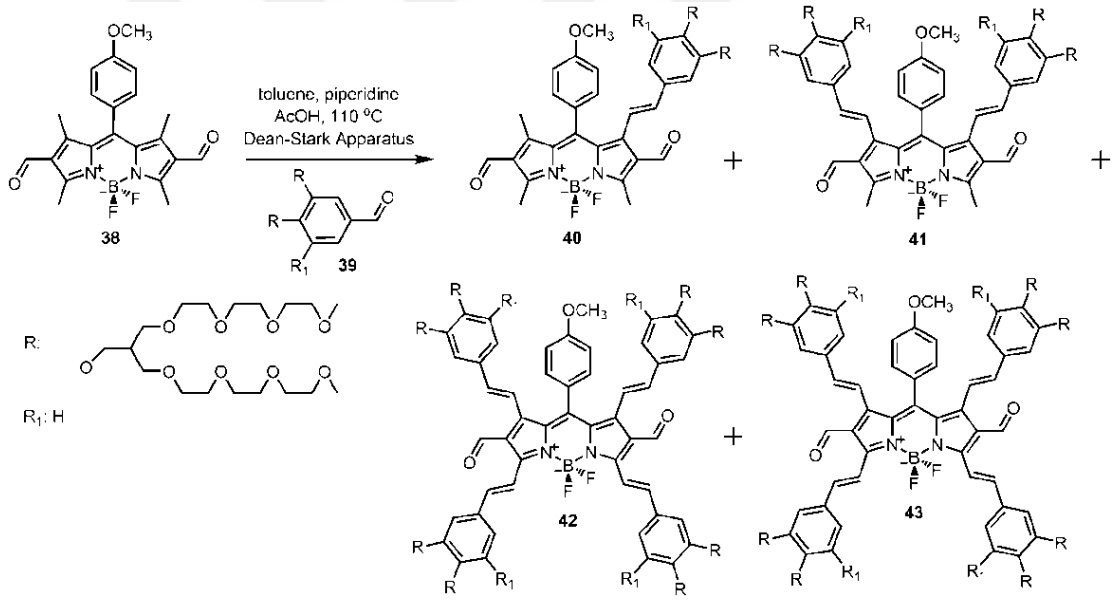

Scheme 3: The functionalization of 2,6-diformyl-BODIPY core, 38.

In the study, different groups were used to functionalize the BODIPY core, **38**. As it is shown in scheme 3, oligo (ethylene glycol) was also used for functionalization so that water solubility and near IR emission of BODIPY derivatives are achieved. By the variety of fictionalization, oligomers, dendrimers or near IR emissive building blocks can be synthesized.

CHAPTER 2

2. Singlet Oxygen Generation with Chemical Excitation of an Erythrosine-Luminol Conjugate

Yesilgul, N.; Uyar, T. B.; Seven, O.; Akkaya, E. U. *ACS Omega*, **2017**, 2 (4), 1367-1371.

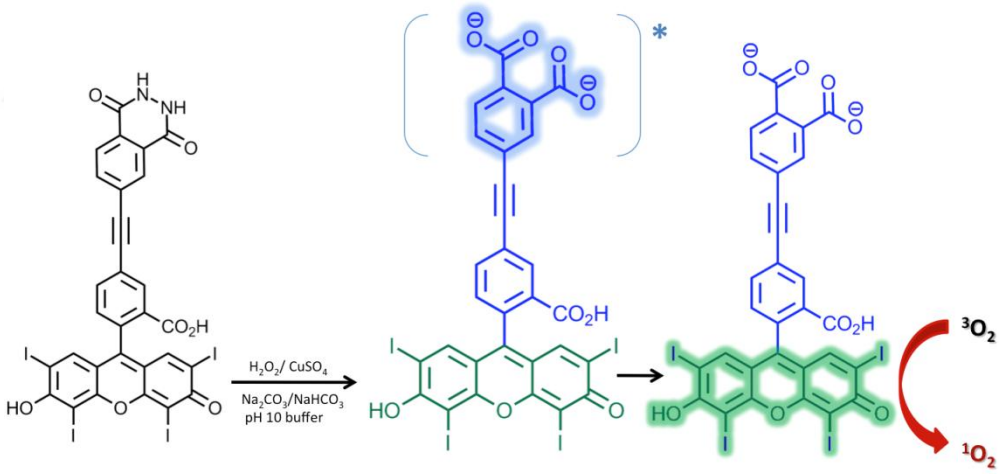

2.1. Objective

Chemical generation of singlet oxygen under biologically relevant conditions is very important considering the role played by singlet oxygen in the cancer therapeutics. We now demonstrate that a luminol derivative can be chemically excited, and transfer excitation energy to the covalently attached photosensitizer derived from erythrosin. Photosensitizer module, when excited in this manner, can generate singlet oxygen in solution. Since hydrogen peroxide is present at a relatively high concentration in cancer cells, singlet oxygen generation through chemical excitation may evolve into an important therapeutic approach.

2.2. Introduction

Singlet oxygen is the primary cytotoxic agent responsible for the photodynamic therapy (PDT) of cancer [134]–[136]. Generation of singlet oxygen requires a photosensitizer, dissolved molecular oxygen and light of an appropriate wavelength for the excitation of that photosensitizer [1], [53], [54], [137]–[141]. Excited photosensitizer should be capable of undergoing efficient intersystem crossing [142]–[145] so that an energy transfer to the ground state molecular oxygen can take place. The fact that light is needed for the generation of singlet oxygen is both an advantage (increased spatial selectivity) and a disadvantage (light does not penetrate tissues more than a few millimeters). Attenuation of light as it passes through the tissues is one of the reasons limiting the clinical practice of PDT to mostly superficial lesions [146]. Despite considerable efforts to alleviate these problems with new light sources, photosensitizers, and novel delivery methods, they seem to remain as intractable as ever [147], [148]. There are proposed alternatives to *in vivo* irradiative generation of singlet oxygen, such as X-ray induced scintillating nanoparticles [149], [150] or persistent luminescent nanoparticles. The former approach attempts to excite using penetrating radiation,[151] whereas the latter separates excitation step from singlet oxygen generation step. Recently, we

also introduced the use of endoperoxide for a potential by-pass of excitation altogether [152], [153].

In this work, our aim was to couple chemical excitation to singlet oxygen generation in a modular unimolecular system. The use of chemiluminescence or bioluminescence as source of excitation for photosensitizers was investigated previously [55], [59], [61], [64], [154], [155]. Unfortunately, the conditions for an efficient (non-radiative) energy transfer required the use of chemiluminescence agent and the photosensitizer in large concentrations, limiting the potential of this approach at the conception. However, through-bond energy transfer to a photosensitizer would circumvent the problem caused by two independent agents, by directly generating singlet oxygen on chemical excitation. The synthesis of the target compound **45** was done in multiple steps from commercially available products. Compound **44** was previously reported [156] as an energy transfer cassette. The final step was the halogenation of xanthene nucleus to introduce heavy iodine atoms to facilitate intersystem crossing. As expected, iodination resulted in significant quenching of the fluorescence as it allows rapid access to the triplet manifold. The general design principle is shown in figure 37.

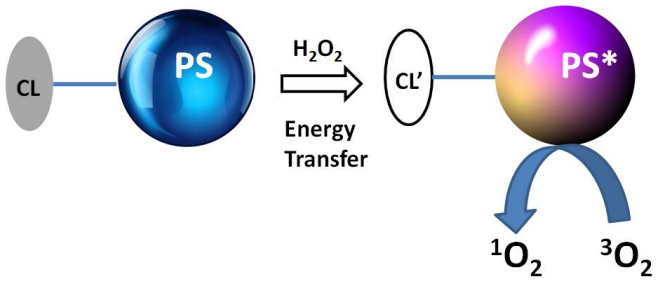

Figure 37: General principle for singlet oxygen generation *via* chemical excitation. Hydrogen peroxide would be a preferred initiator. CL: chemiluminogen module, PS: photosensitizer module, PS*: excited photosensitizer.

2.3. Results and Discussion

The idea is to bring together chemiluminegenic unit to a close proximity to the photosensitizer (Figure 38), thus ensuring a high effective concentration. The chemiluminescence energy transfer is likely to be efficient by a through bond energy transfer, but considering the short distance that the chemiluminogen can be placed in relation to photosensitizer, through space energy transfer can be envisioned.

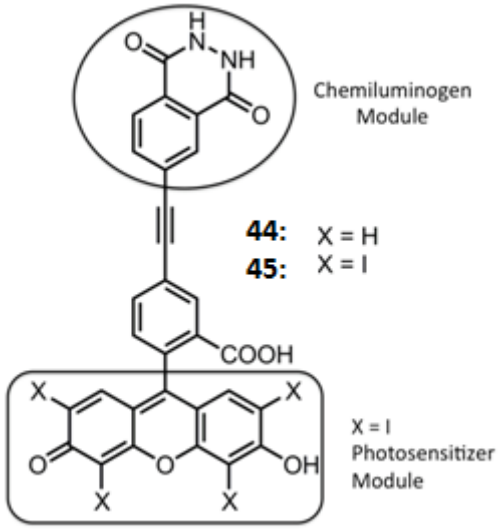

Figure 38: The structure of the immediate precursor 44 and the erythrosine-luminol conjugate 45, which was synthesized and characterized in this study, as a model for intramolecular chemical excitation to generate singlet oxygen.

As the chemiluminescence reaction is triggered, resulting excited state species would then be expected to transfer its energy to the photosensitizer which in turn, would sensitize singlet oxygen. Hydrogen peroxide as a trigger compound is particularly relevant and important for two reasons: i) it is known to be present at high concentrations in tumor cells,[157], [158] ii) there are more than one different chemiluminogen systems (oxalates, acridinium esters, *etc*.) which would be activated by hydrogen peroxide. Absorption spectrum of the compound **45** (Figure 39) shows one peak in the visible region at 530 nm.

Introduction of four iodo substituents causes a red shift in absorbance compared to a typical unsubstituted xanthene dye.

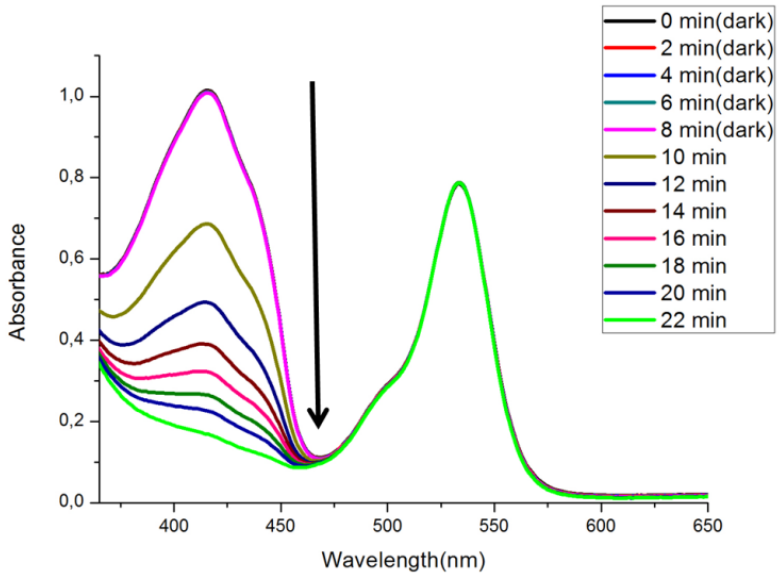

Figure 39: Reaction of the singlet oxygen generated by photosensitization with 47 µM DPBF in DMSO in the presence of erythrosine-luminol conjugate 45. For the first 8 minutes the solution was kept in dark, then irradiated with 520 nm LED array for 16 minutes. Total volume was adjusted to 3.0 mL. Absorbance spectra were recorded in 2-minute intervals.

We first wanted to demonstrate that tetraiodoxanthene (erythrosin) derived module is satisfactory as a photosensitizer. To that end, a solution of the erythrosin-luminol conjugate was prepared in DMSO containing singlet oxygen trap 1,3-diphenyl-isobenzofuran (DPBF). When kept in dark for 8 minutes, there was discernable no change in the absorption spectrum (Figure 39). But when the irradiation with green LED (520 nm, fluence rate 2.5 mW/cm^2) was turned on the absorption peak due to the trap compound DPBF rapidly disappeared in 14 minutes. This indicates that the photosensitizer module which is structurally related to erythrosin, retains a high level of photosensitization capacity within the bifunctional construct.

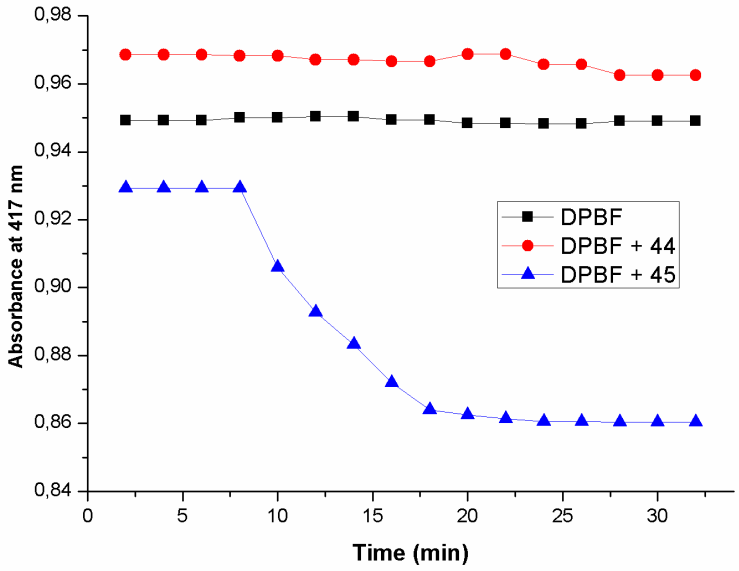

Figure 40: Change in the absorbance of 47.0 µM DPBF in DMSO in the presence of 104.0 µM of compound 44 or 45. The sample solutions contain 300 µl of pH=10.0 buffer solution (Na_2CO_3 and $NaHCO_3$). After 8 minutes, chemical excitation is induced by 300 µl of $1.5x10^{-3}$M $CuSO_4$ and $2x10^{-3}$ M H_2O_2. Total volume was adjusted to 3.0 mL. Absorbance data were recorded in 2-minute intervals.

Chemical generation of singlet oxygen was then studied in DMSO solution (Figure 40) with small amount added of aqueous buffer solution. Careful control experiments were done to eliminate other potential sources for absorbance decrease. Absorption of the singlet oxygen trap (DPBF, black squares) was followed in the presence carbonate buffer (10 % buffer, 90 % DMSO volume percentage), catalytic Cu^{2+} and hydrogen peroxide (final concentration 0.20 mM). Compound **44** under same conditions was also investigated, and showed no change (red circles). However, compound **45**, added to the reaction mixture at t=8.0 minutes, resulted in a rapid decrease, leveling off as expectedly within 12 minutes. This is also in accordance with the typical chemiluminescence kinetics of luminol under comparable conditions. Naturally, due to the solubility restrictions, the chemical excitation was tested under highly suboptimal conditions. However, we estimated chemical yield of singlet oxygen based on the concentration of compound **45**

and the decrease in the absorption of the DPBF as 4.2 %, which is promising considering the chemical and photophysical processes involved in the singlet oxygen generation. The yield is most likely held back due to the solubility of molecular oxygen.

2.4. Conclusion

Our previous work [153] demonstrated that a small amount of singlet oxygen generated within tumors may be sufficient to induce apoptosis. We are confident that, with appropriate modifications to improve water solubility, coupling singlet oxygen generation to hydrogen peroxide levels may evolve into a promising methodology for tumor therapy. Work in that direction is in progress in our laboratory.

2.5. Experimental Details

^{1}H NMR and ^{13}C NMR spectra were recorded on Bruker DPX-400 (operating at 400 MHz for ^{1}H NMR and 100 MHz for ^{13}C NMR). Chemical shifts are reported in units of ppm relative to the solvent peak ($CDCl_3$: 7.27 ppm for ^{1}H and 77.0 ppm for ^{13}C; D_2O: 4.63 ppm for ^{1}H). All spectra were recorded at $25^{0}C$ and coupling constants (*J values*) are given in Hz. Chemical shifts are given in parts per million (ppm). Absorption spectra were performed by using a Varian Cary-100 spectrophotometer. Fluorescence measurements were conducted on a Varian Eclipse spectrofluorometer. Mass spectra were recorded on Agilent Technologies 6530 Accurate-Mass Q-TOF LC/MS. Reactions were monitored by thin layer chromatography using Merck TLC Silica gel 60 F_{254}. Silica gel column chromatography was performed over Merck Silica gel 60 (particle size: 0.040-0.063 mm, 230-400 mesh ASTM). Anhydrous tetrahydrofuran was obtained by refluxing over sodium/benzophenone prior to use. All other reagents and solvents were purchased from Aldrich and used without further purification.1,3-diphenylisobenzofuran (DPBF) was used as singlet oxygen trap.

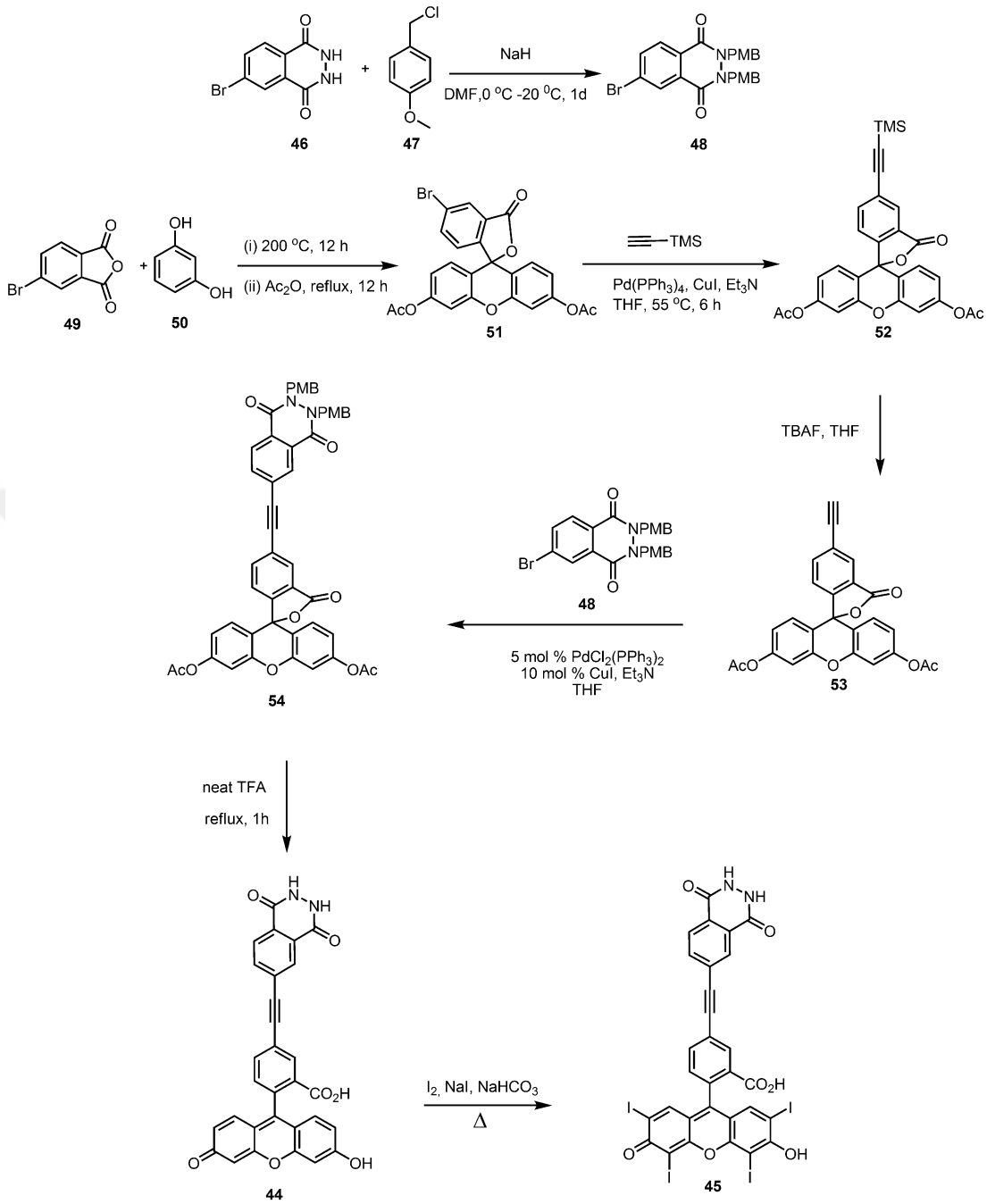

Scheme 4: Synthesis of compound **45** from commercially available and/or easily accessible compounds.

Compound 48

6-bromo-2,3-dihydrophthalazine-1,4-dione (0.300 g, 1.24 mmol) was dissolved in 8.5 mL of dry DMF and cooled to 0 °C. NaH (104.0 mg, 2.6

mmol) was added and reaction mixture was stirred for 45 min, then PMBCl (0.36 mL, 2.6 mmol) was added dropwise. The reaction mixture was stirred at room temperature overnight, and then extracted with EtOAc and water. Organic layer was dried with Na_2SO_4 and evaporated under reduced pressure. The product was purified by silica gel column chromatography using Ethyl Acetate:Hexane (10:90, v/v) as mobile phase. Fraction containing compound 85 was collected then the solvent was removed under reduced pressure (180 mg, 30%).

^{1}H NMR (400 MHz, $CDCl_3$) δ 8.55 (s, 1H), 7.81 (s, 2H), 7.43 (d, *J* = 8.6 Hz, 2H), 7.36 (d, *J* = 8.6 Hz, 2H), 6.92 (d, *J* = 8.6 Hz, 2H), 6.87 (d, *J* = 8.6 Hz, 2H), 5.29 (s, 2H), 5.24 (s, 2H), 3.84 (s, 3H), 3.80 (s, 3H).

^{13}C NMR (100 MHz, $CDCl_3$) δ 159.7, 159.2, 157.1, 149.2, 135.9, 130.6, 130.3, 130.1, 130.1, 129.2, 128.3, 126.7, 125.3, 123.4, 114.0, 113.9, 68.6, 55.3, 53.6.

MS (TOF- ESI): m/z: Calcd: 481.0757 $[M+H]^+$, Found: 481.0628 $[M+H]^+$, Δ=26.91 ppm.

Compound 51

In a round bottomed-flask (100 mL), 4-bromophthalic anhydride (8.75 g, 38.6 mmol) and resorcinol (8.50 g, 77.3 mmol) were heated for 12 hours. Dark brown solid formed. After cooling, 60 mL of acetic anhydride was added and then the mixture was refluxed for 3 hours. The reaction mixture was cooled down to room temperature slowly for recrystallization. Brownish crystals collected and washed with cold acetic anhydride and then with cold ethanol. Recrystalllization was repeated several times until white crystals were collected.

^{1}H NMR (400 MHz, $CDCl_3$) δ 8.18 (dd, *J* = 1.7, 0.4 Hz, 1H), 7.82 (dd, *J* = 8.2, 1.8 Hz, 1H), 7.14 – 7.11 (m, 2H), 7.10 (dd, *J* = 8.3, 0.4 Hz, 1H), 6.85 (s, 4H), 2.34 (s, 6H).

^{13}C NMR (100 MHz, $CDCl_3$) δ 168.9, 167.5, 152.1, 151.5, 151.3, 138.4, 128.7, 128.1, 125.6, 124.2, 117.9, 115.7, 110.5, 81.8, 20.9.

MS (TOF- ESI): m/z: Calcd: 519.005 $[M+Na]^+$, Found: 518.9966 $[M+Na]^+$, Δ=16.16 ppm.

Compound 52

5-Bromofluorescein diacetate **51** (250 mg, 0.5 mmol), CuI (4.8 mg, 0.025 mmol), palladiumtetrakistriphenylphosphine (17.5 mg, 0.025 mmol) were added to 0.5 mL of dry THF in a Schlenk flask under argon atmosphere. NEt_3 (0.7 mL, 5 mmol) was added and lastly trimethylsillyl acetylene (0.14 mL, 1 mmol) was added and the reaction mixture was heated to 72 ^oC for 6 hours. The mixture was concentrated in vacuo and then purified by flash chromotography (25% EtOAc/Hexane). Pale yellow crystals formed (yield: 170 mg, 66%).

^{1}H NMR (400 MHz, $CDCl_3$) δ 8.11 (s, 1H), 7.75 (dd, *J* = 8.0, 1.4 Hz, 1H), 7.14 (d, *J* = 8.0 Hz, 1H), 7.12 – 7.10 (m, 2H), 6.85-6.81 (m, 4H), 2.32 (s, 6H), 0.30 (s, 9H).

^{13}C NMR (100 MHz, $CDCl_3$) δ 169.0, 168.0, 152.0, 151.4, 138.7, 128.8, 128.4, 126.5, 125.6, 124.0, 117.8, 116.2, 110.3, 102.6, 97.5, 81.8, 20.9, 0.01.

MS (TOF- ESI): m/z: Calcd: 519.005 [M], Found: 514.1418 [M] , Δ=5.83 ppm.

Compound 53

5-(2-trimethylsilylethynyl)fluorescein diacetate **52** (200 mg, 0.389 mmol) was dissolved in 6 mL of dry THF. Then, TBAF (0.39 mL, 1.0 M in THF) was added and the mixture was concentrated *in vacuo*. The crude orange solid was purified by flash chromotography (25% EtOAc/Hexane).

^{1}H NMR (400 MHz, $CDCl_3$) δ 8.14 (s, 1H), 7.78 (dd, *J* = 7.9 Hz, 1.4 Hz, 1H), 7.17 (d, *J* = 7.9 Hz, 1H), 7.14 – 7.11 (m, 2H), 6.87-6.83 (m, 4H), 3.25 (s, 1H), 2.33 (s, 6H).

^{13}C NMR (100 MHz, $CDCl_3$) δ 168.8, 168.1, 152.6, 152.2, 151.6, 138.8, 128.8, 128.7, 126.5, 124.6, 124.2, 117.8, 115.9, 110.5, 81.7, 81.5, 79.8, 21.3.

MS (TOF- ESI): m/z: Calcd: 465.0945 $[M+Na]^+$, Found: 465.0856 $[M+Na]^+$, Δ=19.08 ppm.

Compound 54

Compound **48** (335 mg, 0.699 mmol) and compound **53** (335 mg, 0.769 mmol), bis(triphenylphosphine)palladium chloride (26 mg, 0.065 mmol), copper(I) iodide (13 mg, 0.13 mmol), NEt_3 (0.98 mL, 6.99 mmol) and 8.0 mL of dry THF were added to microwave tube. The reaction mixture was microwave irradiated at 120 ^oC about 25 min. The solvent was removed under reduced pressure and the product was purified by silica gel column chromatography using EtOAc/Hexane (25:75, v/v) as mobile phase. White crystals formed (262 mg, 45%).

^{1}H NMR (400 MHz, $CDCl_3$) δ 8.58 (s, 1H), 8.19 (s, 1H), 7.96 (d, *J* = 8.3 Hz, 1H), 7.90– 7.84 (m, 2H), 7.45 (d, *J* = 8.5 Hz, 2H), 7.40 (d, *J* = 8.5 Hz, 2H), 7.22 (d, *J* = 8.0 Hz, 1H), 7.12 (s, 2H), 6.98 – 6.82 (m, 8H), 5.30 (s, 2H), 5.26 (s, 2H), 3.83 (s, 3H), 3.79 (s, 3H), 2.33 (s, 6H).

^{13}C NMR (100 MHz, $CDCl_3$) δ 168.8, 168.1, 159.6, 159.2, 157.6, 152.6, 152.2, 151.5, 149.2, 138.4, 135.2, 130.6, 130.3, 130.1, 129.3, 129.2, 128.9, 128.3, 126.6, 126.0, 125.0, 124.3, 124.2, 123.8, 117.9, 115.9, 113.9, 113.8, 110.5, 90.4, 81.83, 68.5, 55.2, 53.5, 21.1.

MS (TOF- ESI): m/z: Calcd: 842.2476 [M], Found: 842.2399 [M] , Δ=9.14 ppm.

Compound 44

Compound **54** (80 mg, 0.01 mmol) and 8 mL of TFA were mixed and heated to 70^oC for 1 hour. The mixture was concentrated in vacuo. The reaction product was dissolved in 2 mL of 1 M NaOH. Then 2 drops of HCl was added and yellow-orange

solid precipitated. Precipitation was filtrated and washed with water and EtOAc. Yellow solid was afforded (36 mg, 75%).

^{1}H NMR (400 MHz, D_2O) δ 7.88 (s, 1H), 7.83 (s, 1H), 7.79 (d, *J* = 8.2 Hz, 1H), 7.58 (d, *J* = 7.8 Hz, 1H), 7.47 (d, *J* = 8.2 Hz, 1H), 7.24 (d, *J* = 7.8 Hz, 1H), 7.01 (d, *J* = 9.3 Hz, 2H), 6.47 (d, *J* = 9.3 Hz, 2H), 6.33 (s, 2H).

MS (TOF- ESI): m/z: Calcd: 517.103 $[M+H]^+$, Found: 517.0966 $[M+H]^+$, Δ=12.43 ppm.

Compound 45

Compound **44** (16 mg, 0.03 mmol), 0.5 mL of saturated sodium bicarbonate solution, 0.5 mL of 0.1 M NaI solution and 31.4 mg of iodine were mixed and refluxed for about 40 minutes. The mixture was cooled down to room temperature and 0.4 mL of H_2SO_4 was added and extracted with EtOAc. The aqueous layer was separated and organic layer washed with water two times. Finally organic layer washed with 10% sodium thiosulfate solution. Faint red solid was afforded (5 mg, 15%).

^{1}H NMR (400 MHz, MeOD) δ 8.41 (s, 1H), 8.32 – 8.16 (m, 2H), 7.96 (d, *J* = 8.2 Hz, 1H), 7.78 (d, *J* = 8.0 Hz, 1H), 7.30 (d, *J* = 7.9 Hz, 1H), 7.09 (d, *J* = 9.3 Hz, 2H), 6.68 – 6.39 (m, 4H).

MS (TOF- ESI): m/z: Calcd for $C_{30}H_{13}I_3N_2O_7$: 893.78568 [M], Found: 893.74085 [M], Δ=50.16 ppm.

2.5.1. Additional Information

a.

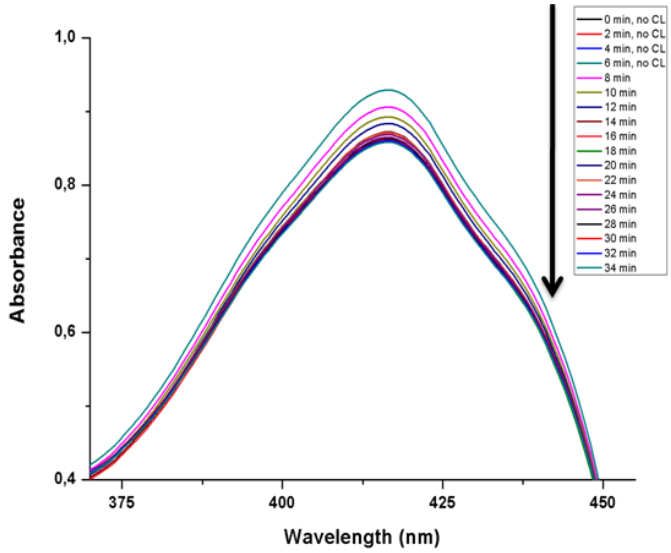

b.

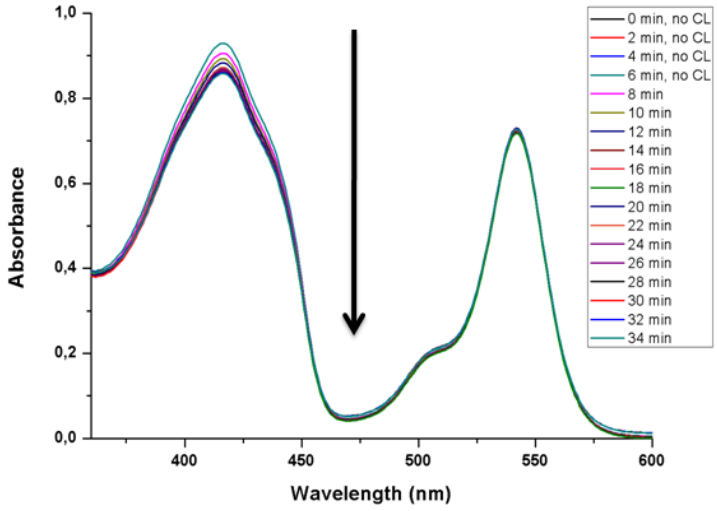

Figure 41: Bleaching of 47 µM DPBF in DMSO in the presence of 104 µM of compound **45**. (Figure 41a) The sample solutions contain 300 µl of pH=10 buffer solution (Na_2CO_3 and $NaHCO_3$). After 6 minutes, chemiluminescence is induced by 300 µl of $1.5x10^{-3}$M $CuSO_4$ and $2x10^{-3}$ M H_2O_2. Absorbance was measured in 2 minutes intervals. During bleaching of DPBF, no change is observed in absorption spectrum of compound **45**. (Figure 41b)

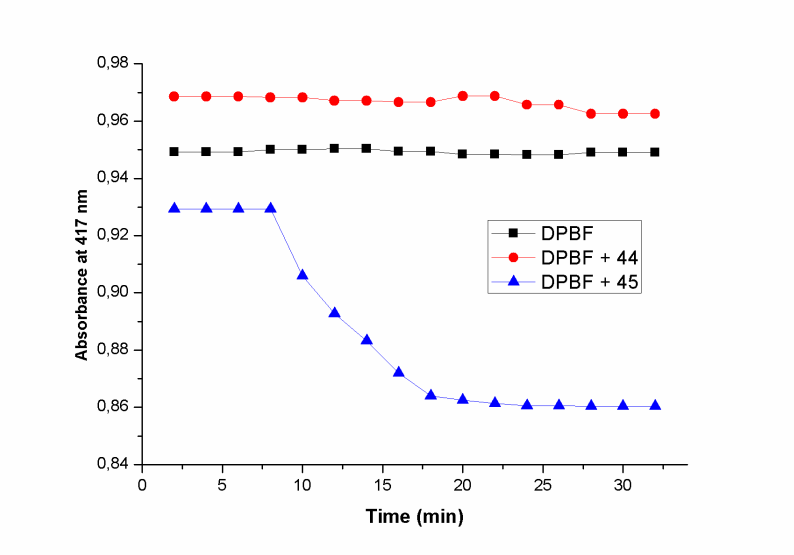

Figure 42: Absorbance of DPBF in DMSO at 417 nm without compound **45** or **44** (square), in the presence of compound 2 (circle), in the presence of compound **45** (triangle).

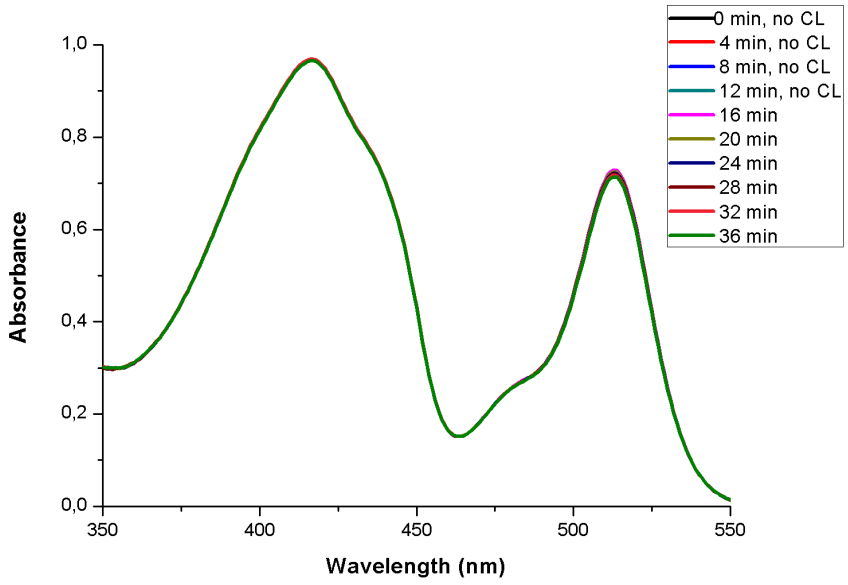

Figure 43: Bleaching of 47 µM DPBF in DMSO in the presence of 104 µM of compound **44**. The sample solutions contain 300 µl of pH=10 buffer solution (Na_2CO_3 and $NaHCO_3$). After 12 minutes, chemiluminescence is induced by 300 µl of $1.5x10^{-3}$M $CuSO_4$ and $2x10^{-3}$ M H_2O_2. Absorbance was measured in 4 minutes intervals.

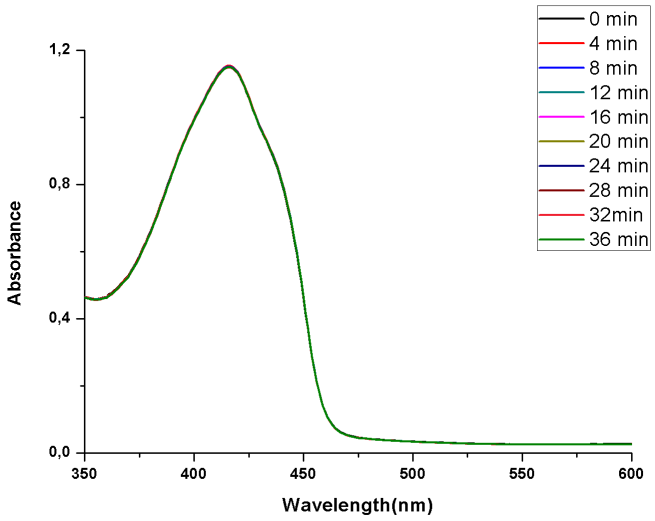

Figure 44: Absorbance of 47 µM DPBF in DMSO. The sample solutions contain 300 µl of pH=10 buffer solution (Na_2CO_3 and $NaHCO_3$) and 300 µl of $1.5x10^{-3}$M $CuSO_4$ and $2x10^{-3}$ M H_2O_2. Absorbance was measured in 4 minutes intervals.

a.

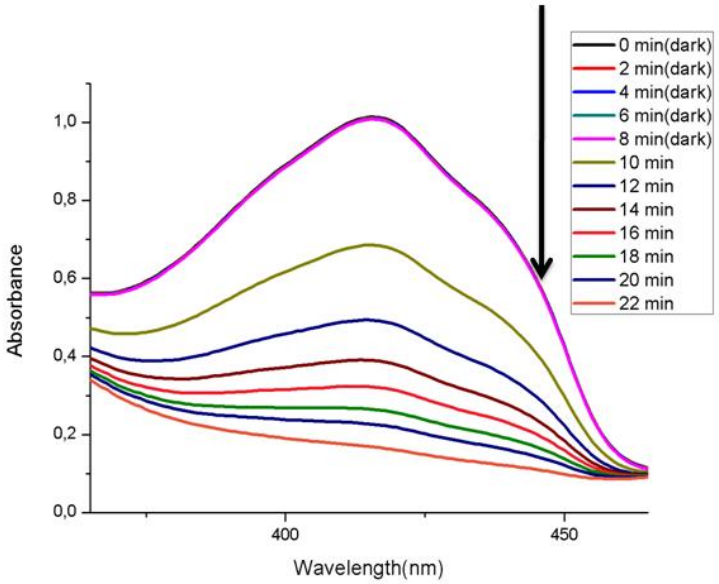

b.

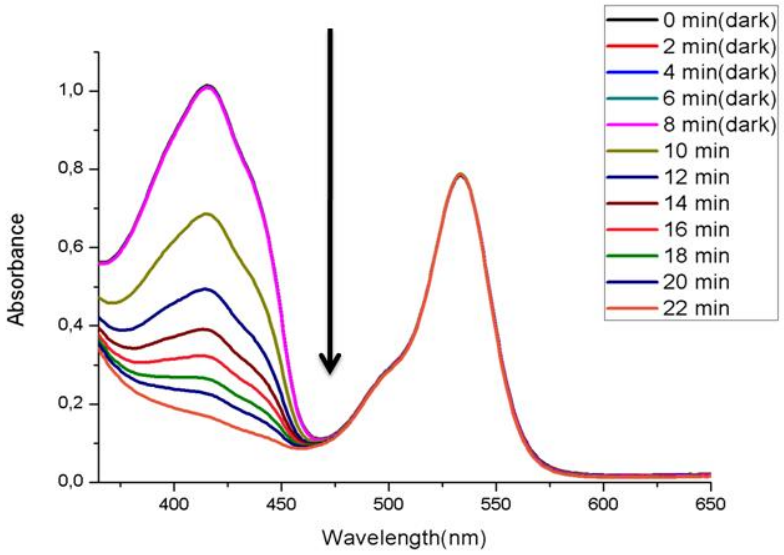

Figure 45: Bleaching of 47 µM DPBF in DMSO in the presence of compound **45** (Figure 45a) For the first 8 minutes sample was kept at dark, then irradiated with 530 nm light for 16 minutes. Absorbance was measured in 2 minutes intervals. During bleaching of DPBF, no change is observed in absorption spectrum of compound **45** (Figure 45 b).

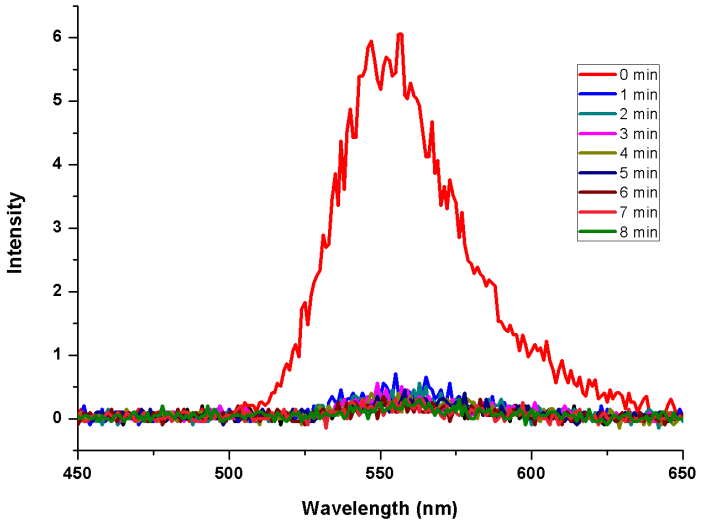

Figure 46: Chemiluminescence intensity of compound **44**. Intensity was measured in 1 minute intervals.

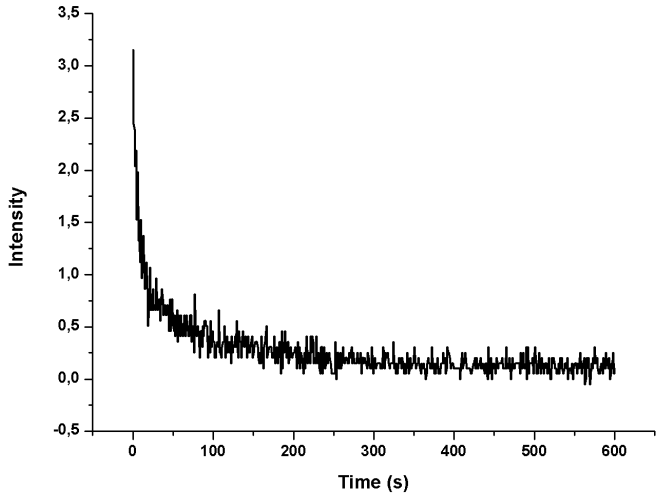

Figure 47: Chemiluminescence intensity decay curve of compound **44**. Intensity was measured in 1 minute intervals.

CHAPTER 3

3. Bodipy-based photosensitizers with long alkyl tails at the *meso* position: efficient singlet oxygen generation in Cremophor-EL micelles

Kilic, B.; **Yesilgul, N.**; Polat, V.; Gercek, Z;Akkaya, E. U.,*Tetrahedron Lett.***2016,** 57, 1317-1320.

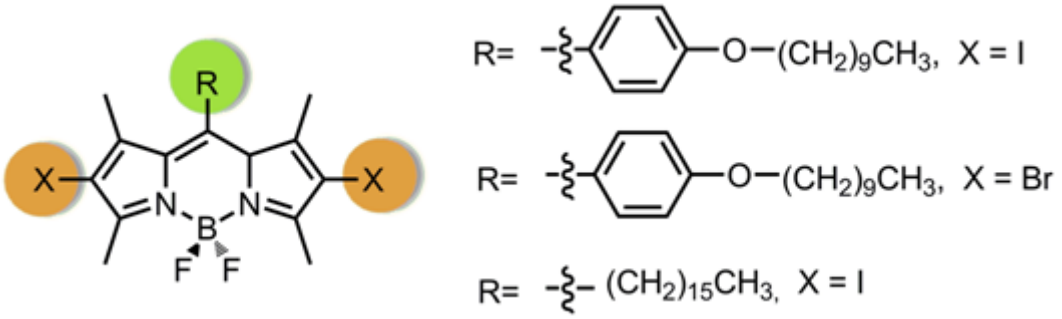

3.1. Objective

Bodipy dyes with *n*-decyloxyphenyl- and pentadecyl- *meso* substituents can easily embed themselves into micellar structures made of Cremophor-EL. In micelles of about 20 nm median size, heavy-atom substituted dyes show remarkable photosensitization properties as evidenced by the rate of the reactions with an anthracene-based selective singlet oxygen trap in buffered aqueous solutions. Considering the ease of Bodipy derivatization and the advantages of Cremophor-EL carried therapeutic agents, these photosensitizing agents may offer novel targeting opportunities, and enhanced chemical and photophysical stability.

3.2. Introduction

Photodynamic therapy is a promising methodology for the treatment of certain cancerous and non-cancerous indications [1], [35], [159]–[164]. The treatment protocol involves bringing together of three components, namely light, molecular oxygen and a photosensitizer. If the excited photosensitizer can efficiently undergo intersystem-crossing to the triplet manifold, excitation energy in turn, can be transferred to the ground state (triplet) molecular oxygen generating singlet excited molecular oxygen. Singlet oxygen produced in this way, is the primary cytotoxic agent in photodynamic therapy [141].

Bodipy-based photosensitizers received considerable attention as alternative photosensitizers in recent years [140], [164]–[168]. The reasons for this attention are twofold: unlike other photostable dyes such as PDIs [169] and squaraines, [170], [171] the absorption peak of these dyes are easily tunable in the entire visible and even in the near IR region of the spectrum,[131] and there are more than one ways to transform these dyes into efficient singlet oxygen generators [172], [173].

One of the most effective ways of drug delivery is liposomal or micellar systems. In this way, in principle, it becomes very straightforward to include various targeting groups in addition to the active agent itself into the micellar or liposomal construct. In this work, we targeted Bodipy derivatives with heavy atoms to facilitate

intersystem crossing. In addition to ensure that these compounds would prefer micellar structure as opposed to bulk aqueous solution, we incorporated long alkyl chains at the *meso* positions (8-) of the Bodipy dyes. The micelle forming agent that we prefer is Cremophor EL. Cremophor EL (a.k.a., Kolliphor EL) is a synthetic, non-ionic surfactant. It is made by the reaction of Castor oil (mostly triglyceride) with ethylene oxide, which provides a polyethylene glycol chain.

3.3. Results and Discussion

The synthesis plan for 8-alkyl and 8-(4'-alkoxy)aryl derivatives differ to some extent. Scheme 5 shows the strategy that we applied for the synthesis of 8-(4'-decyloxy)phenyl-substituted Bodipy dyes. *p*-Hydroxybenzaldehyde was converted to the decyl ether by treatment with 1-bromodecane in acetonitrile under reflux. 4-Decyloxybenzaldehyde (**56**) was then first treated with 2,4-dimethylpyrrole and TFA in DCM, followed by oxidation with DDQ. Without isolation, the dipyrrin intermediate was then treated with Et_3N and BF_3-Et_2O to yield the green fluorescent Bodipy dye **57**. 2,6-positions of the Bodipy core can be brominated and iodinated by different protocols, the reaction with iodic acid and iodine in ethanol at 60 ^oC results in diiodo compound **58**, and room temperature treatment of **57** with NBS results in compound **59**.

In a different approach, palmitoyl chloride was reacted with 2,4-dimethylpyrrole and then difluoroboron bridge was installed, again by BF_3-Et_2O treatment to yield dye **61**. Iodination was done as for the compound **61**, with iodic acid and iodine in ethanol at 60 ^oC yields diiodo compound **62**. All new compounds were characterized by ^1H, ^{13}C NMR spectroscopic methods and HRMS.

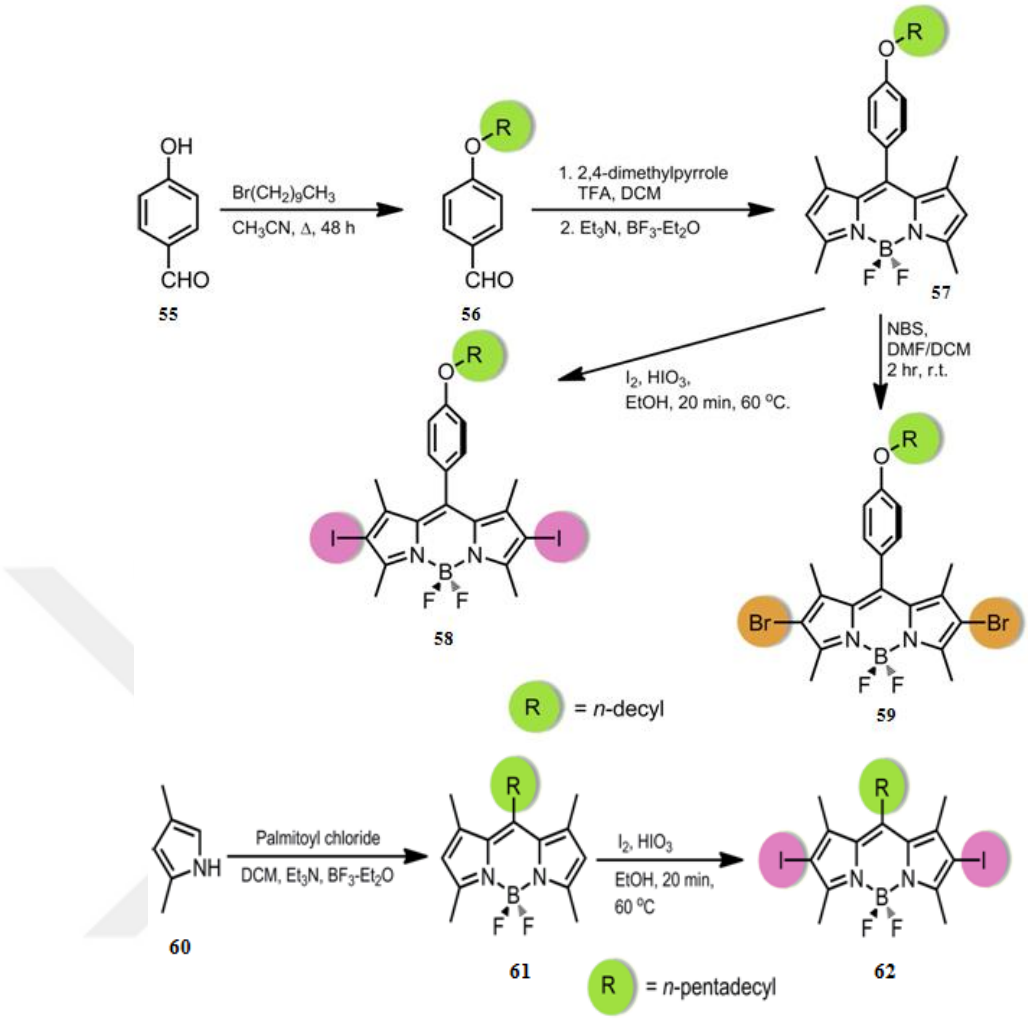

Scheme 5: Synthesis of the targeted photosensitizers **58**, **59** and **62**.

Absorption spectra of the photosensitizers were acquired in DCM, and the major absorption band in the visible corresponding to S_0 - S_1 transition is located around 530 nm (Figure 48). The micelles containing the Bodipy compounds **58**, **59** and **62** were prepared following previous literature. The sizes and the surface charge of the micelles were studied using dynamic light scattering (experimental details, Table 5). Sizes of the micelles vary between 13 to 27 nm. Absorption and emission spectra for the micelle embedded compounds were also acquired in buffered aqueous solutions, and were not altered in any significant extent.

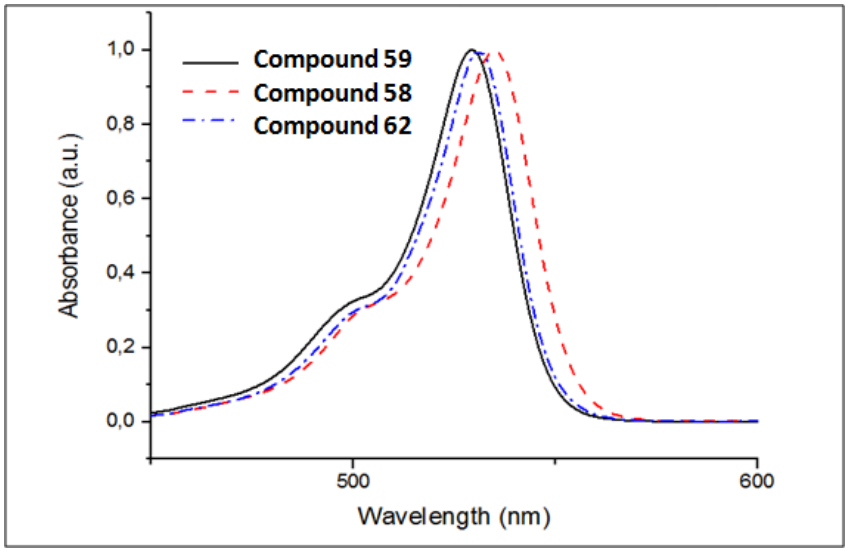

Figure 48: Normalized absorption spectra of photosensitizers **58**, **59** and **62** in DCM.

Singlet oxygen generation capacity of the photosensitizers inmicelles were studied using selective singlet oxygen trap 2,2'-(Anthracene-9,10-diyl)bis(methylene)dimalonic acid. The absorbance of trap molecule was adjusted around 1.0 in oxygen saturated solution. Micellar photosensitizers at 4.0 μM concentration in aqueous buffer solutions were excited in the presence of the above-mentioned trap compound. Initially, a few data points were acquired to eliminate any possibilities for a dark reaction. The the cuvettes were exposed to an LED array optimized for 520 nm. The change in the absorption spectra of the anthracene based trap molecule can be clearly seen in figure 49. It is important to note that when kept in dark, no changes in the absorption takes place, and also, in the absence of photosensitizers under irradiation with the same source, no change in the absorption takes place.

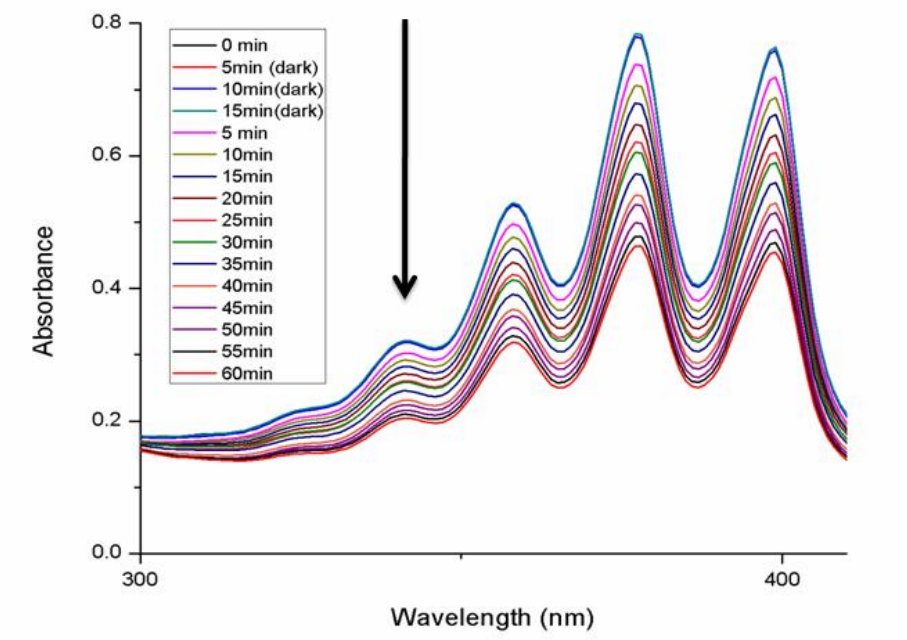

Figure 49: Singlet oxygen mediated bleaching of the trap molecule2,2'-(Anthracene-9,10-diyl)bis(methylene)dimalonic acid in the presence of Bodipy **59** (4.0μM) in water. The light source was an LED array with peak emission at 520nm.

The data for each photosensitizer were plotted as the change in absorption of the trap molecule at 382 nm *versus* irradiation time for each photosensitizer (Figure 50). It is clear that all three photosensitizers show impressive efficiencies for singlet oxygen generation.

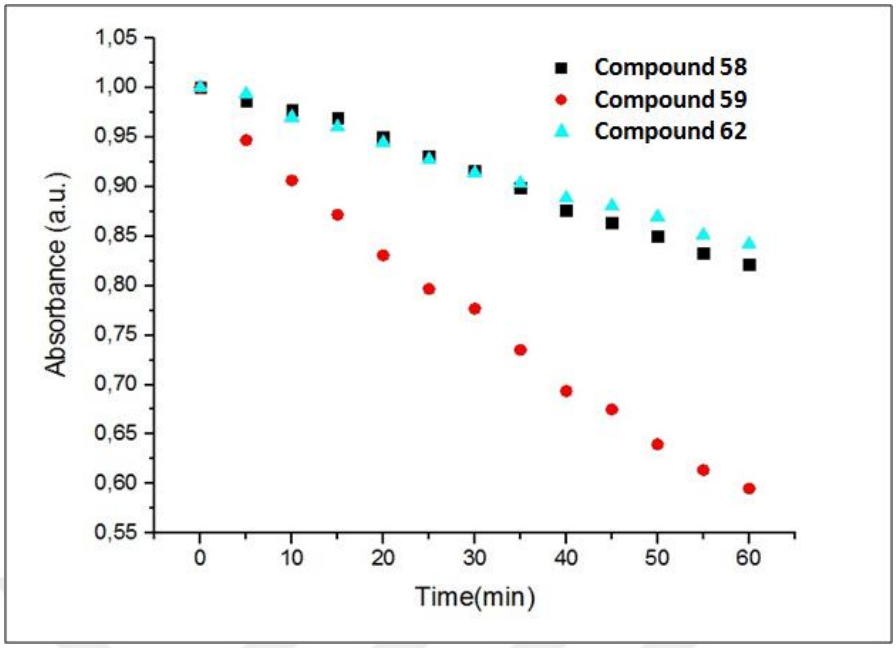

Figure 50: Singlet oxygen mediated bleaching of the trap molecule2,2'-(Anthracene-9,10-diyl)bis(methylene)dimalonic acid in the presence of photosensitizers **58**, **59** and **62** (4.0μM) in water. Absorbance at 382 nm was plotted as a function of time. The light source was an LED array with peak emission at 520nm.

Singlet oxygen quantum yields in Cremophor EL micelles in aqueous solutions were calculated (experimental part) and vary between 0.14 to 0.46. Interestingly, the bromo derivative, photosensitizer **59**, seems to be the most effective compound in micelle-embedded form. Singlet oxygen quantum yield of almost 50% in a micellar construct is truly remarkable.

3.4. Conclusion

In recent years, there have been reported examples of Bodipy based photosensitizers. However, the effect of a micelle embedding side-chain was not reported with long alkyl chain substituted photosensitizers. We demonstrated that in aqueous solutions, stable micelles of such compounds can be prepared, and they can act as effective photosensitizers. We are confident that similarly functionalized Bodipy dyes will find practical applications, within the context of photodynamic therapy. Our work along that direction is in progress.

3.5. Experimental Details

All experimental details are the same as shown in chapter 2. Electrophoretic Light Scattering was performed with Malvern NanoZS zeta potential. Micelles of the target compounds have been prepared according to the literature [174]. In singlet oxygen measurements 1,3-Diphenylisobenzofuran wasused as a singlet oxygen trap in organic solvent measurements and was purchased from supplier. 2,2'-(Anthracene-9,10-diylbis(methylene))dimalonicacid was used a singlet oxygen trap in aqueous solvent and was synthesized according to the literature [175].

Compound 56

4-hydroxybenzaldeyhde (2g, 16.4 mmol) and 1-bromodecane (5.2 ml, 32.8 mmol) were dissolved (150 ml). K_2CO_3 (6.88g, 49.2 mmol) and a few crystals of 18-crown-6 were added. The reaction mixture was refluxed for 48 h. The acetonitrile was evaporated in vacuum and extracted with water and chloroform. Organic phase was dried over Na_2SO_4. After the evaporation of the solvent, silica gel column chromatography using $CHCl_3$/Hexane (5:1, v/v) as the eluent was performed in order to purify the residue (2.4 g, 51%).

^{1}H NMR (400 MHz, $CDCl_3$, 300K): δ, 9.80 (s, 1H), 7.79 (d, *J*= 8.8 Hz, 2H), 6.91 (d, *J*= 8.7 Hz, 2H), 4.05(t, *J*= 6.4 Hz, 2H), 1.80 (q, 2H), 1.35(m, 14H), 0.89(3H) .

^{13}C NMR (100 MHz, $CDCl_3$) δ 190.6, 164.2, 132.0, 129.8, 114.7, 68.4, 31.9, 29.5, 29.3, 29.3, 29.0, 26.0, 22.7, 14.1.

HRMS (ESI) calcd for $C_{17}H_{26}O$ (M+H) 263.2033, found 263.2019 Δ = 5.16 ppm.

Compound 57

2,4-dimethyl pyrrole (5.033 mmol, 408.2 mg) and 4-decyloxybenzaldeyde (2.288 mmol, 300 mg) were dissolved in a 500 mL round-bottomed flask containing 350 mL argon-degassed CH_2Cl_2. To the reaction solution TFA (one drop) was added and

stirred at R.T. for 24h. After that, a solution of DDQ (2.29 mmol, 519.4 mg) in 100 mL CH_2Cl_2 was added to the reaction mixture. After addition of a DDQ solution, the reaction solution was stirred for additional 1 h. Then, 3 mL NEt_3 and 3 mL $BF_3.OEt_2$ were added respectively. TLC was used to monitor the reaction. (eluent $CHCl_3$) The reaction mixture was additionally stirred for 30 min. Thereafter, the resulting solution was washed three times with water and dried over anhydrous Na_2SO_4. After the evaporation of the solvent, silica gel column chromatography using $CHCl_3$ as the eluent was performed in order to purify the residue (0.5 g, 46 %).

^{1}H NMR (400 MHz, $CDCl_3$, 300K): δ; 7.16 (d, *J*=8.7 Hz, 2H), 7.02 (d, J=8.7 Hz, 2H) 5.99 (s, 2H), 4.02 (t, *J*=6.6 Hz, 2H), 2.55 (s, 6H) , 1.84 (m,2H), 1.45 (s, 6H), 1.32(m, 14H) , 0.91 (t , *J*=6.8 Hz, 3H)

^{13}C NMR (100 MHz, $CDCl_3$): δ; 159.8, 155.2, 143.2, 142.0, 131.9, 129.1, 126.8, 121.1, 115.1, 68.2, 31.9, 29.6, 29.6, 29.47, 29.4, 29.3, 26.1, 22.7, 14.6, 14.5, 14.1.

HRMS (ESI) calcd for $C_{29}H_{39}BF_2N_2O$ (M+H) 478.30371, found 478.30871 Δ = 1.05 ppm.

Compound 58

Compound **57** (0.189 mmol, 90 mg) and iodine (0.78 mmol, 200 mg) were added to a 250 mL round bottomed flask and to this solution was added Iodic acid (0.63 mmol, 111.18 mg) dissolved in 2 mL of water. The reaction mixture was stirred at 60 ^{o}C and was monitored by TLC $CHCl_3$: Hexanes (1:1). When all the starting material had been consumed, saturated $Na_2S_2O_3$ solution in water was added and the product was extracted into $CHCl_3$. The solvent was evaporated and the residue was purified by silica gel column chromatography using $CHCl_3$: Hexanes (1:1) as the eluant. Red solid (80 mg, 70%).

^{1}H NMR (400 MHz, $CDCl_3$, 300K) δ 7.13 (d, *J* = 8.5 Hz, 2H), 7.04 (d, *J* = 8.5 Hz, 2H), 4.04 (t, *J* = 6.5 Hz, 2H), 2.66 (s, 6H), 1.97 – 1.77 (m, 2H), 1.64 – 1.45 (m, 8H), 1.33 (s, 12H), 0.92 (dd, *J* = 8.9, 4.4 Hz, 3H).

^{13}C NMR (100 MHz, $CDCl_3$): δ; 160.5, 156.5, 145.7, 141.8, 131.9, 129.3, 126.3, 115.2, 85.7, 68.6, 31.8, 29.6, 29.5, 29.4, 29.3, 26.0, 23.0, 17.1, 16.4, 14.4.

HRMS (ESI) calcd for $C_{29}H_{37}BF_2I_2N_2O$ (M-H) 730.10199, found 730.10249 Δ = 0.68 ppm

Compound 59

Compound **57** (0.23 mmol, 75 mg) was dissolved in a mixture of DMF/DCM (25 ml/25ml). Then N-bromosuccinimide(370 mg, 2.05 mmol) was dissolved in DCM (25ml). NBS in DCM solution was added to the reaction solution dropwise in 15 min. The reaction mixture was stirred at room temperature for 2 hours. Followed by thin layer chromatography the reaction was stopped and the extraction was done with water and DCM. The organic phase was dried with Na_2SO_4 and evaporated by using rotary evaporator. Silica gel column chromatography was carried out to purify the residue by using $CHCl_3$/ Hexane mixture (3:1 v/v) (165 mg, 94.66%).

^{1}H NMR (400 MHz, $CDCl_3$, 300 K): δ_H = 7.15 (d , J=8.7 Hz, 2H), 7.03 (d, J=8.7 Hz, 2H), 4.04 (t, J=6.6 Hz, 2H), 2.62 (s, 6H) , 1.85 (m,2H), 1.53(m, 2H), 1.45 (s, 6H), 1.32(m, 12H) , 0.91 (t, J=6.8 Hz, 3H).

^{13}C NMR (100 MHz, $CDCl_3$): δ_C= 160.15, 153.57, 142.43, 140.43, 130.85, 129.29, 126.01, 115.15, 111.87, 68.56, 32.14, 29.58, 29.56, 29.44, 29.32, 29.23, 26.06, 22.69, 14.11, 13.89, 13.62.

NMR (101 MHz,) δ HRMS (ESI) calcd for $C_{29}H_{37}BBr_2F_2N_2O$ (M-H) 635.1244, found 635.12963 Δ = 8.23 ppm.

Compound 61

2,4-dimethyl pyrrole (10.34 mmol, 1 g) and palmitoylchloride (5.17 mmol, 1.44 g) were added into a round bottom flask (500 ml) containing 300 ml CH_2Cl_2. The solution was refluxed for 1 day at 80 ^{0}C. Then, 5mL of Et_3N and 5 mL of $BF_3.OEt_2$ were successively added and after 30 minutes, the reaction mixture was washed three times with water (3x 75 mL). It was then extracted into the CH_2Cl_2 (3x 75mL) and dried over anhydrous Na_2SO_4. The solvent was evaporated and the residue was purified by silica gel column chromatography using 2:1 (DCM: Hexane) as the eluent. Orange solid was afforded (1.45 g, 59%).

^{1}H NMR (400 MHz, $CDCl_3$, 300 K): δ; 6.1 (s, 2H), 2.99 (t, *J*=8.2 Hz, 2H), 2.54 (s, 6H), 2.45 (s, 6H) , 1.64 (m,2H), 1.49(m, 2H), 1.33(m, 22H) , 0.91 (t, *J*=6.8 Hz, 3H).

^{13}C NMR (100 MHz, $CDCl_3$): δ; 153.6, 146.8, 140.3, 131.5, 121.5, 32.0, 31.8, 30.4, 29.8, 29.7, 29.7, 29.7, 29.6, 29.4, 29.4, 28.4, 22.7, 16.2, 14.2, 14.3.

HRMS (ESI) calcd for $C_{28}H_{45}BF_2N_2$ (M-H) 456.37, found 456.35712 Δ =6.3 ppm.

Compound 62

Compound **61** (0.80 mmol, 400 mg) and Iodine (1.78 mmol, 500 mg) were added to a 250 mL round bottomed flask and to this solution was added iodic acid (2.27 mmol, 400 mg) dissolved in 3 mL of water. The reaction mixture was stirred at 60 ^{o}C and was monitored by TLC 1:1 ($CHCl_3$: Hexanes). When all the starting material had been consumed, saturated $Na_2S_2O_3$ solution in water was added and the product was extracted into $CHCl_3$. The solvent was evaporated and the residue was purified by silica gel column chromatography using 1:1 ($CHCl_3$: Hexanes) as the eluant. Red solid (500 mg, 80%).

^{1}H NMR (400 MHz, $CDCl_3$, 300 K): δ; 3.01 (t, *J*=8.4 Hz, 2H), 2.63 (s, 6H), 2.49 (s, 6H) , 1.63 (m,2H), 1.52(m, 2H), 1.29(m, 22H) , 0.91 (t, *J*=6.82 Hz, 3H).

^{13}C NMR (100 MHz, $CDCl_3$): δ; 155.20, 146.69, 142.12, 131.55, 86.28, 31.93, 31.69, 30.31, 29.69, 29.66, 29.60, 29.56, 29.52, 29.38, 29.36, 29.35, 22.69, 19.03, 16.41, 14.12.

HRMS (ESI) calcd for $C_{28}H_{43}BF2I_2N_2$ (M-H) 709.16, found 709.16034 Δ = 0.56 ppm.

3.5.1. Additional Information

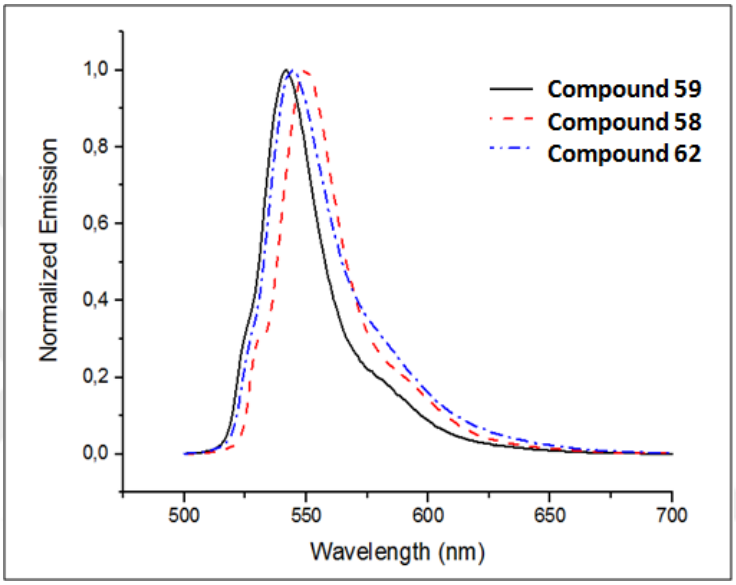

Figure 51: The normalized fluorescence emission of Compound **58**, **59** and **62** in CH_2Cl_2.

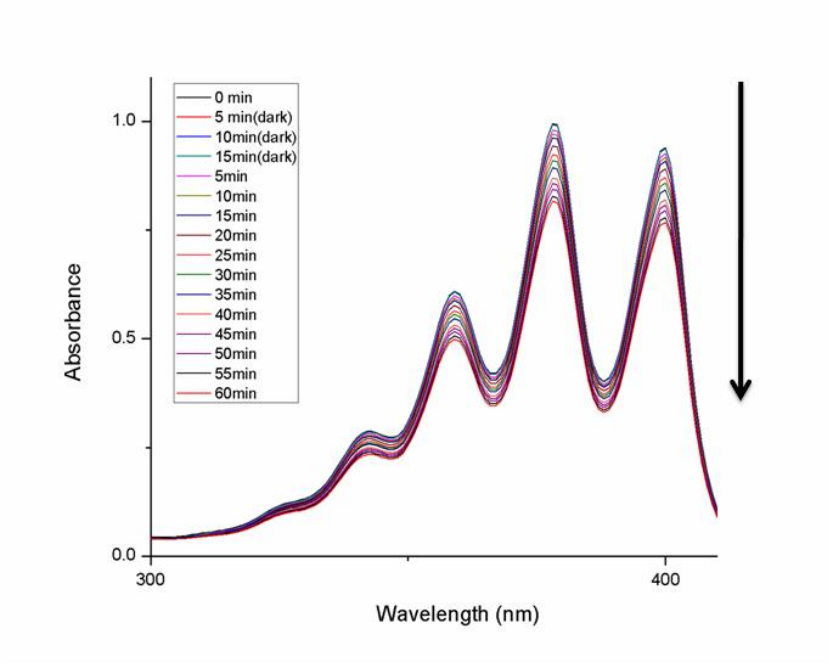

Figure 52: Singlet oxygen mediated bleaching of the trap molecule2,2'-(Anthracene-9,10-diyl)bis(methylene)dimalonic acid in the presence of Bodipy **58** (4.0 μM) in water. The light source was an LED array with peak emission at 520nm.

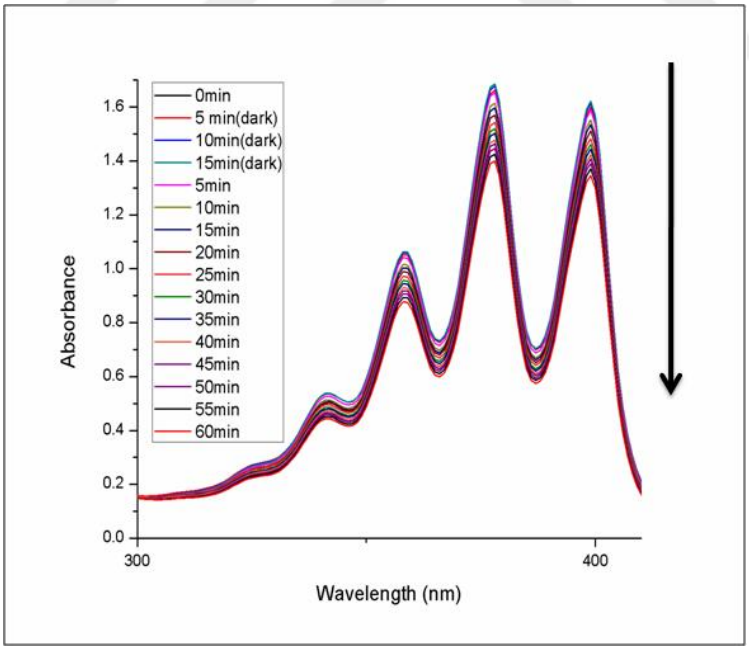

Figure 53: Singlet oxygen mediated bleaching of the trap molecule2,2'-(Anthracene-9,10-diyl)bis(methylene)dimalonic acid in the presence of Bodipy **62** (4.0μM) in water. The light source was an LED array with peak emission at 520nm.

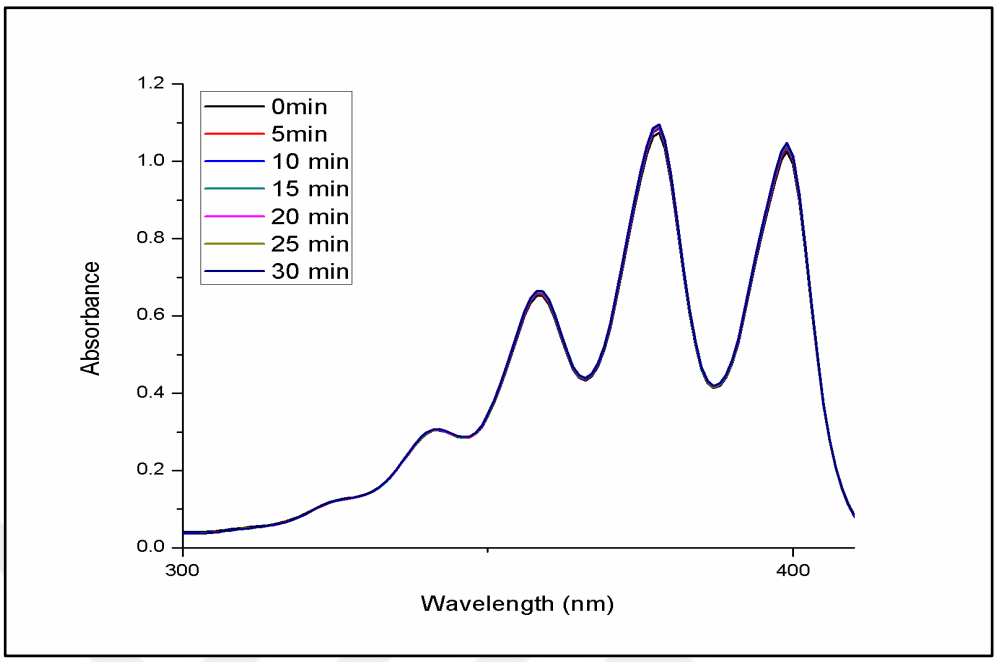

Figure 54: Absorbance spectrum of trap molecule 2,2'-(anthracene-9,10-diylbis(methylene)dimalonic acid in water without photosensitizer.

Singlet Oxygen Quantum Yields

Singlet oxygen quantum yields were calculated according to the literature [172]. The relative quantum yields were calculated with reference to Methylene Blue (MB) in water as 0.52 [176], [177]. Quantum yields for singlet oxygen generation in water were determined by monitoring the photooxidation of trap molecule (2,2'-(Anthracene-9,10-diyl)bis(methylene)dimalonic acid). The absorbance of trap molecule was adjusted around 1.0 in oxygen saturated solution. Then, the photosensitizer (4 μM) was added to cuvette and absorbance of absorbance photosensitizer was adjusted around 0.1- 0.2 in order to diminish the possibility of singlet oxygen quenching by the dyes. After, taking some measurements in dark, we exposed the cuvette to monochromatic light (521 nm) at the peak absorption wavelength. Absorbance was measured for several times after each irradiation. The graphics were plotted as the change in optical density (ΔOD) of trap molecule at 382 nm vs irradiation time for each photosensitizer.

The quantum yields of singlet oxygen generation were calculated by using the following equation. The quantum yields of singlet oxygen generation were calculated by using the following equation:

$$\Phi(^1O_2)bod = \Phi(^1O_2)MB\ (m_{bod}.\ F_{MB}/\ m_{MB}.Fbod)\ (PF_{ref}/\ PF_{bod})$$

where superscripts 'bod' represents the photosensitizers, $\Phi(^1O_2)$ is the quantum yield of singlet oxygen, m is the slope of difference in change in the absorbance of the trap molecule (at 382 nm) with the irradiation time and F is the absorption correction factor, which is given by F=1- 10-OD (OD at the irradiation wavelength). PF is absorbed photonic flux (μEinstein dm^{-3} s^{-1}).

Table 4: $\Phi(^1O_2)$ values of photosensitizer

Compound	**$\Phi(^1O2)$**
Compound 58	0.17
Compound 59	0.46
Compound 62	0.14
MB	0.52

Table 5: Characteristics of micellar compounds **58**, **59** and **62**. Cremophor EL was used for embedding the dye.

Compound	**Zeta potential ζ (mV)**	***Size distribution (nm)***	**Polydispersity index (PdI)**
Compound 58	-5.20	13.16	0.611
Compound 59	-1	26.62	0.161
Compound 62	-11.2	25.20	0.711

CHAPTER 4

4. A Study on Spectral Changes in tetra-benzocrown Modified BODIPY induced by α, ω-diamino Alkanes.

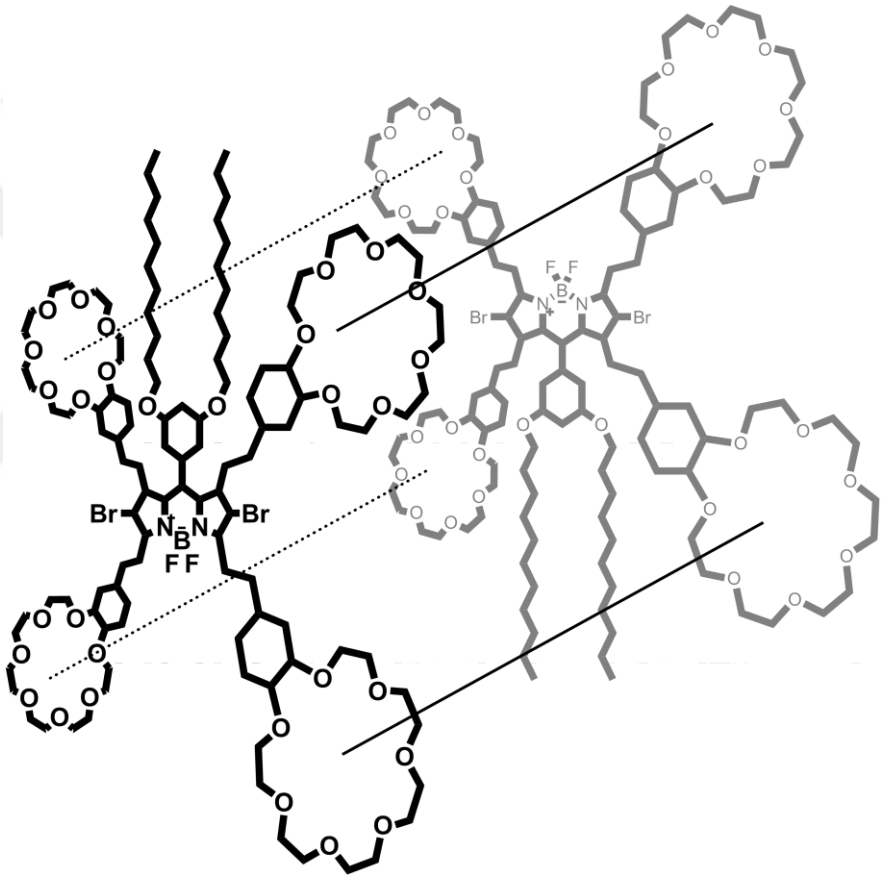

4.1. Objective

A BODIPY derivative functionalized with four crown units was designed and synthesized. The designed BODIPY core binds α,ω-diamino alkanes in different length sizes, including ethylenediamine. An internal hydrogen bond cause a dramatic change in UV-visible spectra and the fluorescence of compound **63** quenched in the case of the shortest diamine by π– π stacking.

4.2. Introduction

Over the past two decades, there are many receptors based on molecular recognition such as size, shape, length, chirality or structure have been designed to recognize various guest molecules. Of these organic compounds, amines are essential to synthetic processes and life as components of amino acids. Biogenic amines with one or more aliphatic primary amine groups are formed by thermal or enzymatic decarboxylation of amino acids [178]. These ubiquitous, naturally-occurring polyamines involved in cellular functions as survival mechanism, cell proliferation and cell growth [179]. For instance, putrescine and cadaverine are two polyamines takes place in regulation of receptor-ligand interactions, membrane stability, signal transduction and transcription. On the other hand, elevated levels of polyamines in cells and in food products can be toxic and are indicators of food toxicity cause to facilitate cell death [180]–[182]. In this regard, interaction of polyamines with other compounds is quite important.

Crown ethers have been used in building supramolecular systems by recognizing and binding specific guest molecules such that they have been used in science and industrial applications [179], [183]. They are popular receptors for biogenic amines and/or because of several different cavity sizes and effective chelation due to oxygen lone pairs [184]. There are several examples of ammonium ion recognition by using crown ether derivatives in literature [185].

BODIPY (4,4-difluuoro-4-bora-3a,4a-diaza-*s*-indacene) dyes are known as an extraordinary class of fluorophores and attribute excellent photophysical properties

such as narrow emission bands, high fluorescence quantum yields, large extinction coefficients and several modification sites allowing desired photophysical changes [52], [186]–[188]. The further substitution of BODIPY core results the synthesis of new BODIPY structures with different properties to solve several specific problems such as water soluble structures for imagining applications, light-harvesting systems, proton sensing and photosensitizers for photodynamic therapy applications [132]. The synthesis of tetra-styryl BODIPY dyes providing desired sensing and photophyscial properties bearing same or different side arms reported before [131], [132].

In this work, we synthesized the BODIPY based chemosensor **63** substituted with the benzo-21-crown-7(B21C7) chelator at four positions. The B21C7 moieties have been extensively studied in supramolecular chemistry. The design of various supramolecular polymers or rotaxane systems, B21C7 has an important role as a host moiety. By the incorporation of crown motifs, the photophysical properties of compound **63** are spectroscopically studied and discussed in the presence of various α,ω-diamino alkanes (ethylenediamine, putrescine, 1,6-diaminohexane, 1,10-diaminodecane) and hexyalamine. The non-covalent interaction between B21C7 units and α,ω-diamino alkanes readily tunes the spectroscopic/photophysical properties as well as the self-organization behavior of compound **63** investigated by UV-vis spectrophotometry and fluorometry (Figure 55).

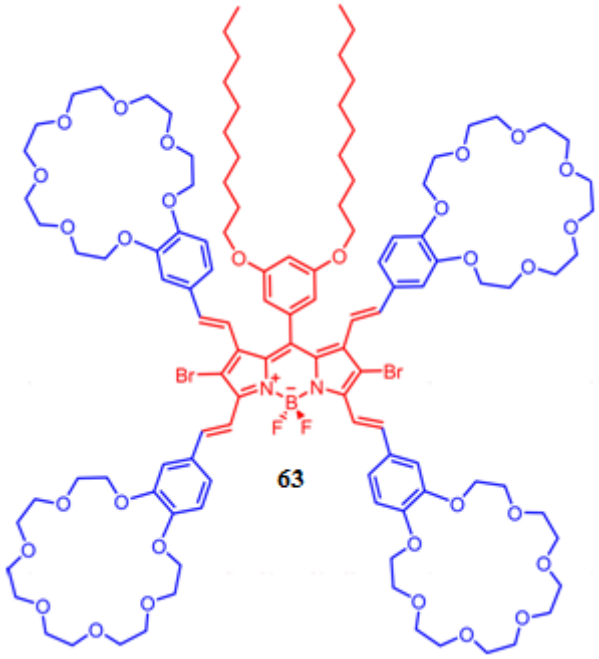

Figure 55: Structure of tetra-crown BODIPY **63.**

4.3. Results and Discussion

Our synthetic strategy was based on recognizing diamine salts by modification of side arms with crown ethers (Scheme 6). Benzo-21-crown-7, **65**, was synthesized starting from tosylation of hexaethylene glycol following the reaction of catechol with hexa(ethylene glycol) ditosylate according to known procedure [189]. The formylation of benzo-21-crown-7 involves hexamethylene tetramine and trifluoroacetic acid i.e. duff formylation [190].

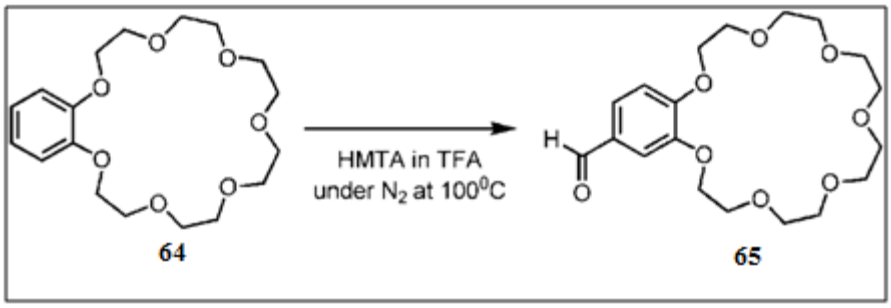

Scheme 6: Synthesis scheme of B21C7 moietiey, compound **65**.

The BODIPY core **66** was synthesized following previously published procedure [191]. Briefly in order to enhance the solubility in non-polar solvents, the decyl groups were introduced through the 8-phenyl substitution in the synthesis of BODIPY core following bromo substitution on 2- and 6- positions. The Knoevenagel condensation reaction was used to functionalize the four side arms (1, 3, 5, 7,-methyl sites) of BODIPY core and ^{1}H NMR and High Resolution Mass Spectrometry (HRMS) was used to characterize compound **63** (Scheme 7).

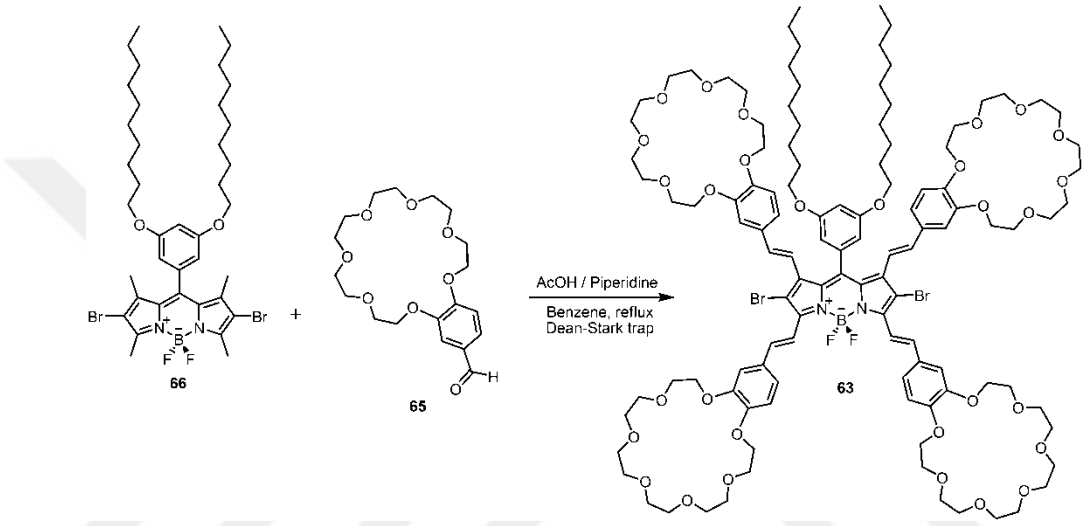

Scheme 7: Synthesis scheme of compound **63.**

The interaction of tetrastyryl BODIPY derivative **63** with guest molecules, α,ω-diamino alkanes, and a mono amine were examined by taking UV-visible spectra in acetonitrile. Protonation of amino compounds were provided by adding trifluoro acetic acid (TFA) in 1:2 molar ratio. UV-visible and fluorescent spectra of BODIPY derivative alone, only with trifluoro acetic acid and also only with one amino compound were measured as control experiments. UV-vis band changes of compound **63** upon addition of 1^{o} amine and 2^{o} amines are shown in figure 56. The addition of an acid as trifluoroacetic acid results in an excellent correspondence of electron pairs of crown ether to primary alkylammonium ion hydrogens, making the binding of complexes stable. The interaction between protonated α,ω-diamino alkanes and compound **63** were resulted a blue shift and intensity decrease for the shorter length of α,ω-diamino alkanes. The blue shift in UV-vis spectra was distinct

for the shortest alkane chain, 1,2-diaminoethane (from 703 nm to 654 nm). The resulting shift of absorption maxima is consistent as one chromophore getting in close proximity to another chromophore. The resulted electronic perturbation of chromophore nucleus cause shifting, broadening or splitting in some cases in the absorption spectra of the chromophore [192]. On the other hand, upon addition of only trifluoroacetic acid, only diaminohexane or a protonated 1^{o} amine -hexylamine- does not cause any significant change in the intensity of absorption spectra.

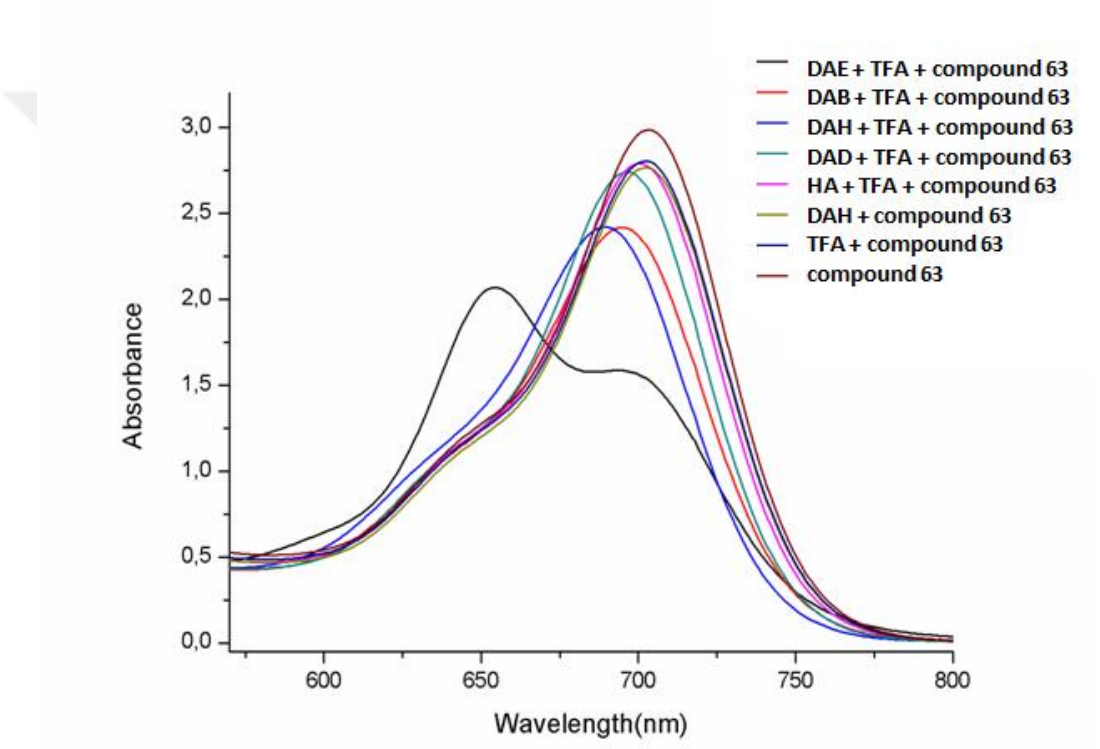

Figure 56: UV-visible spectra of chromophore **63** (33 μM in acetonitrile) treated with diaminoethane (DAE), diaminobutane (DAB), diaminohexane (DAH), diaminodecane (DAD) and hexylamine (HA) with trifluoroacetic acid (TFA). The chromophore **63** was also treated with only diaminohexane and only trifluoroacetic acid. The final concentrations are 66 μM for guest molecules and 132 μM for trifluoroacetic acid.

Thus, with the addition of short chain length protonated α,ω-diamino alkanes, two chromophore **63** gets in close proximity and most likely results in an intermolecular

dimerization. There is a precedent for the observed blue shift suggesting almost parallel stacking (H-dimerization) of two BODIPY dyes where the dimerization occurs by plane to plane stacking to form a sandwich type arrangement (Figure 57) [193]–[196].

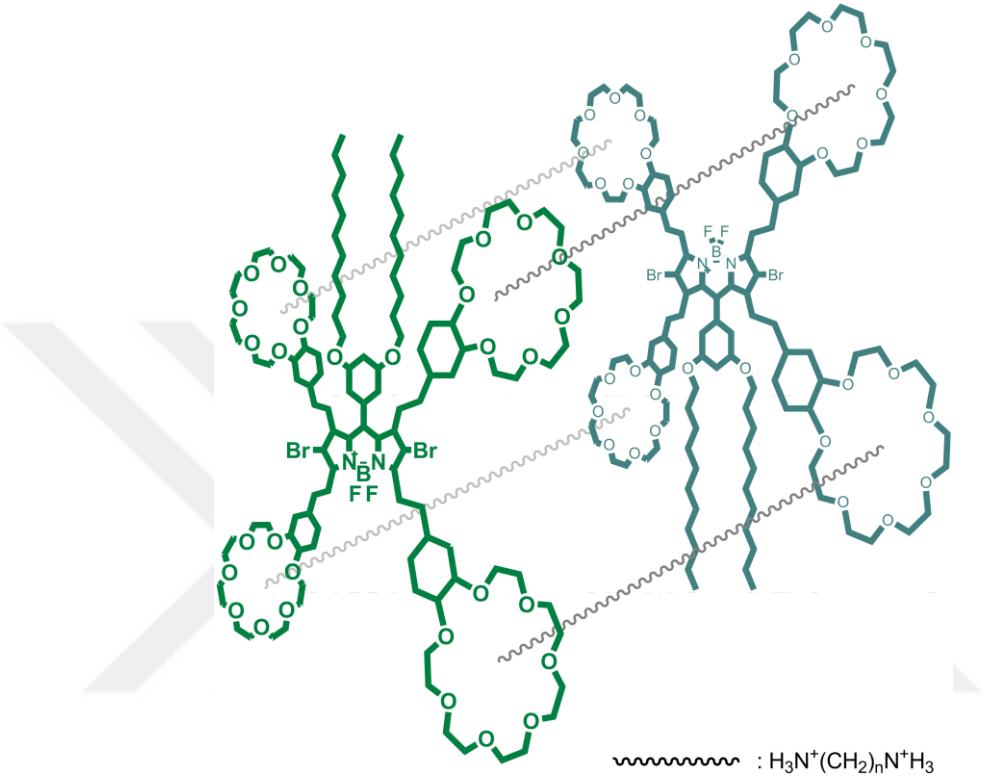

Figure 57: A schematic representation of two chromophore **63** in close proximity.

The selectivity and sensitivity of compound **63** towards protonated α,ω-diamino alkanes were investigated by fluorescence studies to understand the influence of the chain length on emission intensity of chromophore **63** (Figure 58). In fluorescence experiments of compound **63** with protonated α,ω-diamino alkanes (diaminobutane and diaminohexane), while an increase in maximum intensity is observed, the peak positions did not change implying amino alkane-induced fluorescence enhancement due to interaction of the oxygen atoms to protonated α,ω-diamino alkanes. The binding interaction between crown ethers and protonated diaminobutane and diaminohexane inhibits partial electron transfer from oxygen atoms to BODIPY, therefore fluorescence emission is enhanced. On the other hand, diaminodecane does

not promote a significant fluorescence change indicating a very weak binding to crown ether moieties, thus, compound **63** has no selectivity or sensitivity towards a long chain of α,ω-diamino alkane, diaminodecane. The control experiments with protonated hexylamine, trifluoroacetic acid and unprotonated diaminohexane do not show any changes in fluorescence intensity, either.

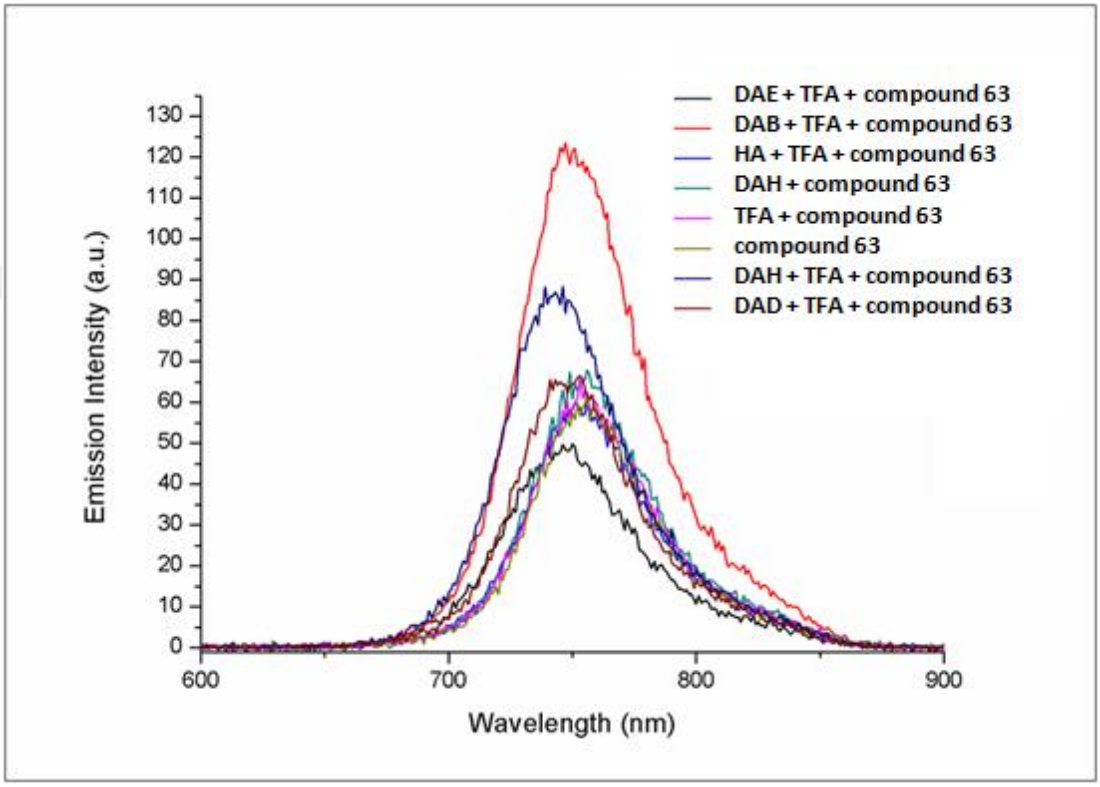

Figure 58: Emission spectra of chromophore **63** (33 μM in acetonitrile) treated with diaminoethane (DAE), diaminobutane (DAB), diaminohexane (DAH), diaminodecane (DAD) and hexylamine (HA) with trifluoroacetic acid (TFA). The chromophore **63** was also treated with only diaminohexane and only trifluoroacetic acid. The final concentrations are 66 μM for guest molecules and 132 μM for trifluoroacetic acid and each mixture was excited at 690 nm.

The fluorescence spectrum of compound **63** also corroborates the results from UV-vis spectroscopy with regard to dimerization upon treatment of the shortest of the protonated α,ω-diamino alkanes, diaminoethane. The fluorescence intensity shows a distinctive decrease indicating that the PET process is largely suppressed in the stacked arrangement of the compound **63** due to formation of the energetically

lower-lying excimer state by the increased contact between the two chromophore **63** by $\pi-\pi$ stacking [185], [197]. Thus, it can be stated that the formed stacked structure of compound **63** with interaction of protonated diaminoethane results the formation of H-dimerization by considering the observed hypsochromic spectral shift of the absorption maxima and the fact that the fluorescence of H-dimerization is quenched.

4.4. Conclusion

In conclusion, we have found in this study the main factors contributing to the changes in photophysical features of compound **63** towards the α,ω-diamino alkanes are: (i) the formation of efficient hydrogen bond between the oxygen donors of crown moieties and the ammonium of α,ω-diamino alkanes; and (ii) optimal length of diamino chains. The control experiments prove that the addition of an acid as trifluoroacetic acid results binding of diamino chains. On the other hand, longer chains such as diaminodecane shows weaker changes when bound to crown moieties and in the case of too short chains as diaminoethane, PET is surpassed by $\pi-\pi$ stacking of chromophore **63**.

4.5. Experimental Details

All experimental details are the same as shown in chapter 2. Compounds **64** and **66** were synthesized according to literature [188], [190]. Anhydrous tetrahydrofuran was obtained by refluxing over sodium/benzophenone prior to use. All other reagents and solvents were purchased from Aldrich and used without further purification.

Compound 65

Benzo-21-crown-7 (470 mg, 1,32mmol) and hexamethylenetetramine (204 mg, 1,45 mmol) were dissolved in trifluoroacetic acid (2.5 ml, 32.65 mmol) and the reaction mixture was refluxed at 100 ^{o}C under N_2 for 24 h. After 24 h, the reaction mixture cooled to 5 ^{o}C then mixed with ice and stirred for 1h. The resulting mixture was extracted with chloroform and the organic layer was dried over Na_2SO_4, evaporated

and residue was purified by silica gel column chromatography using ethyl acetate as the eluent. (colorless oil, 101 mg, 20%).

^{1}H NMR (400 MHz, $CDCl_3$): δ; 3.60 (s, 8H), 3.64-3.70 (m, 4H), 3.71-3.77 (m, 4H), 3.87 (p, *J*= 3.7, 4H), 4.15 (p, *J*= 3.5, 4H), 6.88 (d, *J*= 8.16, 1H), 7.30 (d, *J*=2.1, 1H), 7.36 (d, *J*= 5.04, 1H), 9.75 (s, 1H).

^{13}C NMR (100 MHz, $CDCl_3$): δ ; 67.9, 67.9, 68.1, 68.2, 69.2, 69.2, 69.7, 69.7, 69.8, 69.85, 70.0, 70.1, 110.0, 110.8, 125.5, 128.9, 147.9, 153.0, 189.6.

Compound 63

Compound **66** (0.044 mmol, 35 mg) and compound **65** (0.264 mmol, 101 mg) were added to a 100 mL round-bottomed flask containing 50 mL benzene. Piperidine (0.2 mL) and acetic acid (0.2 mL) were added to this solution. The mixture was heated under reflux by using a Dean Stark trap and it is monitored by TLC with Chloroform as solvent. When all the starting material had been consumed, the mixture was cooled to room temperature and solvent was evaporated. Water (100 mL) added to the residue and the product was extracted into the chloroform (3 x 100 mL). Organic phase dried over Na_2SO_4, evaporated and residue was purified by silica gel column chromatography using $CHCl_3$ as the eluent. Violet solid afforded (30 mg, 30%).

^{1}H NMR (400 MHz, $CDCl_3$): δ = 0.90 (t, *J* = 6.9 Hz, 6H), 1.05-1.26 (m, 28H), 1.40 (p, *J* = 6.9 Hz, 4H), 3.56 (t, *J* = 6.6 Hz, 4H), 3.62 (s, 32H), 3.66-3.71 (m, 16H), 3.73-3.78 (m, 16H), 3.84-3.91 (m, 16H), 4.04 (t, *J* = 4.5 Hz, 4H), 4.09 (t, *J* = 4.6 Hz, 4H), 4.16 (t, *J* = 4.6 Hz, 4H), 4.20 (t, *J* = 4.5 Hz, 4H), 5.7 (d, *J* = 16.5 Hz, 2H), 6.34 (t, *J* = 2.2 Hz, 1H), 6.41 (d, *J* = 2.2 Hz, 2H), 6.47 (d, *J* = 1.7 Hz, 2H), 6.60 (d, *J* = 8.4 Hz, 2H), 6.69 (d, *J* = 8.4 Hz, 2H), 6.87 (d, *J* = 8.4 Hz, 2H), 6.93 (d, *J* = 16.4 Hz, 2H), 7.1 (d, *J* = 1.9 Hz, 2H), 7.22 (d, *J* = 8.5 Hz, 2H), 7.5 (d, *J* = 16.6 Hz, 2H), 8.0 (d, *J* = 16.6 Hz, 2H).

^{13}C NMR (100 MHz, $CDCl_3$): δ = 13.1, 21.7, 24.8, 28.0, 28.3, 28.4, 28.5, 28.6, 30.9, 67.6, 68.2, 68.3, 68.6, 68.7, 68.7, 68.7, 68.8, 69.5, 70.0, 70.0, 70.0, 701, 70.1, 70.2,

70.2, 70.2, 106.9, 109.7, 112.5, 112.7, 112.8, 117.3, 120.3, 120.7, 129.2, 129.5, 134.1, 134.8, 138.5, 139.0, 147.9, 148.0, 148.4, 149.5, 160.2.

CHAPTER 5

5. Towards A Reaction-Based Probe for Reductive Intracellular Conditions

5.1. Objective

Hypoxia is a distinctive property of solid tumors and several other diseases. The bioreductive conditions are accelerated in hypoxic environment. Fluorescent molecular probes have recently been used to determine hypoxic cells. Herein, we report a BODIPY based probe for reductive conditions. In hypoxic conditions, the designed BODIPY based probe resulted in a strong enhancement of emission. Thus, it is a promising probe as a tumor targeting and hypoxia specific purposes.

5.2. Introduction

The low levels of oxygen have been observed in solid malignant tumors but not in healthy cells [198]–[203]. The underlying reason of difference in oxygenation levels is the imperfect neovascularization in tumors due to the imbalance of rapid cellular growth of cancer cells and new blood vessel formations [204]–[210]. Hypoxia can be observed in various diseases such as inflammatory diseases, stroke or cardiac ischemia besides the solid malignant tumors [211]–[215]. Besides, several clinical researches prove that hypoxia increases with malignant tumors [216], [217]. Therefore, tumor targeting and hypoxia specific probes have a considerable importance [218], [219]. There are several literature examples of fluorescent hypoxia targeting probes that most of them have relatively low photostability and based on resorufin, rhodamine, cyanine based dyes or naphthalimides [218], [220]–[222]. Also, it is a well known fact that intracellular reductases such as nitroreductases, quinone reductases, azoreductases or ketoreductases are accelerated by hypoxia resulting accelerated bioreductive reactions [211], [223], [224]. Based on this, in most of the literature examples, the fluorescent probes contains a nitroaryl group or a N=N double bond that in hypoxic conditions these groups turns into $–NH_2$ group and enhances the emission intensity [225]. In cellular conditions, reduced nicotinamide adenine dinucleotide (NADH) serves as an electron donor during the reduction.

Boron-dipyrromethene (BODIPY) dyes are excellent fluorophores for the design of hypoxia targeting probes with their narrow absorption and emission bands, high

emission quantum yields, high molar extinction coefficients and robustness against light [119], [218], [226], [227]. BODIPY dyes have been used as fluorescent membrane markers, sensors for anions and cations, donors and acceptors in FRET systems or indicators for reactive nitrogen and oxygen species [228]–[237]. Although these excellent photophysical properties, there is a limited number of studies of BODIPY dyes in hypoxic conditions [211], [218].

Herein we report the synthesis and characterization of new fluorescent BODIPY probe that the formyl group is introduced in *meso* position of BODIPY core. The resulted target compound is found to be nonfluorescent, however, under reductive conditions, the nucleophile attack on the *meso*-unsaturated BODIPY derivative, a fluorescent product forms. Thus, the *meso*-formyl BODIPY is a good candidate as a fluorogenic probe for a nucleophilic attack (Figure 59).

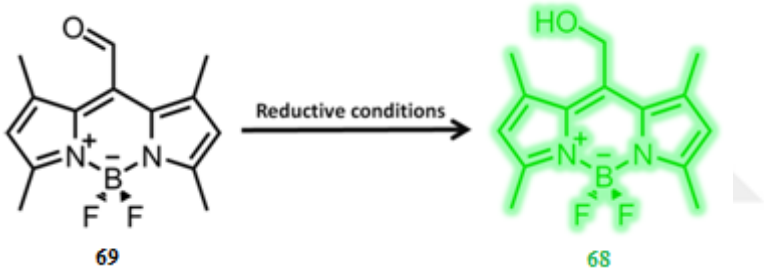

Figure 59: Chemical structure of a hypoxia sensing BODIPY dye.

5.3. Results and Discussion

The *meso*-acetoxymethyl BODIPY, compound **67**, is synthesized by condensation reaction of 1 equivalent of acetoxyacetyl chloride and 2 equivalent of 2,4-dimethyl pyrrole in dichloromethane at 50 ^{o}C followed by *in situ* complexation with $BF_3 \cdot OEt_2$ in the presence of a base, diisopropylamine, at room temperature. Compound **67** is easily converted to the *meso*-hydroxymethyl BODIPY, compound **68**, under basic conditions by addition of 0.1 M of NaOH in dichloromethane:methanol (1:2) environment at room temperature under argon atmosphere. The basic hydrolysis of compound **67** results in approximately %55 yield. The oxidation of compound **68** to

the corresponding *meso*-formyl BODIPY was conducted by using Dess-Martin oxidation conditions and yield was %80 (Scheme 8).

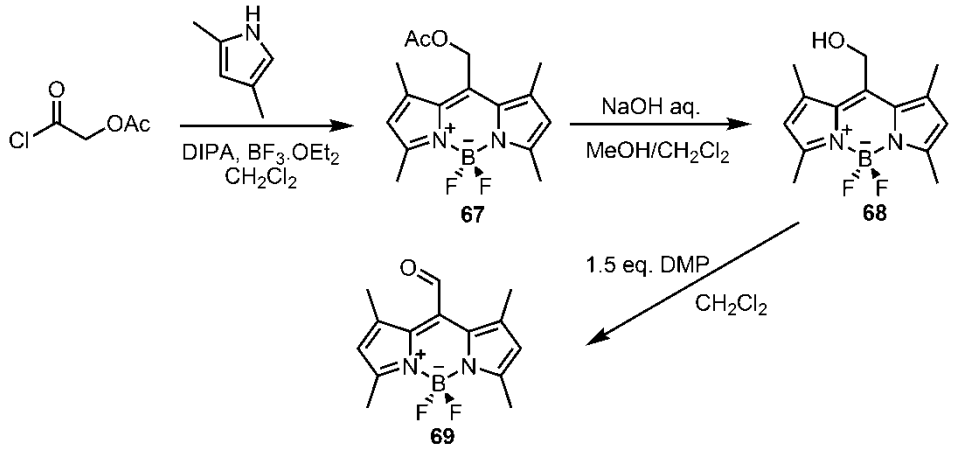

Scheme 8: Synthesis of the *meso*-formyl BODIPY, compound **69**.

We evaluated the spectroscopic properties of *meso*-formyl BODIPY in response to sodium borohydride, $NaBH_4$ under the physiological conditions (pH 7.4 HEPES buffer, 15 mM and ethanol) in the absence and presence of $NaBH_4$ (Figure 60a). Initially, no fluorescence was observed. Upon treatment of increased amount of $NaBH_4$, a dramatic increase in fluorescence intensity was observed and an emission band was formed at 522 nm is consistent with the emission band of compound **69**. As it is expected, the subsequent reduction of the carbonyl group in *meso*-formyl BODIPY by a strong reducing agent transformed to the *meso*-hydroxymethyl BODIPY. The fluorescence change can be observed by naked eye by the addition of solid $NaBH_4$ (Figure 60b).

a.

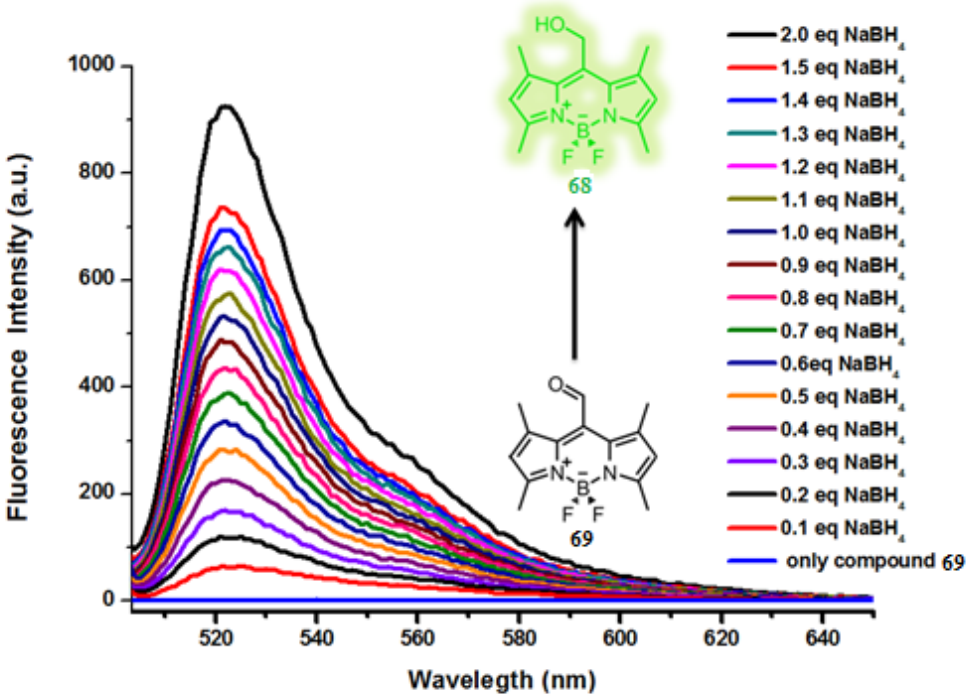

b.

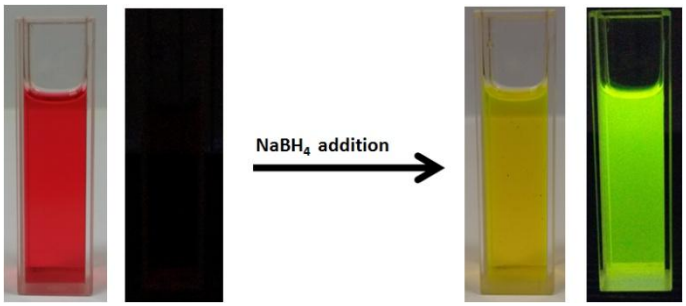

Figure 60: Fluorescence emission spectra of the *meso*-formyl BODIPY, compound **69** (35 µM) in pH 7.4 HEPES buffer (15 mM) and ethanol before and after addition of increased equivalents of sodium borohydride from 0.1 equivalent to 2 equivalent (Figure 60a). The photo of compound 3 (left) under a UV lamp (λ=254 nm and 365 nm, respectively). From left to right, rapid emission enhancement was observed upon addition of sodium borohydride (λ=254 nm and 365 nm, respectively) (Figure 60b).

The observed fluorescence increase of compound **69** is based on the reduction of carbonyl group to a hydroxy group upon addition of sodium borohydride where sodium borohydride behaves as the source of hydride ions, H:¯. The lack of emission of *meso*-formyl BODIPY but not *meso*-hydroxymethyl BODIPY was recently studied by Cosa *et al.* The DFT studies showed that *meso*-unsaturated BODIPY derivatives are in an energetically stabilized conformation due to extended conjugation and BODIPY core is flexible provided by the boron atom. Upon the excitation, the rotation in dihedral angle of the conjugated carbonyl group results shifting one of the dipyrrin groups out of the plane. As a result, internal conversion to ground state competes with the emission. In the presence of the methyl groups in 1- and 7- positions, the energy gap between relaxed excited state and ground state gets smaller, thus, nonradiative deactivation pathways increase. Additionally, the substitution of unsaturated groups besides formyl group in any other positions of BODIPY core cause no significant decrease in emission of the fluorophore indicating position selectivity [238].

The absorption spectrum of compound **69** shows a broader distribution than the observed absorption spectra during the addition of sodium borohydride as it is expected in DFT studies [238]. The large range of ground state conformers in solution causes the broadening in absorption spectra due to the lower energy barrier in meso-formyl BODIPY than meso-hydroxymethyl BODIPY (Figure 61).

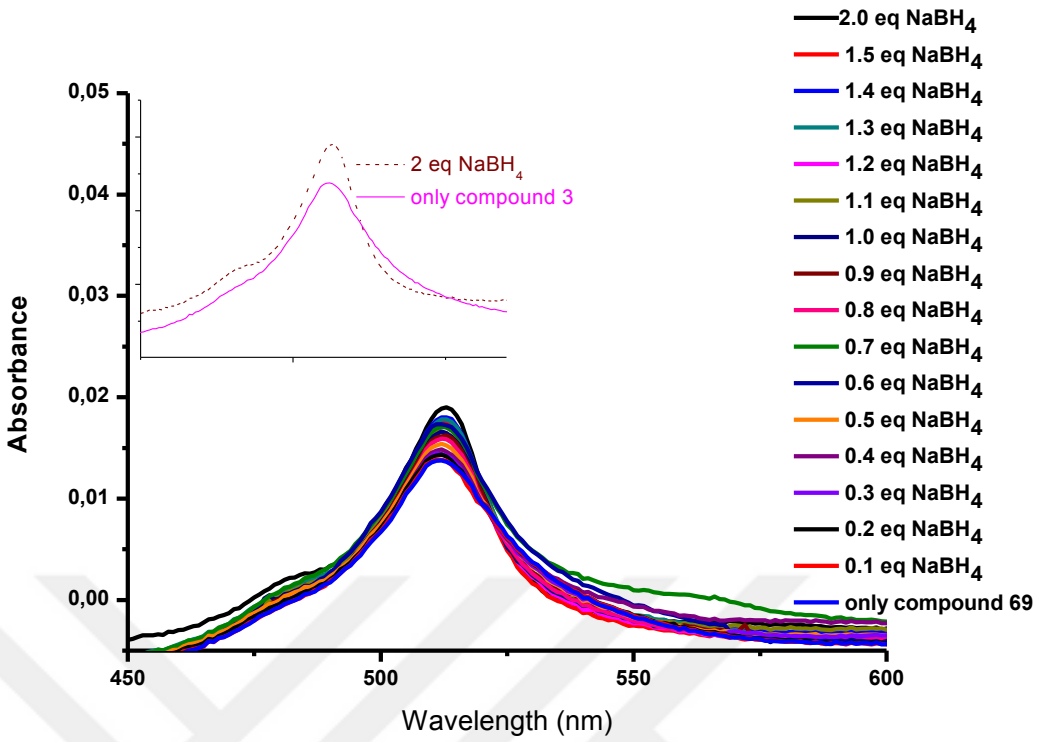

Figure 61: The absorption spectra of the *meso*-formyl BODIPY, compound **69** (35 µM) in pH 7.4 HEPES buffer (15 mM) and ethanol before and after addition of increased equivalents of sodium borohydride from 0.1 equivalent to 2 equivalent.

The above results show the importance of internal steric hindrance caused by 1,7-dimethyl groups causing nonradiative deactivation. Thus, the synthesized *meso*-formyl BODIPY compound has no emission band. In a reductive environment as hypoxic environment or in the presence of sodium borohydride, formyl group is reduced to hydroxyl group. The reduction of compound **69** resulted in a strong enhancement of emission.

5.4. Conclusion

In conclusion, we have developed a new fluorescent indicator, compound **69**, based on BODIPY and it was shown to work in reductive environment of aqueous $NaBH_4$. In hypoxic conditions, the amount of intracellular reductases increases. The reduced form of coenzyme nicotinamide adenine dinucleotide, NADH, is the reducing agent

works in reduction of aldehydes and ketones in biological systems. The synthesized *meso*-formyl BODIPY compound was introduced 1,7-dimethyl groups to provide internal steric hindrance causing non-radiative emission. The reductive environment is provided by sodium borohydride for the reduction of formyl group. The reduction of *meso*-formyl BODIPY resulted in a strong enhancement of emission. It is, therefore, *meso*-formyl BODIPY provides a promising strategy for tumor targeting hypoxia probes for further studies.

5.5. Experimental Details

All experimental details are the same as shown in chapter 2.

Compound 67

Acetoxyacetyl chloride (1.60 mL, 14.8 mmol, 1 eq) was added to the solution of 2,4-Dimethyl pyrrole (2.55 mL, 24.8 mmol, 1.6 eq) was dissolved in dry CH_2Cl_2. The reaction mixture was stirred at 40 °C under argon atmosphere for 2 hours. Then, the mixture was cooled to room temperature and diisopropylethylamine (8.58 mL, 49.3 mmol, 3.3 eq) was added then $BF3{\cdot}OEt_2$ (6.18 mL, 49.3 mmol, 3.3 eq) and the reaction mixture left stirring for 30 min. The solvent was evaporated and purified by a silica gel flash column and eluted with DCM: Hexane (1:3) to give compound **67** as orange crystals (2.5 g, 65% yield)

^{1}H NMR (400 MHz, $CDCl_3$): δ; 6.00 (s, 2H), 5.32 (s, 2H), 2.55 (s, 6H), 2.38 (s, 6H), 2.15 (s, 3H).

^{13}C NMR (100 MHz, $CDCl_3$): δ; 170.3, 156.9, 141.1, 133.5, 132.3, 122.4, 57.7, 20.7, 15.7, 14.6.

HRMS (TOF-ESI): m/z calcd for $C_{16}H_{19}BF_2N_2O_2$: 342.14362 $[M+Na]^+$; found: 342.14803 $[M+Na]^+$, Δ = -12.9 ppm.

Compound 68

Compound **67** (140 mg, 0.44 mmol) was dissolved in DCM: MeOH (4.3 mL:8.6 mL) mixture and then 0.1 M of NaOH aq (1.7 mL) was added. The reaction mixture was stirred at room temperature until the consumption of compound **67** under argon atmosphere. The solvent was removed and the residue was redissolved in DCM, washed with water, dried, and evaporated. The solvent was evaporated and purified by a silica gel flash column and eluted with hexane: EtOAc (1:1) to give compound **68** as orange powder (90 mg, 60% yield)

^{1}H NMR (400 MHz, DMSO): δ; 6.24 (s, 2H, pyrrole-H), 5.50 (t, J = 3.9 Hz, 1H, OH), 4.72 (d, J = 4.5 Hz, 2H, CH_2), 2.57 (s, 6H, CH_3), 2.41 (s, 6H, CH_3).

^{13}C NMR (100 MHz, DMSO): δ; 155.2, 142.4, 141.7, 132.5, 121.7, 55.1,

Compound 69

Compound **68** (0.2 g, 0.70 mmol), and Dess-Martin periodinane (0.46 g, 1.05 mmol) were mixed in dry DCM under argon atmosphere at 0 ^{o}C and the reaction mixture was stirred for 30 min. The reaction mixture was washed with $Na_2S_2O_3$ and $NaHCO_3$, respectively and water then dried over Na_2SO_4. The solvent was removed and purified by a silica gel flash column and eluted with DCM to give compound **69** as red crystals (173 mg, 90% yield)

^{1}H NMR (400 MHz, $CDCl_3$): δ; 10.58 (s, 1H), 6.10 (s, 2H), 2.56 (s, 6H), 2.15 (s, 6H).

^{13}C NMR (100 MHz, $CDCl_3$): δ; 193.3, 158.9, 141.4, 136.2, 129.0, 121.7, 29.6, 15.7, 14.4.

HRMS (TOF-ESI): m/z calcd for $C_{14}H_{15}BF_2N_2O$: 274.12091 $[M-H]^-$; found: 274.11621 $[M-H]^-$, Δ = 17.13 ppm.

CHAPTER 6

6. Supramolecular Control of Through Space Energy Transfer

6.1. Objective

A mechanically interlocked antennae system, [2]rotaxane, composed of boradiazaindacene (BODIPY) units was designed and synthesized. The new energy transfer cassette shows efficient Förster resonance energy transfer from two donor BODIPY units to a dibenzo[24]crown-8 (DB24C8) functionalized distyryl-BODIPY (Figure 62).

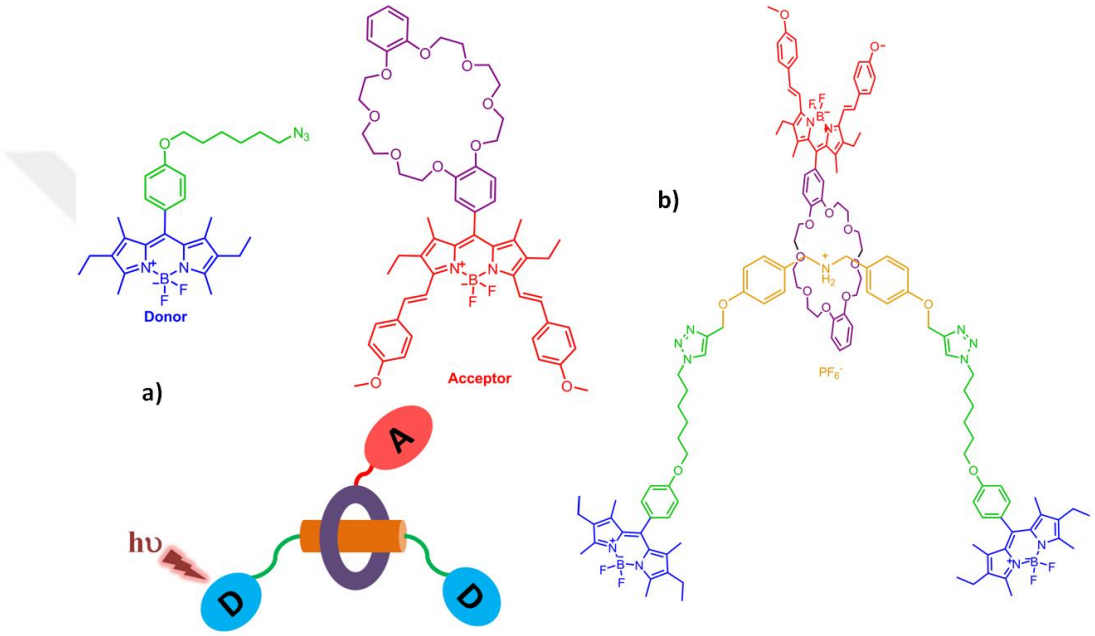

Figure 62: (a)Schematic representation of BODIPY-based [2]rotaxane showing that a macrocycle (purple) was mechanically interlocked through a linker (orange), terminated by two BODIPY end groups (blue). The energy cassette components were tagged by the donor D (blue) and acceptor A (red). (b) Chemical structure of the [2]rotaxane **83**.

6.2. Introduction

A natural light-harvesting system where photochemical conversion of solar energy takes place is an efficient process to produce photosynthetic proteins [239], [240]. Excitation energy transfer (ET) plays an important role in this highly effective working system [241], [242]. For example, in bacterial photosynthetic units, solar energy is transferred and collected from outer LH-II complex or LH-III complex, in

the case of purple bacteria antenna system, to the reaction center [243]. Mimicking such light-harvesting antennae has attracted considerable attention from biologists and chemists [242], [244]–[246]. In an artificial light-harvesting system, donor and acceptor moieties are placed in close proximity by covalent bonds although noncovalent interactions provide more tenability, versatility and ease of modulation on antennae systems as naturally occurring energy transfer cassettes and energy transfer takes place from donor chromophore to core in unidirectional and effective way [243], [247]–[249].

Mechanically interlocked molecules (MIMs) such as rotaxanes, polyrotaxanes, catenanes, and polycatenanes have been extensively studied in the construction of molecular muscles, molecular machines, shuttles or molecular wires [250]–[253]. The controllable construction in the axle or in the wheel components provides ease of adding specific functions to total system, controlling interactions of components or determining the distance between different units such as light-harvesting systems between donor and acceptor parts, therefore, MIMs are attractive choices for designing energy transfer cassettes [254], [255]. The energy tansfer between mechanically linked chromophores favors Förster type energy transfer in which energy trasnfer occurs through space [99], [256], [257].

In this study, we synthesized an efficient Förster type energy transfer system by formation of a [2]rotaxane that contains three chromophoric units, namely, difluoroboradiaza-s-indacene (BODIPY) dyes one with a DB24C8 ring on meso-position of BODIPY core. As shown in figure 62, [2]rotaxane **83** has constructed from two BODIPY arms connected to a linker, dibenzylammonium (DBA) unit, and it has mechanically interlocked to BODIPY functionalized DB24C8 ring. The strong interaction of DB24C8 macrocycle with ammonium cations is well known. Thus, the interaction, specially, hydrogen bonding and π–π stacking, between DB24C8 and DBA is well studied as a building method in MIMs structures. Meanwhile, Cu(I)-catalyzed azide-alkyn click reaction on DBA unit has been used to design various complex molecules due to its high efficiency, tolerance to mild reaction conditions and different functional groups. Two azide terminated BODIPY derivatives as donor

fluorophores introduced into DBA linker and they also serve as stopper units, meanwhile, a BODIPY-functionalized DB24C8 macrocycle was introduced as an acceptor and formed molecular thread structure. BODIPY dyes are good candidates as energy transfer fluorophores not only with their high photostability or sharp emission and absorption bands but also with high fluorescence quantum yield and high molar extinction coefficient.

6.3. Results and Discussion

Synthesis and Characterization

The synthesis of acceptor unit **74** is outlined in scheme 9. Aldehyde **72** is prepared from tosylation of the previously prepared alcohol **70** according to literature [258]**.** The B24C8-BODIPY core was synthesized by three step one pot BODIPY synthesis with aldehyde **72** by using 3-ethyl-2,4-dimethylpyrrole. The introduction of two styryl groups in 3-, and 5-, positions of BODIPY core was achieved with Knoevenagel condensation reaction by using piperidine and acetic acid in refluxing benzene by using Dean-Stark apparatus to remove water from reaction media. The preparation of dibenzylammonium unit **79** involves the condensation of the aldehyde **76** and benzyl amine **77** following reduction, protonation and finally anion exchange reactions.

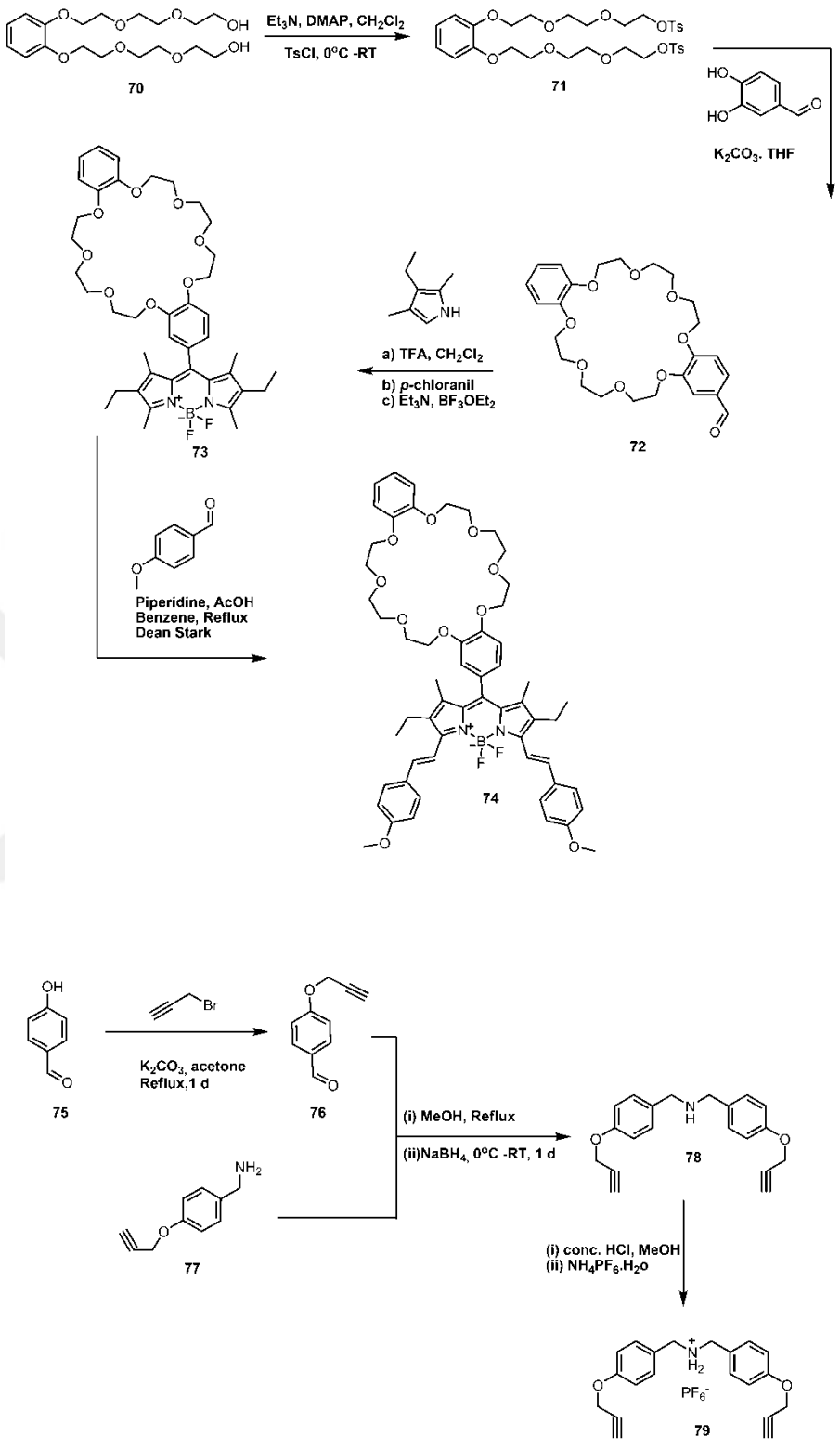

Scheme 9: Synthesis scheme of acceptor and linker parts of [2]rotaxane.

The synthesis of donor **82** involves first the synthesis of bromo-tethered aromatic adehyde **80** following a classical BODIPY reaction with 3-ethyl-2,4-dimethylpyrrole and finally the reaction with NaN_3 in polar aprotic solvent such as DMF (Scheme 10).

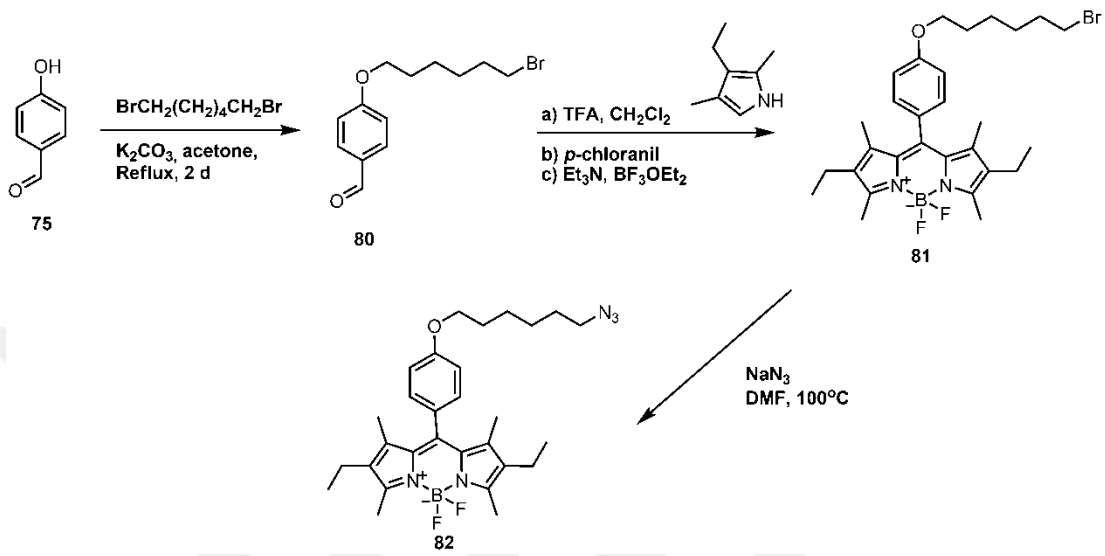

Scheme 10: Synthesis scheme of the donor part of [2]rotaxane.

The synthetic procedure of target BODIPY based [2]rotaxane **83** is shown in scheme 11. First, dibenzylammonium unit **79** and the acceptor BODIPY **74** were treated in DCM for 24 h, thus, a self-complexing pseudorotaxane forms. Then, using the 1,3 dipolar cycloaddition reaction (CuAAC) catalyst and the addition of azido-BODIPY derivative **82**, triazole formation achieved and compound **83** is synthesized.

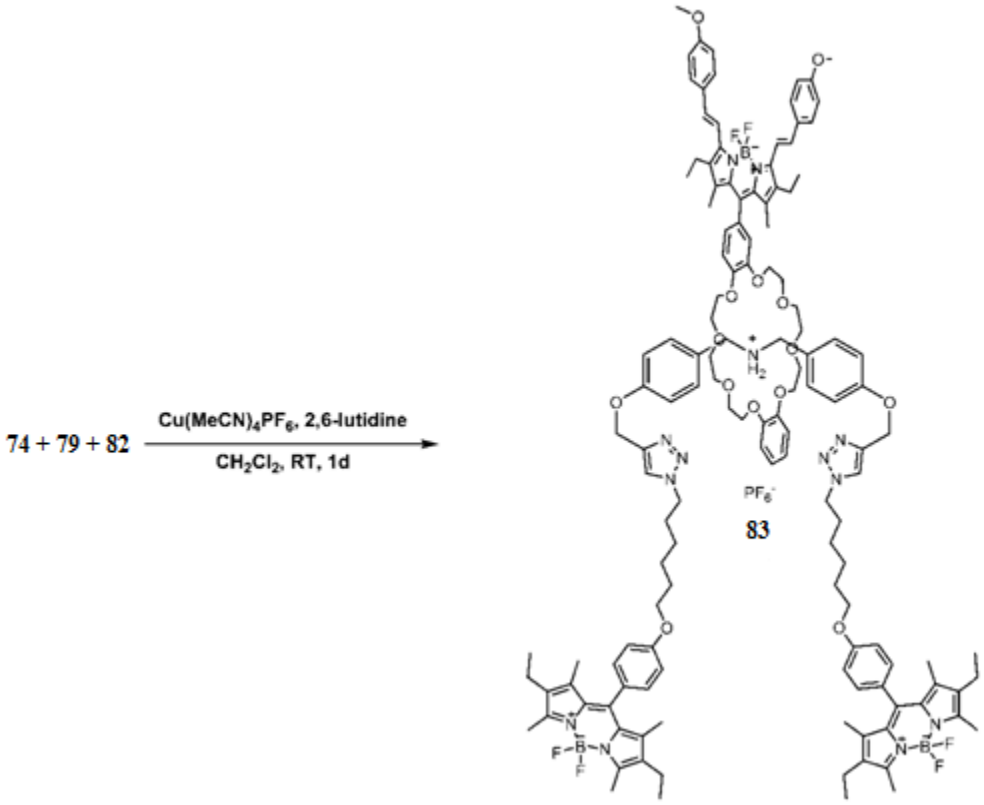

Scheme 11: Synthesis scheme of [2]rotaxane.

We first investigated the photophysical properties of [2]rotaxane **83**, the acceptor BODIPY **74** and the donor BODIPY **82**. The absorption spectra of these three compounds and **M** (a mixture of compounds **74** and **82** with a molar ratio of 1:2, respectively) in chloroform are shown in figure 63. The absorption spectrum of compound **83** showed two distinct absorption bands at λ= 526 nm and λ= 659 nm. In order to show the importance of the mechanical linkage in energy transfer system, the absorption spectrum of **M** and **83** were compared. The absorption spectrum of **M** was almost the same as of [2]rotaxane **83** which can be formed from the addition of the absorption spectra of **74** and **82**.

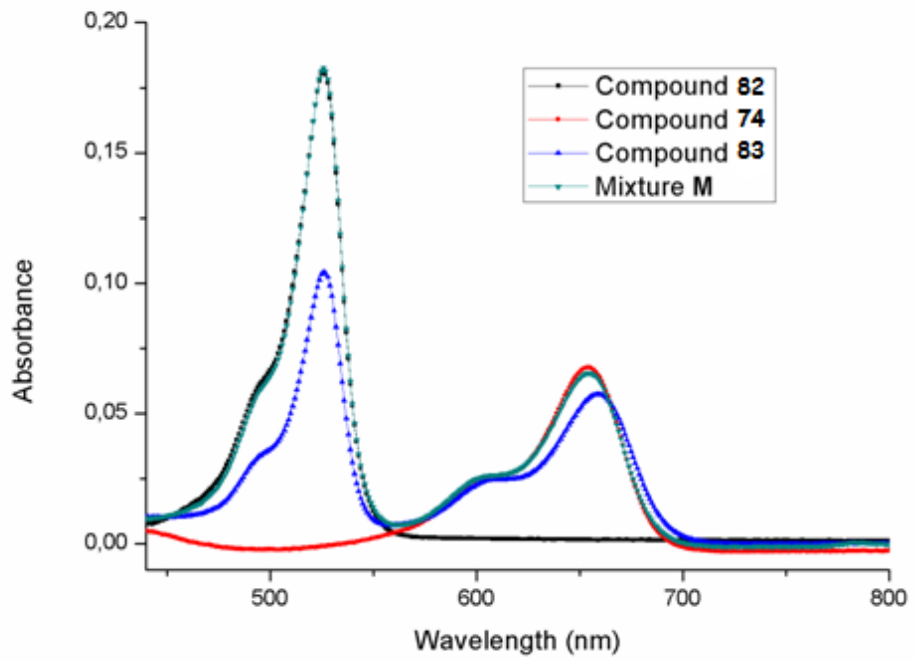

Figure 63: The absorption spectra of [2]rotaxane **83** ($1x10^{-6}$ M), compound **74** ($1x10^{-6}$ M), compound **82**($2x10^{-6}$ M), and mixture **M** (a mixture of **74** and **82** in a molar ratio of 1:2).

Figure 64 shows the fluorescence spectra of **74**, **82**, **83** and **M** in chloroform at room temperature under the same excitation wavelength (λ= 500). The emission maximum λ_{max} of **82** and **74** peaked at 537 nm and 673 nm, respectively. Additionally, the absorption spectrum of the acceptor distyryl-BODIPY unit **74** showed a large overlap with the emission of the donor BODIPY **82** indicating fluorescence resonance energy transfer is ideal for through interactions between transition dipoles (Figure 65) [259], [260]. The emission spectrum of **M** consisted of the addition of individual emission spectra of **82** and **74** when excited at λ = 500 nm. Therefore, the donor **74** and acceptor **82** behave as individually and as non interacting fluorophores in the mixture **M**. However, there is a distinctive difference in the emission spectrum of [2]rotaxane **83** compared with the mixture system **M**; the emission spectrum of [2]rotaxane **83** became a very weak at λ= 537 nm that shows the quenching of the shorter wavelength and a peak was raised at a longer wavelength, λ= 676 nm. This indicated

an efficient energy transfer from azido-BODIPY derivative **82** to the acceptor distyryl-BODIPY unit **74**. The comparision of the mixture system and [2]rotaxane **83** proves the importance of the mechanical linkage between the acceptor and the donor units by shortening the distance between fluorophores and therefore promoted Förster type energy transfer through space.

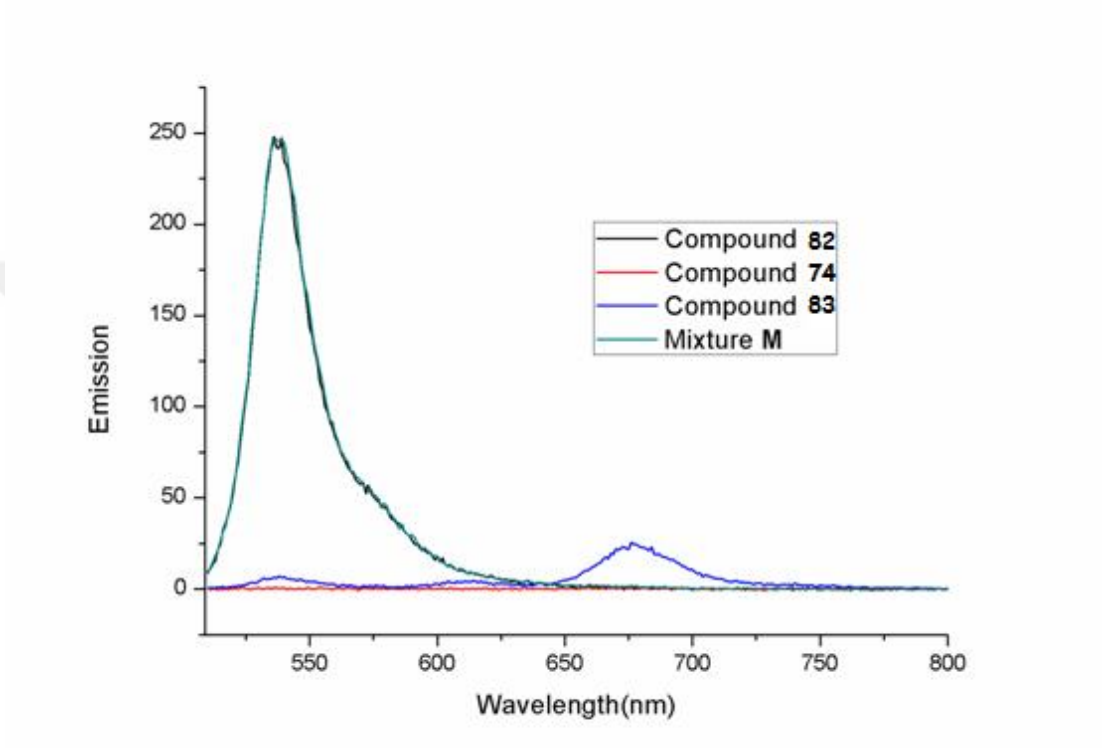

Figure 64: The emission spectra of [2]rotaxane **83** ($1x10^{-6}$ M), compound **74** ($1x10^{-6}$ M), compound **82** ($2x10^{-6}$ M), and mixture **M** (a mixture of **74** and **82** in a molar ratio of 1:2). The excitation wavelength of the fluorescent spectra is 500 nm.

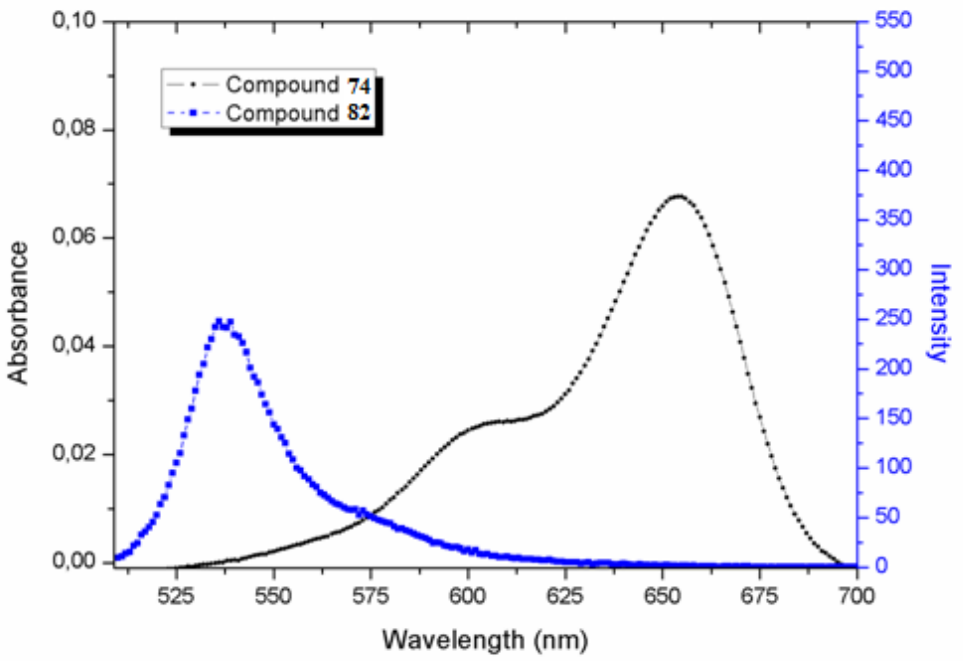

Figure 65: The absorption spectrum of compound **74** ($1x10^{-6}$ M) and the emission spectrum of compound **82** ($2x10^{-6}$ M) in chloroform.

The figure 66 shows the emission spectra of the admixtured system with the rotaxane system excited under two different wavelengths (500 and 673 nm). The [2]rotaxane system shows an emission peak independently to the excitation wavelength indicating that energy is effectively transferred to one chromophore [247], on the other hand, mixture has two distinct emission peaks dependent on the excitation wavelength. This can be explained by existence of two independent chromophores in the mixture system.

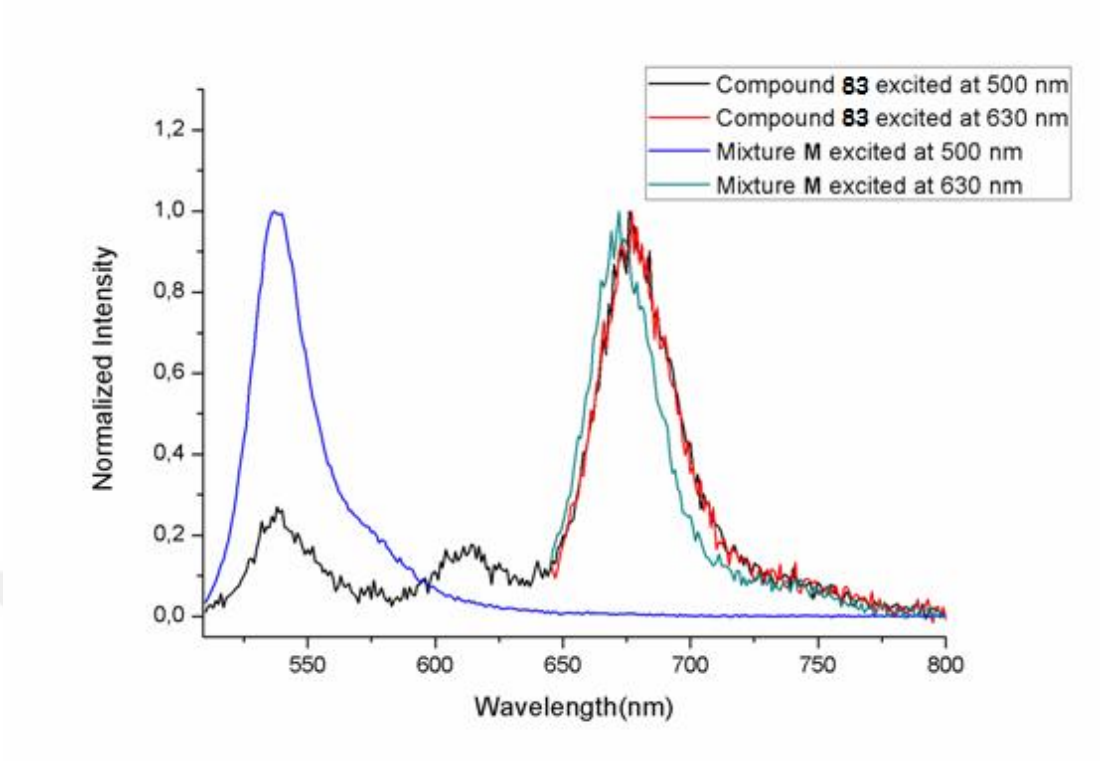

Figure 66: The emission spectra of [2]rotaxane **83** ($1x10^{-6}$ M) and mixture **M** (a mixture of **74** and **82** in a molar ratio of 1:2) in chloroform recorded at different excitation wavelengths (500 nm and 630 nm) at room temperature.

To understand the energy transfer process better, time resolved fluorescence spectroscopy was performed for [2]rotaxane **83** and the donor **82** (Table 6). The emission decay of compound **83** is biexponential, which is reasonable because of the residual emission from the shorter wavelength chromophore addition to the emission from the longer wavelength chromophore. When the reduced emission lifetime of donor chromophore is considered, energy transfer efficiency can be calculated as 97% for light harvester **83**. However, the comparison of absorption and excitation spectra (normalized at absorption wavelength of the acceptor) shows that percent energy transfer efficiency is about 30-40% (Figure 67). The difference in energy transfer efficiency is reasonable considering additional vibrational and nonradiative pathways in large molecules as rotaxanes.

Table 6: Fluorescence lifetime (τ) of 14 and 13 obtained from the time-resolved fluorescence measurement in $CHCl_3$ solution.

compound[a]	**l_{ems} (nm)**	**τ (ns)**[b]	**efficiency**
83	676	4.8 (40%) 0.22 (60%)	97%
82	537	4.94	-
74	673	-	-

[a] Data acquired in $CHCl_3$ in dilute solutions. [b] Data in parentheses refer to weight percentage of the contribution to emission decay.

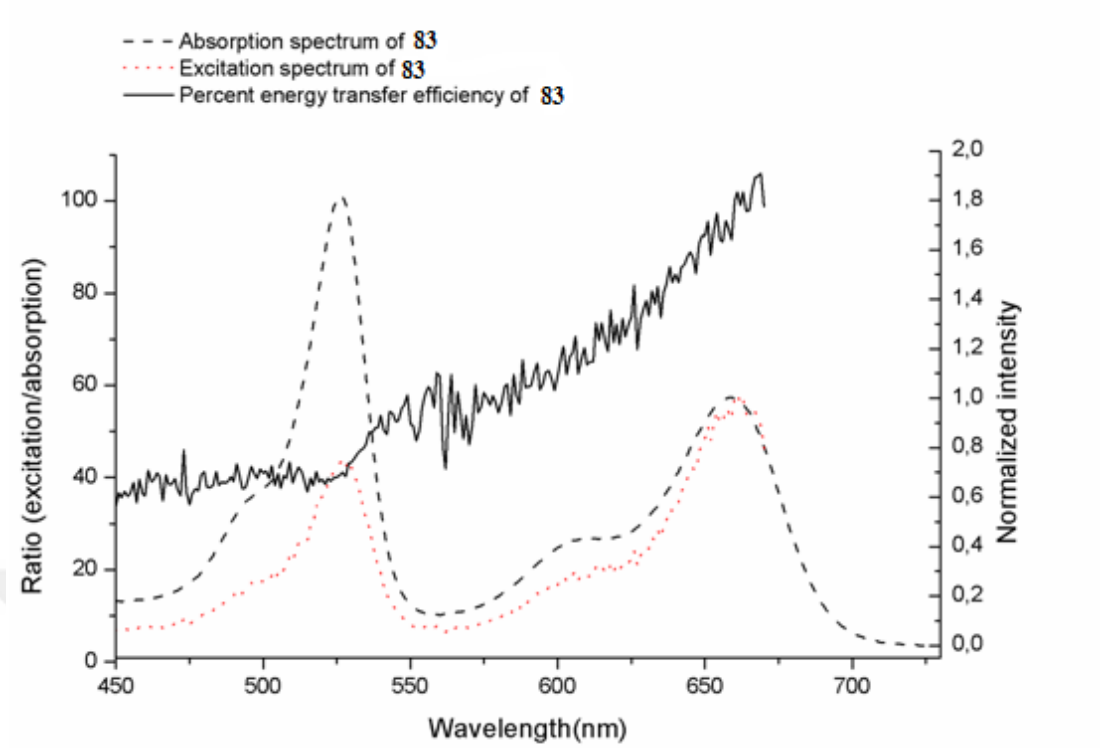

Figure 67: Percent energy transfer efficiency of **83** (solid line) as a function of wavelength of excitation. Excitation spectrum of **83** (dotted line) and absorption spectrum of **83** (dashed line), normalized at 660 nm. (Emission data were collected at 673 nm.)

6.4. Conclusion

In conclusion, we have developed a new BODIPY based mechanically interlocked light harvesting system by synthesis and characterization of **83**. Through the introduction of two BODIPY donor units to B24C8 introduced BODIPY acceptor via linker, an efficient energy transfer process was provided.

6.5. Experimental Details

All experimental details are the same as shown in chapter 2.

Synthesis

Compound 71

Compound **70** (5.6 g, 15 mmol), triethylamine (8.7 mL, 62 mmol) and 4-dimethylamino pyridine (10 mg, 0.15 mmol) were mixed in DCM (60 mL) at 0 ^{o}C in ice bath. 4- toluenesulfonyl chloride (7.2 g, 38 mmol) dissolved in DCM (150 mL) was added dropwise to the reaction mixture with vigorously stirring. After keeping at 0 ^{o}C for 1 h, the ice bath was removed. The reaction mixture was stirred at room temperature overnight. The reaction mixture was washed with 0.1 M HCl (twice) and saturated NaCl solutions (twice). The organic layer was dried over Na_2SO_4 and concentrated by evaporation. The crude product was purified by column chromatography (Silica gel, EtOAc/Hexane: 1/6 (v/v)). Compound **2** was obtained as colorless oil.

^{1}H NMR (400 MHz, $CDCl_3$): δ; 7.81 (d, *J*= 8Hz, 4H), 7.34 (d, *J*=8 Hz, 4H), 6.93 (s, 4H), 4.18-4.14 (q,*J*=4 Hz, 8H), 3.84 (t, *J*= 4 Hz, 4H), 3.72-3.68 (m, 8H), 3.64-3.61 (m, 4H), 2.45 (s, 6H).

^{13}C NMR (100 MHz, $CDCl_3$) δ; 149.0, 144.8, 133.1, 129.8, 128.0, 121.7, 115.0, 70.8, 70.8, 69.8, 69.3, 68. 9, 68.7, 21.6 ppm.

MS (TOF- ESI): m/z: Calcd: 705.20099 $[M+Na]^+$, Found:705.20470$[M+Na]^+$, Δ:-5.26 ppm

Compound 72

Under argon atmosphere, 3,4-dihydroxybenzaldehyde (1.38 g, 10 mmol), K_2CO_3 (16.3 g, 50 mmol) were mixed in THF (300 mL). The mixture was heated under reflux for 1 h, then compound **71** (6.83 g, 10 mmol) in THF (100 mL) was added. The reaction mixture was heated under reflux for 24 h. After cooling to room temperature the solvent was removed by evaporation. The residue was dissolved in DCM (200 mL) and washed with 1 M HCl and saturated NaCl aqueous solutions. The organic layer was dried over Na_2SO_4 and concentrated by evaporation. The

crude product was purified by column chromatography (Silica gel, EtOAC/MEOH: 10/1). Compound **72** was obtained as off-white solid.

^{1}H NMR (400 MHz, $CDCl_3$): δ; 9.77 (s, 1H), 7.40-7.33 (m, 2H), 6.92 -6.82 (m, 5H), 4.19 -4.11 (m, 8H), 3.92-3.78 (m, 16H).

^{13}C NMR (100 MHz, $CDCl_3$) δ; 190.8, 154.3, 149.2, 148.9, 148.9, 130.2, 126.7, 121.4, 121.4, 114.1, 112.0, 111.2, 71.5, 71.4, 71.3, 69.9, 69.7, 69.5, 69.4, 69.4, 69.3 ppm.

MS (TOF- ESI): m/z: Calcd: 499.19385$[M+Na]^+$, Found: 499.19847$[M+Na]^+$, Δ:-9,31 ppm.

Compound 73

CH_2Cl_2 (300 ml) was purged with Argon for 30 min. Compound **72** (500 mg, 1.04 mmol) and 3-ethyl-2,4-dimethyl pyrrole (0.33 mL, 2.41 mmol) were added. The color of the solution turned into red after the addition of 2 drops of trifluoroacetic acid. The reaction mixture was stirred at room temperature overnight. Then, *p*-chloranil (283mg, 1.15 mmol) was added and the reaction mixture was stirred at room temperature for 2 h. Then triethyl amine (1.3 mL) and boron trifluoride diethyl etherate (1.3 mL) were added sequentially. After stirring at room temperature for 30 min, the reaction mixture was extracted with water. Organic layer was dried over Na_2SO_4 and concentrated by evaporation. The crude product was purified by column chromatography (Slica gel, EtOAC/Hexane: 2/1 (v/v)). Compound **73** was obtained as red solid.

^{1}H NMR (400 MHz, $CDCl_3$): δ; 6.98-6.90 (m, 5H), 6.82 (d, *J*=8 Hz, 2H), 4.24-4.17 (m, 6H), 4.15-4.11 (m, 2H), 3.87- 4.02 (m, 16H), 2.54 (s, 6H), 2.32 (q, *J*= 8 Hz, 4H), 1.38 (s, 6H), 1.00 (t, *J*= 8 Hz, 6H).

^{13}C NMR (100 MHz, $CDCl_3$) δ: 153.63, 149.58, 149.30, 149.00, 139.9, 138.42, 132.68, 131.01, 128.45, 121.50, 121.47, 114.20, 114.17, 113.85, 71.47, 71.40, 71.30, 69.98, 69.91, 69.87, 69.59, 69.45, 69.40, 69.31, 17.06, 14.59, 12.47, 11.79 ppm.

MS (TOF- ESI): m/z: Calcd: 772.37916 $[M+Na]^+$, Found: 772.38675$[M+Na]^+$, Δ:-9.86 ppm.

Compound 74

Compound **73** (259 mg, 0.345 mmol) and 4-methoxy benzaldehyde (105 µL, 0.862 mmol) were dissolved in benzene (40 mL). Piperidine (0.32 mL) and acetic acid (0.32 mL) were added to the reaction mixture. The reaction mixture was refluxed using Dean Stark apparatus until all aldehyde was consumed. After the reaction was completed, it was extracted with DCM and water. Organic layer was dried over Na_2SO_4 and concentrated by evaporation. The crude product was purified by silica gel column chromatography (first DCM/ MeOH: 95/5 then EtOAC/Hexane: 2/1 (v/v)). Compound **74** was obtained as green solid.

^{1}H NMR (400 MHz, CDCl3): δ; 7.68 (d, *J*=16,8 Hz, 2H), 7.59 (d, *J*= 7.6 Hz, 4 H), 7.23 (d, J= 16 Hz, 2H), 7.01-7.91 (m, 9 H), 6.85 (d, *J*=10 Hz, 2 H),4.29-4.12 (m, 10H), 4.01-3.91 (m, 14H), 3.88 (s, 6H), 4.02 (q, *J*=8 Hz, 4H), 1.43 (s, 6H), 1.18 (t, *J*= 8Hz, 6H).

^{13}C NMR (100 MHz, CDCl3) δ: 160.2, 150.4, 149.6, 149.4, 138.8, 137.7, 135.3, 133.5, 130.4, 128.8, 121.5,121.5, 118.2, 114.2, 71.5, 71.4, 71.3, 71.3, 70.0, 69.9, 69.9, 69.6, 69.5, 69.4, 69.4, 55.4, 29.7, 18.4, 14.0, 11.6 ppm.

MS (TOF- ESI): m/z: Calcd: 985.47312 M^*, Found: 985.46501 M^*, Δ: 8.23 ppm.

Compound 76

To a solution of K_2CO_3 (1.50 g, 7.3 mmol) in acetonitrile (100 ml), 4-hydroxybenzaldehyde (0.1 g, 0.82 mmol) and propargyl bromide (0.11 g, 0.90 mmol) was added and the mixture was refluxed for 2 d under argon atmosphere, then, the reaction mixture was cooled and concentrated under reduced pressure. The residue was dissolved in CH_2Cl_2 (100 ml) and filtrated, then, washed with water (100 ml) three times. The organic phase was dried with Na_2SO_4 and concentrated under

reduced pressure. The crude product was purified by column chromatography (eluent: $CHCl_3$) to afford white solid. (0.98 g, 74%)

^{1}H NMR (400 MHz, $CDCl_3$) δ; 9.90 (s, 1H), 7.85 (d, *J* = 8.5 Hz, 2H), 7.09 (d, *J* = 8.5 Hz, 2H), 4.78 (s, 2H), 2.59 (s, 1H).

^{13}C NMR (100 MHz, $CDCl_3$) δ; 190.6, 162.4, 132.3, 130.59, 115.16, 77.58, 76.40, 56.11.

MS (TOF- ESI): m/z: Calcd: 161.05971 $[M+H]^+$, Found: 161.05090 $[M+H]^+$, Δ: 54.68 ppm.

Compound 78

Compound **76** (0.43 g, 2.67 mmol) and compound **77** (0.43 g, 2.67 mmol) were mixed in methanol (20 ml) and refluxed for 24 h, then, the reaction mixture was cooled to 0^{o}C and $NaBH_4$ (1.0 g, 26.4 mmol) was added portion wise. The reaction mixture was stirred at room temperature for 24 h. Water was added to the reaction and the mixture was concentrated under vacuum pressure. The residue was dissolved in CH_2Cl_2 (100 ml) and was washed with water (100 ml) three times. The organic phase was dried with Na_2SO_4 and concentrated under reduced pressure. The crude product was purified by column chromatography (eluent: 100:1 DCM/MeOH) to afford yellow oil. (0.50 g, 61%)

^{1}H NMR (400 MHz, $CDCl_3$) δ; 7.30 (d, *J* = 8.4 Hz, 4H), 6.97 (d, *J* = 8.5 Hz, 4H), 4.69 (d, *J* = 2.3 Hz, 4H), 3.76 (s, 4H), 2.56 (t, *J* = 2.3 Hz, 2H).

^{13}C NMR (100 MHz, $CDCl_3$) δ; 156.7, 133.4, 129.4, 114.9, 78.8, 75.65, 55.9, 52.4.

MS (TOF- ESI): m/z: Calcd: 306.14886 M^*, Found: 306.14327 M^*, Δ: 18.24 ppm.

Compound 79

Compound **78** (0.50 g, 1.61 mmol) was dissolved in methanol (15 ml) and concentrated HCl was added to adjust pH lower than 2, then, the solvent was

removed in vacuo. The reaction residue was dissolved in acetone (15 ml) and a saturated solution of NH_4PF_6 was added drop wise until the reaction mixture became clear. The solvent was removed under reduced pressure and water was added to the residue. The resulting mixture was filtered and washed with water several times and dried to give white solid. (0.68 g, 94%)

^{1}H NMR (400 MHz, MeOD) δ; 7.44 (d, *J* = 8.7 Hz, 4H), 7.07 (d, *J* = 8.8 Hz, 4H), 4.77 (d, *J* = 2.4 Hz, 4H), 4.18 (s, 4H), 2.95 (t, *J* = 2.4 Hz, 2H).

^{13}C NMR (100 MHz, MeOD) δ; 158.63, 131.22, 123.72, 115.24, 78.08, 75.67, 55.33, 50.03.

MS (TOF- ESI): m/z: $[M–PF_6]+$ Calcd: $C_{20}H_{20}NO_2$ 306.1494 M; found: 306.15104 M, Δ: -5.34 ppm.

Compound 80

4-hydroxybenzaldehyde (1.0 g, 8.20 mmol), 1,6-dibromo hexane (2.2 g, 9.0 mmol) and K_2CO_3 (2.12 g, 14.5 mmol) were refluxed in freshly distilled acetone (50 ml) for 48 h under argon atmosphere, then, the reaction mixture was cooled and concentrated under reduced pressure. The crude product was dissolved in CH_2Cl_2 (100 ml) and washed with water (100 ml) three times. The organic layer was dried with Na_2SO_4 and concentrated under reduced pressure. The crude product was purified by column chromatography (eluent: 3:1 Hexane/EtOAc) to afford yellow oil. (0.94 g, 40%)

^{1}H NMR (400 MHz, $CDCl_3$) δ; 9.89 (s, 1H), 7.84 (d, *J* = 8.7 Hz, 2H), 7.00 (d, *J* = 8.7 Hz, 2H), 4.06 (t, *J* = 6.4 Hz, 2H), 3.44 (t, *J* = 6.7 Hz, 2H), 2.12 – 1.81 (m, 4H), 1.61 – 1.44 (m, 4H).

^{13}C NMR (100 MHz, $CDCl_3$) δ; 190.8, 164.1, 132.0, 129.8, 114.7, 68.1, 33.7, 32.6, 28.9, 27.9, 25.2.

MS (TOF- ESI): m/z: Calcd: 285.04847 $[M+H]^+$, Found: 285.04886 $[M+H]^+$, Δ: -1.37 ppm.

Compound 81

Argon gas bubbled through CH_2Cl_2 (200 ml) for 30 min then compound **80** (0.50 g, 1.75 mmol) and 3-ethyl-2,4-dimethyl pyrrole (0.52 g, 4.21 mmol) was dissolved in it. Finally, 3 drops of TFA was added. The reaction mixture was stirred at room temperature over night. Then, *p*-chloranil (0.43 g, 1.75 mmol) was added and the mixture was stirred additional 1h. Et_3N (3.0 ml) was added drop wise over a period of 15 min following $BF_3.OEt_2$ (3.0 ml) was added drop wise over a period of 30 min. The resulting dark colored solution was stirred for 2 h at room temperature. The reaction mixture was washed with water (100 ml) three times. The organic layer was dried with Na_2SO_4 and concentrated under reduced pressure. The crude product was purified by column chromatography (eluent: $CHCl_3$) to afford dark red solid (0.30 g, 31%).

^{1}H NMR (400 MHz, $CDCl_3$) δ; 7.17 (d, *J* = 8.6 Hz, 2H), 7.01 (d, *J* = 8.6 Hz, 2H), 4.05 (t, *J* = 6.4 Hz, 2H), 3.47 (t, *J* = 6.8 Hz, 2H), 2.55 (s, 6H), 2.32 (q, *J* = 7.5 Hz, 4H), 2.01 – 1.83 (m, 4H), 1.62 – 1.54 (m, 4H), 1.36 (s, 6H), 1.00 (t, *J* = 7.5 Hz, 6H).

^{13}C NMR (100 MHz, $CDCl_3$) δ; 159.5, 153.6, 140.5, 138.9, 132.7, 131.1, 129.5, 127.8, 115.0, 67.9, 33.8, 32.7, 29.1, 28.0, 25.3, 17.1, 14.6, 12.5, 11.9.

MS (TOF- ESI): m/z: Calcd: 580.21572 $[M+Na]^+$, Found: 580.22127 $[M+Na]^+$, Δ: -9.57 ppm.

Compound 82

Compound **81** (0.40 g, 0.72 mmol) and NaN_3 (0.12 g, 1.79 mmol) were dissolved in DMSO (20 ml) and the reaction mixture was heated to 100 ^oC for 2 h. The reaction was controlled by TLC. When the reaction was complete, it was cooled to room temperature and $CHCl_3$ (100 ml) was added and washed with water (100 ml) six times. The organic layer was dried with Na_2SO_4 and concentrated under reduced pressure. The crude product was used without further purification. Dark red solid (0.35 g, 97%) was afforded.

^{1}H NMR (400 MHz, $CDCl_3$) δ; 7.17 (d, *J* = 8.4 Hz, 2H), 7.01 (d, *J* = 8.4 Hz, 2H), 4.04 (t, *J* = 6.4 Hz, 2H), 3.32 (t, *J* = 6.8 Hz, 2H), 2.55 (s, 6H), 2.32 (q, *J* = 7.5 Hz, 4H), 1.94 – 1.80 (m, 2H), 1.71-1.64 (m, 2H), 1.61 – 1.49 (m, 4H), 1.36 (s, 6H), 1.00 (t, *J* = 7.5 Hz, 6H).
^{13}C NMR (100 MHz, $CDCl_3$) δ; 159.5, 153.5, 140.4, 138.4, 132.6, 131.2, 129.4, 127.8, 115.0, 67.9, 51.4, 29.1, 28.8, 26.6, 25.7, 17.1, 14.6, 12.5, 11.8.

MS (TOF- ESI): m/z: Calcd: 521.32466 $[M+H]^+$, Found: 521.32041 $[M+H]^+$, Δ: 8.14 ppm.

Compound 83

A solution of compound **74** (326 mg, 0.33 mmol) and compound **79** (100 mg, 0.22 mmol) was dissolved in degassed DCM (15 ml) and stirred at room temperature for 4 hours. Then, compound **82** (252 mg, 0.48 mmol) in 5 ml of DCM and $Cu(CH_3CN)_4PF_6$ (74 mg, 0.20 mmol) and 2,6-lutidine (5 μL, 0.107 mmol) were added. The resulting mixture was stirred at room temperature for 1 day. After 1 day, DCM (25 ml) was added to reaction mixture and it was washed with water (30 ml). The organic layer was dried with Na_2SO_4 and concentrated under reduced pressure. The crude product was purified with column chromatography over silica gel (9:1 DCM/MeOH). Compound **83** was afforded as dark purple solid (175 mg, 32%) was afforded.

^{1}H NMR (400 MHz, $CDCl_3$): δ_H 7,83 (s, 2H), 7.66 (d, *J*=16.8 Hz, 2H), 7.58 (d, *J*=8.8 Hz, 4H), 7.38 (, *J*=1.2 Hz, 4H), 7.25 (d, *J*= 8. Hz, 2H), 7.15 (d, *J*=8.4 Hz, 4H), 7.05 (d, *J*=8 Hz, 2H), 7 (s, 2H), 6.97 (d, *J*= 4.8 Hz, 4H), 6.94 (d, *J*= 4.8 Hz, 4H), 6.90 (d, *J*=8 Hz, 4H), 6.82 (s, 1H), 6.78-6.73 (m, 2H), 5.19(s, 4H) 4.50 (m, 2H), 4.41 (t, *J*= 7.2 Hz), 4.31-4.26 (m, 2H), 4.19-4.16 m, 2H), 4.11-4.10 (m 2H), 4.05-4.04 (m, 2H), 4.01 (t, *J*= 6.4 Hz, 4H), 395-3.93 (m, 2H), 3.90-3.88 (m, 2H), 3.87 (s, 6H, Ar-OCH_3), 3.73-3.69 (m, 2H), 3.67-364 (m, 2H), 3.52 -3.42 (m, 6H), 3.37-3.34 (m,2H), 2.54 (s, 12H), 2.31 (q, J_1= 7.2 Hz, J_2=7.6 Hz, 10 H), 2.04-1.95 (m, 6H), 1.88-1.80 (m, 6H), 1.47-1.44 (m, 4H), 1.35 (s, 12H), 1.25 (s, 6H), 1.13 (t, *J*=7.2 Hz, 6H), 1.00 (t, *J*=7.2 Hz, 12H).

^{13}C NMR (100 MHz, $CDCl_3$) δ; 160.29, 159.48, 159.02, 153.43, 150.60, 148.53, 148.36, 147.20, 143.23, 140.41, 138.50, 138.30, 135.61, 133.67, 132.61, 130.76, 130.23, 129.42, 128.81, 128.33, 127.71, 123.98, 123.50, 121.97, 118.00, 115.07, 114.98, 114.26, 70.70, 67.82, 61.63, 55.39, 52.07, 50.32, 30.24, 29.70, 29.70, 29.05, 26.30, 25.55, 22.69, 18.36, 17.07, 14.62, 14.02, 12.49, 12.46, 12.44, 11.87, 11.41.

MS (TOF- ESI): m/z: $[M–PF_6]^+$ Calcd: $C_{135}H_{161}B_3F_6N_{13}O_{14}$ 2333.2651; found: 2333.23999, Δ: 10.76 ppm.

EPILOGUE

In this thesis, we proposed new approaches to fluorescent dyes in different areas. Along this way, five different studies were studied by derivatization of fluorescent dyes but mainly BODIPY dyes. Of course, BODIPY dyes with their distinctive properties highly attractable and well preferred fluorescent fluorophores in supramolecular applications as well as in our studies.

In chapter 2, we have demonstrated chemical generation of singlet oxygen. In our design, photosensitizer module consists of two parts: one is erythrosine based photosensitizer and the other one is luminol where chemical excitation starts. In tumor cells, hydrogen peroxide concentration increases. In the presence of hydrogen peroxide, luminol module is chemically excited and transfers its energy to erythrosine part, which is attached covalently. We showed that chemical excitation of a photosensitizer unit is a promising method due to elimination of light source in therapeutic applications.

A novel design of BODIPY based photosensitizers were designed and synthesized in chapter 3. In the design, long alkyl chains substituted to photosensitizer core and stable micelles of designed photosensitizers were studied in aqueous solutions. The synthesized photosensitizers worked effectively in aqueous solutions.

In chapter 4, a BODIPY derivative substituted with four crown units was synthesized. The photophysical properties of designed BODIPY were studied in the presence of alkanes of different chain lengths. The effect of formation of hydrogen bonding was observed successfully in UV-vis and fluorescence spectra in the presence of alkane chains. On the other hand, with the shortest chain of diamino alkanes, PET was quenched due to $\pi-\pi$ stacking.

In chapter 5, a novel fluorescent indicator which could potentially work in bioreductive conditions as hypoxic environment was synthesized. In solution,

reductive environment was provided by sodium borohydride. The reduction of final BODIPY derivative was observed with strong enhancement in emission. Since hypoxia increases in cancer cells, the synthesized probe is promising for tumor imaging purposes.

In the final chapter, a novel BODIPY based mechanically interlocked light harvesting system was designed. Energy transfer was shown to proceed efficiently from two BODIPY derived donor units to B21C7 substituted BODIPY acceptor through a linker with 97% efficiency. The use of mechanical linkage in construction of light harvesting system provided ease of substitution between donor and acceptor units.

To conclude, we reported five studies in different areas: singlet oxygen generation by chemical excitation and by formation of micelles, photophysical studies in the presence of different diamino alkane chains, hypoxia targeting fluorescent indicators and energy transfer cassettes. Our results showed promising results and further work in these areas expected to yield potential outcome.

BIBLIOGRAPHY

[1] D. E. J. G. J. Dolmans, D. Fukumura, and R. K. Jain, "Photodynamic therapy for cancer," *Nat Rev Cancer*, vol. 3, no. 5, pp. 380–387, May 2003.

[2] M. Triesscheijn, P. Baas, J. H. M. Schellens, and F. A. Stewart, "Photodynamic therapy in oncology," *Oncologist*, vol. 11, no. 9, pp. 1034–1044, 2006.

[3] S. Miyamoto, G. E. Ronsein, F. M. Prado, M. Uemi, T. C. Corrêa, I. N. Toma, A. Bertolucci, M. C. B. Oliveira, F. D. Motta, M. H. G. Medeiros, and P. Di Mascio, "Biological hydroperoxides and singlet molecular oxygen generation," *IUBMB Life*, vol. 59, no. 4, pp. 322–331, 2007.

[4] K. J. Davies, "Protein damage and degradation by oxygen radicals. I. general aspects," *J. Biol. Chem.*, vol. 262, no. 20, pp. 9895–9901, 1987.

[5] R. Richards-Kortum and E. Sevick-Muraca, "Quantitative optical spectroscopy for tissue diagnosis," *Annu. Rev. Phys. Chem.*, vol. 47, pp. 555–606, 1996.

[6] J. D. Spikes, *Primary photo-processes in biology and medicine*. Newyork, 1985.

[7] J. S. Daniell, M D; Hill, "A history of photodynamic therapy," *Aust. NZ J Surg*, vol. 61, pp. 340–348, 1991.

[8] O. Raab, "Uber die Wirkung fluoreszierender Stoffe auf Infusorien," *Z. Biol.*, vol. 39, pp. 524–526, 1900.

[9] N. R. Finsen, "Phototherapy," Edward Arnold: London, 1901.

[10] H. Schwartz, S. K., Abolon, K. & Vermund, "Some relationships of porphyrins, X-rays and tumors," *Univ. Minn. Med. Bull*, vol. 27, pp. 7–8, 1955.

[11] A. M. Lipson, R. L., Baldes, E. J. & Olsen, “Hematoporphyrin derivative: a new aid for endoscopic detection of malignant disease,” *J. Thorac. Cardiovasc. Surg.*, vol. 42, pp. 623–629, 1961.

[12] L. R.L. and B. E.J., “THe photodynamic properties of a particular hematoporphyrin derivative,” *Arch. Dermatol.*, vol. 82, no. 4, pp. 508–516, Oct. 1960.

[13] I. Diamond, A. Mcdonagh, C. Wilson, S. Granelli, S. Nielsen, and R. Jaenicke, “Photodynamic theraphu of malignant tumors,” *Lancet*, vol. 300, no. 7788, pp. 1175–1177, 1972.

[14] E. Snell, “Photodynamic destruction of human bladder carcinoma,” *Br. J. Cancer*, vol. 31, no. 2, pp. 237–244, 1975.

[15] T. J. Dougherty, J. E. Kaufman, A. Goldfarb, K. R. Weishaupt, D. Boyle, and A. Mittleman, “Photoradiation therapy for the treatment of malignant tumors,” *Cancer Res.*, vol. 38, no. 8, pp. 2628–2635, Aug. 1978.

[16] S. G. Bown, A. Z. Rogowska, D. E. Whitelaw, W. R. Lees, L. B. Lovat, P. Ripley, L. Jones, P. Wyld, A. Gillams, and A. W. R. Hatfield, “Photodynamic therapy for cancer of the pancreas,” *Gut*, vol. 50, no. 4, pp. 549–57, 2002.

[17] H. I. Pass, T. F. DeLaney, Z. Tochner, P. E. Smith, B. K. Temeck, H. W. Pogrebniak, K. C. Kranda, A. Russo, W. S. Friauf, and J. W. Cole, “Intrapleural photodynamic therapy: results of a phase I trial,” *Ann. Surg. Oncol.*, vol. 1, no. 1, pp. 28–37, Jan. 1994.

[18] R. R. Allison, T. S. Mang, and B. D. Wilson, “Photodynamic therapy for the treatment of nonmelanomatous cutaneous malignancies,” *Semin. Cutan. Med. Surg.*, vol. 17, no. 2, pp. 153–163, Jun. 1998.

[19] M. A. Biel, “Photodynamic therapy of head and neck cancers,” *Methods Mol. Biol.*, vol. 635, pp. 281–293, 2010.

[20] E. A. Popovic, A. H. Kaye, and J. S. Hill, “Photodynamic therapy of brain tumors,” *J. Clin. Laser Med. Surg.*, vol. 14, no. 5, pp. 251–261, Oct. 1996.

[21] M. D. Daniell and J. S. Hill, “A history of photodynamic therapy,” *Aust. N. Z. J. Surg.*, vol. 61, no. 5, pp. 340–348, May 1991.

[22] M. O. Senge and J. C. Brandt, “Temoporfin (Foscan®, 5,10,15,20-tetra(m-hydroxyphenyl)chlorin) a second generation photosensitizer,” *Photochem. Photobiol.*, vol. 87, no. 6, pp. 1240–1296, 2011.

[23] Z. S. Silva, S. K. Bussadori, K. P. S. Fernandes, Y.-Y. Huang, and R. M. Hamblin, “Animal models for photodynamic therapy (PDT),” *Biosci. Rep.*, vol. 35, pp. 1–14, 2015.

[24] N. L. Oleinick, R. L. Morris, and I. Belichenko, “The role of apoptosis in response to photodynamic therapy: what, where, why, and how,” *Photochem. Photobiol. Sci.*, vol. 1, no. 1, pp. 1–21, 2002.

[25] B. W. Henderson and T. J. Dougherty, “How does photodynamic theraphy work?,” *Photochem. Photobiol.*, vol. 55, no. 1, pp. 145–157, Jan. 1992.

[26] F. Cairnduff, M. R. Stringer, E. J. Hudson, D. V Ash, and S. B. Brown, “Superficial photodynamic therapy with topical 5-aminolaevulinic acid for superficial primary and secondary skin cancer,” *Br. J. Cancer*, vol. 69, no. 3, pp. 605–608, 1994.

[27] M. J. Davies, “Singlet oxygen-mediated damage to proteins and its consequences,” *Biochem. Biophys. Res. Commun.*, vol. 305, no. 3, pp. 761–770, Jun. 2003.

[28] S. Pervaiz and M. Olivo, “Art and science of photodynamic therapy,” *Clin. Exp. Pharmacol. Physiol.*, vol. 33, no. 5–6, pp. 551–556, 2006.

[29] A. Castano, P. Mroz, and M. Hamblin, “Photodynamic therapy and anti-tumour immunity,” *Nat. Rev. Cancer*, vol. 6, no. 7, pp. 535–545, 2006.

[30] N. J. Turro, *In modern molecular photochemistry*. University Science Books: Sausalito, CA, 1991.

[31] S. K. Lower and M. A. El-Sayed, “The Triplet State and Molecular Electronic Processes in Organic Molecules,” *Chem. Rev.*, vol. 66, no. 2, pp. 199–241, Apr. 1966.

[32] P. Agostinis, K. Berg, K. A. Cengel, T. H. Foster, A. W. Girotti, S. O. Gollnick, S. M. Hahn, M. R. Hamblin, A. Juzeniene, D. Kessel, M. Korbelik, J. Moan, P. Mroz, D. Nowis, J. Piette, B. C. Wilson, and J. Golab, “Photodynamic therapy of cancer: An update,” *CA. Cancer J. Clin.*, vol. 61, no. 4, pp. 250–81, Jan. .

[33] A. Nowak-Stepniowska, P. Pergol, and A. Padzik-Graczyk, “Photodynamic method of cancer diagnosis and therapy: Mechanisms and applications,” *Postepy Biochem.*, vol. 59, no. 1, pp. 53–63, 2013.

[34] V. J. Pansare, S. Hejazi, W. J. Faenza, and R. K. Prud’homme, “Review of long-wavelength optical and NIR imaging materials: contrast agents, fluorophores, and multifunctional nano carriers,” *Chem. Mater.*, vol. 24, no. 5, pp. 812–827, 2012.

[35] J. F. Lovell, T. W. B. Liu, J. Chen, and G. Zheng, “Activatable photosensitizers for imaging and therapy,” *Chem. Rev.*, vol. 110, no. 5, pp. 2839–2857, May 2010.

[36] T. C. Zhu and J. C. Finlay, “The role of photodynamic therapy (PDT) physics,” *Med. Phys.*, vol. 35, no. 7, pp. 3127–3136, Jul. 2008.

[37] H. He, P.-C. Lo, and D. K. P. Ng, “A glutathione-activated phthalocyanine-based photosensitizer for photodynamic therapy,” *Chemistry*, vol. 20, no. 21, pp. 6241–5, May 2014.

[38] J. L. Sessler, T. Murai, V. Lynch, and M. Cyr, “An ‘expanded porphyrin’: the

synthesis and structure of a new aromatic pentadentate ligand," *J. Am. Chem. Soc.*, vol. 110, no. 16, pp. 5586–5588, Aug. 1988.

[39] R. A. Sessler, J.L. and Miller, "Texaphyrins: New drugs with diverse clinical applications in radiation and photodynamic therapy," *Biochem. Pharmacol.*, vol. 59, pp. 733–739, 2000.

[40] P. Jichlinski and H. J. Leisinger, "Photodynamic therapy in superficial bladder cancer: past, present and future," *Urol. Res.*, vol. 29, no. 6, pp. 396–405, Dec. 2001.

[41] P. Puolakkainen and T. Schroder, "Photodynamic therapy of gastrointestinal tumors: a review," *Dig. Dis.*, vol. 10, no. 1, pp. 53–60, 1992.

[42] R. L. Prosst, H. C. Wolfsen, and J. Gahlen, "Photodynamic therapy for esophageal diseases: a clinical update," *Endoscopy*, vol. 35, no. 12, pp. 1059–1068, Dec. 2003.

[43] M. G. Dilkes, E. Benjamin, S. Ovaisi, and A. S. Banerjee, "Treatment of primary mucosal head and neck squamous cell carcinoma using photodynamic therapy: results after 25 treated cases," *J. Laryngol. Otol.*, vol. 117, no. 9, pp. 713–717, Sep. 2003.

[44] P. Baas, A. E. Saarnak, H. Oppelaar, H. Neering, and F. A. Stewart, "Photodynamic therapy with meta-tetrahydroxyphenylchlorin for basal cell carcinoma: a phase I/II study," *Br. J. Dermatol.*, vol. 145, no. 1, pp. 75–78, Jul. 2001.

[45] V. Gayl Schweitzer, "Photofrin-mediated photodynamic therapy for treatment of aggressive head and neck nonmelanomatous skin tumors in elderly patients," *Laryngoscope*, vol. 111, no. 6, pp. 1091–1098, Jun. 2001.

[46] N. C. Zeitouni, A. R. Oseroff, and S. Shieh, "Photodynamic therapy for nonmelanoma skin cancers. Current review and update.," *Mol. Immunol.*, vol.

39, no. 17–18, pp. 1133–1136, Jul. 2003.

[47] T.-W. Wong, K. Aizawa, I. Sheyhedin, C. Wushur, and H. Kato, “Pilot study of topical delivery of mono-L-aspartyl chlorin e6 (NPe6): implication of topical NPe6-photodynamic therapy,” *J. Pharmacol. Sci.*, vol. 93, no. 2, pp. 136–142, Oct. 2003.

[48] Z. Huang, “A review of progress in clinical photodynamic therapy,” *Technol. Cancer Res. Treat.*, vol. 4, no. 3, pp. 283–293, Jun. 2005.

[49] T. Yogo, Y. Urano, Y. Ishitsuka, F. Maniwa, and T. Nagano, “Highly efficient and photostable photosensitizer based on BODIPY chromophore,” *J. Am. Chem. Soc.*, vol. 127, no. 35, pp. 12162–12163, Sep. 2005.

[50] K. Umezawa, Y. Nakamura, H. Makino, D. Citterio, and K. Suzuki, “Bright, color-Tunable fluorescent dyes in the visible−Near-Infrared region,” *J. Am. Chem. Soc.*, vol. 130, no. 5, pp. 1550–1551, Feb. 2008.

[51] W. M. Gallagher, L. T. Allen, C. O’Shea, T. Kenna, M. Hall, A. Gorman, J. Killoran, and D. F. O’Shea, “A potent nonporphyrin class of photodynamic therapeutic agent: cellular localisation, cytotoxic potential and influence of hypoxia,” *Br J Cancer*, vol. 92, no. 9, pp. 1702–1710, Apr. 2005.

[52] J. Killoran, L. Allen, J. F. Gallagher, W. M. Gallagher, and D. F. or minute]Shea, “Synthesis of BF2 chelates of tetraarylazadipyrromethenes and evidence for their photodynamic therapeutic behaviour,” *Chem. Commun.*, no. 17, pp. 1862–1863, 2002.

[53] S. Atilgan, Z. Ekmekci, A. L. Dogan, D. Guc, and E. U. Akkaya, “Water soluble distyryl-Boradiazaindacenes as efficient photosensitizers for photodynamic therapy,” *Chem. Commun.*, no. 42, pp. 4398–4400, 2006.

[54] S. Ozlem and E. U. Akkaya, “Thinking outside the silicon box: Molecular AND logic as an additional layer of selectivity in singlet oxygen generation

for photodynamic therapy," *J. Am. Chem. Soc.*, vol. 131, no. 1, pp. 48–49, Jan. 2009.

[55] R. Laptev, M. Nisnevitch, G. Siboni, Z. Malik, and M. A. Firer, "Intracellular chemiluminescence activates targeted photodynamic destruction of leukaemic cells," *Br. J. Cancer*, vol. 95, no. 2, pp. 189–196, Jul. 2006.

[56] S. Yano, S. Hirohara, M. Obata, Y. Hagiya, S. Ogura, A. Ikeda, H. Kataoka, M. Tanaka, and T. Joh, "Current states and future views in photodynamic therapy," *J. Photochem. Photobiol. C Photochem. Rev.*, vol. 12, no. 1, pp. 46–67, 2011.

[57] M. Ethirajan, Y. Chen, P. Joshi, and R. K. Pandey, "The role of porphyrin chemistry in tumor imaging and photodynamic therapy," *Chem. Soc. Rev.*, vol. 40, no. 1, pp. 340–362, Jan. 2011.

[58] C. M. Magalhaes, J. C. G. Esteves da Silva, and L. Pinto da Silva, "Chemiluminescence and bioluminescence as an excitation source in the photodynamic therapy of cancer: A critical review," *Chemphyschem*, vol. 17, no. 15, pp. 2286–2294, Aug. 2016.

[59] M. Bancirova and J. Lasovsky, "The photodynamic effect: The comparison of chemiexcitation by luminol and phthalhydrazide," *Luminescence*, vol. 26, no. 6, pp. 410–415, 2011.

[60] Y. R. Kim, S. Kim, J. W. Choi, S. Y. Choi, S.-H. Lee, H. Kim, S. K. Hahn, G. Y. Koh, and S. H. Yun, "Bioluminescence-activated deep-tissue photodynamic therapy of cancer," *Theranostics*, vol. 5, no. 8, pp. 805–817, 2015.

[61] H. Yuan, H. Chong, B. Wang, C. Zhu, L. Liu, Q. Yang, F. Lv, and S. Wang, "Chemical molecule-induced light-activated system for anticancer and antifungal activities," *J. Am. Chem. Soc.*, vol. 134, no. 32, pp. 13184–13187, Aug. 2012.

[62] M. L. Schipper, M. R. Patel, and S. S. Gambhir, “Evaluation of firefly luciferase bioluminescence mediated photodynamic toxicity in cancer cells,” *Mol. Imaging Biol.*, vol. 8, no. 4, pp. 218–225, 2006.

[63] C.-Y. Hsu, C.-W. Chen, H.-P. Yu, Y.-F. Lin, and P.-S. Lai, “Bioluminescence resonance energy transfer using luciferase-immobilized quantum dots for self-illuminated photodynamic therapy,” *Biomaterials*, vol. 34, no. 4, pp. 1204–1212, Jan. 2013.

[64] T. Theodossiou, J. S. Hothersall, E. A. Woods, K. Okkenhaug, J. Jacobson, and A. J. MacRobert, “Firefly luciferin-activated Rose Bengal: In vitro photodynamic therapy by intracellular chemiluminescence in transgenic NIH 3T3 cells,” *Cancer Res.*, vol. 63, no. 8, pp. 1818–1821, Apr. 2003.

[65] L. Pinto da Silva and J. C. G. Esteves da Silva, “Firefly chemiluminescence and bioluminescence: efficient generation of excited states,” *Chemphyschem*, vol. 13, no. 9, pp. 2257–2262, Jun. 2012.

[66] I. Navizet, Y.-J. Liu, N. Ferre, D. Roca-Sanjuan, and R. Lindh, “The chemistry of bioluminescence: an analysis of chemical functionalities,” *Chemphyschem*, vol. 12, no. 17, pp. 3064–3076, Dec. 2011.

[67] J. Vieira, L. Pinto da Silva, and J. C. G. Esteves da Silva, “Advances in the knowledge of light emission by firefly luciferin and oxyluciferin,” *J. Photochem. Photobiol. B Biol.*, vol. 117, pp. 33–39, Dec. 2012.

[68] L. P. da Silva and J. C. G. Esteves da Silva, “Computational studies of the Luciferase light-emitting product: Oxyluciferin,” *J. Chem. Theory Comput.*, vol. 7, no. 4, pp. 809–817, Apr. 2011.

[69] T. Hirano, “The reaction mechanism of calcium-activated photoprotein bioluminescence,” *Curr. Pharm. Biotechnol.*, vol. 13, no. 14, pp. 2551–2561, Nov. 2012.

[70] M. Matsumoto, “Advanced chemistry of dioxetane-based chemiluminescent substrates originating from bioluminescence,” *J. Photochem. Photobiol. C Photochem. Rev.*, vol. 5, no. 1, pp. 27–53, 2004.

[71] F. A. Augusto, G. A. de Souza, S. P. de Souza Junior, M. Khalid, and W. J. Baader, “Efficiency of electron transfer initiated chemiluminescence,” *Photochem. Photobiol.*, vol. 89, no. 6, pp. 1299–1317, 2013.

[72] L. Pinto da Silva and J. C. G. Esteves da Silva, “Interstate crossing-induced chemiexcitation as the reason for the chemiluminescence of dioxetanones,” *Chemphyschem*, vol. 14, no. 5, pp. 1071–1079, Apr. 2013.

[73] L. H. Catalani and T. Wilson, “Electron transfer and chemiluminescence. Two inefficient systems: 1,4-dimethoxy-9,10-diphenylanthracene peroxide and diphenoyl peroxide,” *J. Am. Chem. Soc.*, vol. 111, no. 7, pp. 2633–2639, Mar. 1989.

[74] L. Yue, Y.-J. Liu, and W.-H. Fang, “Mechanistic insight into the chemiluminescent decomposition of firefly dioxetanone,” *J. Am. Chem. Soc.*, vol. 134, no. 28, pp. 11632–11639, Jul. 2012.

[75] G. Merenyi, J. Lind, and T. E. Eriksen, “Luminol chemiluminescence: chemistry, excitation, emitter,” *J. Biolumin. Chemilumin.*, vol. 5, no. 1, pp. 53–56, 1990.

[76] A. L. Rose and T. D. Waite, “Chemiluminescence of luminol in the presence of iron(II) and oxygen: oxidation mechanism and implications for its analytical use,” *Anal. Chem.*, vol. 73, no. 24, pp. 5909–5920, Dec. 2001.

[77] A. Gaikwad, M. Silva, and D. Perez-Bendito, “Selective stopped-flow determination of manganese with luminol in the absence of hydrogen peroxide,” *Anal. Chim. Acta*, vol. 302, no. 2–3, pp. 275–282, 1995.

[78] V. Balzani, A. Credi, and M. Venturi, “Light-harvesting antennae,” in

Molecular Devices and Machines – A Journey into the Nano World, Wiley-VCH Verlag GmbH & Co. KGaA, 2004, pp. 96–131.

[79] N. J. Turro, *Modern molecular photochemistry*. University Science Books, Sausalito, 1991.

[80] T. Forster, "10th Spiers Memorial Lecture. Transfer mechanisms of electronic excitation," *Discuss. Faraday Soc.*, vol. 27, no. 0, pp. 7–17, 1959.

[81] T. Forster, "Energiewanderung und fluoreszenz," *Naturwissenschaften*, vol. 33, no. 6, pp. 166–175, 1946.

[82] F. Barigelletti and L. Flamigni, "Photoactive molecular wires based on metal complexes," *Chem. Soc. Rev.*, vol. 29, no. 1, pp. 1–12, 2000.

[83] G. D. Scholes, "Long-range resonance energy transfer in molecular systems," *Annu. Rev. Phys. Chem.*, vol. 54, pp. 57–87, 2003.

[84] R. M. Clegg, "The history of FRET : From conception through the labors of birth," *Rev. Fluoresc.*, vol. 3, pp. 1–45, 2006.

[85] "Fluorescence resonance energy transfer (FRET)." [Online]. Available: https://www.thermofisher.com/tr/en/home/references/molecular-probes-the-handbook/technical-notes-and-product-highlights/fluorescence-resonance-energy-transfer-fret.html. [Accessed: 21-Aug-2016].

[86] B. Valeur, *Molecular fluorescence, principles and applications*. Wiley-WC, 2002.

[87] M. D. Yilmaz, O. A. Bozdemir, and E. U. Akkaya, "Light harvesting and efficient energy transfer in a Boron-dipyrrin (BODIPY) functionalized perylenediimide derivative," *Org. Lett.*, vol. 8, no. 13, pp. 2871–2873, Jun. 2006.

[88] D. L. Dexter, "A theory of sensitized luminescence in solids," *J. Chem. Phys.*,

vol. 21, p. 836, 1953.

[89] C.-W. Wan, A. Burghart, J. Chen, F. Bergström, L. B.-Å. Johansson, M. F. Wolford, T. G. Kim, M. R. Topp, R. M. Hochstrasser, and K. Burgess, "Anthracene–BODIPY cassettes: Syntheses and energy transfer," *Chem. – A Eur. J.*, vol. 9, no. 18, pp. 4430–4441, 2003.

[90] A. Harriman, L. J. Mallon, K. J. Elliot, A. Haefele, G. Ulrich, and R. Ziessel, "Length dependence for intramolecular energy transfer in three- and four-color donor−spacer−acceptor arrays," *J. Am. Chem. Soc.*, vol. 131, no. 37, pp. 13375–13386, 2009.

[91] P. F. Barbara, "Molecular machines special issue," *Acc. Chem. Res.*, vol. 34, no. 6, p. 409, Jun. 2001.

[92] P. L. Anelli, N. Spencer, and J. F. Stoddart, "A molecular shuttle," *J. Am. Chem. Soc.*, vol. 113, no. 13, pp. 5131–5133, Jun. 1991.

[93] M. Cavallini, F. Biscarini, S. Léon, F. Zerbetto, G. Bottari, and D. A. Leigh, "Information storage using supramolecular surface patterns," *Science (80-.).*, vol. 299, no. 5606, p. 531 LP-531, Jan. 2003.

[94] C. J. Easton, S. F. Lincoln, L. Barr, and H. Onagi, "Molecular reactors and machines: applications, potential, and limitations," *Chemistry*, vol. 10, no. 13, pp. 3120–8, Jul. 2004.

[95] V. Balzani, M. Gómez-López, and J. F. Stoddart, "Molecular machines," *Acc. Chem. Res.*, vol. 31, no. 7, pp. 405–414, Jul. 1998.

[96] H. Murakami, A. Kawabuchi, K. Kotoo, M. Kunitake, and N. Nakashima, "A light-driven molecular shuttle based on a rotaxane," *J. Am. Chem. Soc.*, vol. 119, no. 32, pp. 7605–7606, Aug. 1997.

[97] N. Armaroli, V. Balzani, J.-P. Collin, P. Gaviña, J.-P. Sauvage, and B. Ventura, "Rotaxanes Incorporating Two Different Coordinating Units in Their

Thread: Synthesis and Electrochemically and Photochemically Induced Molecular Motions," *J. Am. Chem. Soc.*, vol. 121, no. 18, pp. 4397–4408, May 1999.

[98] T. Ogoshi, D. Yamafuji, T. Yamagishi, and A. M. Brouwer, "Forster resonance energy transfer by formation of a mechanically interlocked [2]rotaxane," *Chem. Commun.*, vol. 49, no. 48, pp. 5468–5470, 2013.

[99] H. Onagi and J. Rebek, Jr., "Fluorescence resonance energy transfer across a mechanical bond of a rotaxane," *Chem. Commun.*, no. 36, pp. 4604–4606, 2005.

[100] Z. Xu, J. Yoon, and D. R. Spring, "Fluorescent chemosensors for Zn(2+).," *Chem. Soc. Rev.*, vol. 39, no. 6, pp. 1996–2006, Jun. 2010.

[101] K. Rurack and U. Resch-Genger, "Rigidization, preorientation and electronic decoupling. The 'magic triangle' for the design of highly efficient fluorescent sensors and switches," *Chem. Soc. Rev.*, vol. 31, no. 2, pp. 116–127, Mar. 2002.

[102] B. Valeur and I. Leray, "Design principles of fluorescent molecular sensors for cation recognition," *Coord. Chem. Rev.*, vol. 205, no. 1, pp. 3–40, 2000.

[103] H. G. Loehr and F. Voegtle, "Chromo- and fluoroionophores. A new class of dye reagents," *Acc. Chem. Res.*, vol. 18, no. 3, pp. 65–72, 1985.

[104] N. Mateeva, V. Enchev, L. Antonov, T. Deligeorgiev, and M. Mitewa, "Spectroscopic study of the complexation of an zza-15-crown-5 containing chromofluoroionophore with Ba2+ and Ca2+ cations," *J. Incl. Phenom. Mol. Recognit. Chem.*, vol. 20, no. 4, pp. 323–333, 1994.

[105] M. M. Martin, P. Plaza, Y. H. Meyer, L. Bégin, J. Bourson, and B. Valeur, "A new concept of photogeneration of cations: Evidence for photoejection of Ca2+ and Li+ from complexes with a crown-ether-linked merocyanine by

picosecond spectroscopy," *J. Fluoresc.*, vol. 4, no. 4, pp. 271–273, 1994.

[106] C. N. Baki and E. U. Akkaya, "Boradiazaindacene-appended calix[4]arene: Fluorescence sensing of pH near neutrality," *J. Org. Chem.*, vol. 66, no. 4, pp. 1512–1513, Feb. 2001.

[107] A. P. de Silva, H. Q. N. Gunaratne, and K. R. A. S. Sandanayake, "A new benzo-annelated cryptand and a derivative with alkali cation-sensitive fluorescence," *Tetrahedron Lett.*, vol. 31, no. 36, pp. 5193–5196, 1990.

[108] K. Kubo, N. Kato, and T. Sakurai, "Synthesis and complexation behavior of diaza-18-crown-6 carrying two pyrenylmethyl groups," *Bull. Chem. Soc. Jpn.*, vol. 70, no. 12, pp. 3041–3046, 1997.

[109] T. Bioscience, "Based applications: DNA & RNA probes for fluorescence." [Online]. Available: http://taeshinbio.co.kr/bbs/board.php?bo_table=IDT&wr_id=8. [Accessed: 24-May-2017].

[110] A. Baeyer, "Ueber eine neue Klasse von Farbstoffen," *Berichte der Dtsch. Chem. Gesellschaft*, vol. 4, no. 2, pp. 555–558, Jun. 1871.

[111] F. H. Kasten, *Introduction to fluorescent probes: properties, history and applications*. Academic Press, 1999.

[112] D. C. Neckers and O. M. Valdes-Aguilera, "Photochemistry of the Xanthene dyes," in *Advances in Photochemistry*, John Wiley & Sons, Inc., 2007, pp. 315–394.

[113] T. A. Gust, D.; Moore, "Advances in photochemistry," in *Mimicking Photosynthetic Electron and Energy Transfer*, 1991, pp. 1–65.

[114] R. V. Rathod, S. Bera, M. Singh, and D. Mondal, "A colorimetric and fluorometric investigation of Cu(II) ion in aqueous medium with a fluorescein-based chemosensor," *RSC Adv.*, vol. 6, no. 41, pp. 34608–34615,

2016.

[115] Y.-X. Wu, X.-B. Zhang, J.-B. Li, C.-C. Zhang, H. Liang, G.-J. Mao, L.-Y. Zhou, W. Tan, and R.-Q. Yu, “Bispyrene-fluorescein hybrid based FRET cassette: a convenient platform toward ratiometric time-resolved probe for bioanalytical applications,” *Anal. Chem.*, vol. 86, no. 20, pp. 10389–10396, Oct. 2014.

[116] S. H. Lim, C. Thivierge, P. Nowak-Sliwinska, J. Han, H. van den Bergh, G. Wagnières, K. Burgess, and H. B. Lee, “In vitro and In vivo photocytotoxicity of boron dipyrromethene derivatives for photodynamic therapy,” *J. Med. Chem.*, vol. 53, no. 7, pp. 2865–2874, Apr. 2010.

[117] A. Schmitt, B. Hinkeldey, M. Wild, and G. Jung, “Synthesis of the core compound of the BODIPY dye class,” *J. Fluoresc.*, vol. 19, no. 4, pp. 755–758, 2009.

[118] A. Loudet and K. Burgess, “BODIPY dyes and their derivatives: syntheses and spectroscopic properties.,” *Chem. Rev.*, vol. 107, no. 11, pp. 4891–4932, Nov. 2007.

[119] G. Ulrich, R. Ziessel, and A. Harriman, “The chemistry of fluorescent bodipy dyes: versatility unsurpassed,” *Angew. Chem. Int. Ed. Engl.*, vol. 47, no. 7, pp. 1184–201, Jan. 2008.

[120] H. Wang, F. R. Fronczek, M. G. H. Vicente, and K. M. Smith, “Functionalization of 3,5,8-trichlorinated BODIPY dyes,” *J. Org. Chem.*, vol. 79, no. 21, pp. 10342–10352, Nov. 2014.

[121] A. Coskun and E. U. Akkaya, “Difluorobora-s-diazaindacene dyes as highly selective dosimetric reagents for fluoride anions,” 2004.

[122] Z. Dost, S. Atilgan, and E. U. Akkaya, “Distyryl-boradiazaindacenes: facile synthesis of novel near IR emitting fluorophores,” *Tetrahedron*, vol. 62, no.

36, pp. 8484–8488, 2006.

[123] N. Saki, T. Dinc, and E. U. Akkaya, “Excimer emission and energy transfer in cofacial boradiazaindacene (BODIPY) dimers built on a xanthene scaffold,” *Tetrahedron*, vol. 62, no. 11, pp. 2721–2725, 2006.

[124] K. Rurack, M. Kollmannsberger, and J. Daub, “Molecular switching in the near infrared (NIR) with a functionalized boron-dipyrromethene dye,” *Angew. Chem. Int. Ed. Engl.*, vol. 40, no. 2, pp. 385–387, Jan. 2001.

[125] K. Sonogashira, Y. Tohda, and N. Hagihara, “A convenient synthesis of acetylenes: catalytic substitutions of acetylenic hydrogen with bromoalkenes, iodoarenes and bromopyridines,” *Tetrahedron Lett.*, vol. 16, no. 50, pp. 4467–4470, 1975.

[126] G. Ulrich, C. Goze, M. Guardigli, A. Roda, and R. Ziessel, “Pyrromethene dialkynyl borane complexes for ‘cascatelle’ energy transfer and protein labeling,” *Angew. Chem. Int. Ed. Engl.*, vol. 44, no. 24, pp. 3694–8, Jun. 2005.

[127] K. Rurack, M. Kollmannsberger, and J. Daub, “A highly efficient sensor molecule emitting in the near infrared (NIR): 3,5-distyryl-8-(p-dimethylaminophenyl)difluoroboradiaza-s-indacene,” *New J. Chem.*, vol. 25, no. 2, pp. 289–292, 2001.

[128] H. Y. Lee, D. R. Bae, J. C. Park, H. Song, W. S. Han, and J. H. Jung, “A selective fluoroionophore based on BODIPY-functionalized magnetic silica nanoparticles: removal of Pb2+ from human blood,” *Angew. Chem. Int. Ed. Engl.*, vol. 48, no. 7, pp. 1239–43, Jan. 2009.

[129] X. Qi, S. K. Kim, S. J. Han, L. Xu, A. Y. Jee, H. N. Kim, C. Lee, Y. Kim, M. Lee, S.-J. Kim, and J. Yoon, “New BODIPY–triazine based tripod fluorescent systems,” 2008.

[130] R. Guliyev, A. Coskun, and E. U. Akkaya, “Design strategies for ratiometric

chemosensors: modulation of excitation energy transfer at the energy donor site," *J. Am. Chem. Soc.*, vol. 131, no. 25, pp. 9007–9013, Jul. 2009.

[131] O. Buyukcakir, O. A. Bozdemir, S. Kolemen, S. Erbas, and E. U. Akkaya, "Tetrastyryl-Bodipy dyes: Convenient synthesis and characterization of elusive near IR fluorophores," *Org. Lett.*, vol. 11, no. 20, pp. 4644–4647, 2009.

[132] T. Bura, P. Retailleau, G. Ulrich, and R. Ziessel, "Highly substituted bodipy dyes with spectroscopic features sensitive to the environment," *J. Org. Chem.*, vol. 76, no. 4, pp. 1109–1117, 2011.

[133] S. Zhu, J. Zhang, G. Vegesna, A. Tiwari, F.-T. Luo, M. Zeller, R. Luck, H. Li, S. Green, and H. Liu, "Controlled Knoevenagel reactions of methyl groups of 1,3,5,7-tetramethyl BODIPY dyes for unique BODIPY dyes," *RSC Adv.*, vol. 2, no. 2, pp. 404–407, 2012.

[134] P. Agostinis, K. Berg, K. A. Cengel, T. H. Foster, A. W. Girotti, S. O. Gollnick, S. M. Hahn, M. R. Hamblin, A. Juzeniene, D. Kessel, M. Korbelik, J. Moan, P. Mroz, D. Nowis, J. Piette, B. C. Wilson, and J. Golab, "Photodynamic therapy of cancer: An update," *CA. Cancer J. Clin.*, vol. 61, no. 4, pp. 250–281, 2011.

[135] A. E. O'Connor, W. M. Gallagher, and A. T. Byrne, "Porphyrin and nonporphyrin photosensitizers in oncology: Preclinical and clinical advances in photodynamic therapy," *Photochem. Photobiol.*, vol. 85, no. 5, pp. 1053–1074, 2009.

[136] A. Juzeniene, Q. Peng, and J. Moan, "Milestones in the development of photodynamic therapy and fluorescence diagnosis," *Photochem. Photobiol. Sci.*, vol. 6, no. 12, pp. 1234–1245, Dec. 2007.

[137] A. P. Castano, T. N. Demidova, and M. R. Hamblin, "Mechanisms in photodynamic therapy: Part one-photosensitizers, photochemistry and cellular

localization," *Photodiagnosis Photodyn. Ther.*, vol. 1, no. 4, pp. 279–293, Dec. 2004.

[138] F. Yukruk, A. L. Dogan, H. Canpinar, D. Guc, and E. U. Akkaya, "Water-soluble green perylenediimide (PDI) dyes as potential sensitizers for photodynamic therapy," *Org. Lett.*, vol. 7, no. 14, pp. 2885–2887, 2005.

[139] S. Erbas, A. Gorgulu, M. Kocakusakogullari, and E. U. Akkaya, "Non-covalent functionalized SWNTs as delivery agents for novel Bodipy-based potential PDT sensitizers," *Chem. Commun.*, no. 33, pp. 4956–4958, 2009.

[140] S. Kolemen, M. Isik, G. M. Kim, D. Kim, H. Geng, M. Buyuktemiz, T. Karatas, X.-F. Zhang, Y. Dede, J. Yoon, and E. U. Akkaya, "Intracellular modulation of excited-state dynamics in a chromophore dyad: Differential enhancement of photocytotoxicity targeting cancer cells," *Angew. Chem. Int. Ed. Engl.*, vol. 54, no. 18, pp. 5340–5344, Apr. 2015.

[141] T. J. Dougherty, C. J. Gomer, B. W. Henderson, G. Jori, D. Kessel, M. Korbelik, J. Moan, and Q. Peng, "Photodynamic therapy," *J. Natl. Cancer Inst.*, vol. 90, no. 12, pp. 889–905, Jun. 1998.

[142] J. Moan and Q. Peng, "An outline of the hundred-year history of PDT," *Anticancer Res.*, vol. 23, no. 5A, pp. 3591–3600, 2003.

[143] T. Ozdemir, J. L. Bila, F. Sozmen, L. T. Yildirim, and E. U. Akkaya, "Orthogonal Bodipy trimers as photosensitizers for photodynamic action," *Org. Lett.*, vol. 18, no. 19, pp. 4821–4823, 2016.

[144] S. G. Awuah, J. Polreis, V. Biradar, and Y. You, "Singlet oxygen generation by novel NIR BODIPY dyes," *Org. Lett.*, vol. 13, no. 15, pp. 3884–3887, 2011.

[145] N. Adarsh, R. R. Avirah, and D. Ramaiah, "Tuning photosensitized singlet oxygen generation efficiency of novel aza-BODIPY dyes," *Org. Lett.*, vol. 12,

no. 24, pp. 5720–5723, 2010.

[146] S. Stolik, J. A. Delgado, A. Perez, and L. Anasagasti, “Measurement of the penetration depths of red and near infrared light in human ‘ex vivo’ tissues,” *J. Photochem. Photobiol. B Biol.*, vol. 57, no. 2–3, pp. 90–93, Sep. 2000.

[147] S. Erbas-Cakmak and E. U. Akkaya, “Toward Singlet Oxygen Delivery at a Measured Rate: A Self-Reporting Photosensitizer,” *Org. Lett.*, vol. 16, no. 11, pp. 2946–2949, 2014.

[148] M. Klaper, W. Fudickar, and T. Linker, “Role of distance in singlet oxygen applications: A model system,” *J. Am. Chem. Soc.*, vol. 138, no. 22, pp. 7024–7029, 2016.

[149] S. Clement, W. Deng, E. Camilleri, B. C. Wilson, and E. M. Goldys, “X-ray induced singlet oxygen generation by nanoparticle-photosensitizer conjugates for photodynamic therapy: Determination of singlet oxygen quantum yield,” *Sci. Rep.*, vol. 6, p. 19954, Jan. 2016.

[150] Y. Liu, W. Chen, S. Wang, and A. G. Joly, “Investigation of water-soluble X-Ray luminescence nanoparticles for photodynamic activation,” *Appl. Phys. Lett.*, vol. 92, no. 4, pp. 1–4, 2008.

[151] A.-L. Bulin, C. Truillet, R. Chouikrat, F. Lux, C. Frochot, D. Amans, G. Ledoux, O. Tillement, P. Perriat, M. Barberi-Heyob, and C. Dujardin, “X-ray-induced singlet oxygen activation with nanoscintillator-coupled porphyrins,” *J. Phys. Chem. C*, vol. 117, no. 41, pp. 21583–21589, 2013.

[152] I. S. Turan, D. Yildiz, A. Turksoy, G. Gunaydin, and E. U. Akkaya, “A bifunctional photosensitizer for enhanced fractional photodynamic therapy: Singlet oxygen generation in the presence and absence of light,” *Angew. Chemie Int. Ed.*, vol. 55, no. 8, pp. 2875–2878, 2016.

[153] S. Kolemen, T. Ozdemir, D. Lee, G. M. Kim, T. Karatas, J. Yoon, and E. U.

Akkaya, “Remote-controlled release of singlet oxygen by the plasmonic heating of endoperoxide-modified gold nanorods: Towards a paradigm change in photodynamic therapy,” *Angew. Chemie*, vol. 128, no. 11, pp. 3670–3674, 2016.

[154] M. J. Phillip and P. P. Maximuke, “Chemiluminescence and Hematoporphyrin Derivative: A Novel Therapy for Mammary Adenocarcinomas in Mice,” *Oncology*, vol. 46, no. 4, pp. 266–272, 1989.

[155] C. M. Magalhães, J. C. G. da Silva, and L. da Silva, “Chemiluminescence and bioluminescence as an excitation source in the photodynamic therapy of cancer: A critical review,” *ChemPhysChem*, vol. 17, no. 15, pp. 2286–2294, 2016.

[156] J. Han, J. Jose, E. Mei, and K. Burgess, “Chemiluminescent energy-transfer cassettes based on fluorescein and nile red,” *Angew. Chemie Int. Ed.*, vol. 46, no. 10, pp. 1684–1687, 2007.

[157] T. P. Szatrowski and C. F. Nathan, “Production of large amounts of hydrogen peroxide by human tumor cells,” *Cancer Res.*, vol. 51, no. 3, pp. 794–798, Feb. 1991.

[158] A. Glasauer and N. S. Chandel, “Targeting antioxidants for cancer therapy,” *Biochem. Pharmacol.*, vol. 92, no. 1, pp. 90–101, Nov. 2014.

[159] R. Bonnett, “Photosensitizers of the porphyrin and phthalocyanine series for photodynamic therapy,” *Chem. Soc. Rev.*, vol. 24, no. 1, pp. 19–33, 1995.

[160] S. B. Brown, E. A. Brown, and I. Walker, “The present and future role of photodynamic therapy in cancer treatment,” *Lancet. Oncol.*, vol. 5, no. 8, pp. 497–508, Aug. 2004.

[161] A. P. Castano, P. Mroz, and M. R. Hamblin, “Photodynamic therapy and anti-tumour immunity,” *Nat. Rev. Cancer*, vol. 6, no. 7, pp. 535–545, Jul. 2006.

[162] C. A. Robertson, D. H. Evans, and H. Abrahamse, “Photodynamic therapy (PDT): A short review on cellular mechanisms and cancer research applications for PDT,” *J. Photochem. Photobiol. B Biol.*, vol. 96, no. 1, pp. 1–8, Jul. 2009.

[163] J. Zhao, W. Wu, J. Sun, and S. Guo, “Triplet photosensitizers: From molecular design to applications,” *Chem. Soc. Rev.*, vol. 42, no. 12, pp. 5323–5351, 2013.

[164] A. Kamkaew, S. H. Lim, H. B. Lee, L. V. Kiew, L. Y. Chung, and K. Burgess, “BODIPY dyes in photodynamic therapy,” *Chem. Soc. Rev.*, vol. 42, no. 1, pp. 77–88, 2013.

[165] S. Erbas-Cakmak and E. U. Akkaya, “Cascading of molecular logic gates for advanced functions: A self-reporting, activatable photosensitizer,” *Angew. Chemie Int. Ed.*, vol. 52, no. 43, pp. 11364–11368, 2013.

[166] S. Erbas-Cakmak, O. A. Bozdemir, Y. Cakmak, and E. U. Akkaya, “Proof of principle for a molecular 1 : 2 demultiplexer to function as an autonomously switching theranostic device,” *Chem. Sci.*, vol. 4, no. 2, pp. 858–862, 2013.

[167] I. S. Turan, F. P. Cakmak, D. C. Yildirim, R. Cetin-Atalay, and E. U. Akkaya, “Near-IR absorbing BODIPY derivatives as glutathione-activated photosensitizers for selective photodynamic action,” *Chem. – A Eur. J.*, vol. 20, no. 49, pp. 16088–16092, 2014.

[168] S. D. Topel, G. T. Cin, and E. U. Akkaya, “Near IR excitation of heavy atom free Bodipy photosensitizers through the intermediacy of upconverting nanoparticles,” *Chem. Commun. (Cambridge, England)*, vol. 50, no. 64, pp. 8896–8899, Aug. 2014.

[169] O. Ozcan, F. Yukruk, E. U. Akkaya, and D. Uner, “Dye sensitized CO2 reduction over pure and platinized TiO2,” *Top. Catal.*, vol. 44, no. 4, pp. 523–528, 2007.

[170] U. Oguz and E. U. Akkaya, “A squaraine-based sodium selective fluorescent chemosensor,” *Tetrahedron Lett.*, vol. 39, no. 32, pp. 5857–5860, 1998.

[171] B. Kukrer and E. U. Akkaya, “Red to near IR fluorescent signalling of carbohydrates,” *Tetrahedron Lett.*, vol. 40, no. 51, pp. 9125–9128, 1999.

[172] Y. Cakmak, S. Kolemen, S. Duman, Y. Dede, Y. Dolen, B. Kilic, Z. Kostereli, L. T. Yildirim, A. L. Dogan, D. Guc, and E. U. Akkaya, “Designing excited states: Theory-guided access to efficient photosensitizers for photodynamic action,” *Angew. Chemie Int. Ed.*, vol. 50, no. 50, pp. 11937–11941, 2011.

[173] L. Huang, X. Yu, W. Wu, and J. Zhao, “Styryl Bodipy-C60 dyads as efficient heavy atom free organic triplet photosensitizers,” *Org. Lett.*, vol. 14, no. 10, pp. 2594–2597, 2012.

[174] S. O. McDonnell, M. J. Hall, L. T. Allen, A. Byrne, W. M. Gallagher, and D. F. O’Shea, “Supramolecular photonic therapeutic agents,” *J. Am. Chem. Soc.*, vol. 127, no. 47, pp. 16360–16361, 2005.

[175] G. R. Martinez, F. Garcia, L. H. Catalani, J. Cadet, M. C. B. Oliveira, G. E. Ronsein, S. Miyamoto, M. H. G. Medeiros, and P. Di Mascio, “Synthesis of a hydrophilic and non-ionic anthracene derivative, the N,N′-di-(2,3-dihydroxypropyl)-9,10-anthracenedipropanamide as a chemical trap for singlet molecular oxygen detection in biological systems,” *Tetrahedron*, vol. 62, no. 46, pp. 10762–10770, 2006.

[176] J. A. Bonacin, F. M. Engelmann, D. Severino, H. E. Toma, and M. S. Baptista, “Singlet oxygen quantum yields (Φd) in water using beetroot extract and an array of LEDs,” *J. Braz. Chem. Soc.*, vol. 20, no. 1, pp. 31–36, 2009.

[177] F. Ronzani, A. Trivella, E. Arzoumanian, S. Blanc, M. Sarakha, C. Richard, E. Oliveros, and S. Lacombe, “Comparison of the photophysical properties of three phenothiazine derivatives: Transient detection and singlet oxygen production,” *Photochem. Photobiol. Sci.*, vol. 12, no. 12, pp. 2160–2169,

2013.

[178] M. H. Silla Santos, “Biogenic amines: Their importance in foods,” *Int. J. Food Microbiol.*, vol. 29, no. 2–3, pp. 213–231, 1996.

[179] A. Gugliucci, “Polyamines as clinical laboratory tools,” *Clin. Chim. Acta*, vol. 344, no. 1–2, pp. 23–35, Jun. 2004.

[180] T. Eisenberg, H. Knauer, A. Schauer, S. Buttner, C. Ruckenstuhl, D. Carmona-Gutierrez, J. Ring, S. Schroeder, C. Magnes, L. Antonacci, H. Fussi, L. Deszcz, R. Hartl, E. Schraml, A. Criollo, E. Megalou, D. Weiskopf, P. Laun, G. Heeren, M. Breitenbach, B. Grubeck-Loebenstein, E. Herker, B. Fahrenkrog, K.-U. Frohlich, F. Sinner, N. Tavernarakis, N. Minois, G. Kroemer, and F. Madeo, “Induction of autophagy by spermidine promotes longevity,” *Nat. Cell Biol.*, vol. 11, no. 11, pp. 1305–1314, Nov. 2009.

[181] K. Soda, Y. Dobashi, Y. Kano, S. Tsujinaka, and F. Konishi, “Polyamine-rich food decreases age-associated pathology and mortality in aged mice,” *Exp. Gerontol.*, vol. 44, no. 11, pp. 727–732, Nov. 2009.

[182] A. R. Shalaby, “Significance of biogenic amines to food safety and human health,” *Food Res. Int.*, vol. 29, no. 7, pp. 675–690, 1996.

[183] C. Liu, D. Walter, D. Neuhauser, and R. Baer, “Molecular recognition and conductance in crown ethers,” *J. Am. Chem. Soc.*, vol. 125, no. 46, pp. 13936–13937, 2003.

[184] G. R. C. Hamilton, S. K. Sahoo, S. Kamila, N. Singh, N. Kaur, B. W. Hyland, and J. F. Callan, “Optical probes for the detection of protons, and alkali and alkaline earth metal cations,” *Chem. Soc. Rev.*, vol. 44, no. 13, pp. 4415–4432, 2015.

[185] A. Spath and B. Konig, “Molecular recognition of organic ammonium ions in solution using synthetic receptors,” *Beilstein J. Org. Chem.*, vol. 6, 2010.

[186] L. Jiao, C. Yu, T. Uppal, M. Liu, Y. Li, Y. Zhou, E. Hao, X. Hu, and M. G. H. Vicente, “Long wavelength red fluorescent dyes from 3,5-diiodo-BODIPYs,” *Org. Biomol. Chem.*, vol. 8, no. 11, pp. 2517–2519, 2010.

[187] J. Isaad and A. El Achari, “A water soluble fluorescent BODIPY dye with azathia-crown ether functionality for mercury chemosensing in environmental media,” *Analyst*, vol. 138, no. 13, pp. 3809–3819, 2013.

[188] M. M. Salim, E. A. Owens, T. Gao, J. H. Lee, H. Hyun, H. S. Choi, and M. Henary, “Hydroxylated near-infrared BODIPY fluorophores as intracellular pH sensors.,” *Analyst*, vol. 139, no. 19, pp. 4862–73, 2014.

[189] C. Zhang, S. Li, J. Zhang, K. Zhu, N. Li, and F. Huang, “Benzo-21-crown-7/secondary dialkylammonium salt [2]pseudorotaxane- and [2]rotaxane-type threaded structures,” *Org. Lett.*, vol. 9, no. 26, pp. 5553–5556, 2007.

[190] N. G. R. Rao, K. R. Kumar, and A. Pradesh, “Synthesis and evaluation of dibenzo- 18 -crown -6 ether containing hydrazone derivative as antibacterial drug derivatives,” *J. Chem. Pharm. Res.*, vol. 2, no. 4, pp. 671–679, 2010.

[191] Ö. A. Bozdemir, O. Büyükcakir, and E. U. Akkaya, “Novel molecular building blocks based on the Boradiazaindacene chromophore: Applications in fluorescent metallosupramolecular coordination polymers,” *Chem. – A Eur. J.*, vol. 15, no. 15, pp. 3830–3838, 2009.

[192] M. A. H. Alamiry, A. C. Benniston, G. Copley, A. Harriman, and D. Howgego, “Intramolecular excimer formation for covalently linked boron dipyrromethene dyes,” *J. Phys. Chem. A*, vol. 115, no. 44, pp. 12111–12119, 2011.

[193] E. A. Margulies, L. E. Shoer, S. W. Eaton, and M. R. Wasielewski, “Excimer formation in cofacial and slip-stacked perylene-3,4:9,10-bis(dicarboximide) dimers on a redox-inactive triptycene scaffold,” *Phys. Chem. Chem. Phys.*, vol. 16, no. 43, pp. 23735–42, 2014.

[194] J. M. Giaimo, J. V Lockard, L. E. Sinks, A. M. Scott, T. M. Wilson, and M. R. Wasielewski, “Excited singlet states of covalently bound, cofacial dimers and trimers of perylene-3,4:9,10-bis(dicarboximide)s,” *J. Phys. Chem. A*, vol. 112, no. 11, pp. 2322–2330, Mar. 2008.

[195] I. Mikhalyov, N. Gretskaya, F. Bergstrom, and L. B.-A. Johansson, “Electronic ground and excited state properties of dipyrrometheneboron difluoride (BODIPY): Dimers with application to biosciences,” *Phys. Chem. Chem. Phys.*, vol. 4, no. 22, pp. 5663–5670, 2002.

[196] Y. Tokoro, A. Nagai, and Y. Chujo, “Nanoparticles via H-aggregation of amphiphilic BODIPY dyes,” *Tetrahedron Lett.*, vol. 51, no. 26, pp. 3451–3454, 2010.

[197] S. K. Kim, M. Y. Bang, S. H. Lee, K. Nakamura, S. W. Cho, and J. Yoon, “New fluorescent chemosensors for cationic guests: 1,8-Bis(azacrown)anthracenes,” *J. Incl. Phenom.*, vol. 43, no. 1–2, pp. 71–75, 2002.

[198] H. Yasuda, “Solid tumor physiology and hypoxia-induced chemo/radio-resistance: Novel strategy for cancer therapy: Nitric oxide donor as a therapeutic enhancer,” *Biol. Chem.*, vol. 19, no. 2, pp. 205–216, 2008.

[199] W. Mueller-Klieser, P. Vaupel, R. Manz, and R. Schmidseder, “Intracapillary oxyhemoglobin saturation of malignant tumors in humans,” *Int. J. Radiat. Oncol. Biol. Phys.*, vol. 7, no. 10, pp. 1397–1404, Oct. 1981.

[200] R. M. Sutherland, “Cell and environment interactions in tumor microregions: The multicell spheroid model,” *Science (80-.).*, vol. 240, no. 4849, pp. 177–184, Apr. 1988.

[201] R. M. Sutherland, “Importance of critical metabolites and cellular interactions in the biology of microregions of tumors,” *Cancer*, vol. 58, no. 8, pp. 1668–1680, Oct. 1986.

[202] M. Hockel and P. Vaupel, “Tumor hypoxia: definitions and current clinical, biologic and molecular aspects,” *J. Natl. Cancer Inst.*, vol. 93, no. 4, pp. 266–276, Feb. 2001.

[203] P. Vaupel and A. Mayer, “Hypoxia in cancer: Significance and impact on clinical outcome,” *Cancer Metastasis Rev.*, vol. 26, no. 2, pp. 225–239, Jun. 2007.

[204] X. Zheng, X. Wang, H. Mao, W. Wu, B. Liu, and X. Jiang, “Hypoxia-specific ultrasensitive detection of tumours and cancer cells in vivo,” *Nat. Commun.*, vol. 6, p. 5834, 2015.

[205] P. Vaupel, F. Kallinowski, and P. Okunieff, “Blood flow, oxygen and nutrient supply and metabolic microenvironment of human tumors: A review,” *Cancer Res.*, vol. 49, no. 23, pp. 6449–6465, Dec. 1989.

[206] H. Harada, M. Inoue, S. Itasaka, K. Hirota, A. Morinibu, K. Shinomiya, L. Zeng, G. Ou, Y. Zhu, M. Yoshimura, W. G. McKenna, R. J. Muschel, and M. Hiraoka, “Cancer cells that survive radiation therapy acquire HIF-1 activity and translocate towards tumour blood vessels,” *Nat. Commun.*, vol. 3, p. 783, Apr. 2012.

[207] D. Hanahan and R. A. Weinberg, “The hallmarks of cancer,” *Cell*, vol. 100, no. 1, pp. 57–70, Jan. 2000.

[208] M.-C. Hung, G. B. Mills, and D. Yu, “Oxygen sensor boosts growth factor signaling,” *Nature Medicine*, vol. 15, no. 3. United States, pp. 246–247, Mar-2009.

[209] R. B. P. Elmes, “Bioreductive fluorescent imaging agents: applications to tumour hypoxia,” *Chem. Commun.*, vol. 52, pp. 8935–8956, 2016.

[210] W. A. Denny, “Prodrug strategies in cancer therapy,” *Eur. J. Med. Chem.*, vol. 36, no. 7–8, pp. 577–595, 2001.

[211] J. Xu, S. Sun, Q. Li, Y. Yue, Y. Li, and S. Shao, “A rapid response ‘Turn-On’ fluorescent probe for nitroreductase detection and its application in hypoxic tumor cell imaging,” *Analyst*, vol. 140, no. 2, pp. 574–81, 2015.

[212] J. H. Crawford, T. S. Isbell, Z. Huang, S. Shiva, B. K. Chacko, A. N. Schechter, V. M. Darley-Usmar, J. D. Kerby, J. D. J. Lang, D. Kraus, C. Ho, M. T. Gladwin, and R. P. Patel, “Hypoxia, red blood cells, and nitrite regulate NO-dependent hypoxic vasodilation,” *Blood*, vol. 107, no. 2, pp. 566–574, Jan. 2006.

[213] M. T. Gladwin, N. J. H. Raat, S. Shiva, C. Dezfulian, N. Hogg, D. B. Kim-Shapiro, and R. P. Patel, “Nitrite as a vascular endocrine nitric oxide reservoir that contributes to hypoxic signaling, cytoprotection and vasodilation,” *Am. J. Physiol.*, vol. 291, no. 5, pp. 2026–2035, Nov. 2006.

[214] Y. Tang, A. Lu, B. J. Aronow, K. R. Wagner, and F. R. Sharp, “Genomic responses of the brain to ischemic stroke, intracerebral haemorrhage, kainate seizures, hypoglycemia, and hypoxia,” *Eur. J. Neurosci.*, vol. 15, no. 12, pp. 1937–1952, Jun. 2002.

[215] C. Murdoch, M. Muthana, and C. E. Lewis, “Hypoxia regulates macrophage functions ininflammation,” *J. Immunol.*, vol. 175, no. 10, pp. 6257–6263, Nov. 2005.

[216] M. Hockel, K. Schlenger, B. Aral, M. Mitze, U. Schaffer, and P. Vaupel, “Association between tumor hypoxia and malignant progression in advanced cancer of the uterine cervix,” *Cancer Res.*, vol. 56, no. 19, pp. 4509–4515, Oct. 1996.

[217] E. K. Rofstad, H. Rasmussen, K. Galappathi, B. Mathiesen, K. Nilsen, and B. A. Graff, “Hypoxia Promotes lymph node metastasis in human melanoma xenografts by up-regulating the urokinase-type plasminogen activator receptor,” *Cancer Res.*, vol. 62, no. 6, pp. 1847–1853, Mar. 2002.

[218] S. Wang, H. Liu, J. Mack, J. Tian, B. Zou, H. Lu, Z. Li, J. Jiang, and Z. Shen, "A BODIPY-based 'Turn-On' fluorescent probe for hypoxic cell imaging," *Chem. Commun.*, vol. 51, no. 69, pp. 13389–92, 2015.

[219] E. T. Shinohara and A. Maity, "Increasing sensitivity to radiotherapy and chemotherapy by using novel biological agents that alter the tumor microenvironment," *Curr. Mol. Med.*, vol. 9, no. 9, pp. 1034–1045, Dec. 2009.

[220] Z. Li, X. Gao, W. Shi, X. Li, and H. Ma, "7-((5-Nitrothiophen-2-yl)methoxy)-3H-phenoxazin-3-one as a spectroscopic off-on probe for highly sensitive and selective detection of nitroreductase," *Chem. Commun. (Camb).*, vol. 49, no. 52, pp. 5859–5861, Jul. 2013.

[221] W. Piao, S. Tsuda, Y. Tanaka, S. Maeda, F. Liu, S. Takahashi, Y. Kushida, T. Komatsu, T. Ueno, T. Terai, T. Nakazawa, M. Uchiyama, K. Morokuma, T. Nagano, and K. Hanaoka, "Development of azo-based fluorescent probes to detect different levels of hypoxia," *Angew. Chem. Int. Ed. Engl.*, vol. 52, no. 49, pp. 13028–13032, Dec. 2013.

[222] L. Cui, Y. Zhong, W. Zhu, Y. Xu, Q. Du, X. Wang, X. Qian, and Y. Xiao, "A new prodrug-derived ratiometric fluorescent probe for hypoxia: high selectivity of nitroreductase and imaging in tumor cell," *Org. Lett.*, vol. 13, no. 5, pp. 928–931, Mar. 2011.

[223] T. Guo, L. Cui, J. Shen, W. Zhu, Y. Xu, and X. Qian, "A highly sensitive long-wavelength fluorescence probe for nitroreductase and hypoxia: Selective detection and quantification," *Chem. Commun. (Camb).*, vol. 49, no. 92, pp. 10820–10822, 2013.

[224] K. Kiyose, K. Hanaoka, D. Oushiki, T. Nakamura, M. Kajimura, M. Suematsu, H. Nishimatsu, T. Yamane, T. Terai, Y. Hirata, and T. Nagano, "Hypoxia-sensitive fluorescent probes for in vivo real-time fluorescence imaging of acute ischemia," *J. Am. Chem. Soc.*, vol. 132, no. 45, pp. 15846–15848, Nov. 2010.

[225] H. M. Vlastos, Georges and Verkooijen, “Minimally invasive approaches for diagnosis and treatment of early-stage breast cancer,” *Oncologist*, vol. 12, no. 1, pp. 1–10, 2007.

[226] N. Boens, V. Leen, and W. Dehaen, “Fluorescent indicators based on BODIPY,” *Chem. Soc. Rev.*, vol. 41, no. 3, pp. 1130–1172, Feb. 2012.

[227] A. B. Descalzo, H.-J. Xu, Z. Shen, and K. Rurack, “Red/near-infrared Boron-dipyrromethene dyes as strongly emitting fluorophores,” *Ann. N. Y. Acad. Sci.*, vol. 1130, pp. 164–171, 2008.

[228] K. Krumova and G. Cosa, “Bodipy dyes with tunable redox potentials and functional groups for further tethering: Preparation, electrochemical, and spectroscopic characterization,” *J. Am. Chem. Soc.*, vol. 132, no. 49, pp. 17560–17569, 2010.

[229] M. Dahim, N. K. Mizuno, X.-M. Li, W. E. Momsen, M. M. Momsen, and H. L. Brockman, “Physical and photophysical characterization of a BODIPY phosphatidylcholine as a membrane probe,” *Biophys. J.*, vol. 83, no. 3, pp. 1511–1524, Sep. 2002.

[230] T. E. Wood and A. Thompson, “Advances in the chemistry of dipyrrins and their complexes,” *Chem. Rev.*, vol. 107, no. 5, pp. 1831–1861, May 2007.

[231] W. Qin, T. Rohand, W. Dehaen, J. N. Clifford, K. Driesen, D. Beljonne, B. Van Averbeke, M. Van der Auweraer, and N. Boens, “Boron dipyrromethene analogs with phenyl, styryl and ethynylphenyl substituents: Synthesis, photophysics, electrochemistry and quantum-chemical calculations,” *J. Phys. Chem. A*, vol. 111, no. 35, pp. 8588–8597, Sep. 2007.

[232] J. Korlach, P. Schwille, W. W. Webb, and G. W. Feigenson, “Characterization of lipid bilayer phases by confocal microscopy and fluorescence correlation spectroscopy,” *Proc. Natl. Acad. Sci. U. S. A.*, vol. 96, no. 15, pp. 8461–8466, Jul. 1999.

[233] E. H. Pap, G. P. Drummen, V. J. Winter, T. W. Kooij, P. Rijken, K. W. Wirtz, J. A. Op den Kamp, W. J. Hage, and J. A. Post, "Ratio-fluorescence microscopy of lipid oxidation in living cells using C11-BODIPY(581/591)," *FEBS Lett.*, vol. 453, no. 3, pp. 278–282, Jun. 1999.

[234] X. Peng, J. Du, J. Fan, J. Wang, Y. Wu, J. Zhao, S. Sun, and T. Xu, "A Selective fluorescent sensor for imaging Cd2+ in living cells.," *J. Am. Chem. Soc.*, vol. 129, no. 6, pp. 1500–1501, Feb. 2007.

[235] A. Khatchadourian, K. Krumova, S. Boridy, A. T. Ngo, D. Maysinger, and G. Cosa, "Molecular imaging of lipid peroxyl radicals in living cells with a BODIPY−α-tocopherol adduct," *Biochemistry*, vol. 48, no. 24, pp. 5658–5668, Jun. 2009.

[236] H. Zhu, J. Fan, M. Li, J. Cao, J. Wang, and X. Peng, "A 'Distorted-BODIPY'-based fluorescent probe for imaging of cellular viscosity in live cells," *Chemistry*, vol. 20, no. 16, pp. 4691–4696, 2014.

[237] M. T. Whited, N. M. Patel, S. T. Roberts, K. Allen, P. I. Djurovich, S. E. Bradforth, and M. E. Thompson, "Symmetry-breaking intramolecular charge transfer in the excited state of meso-linked BODIPY dyads," *Chem. Commun. (Camb).*, vol. 48, no. 2, pp. 284–286, 2012.

[238] R. Lincoln, L. E. Greene, C. Bain, J. O. Flores-Rizo, D. S. Bohle, and G. Cosa, "When push comes to shove: Unravelling the mechanism and scope of nonemissive meso-unsaturated BODIPY dyes," *J. Phys. Chem. B*, vol. 119, no. 13, pp. 4758–4765, 2015.

[239] X. Hu, A. Damjanović, T. Ritz, and K. Schulten, "Architecture and mechanism of the light-harvesting apparatus of purple bacteria," *Proc. Natl. Acad. Sci.*, vol. 95, no. 11, pp. 5935–5941, May 1998.

[240] A. W. Roszak, T. D. Howard, J. Southall, A. T. Gardiner, C. J. Law, N. W. Isaacs, and R. J. Cogdell, "Crystal structure of the RC-LH1 core complex

from Rhodopseudomonas Palustris," *Science*, vol. 302, no. 5652, pp. 1969–1972, Dec. 2003.

[241] K. Sakamoto, Y. Takashima, N. Hamada, H. Ichida, H. Yamaguchi, H. Yamamoto, and A. Harada, "Selective photoinduced energy transfer from a thiophene rotaxane to acceptor," *Org. Lett.*, vol. 13, no. 4, pp. 672–675, 2011.

[242] A. S. D. Sandanayaka, H. Sasabe, T. Takata, and O. Ito, "Photoinduced electron transfer processes of fullerene rotaxanes containing various electron-donors," *J. Photochem. Photobiol. C Photochem. Rev.*, vol. 11, no. 2–3, pp. 73–92, 2010.

[243] G. McDermott, S. M. Prince, A. A. Freer, A. M. Hawthornthwaite-Lawless, M. Z. Papiz, R. J. Cogdell, and N. W. Isaacs, "Crystal structure of an integral membrane light-harvesting complex from photosynthetic bacteria," *Nature*, vol. 374, no. 6522, pp. 517–521, Apr. 1995.

[244] D.-L. Jiang and T. Aida, "Photoisomerization in dendrimers by harvesting of low-energy photons," *Nature*, vol. 388, no. 6641, pp. 454–456, Jul. 1997.

[245] D. Liu, S. De Feyter, M. Cotlet, A. Stefan, U.-M. Wiesler, A. Herrmann, D. Grebel-Koehler, J. Qu, K. Müllen, and F. C. De Schryver, "Fluorescence and intramolecular energy transfer in polyphenylene dendrimers," *Macromolecules*, vol. 36, no. 16, pp. 5918–5925, 2003.

[246] Y. Pan, M. Lu, Z. Peng, and J. S. Melinger, "Synthesis and optical properties of unsymmetrical conjugated dendrimers focally anchored with perylenes in different geometries," *J. Org. Chem.*, vol. 68, no. 18, pp. 6952–6958, 2003.

[247] J.-L. Wang, J. Yan, Z.-M. Tang, Q. Xiao, Y. Ma, and J. Pei, "Gradient shape-persistent π-conjugated dendrimers for light-harvesting: Synthesis, photophysical properties, and energy funneling," *J. Am. Chem. Soc.*, vol. 130, no. 30, pp. 9952–9962, 2008.

[248] T. Park, E. M. Todd, S. Nakashima, and S. C. Zimmerman, “A quadruply hydrogen bonded heterocomplex displaying high-fidelity recognition,” *J. Am. Chem. Soc.*, vol. 127, no. 51, pp. 18133–18142, Dec. 2005.

[249] R. P. Sijbesma, F. H. Beijer, L. Brunsveld, B. J. Folmer, J. H. Hirschberg, R. F. Lange, J. K. Lowe, and E. W. Meijer, “Reversible polymers formed from self-complementary monomers using quadruple hydrogen bonding,” *Science (80-.).*, vol. 278, no. 5343, pp. 1601–1604, Nov. 1997.

[250] A. Harada, A. Hashidzume, H. Yamaguchi, and Y. Takashima, “Polymeric rotaxanes,” *Chem. Rev.*, vol. 109, no. 11, pp. 5974–6023, 2009.

[251] S. Saha and J. F. Stoddart, “Photo-driven molecular devices,” pp. 77–92, 2007.

[252] J. D. Crowley, D. A. Leigh, P. J. Lusby, R. T. McBurney, L.-E. Perret-Aebi, C. Petzold, A. M. Z. Slawin, and M. D. Symes, “A switchable palladium-complexed molecular shuttle and its metastable positional isomers,” *J. Am. Chem. Soc.*, vol. 129, no. 48, pp. 15085–15090, 2007.

[253] L. Kobr, K. Zhao, Y. Shen, A. Comotti, S. Bracco, R. K. Shoemaker, P. Sozzani, N. A. Clark, J. C. Price, C. T. Rogers, and J. Michl, “Inclusion compound based approach to arrays of artificial dipolar molecular rotors. A surface inclusion,” *J. Am. Chem. Soc.*, vol. 134, no. 24, pp. 10122–10131, 2012.

[254] M. E. Gallina, B. Baytekin, C. Schalley, and P. Ceroni, “Light-harvesting in multichromophoric rotaxanes,” *Chem. – A Eur. J.*, vol. 18, no. 5, pp. 1528–1535, 2012.

[255] Z.-J. Zhang, Y.-M. Zhang, and Y. Liu, “Controlled molecular self-assembly behaviors between cucurbituril and bispyridinium derivatives,” *J. Org. Chem.*, vol. 76, no. 11, pp. 4682–4685, 2011.

[256] C. Devadoss, P. Bharathi, and J. S. Moore, “Energy transfer in dendritic macromolecules: Molecular size effects and the role of an energy gradient,” *J. Am. Chem. Soc.*, vol. 118, no. 40, pp. 9635–9644, 1996.

[257] K. Hiratani, M. Kaneyama, Y. Nagawa, E. Koyama, and M. Kanesato, “Synthesis of [1]rotaxane via covalent bond formation and its unique fluorescent response by energy transfer in the presence of lithium ion,” *J. Am. Chem. Soc.*, vol. 126, no. 42, pp. 13568–13569, 2004.

[258] D. Liu, D. Wang, M. Wang, Y. Zheng, K. Koynov, G. K. Auernhammer, H.-J. Butt, and T. Ikeda, “Supramolecular organogel based on crown ether and secondary ammoniumion functionalized glycidyl triazole polymers,” *Macromolecules*, vol. 46, no. 11, pp. 4617–4625, 2013.

[259] T. Förster, “Zwischenmolekulare energiewanderung und fluoreszenz,” *Ann. Phys.*, vol. 437, no. 1–2, pp. 55–75, 1948.

[260] J.-Y. Wang, J.-M. Han, J. Yan, Y. Ma, and J. Pei, “A mechanically interlocked [3]rotaxane as a light-harvesting antenna: Synthesis, characterization, and intramolecular energy transfer,” *Chem. – A Eur. J.*, vol. 15, no. 14, pp. 3585–3594, 2009.

APPENDIX

A1. Singlet Oxygen Generation with Chemical Excitation of an Erythrosine-Luminol Conjugate (^{1}H, ^{13}C and Mass Spectra)

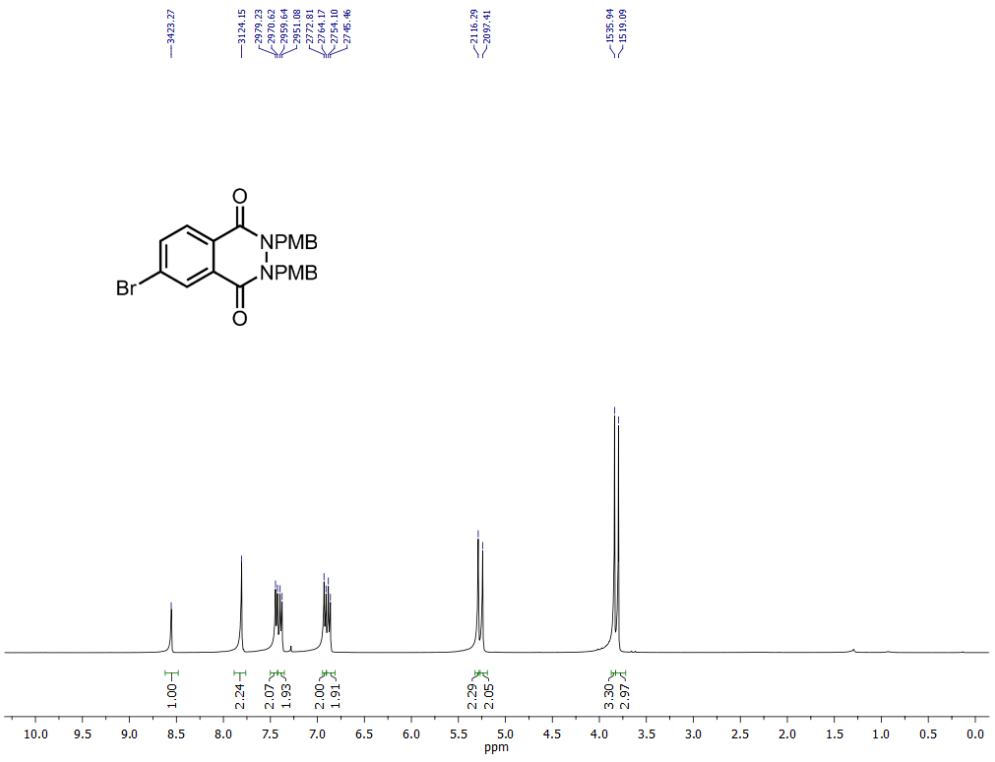

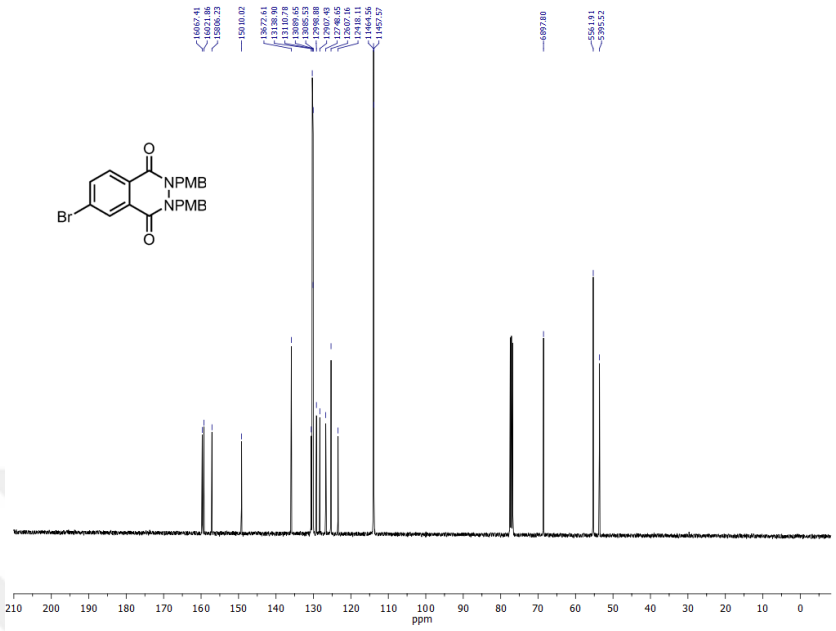
NPMB
NPMB
Br
O
O
O
ppm

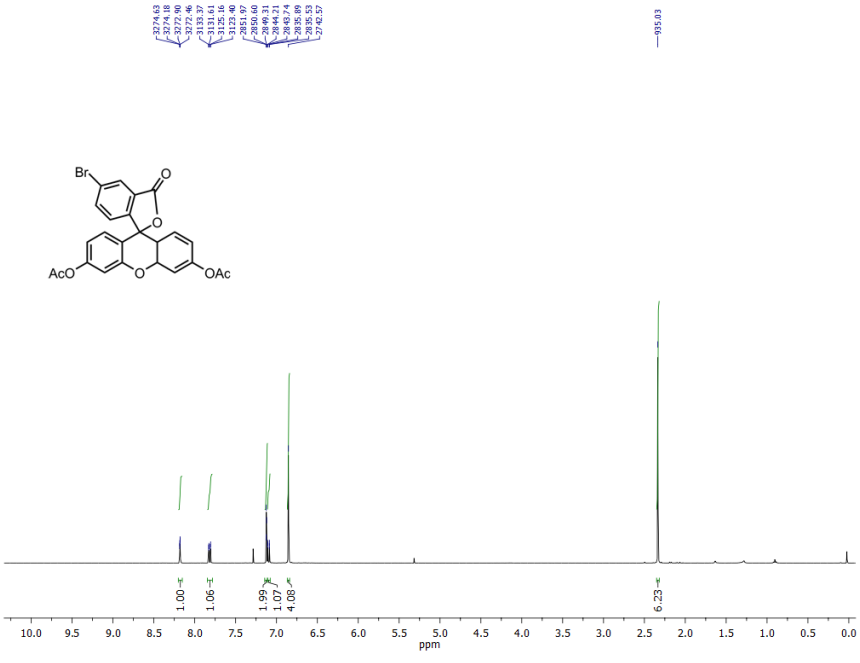
Br
O
O
AcO
OAc
O
ppm

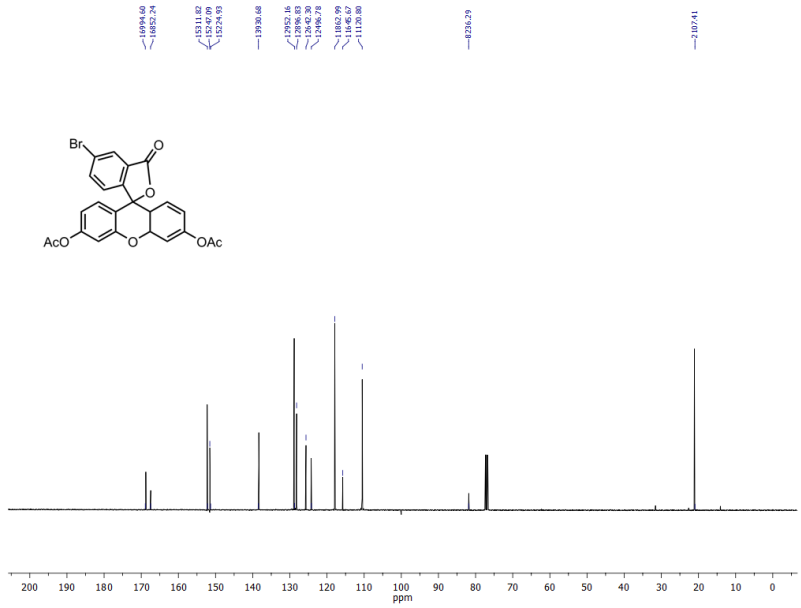
169.94
168.52
153.11
152.89
152.54
139.50
129.52
128.96
126.70
119.05
111.80
82.29
21.07
Br
O
O
AcO
O
OAc
200
190
180
170
160
150
140
130
120
110
100
90
80
70
60
50
40
30
20
10
0
ppm


3046.89
3107.65
3106.28
3099.70
3098.31
2865.96
2850.98
2846.72
2846.02
2845.17
2741.50
2740.76
2734.04
2732.40
2723.94
929.89
119.23

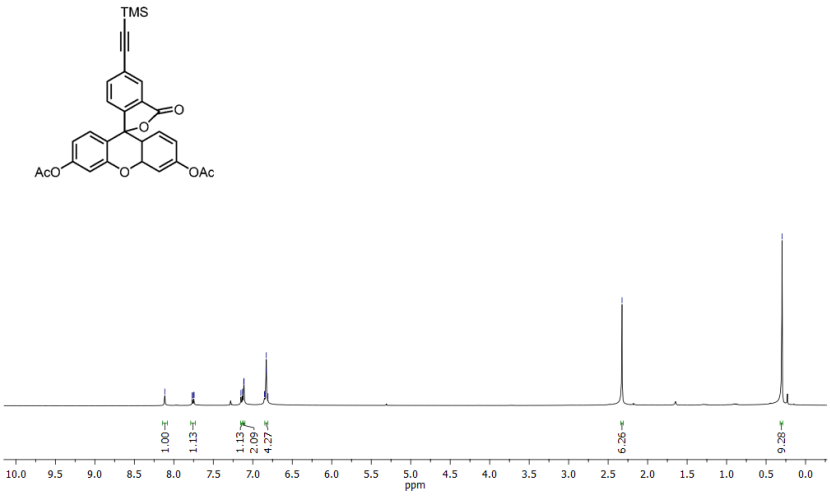
TMS
O
O
AcO
O
OAc
1.00
1.13
1.13
2.09
4.27
6.26
9.28
10.0
9.5
9.0
8.5
8.0
7.5
7.0
6.5
6.0
5.5
5.0
4.5
4.0
3.5
3.0
2.5
2.0
1.5
1.0
0.5
0.0
ppm

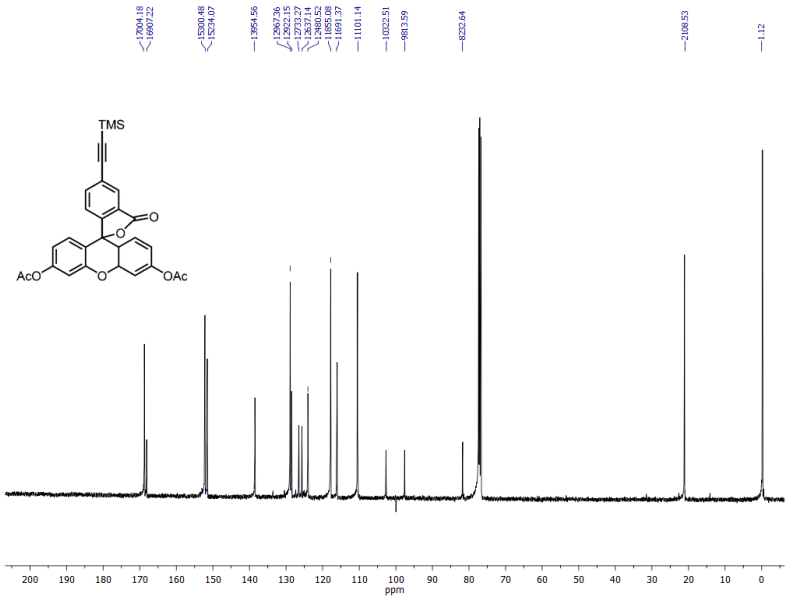
TMS
AcO
OAc
O
O
O
ppm

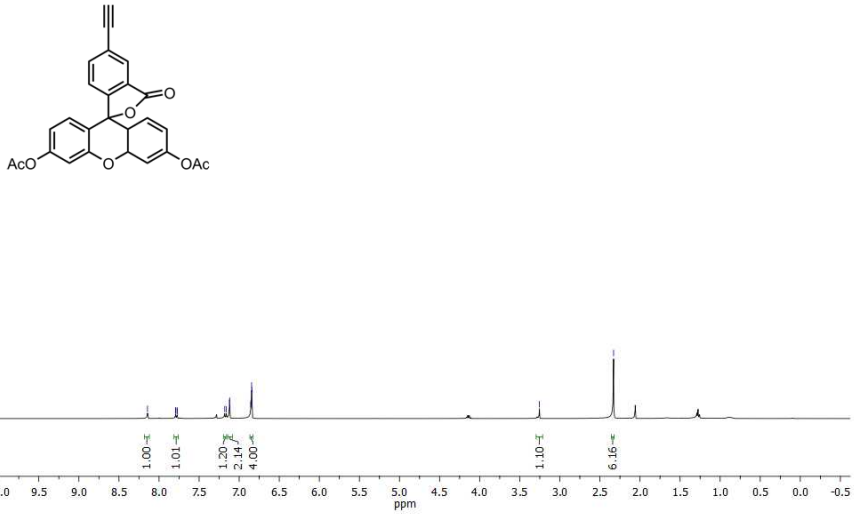
AcO
OAc
O
O
O
ppm

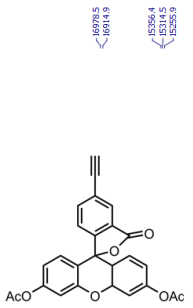
AcO
OAc

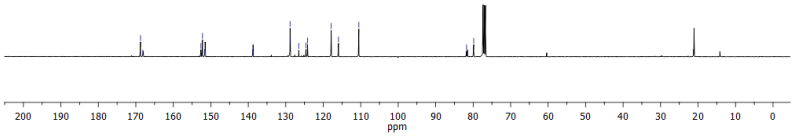
ppm

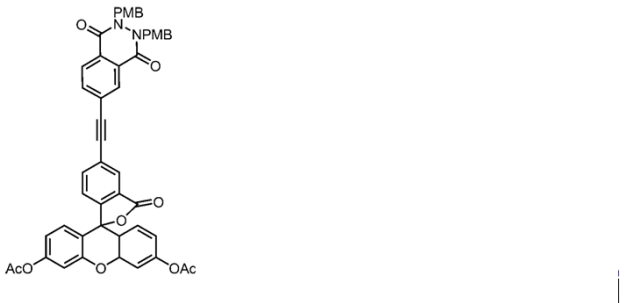
PMB
NPMB
AcO
OAc

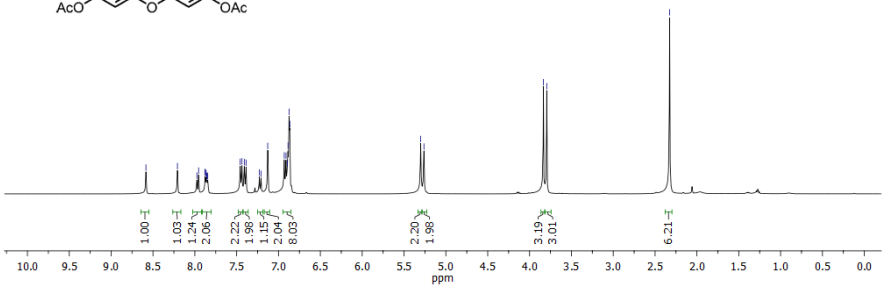
ppm

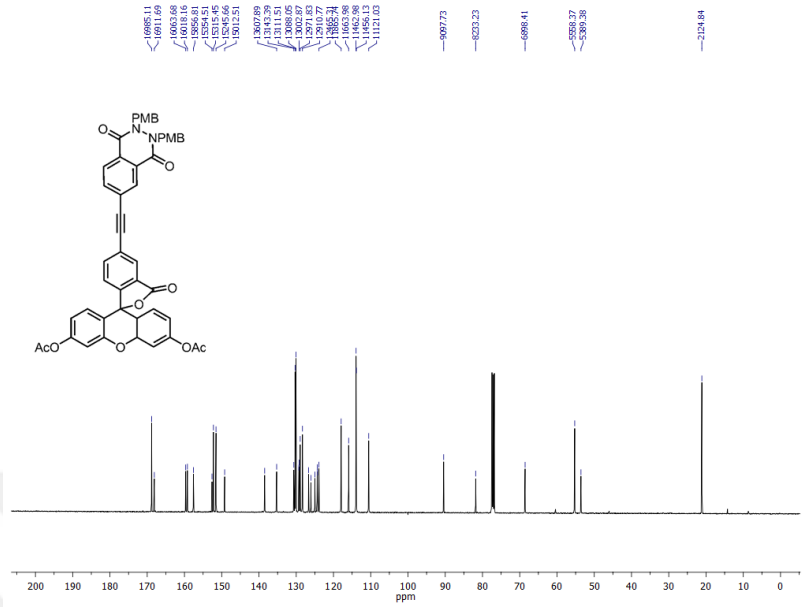
PMB
NPMB
AcO
OAc
ppm

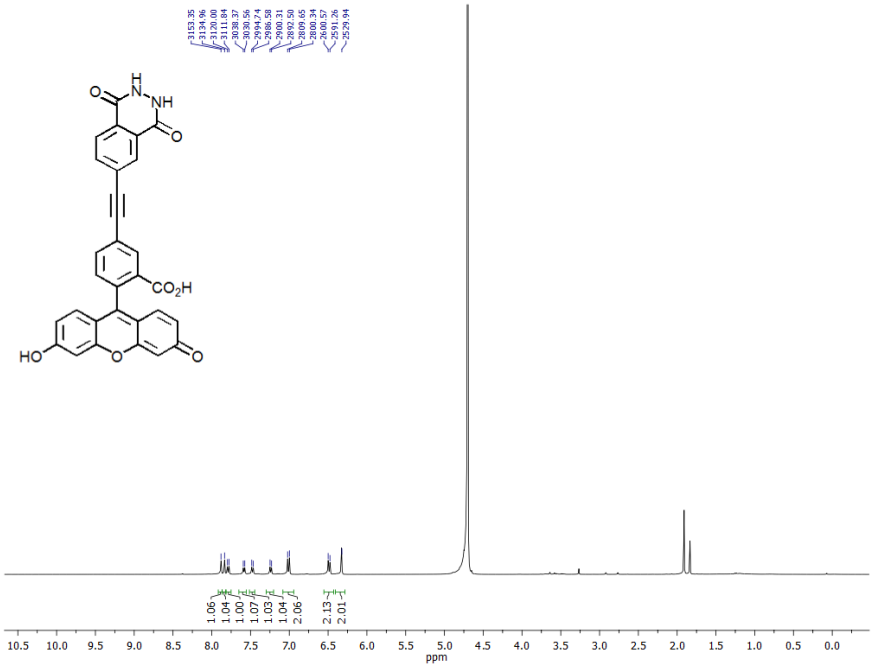
NH
CO2H
HO
ppm

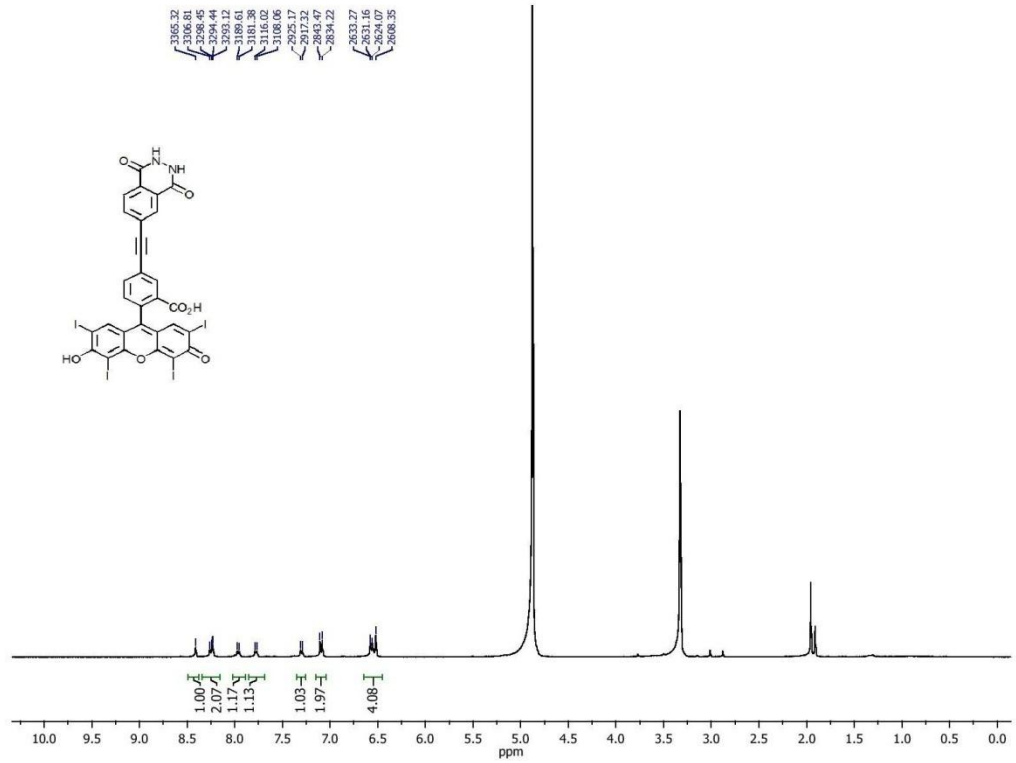
3365.32
3306.81
3298.45
3294.44
3293.12
3189.61
3181.38
3116.02
3108.06
2925.17
2917.32
2843.47
2834.22
2633.27
2631.16
2624.07
2608.35
1.00
2.07
1.17
1.13
1.03
1.97
4.08
10.0 9.5 9.0 8.5 8.0 7.5 7.0 6.5 6.0 5.5 5.0 4.5 4.0 3.5 3.0 2.5 2.0 1.5 1.0 0.5 0.0
ppm

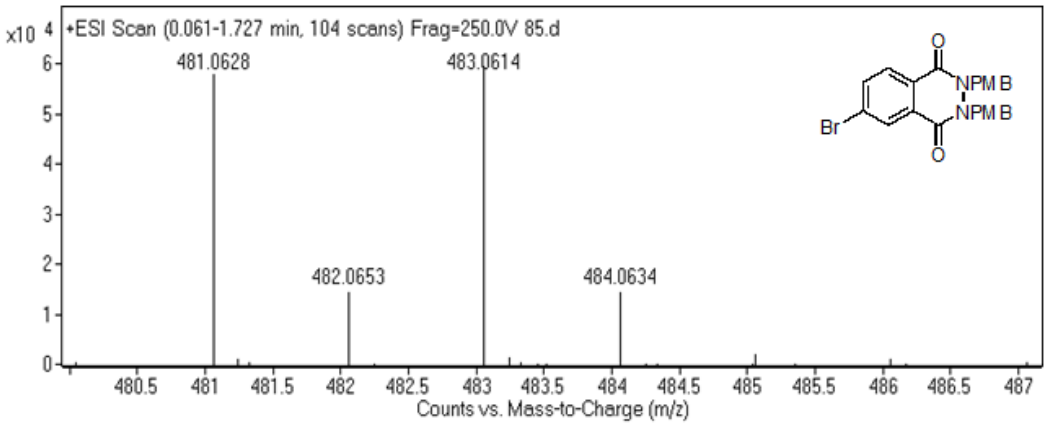
x10 4
+ESI Scan (0.061-1.727 min, 104 scans) Frag=250.0V 85.d
481.0628
483.0614
482.0653
484.0634
NPMB
NPMB
Br
480.5 481 481.5 482 482.5 483 483.5 484 484.5 485 485.5 486 486.5 487
Counts vs. Mass-to-Charge (m/z)

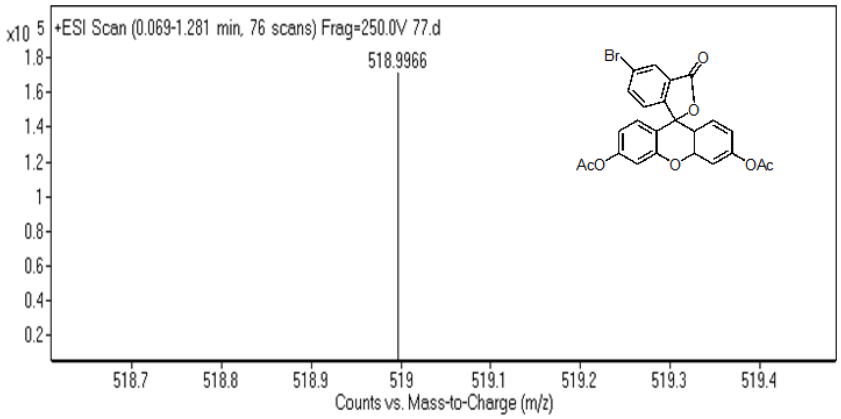
x10 5
+ESI Scan (0.069-1.281 min, 76 scans) Frag=250.0V 77.d
518.9966
Br
O
O
AcO
O
OAc
1.8
1.6
1.4
1.2
1
0.8
0.6
0.4
0.2
518.7
518.8
518.9
519
519.1
519.2
519.3
519.4
Counts vs. Mass-to-Charge (m/z)

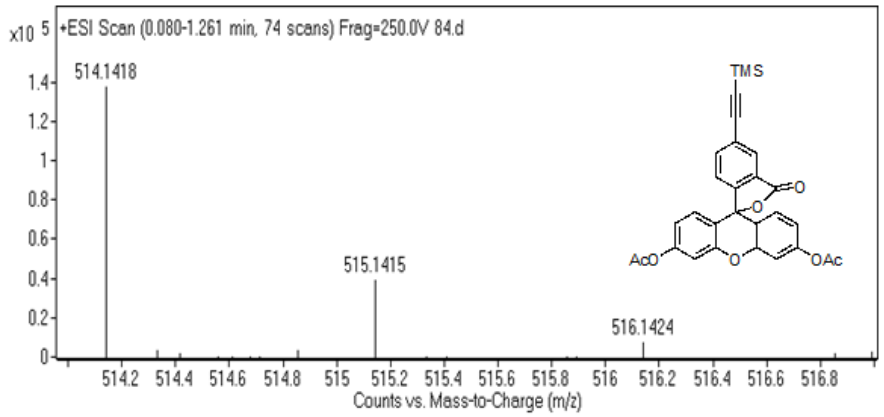
x10 5
+ESI Scan (0.080-1.261 min, 74 scans) Frag=250.0V 84.d
514.1418
515.1415
516.1424
TMS
O
O
AcO
O
OAc
1.4
1.2
1
0.8
0.6
0.4
0.2
0
514.2
514.4
514.6
514.8
515
515.2
515.4
515.6
515.8
516
516.2
516.4
516.6
516.8
Counts vs. Mass-to-Charge (m/z)

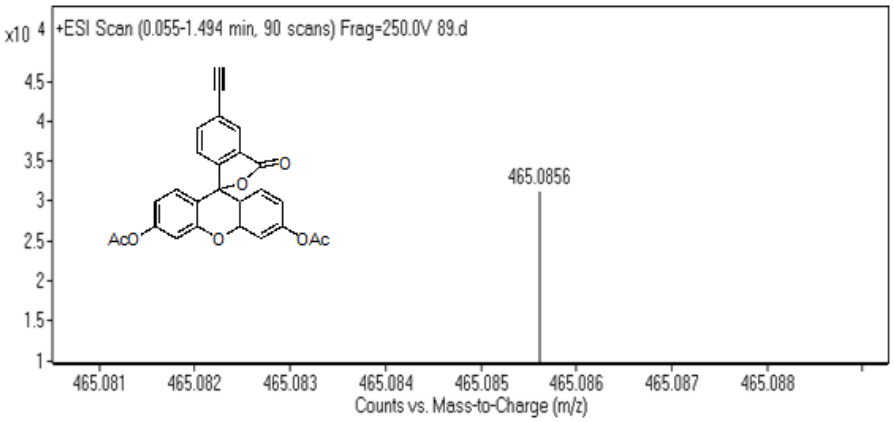
x10 4
+ESI Scan (0.055-1.494 min, 90 scans) Frag=250.0V 89.d
465.0856
O
O
AcO
O
OAc
4.5
4
3.5
3
2.5
2
1.5
1
465.081
465.082
465.083
465.084
465.085
465.086
465.087
465.088
Counts vs. Mass-to-Charge (m/z)

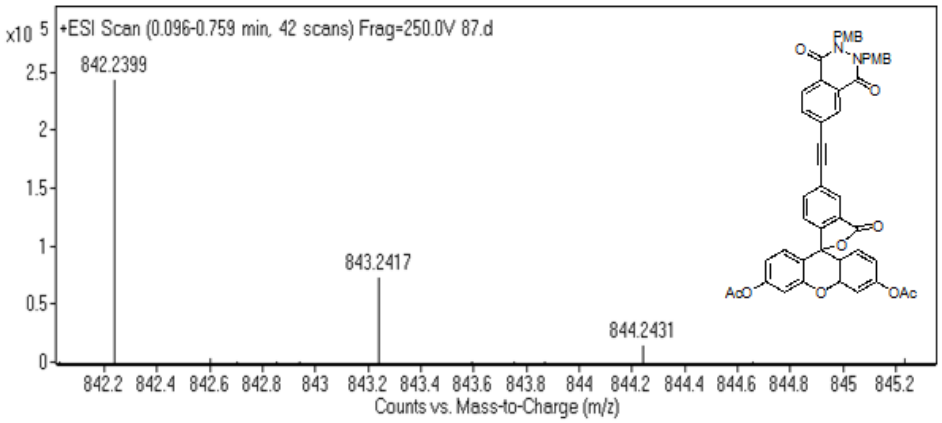
x10 5
+ESI Scan (0.096-0.759 min, 42 scans) Frag=250.0V 87.d
842.2399
843.2417
844.2431
PMB
NPMB
AcO
OAc
Counts vs. Mass-to-Charge (m/z)

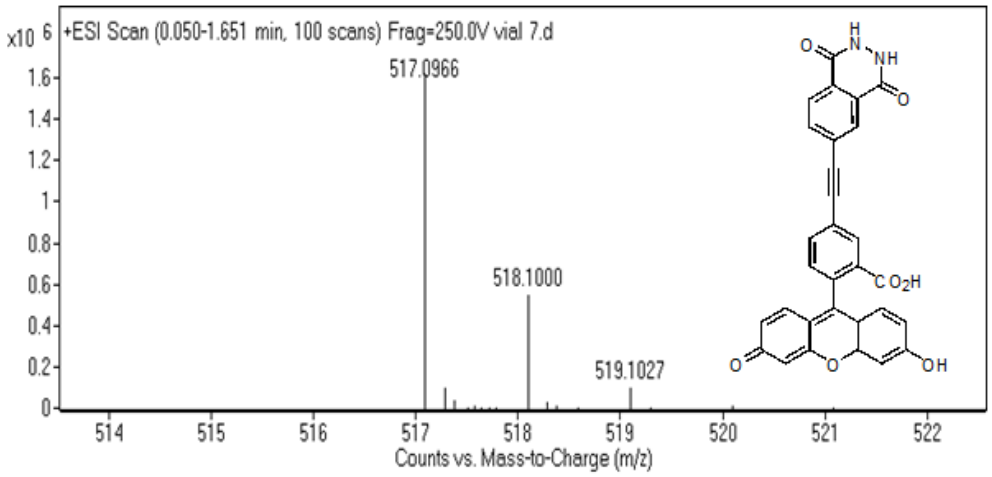
x10 6
+ESI Scan (0.050-1.651 min, 100 scans) Frag=250.0V vial 7.d
517.0966
518.1000
519.1027
CO2H
OH
Counts vs. Mass-to-Charge (m/z)

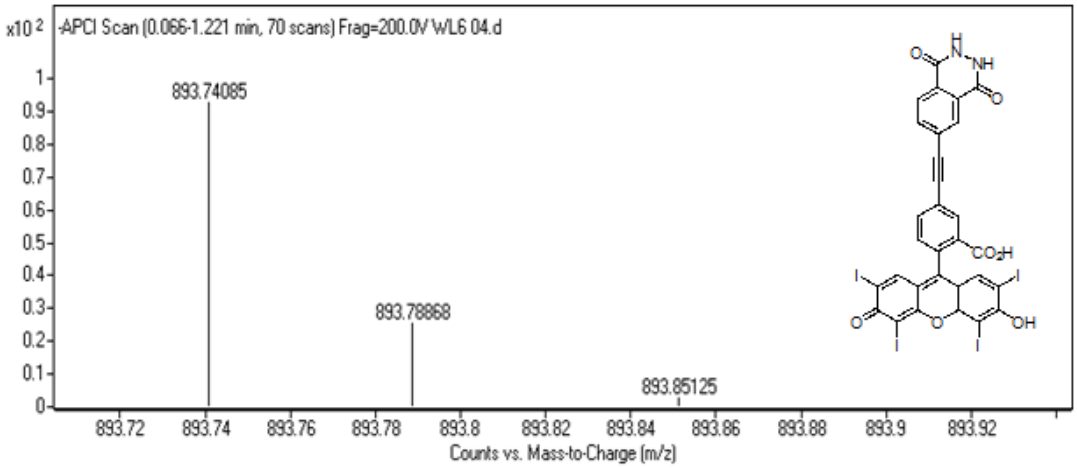
x10 2
-APCI Scan (0.066-1.221 min, 70 scans) Frag=200.0V WL6 04.d
893.74085
893.78868
893.85125
CO2H
OH
Counts vs. Mass-to-Charge (m/z)

A2. Bodipy-based photosensitizers with long alkyl tails at the *meso* position: efficient singlet oxygen generation in Cremophor-EL micelles (^{1}H, ^{13}C, Mass Spectra, Size Distribution Analyses and Zeta Potential Measurements)

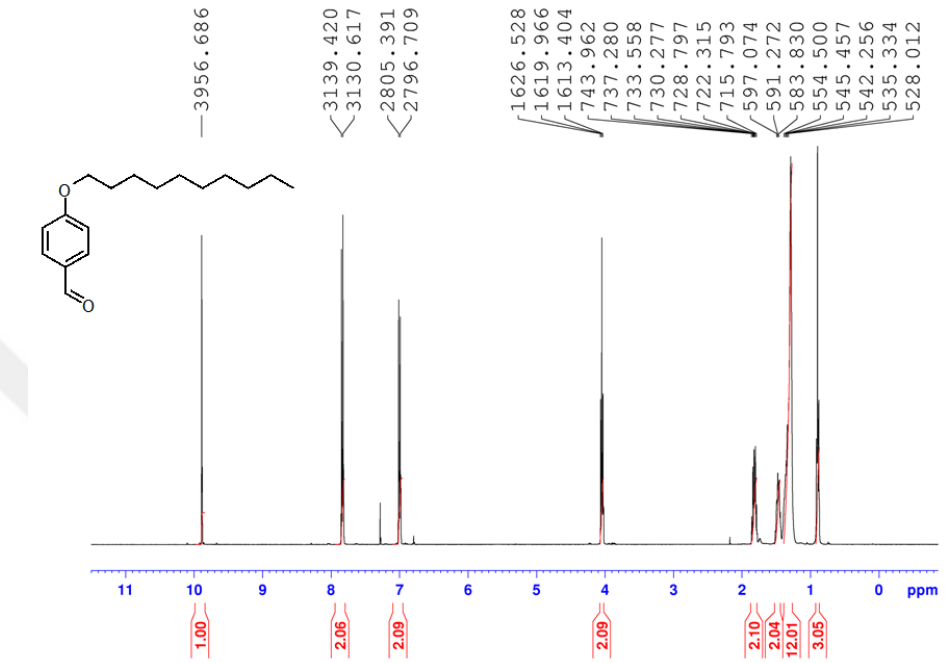

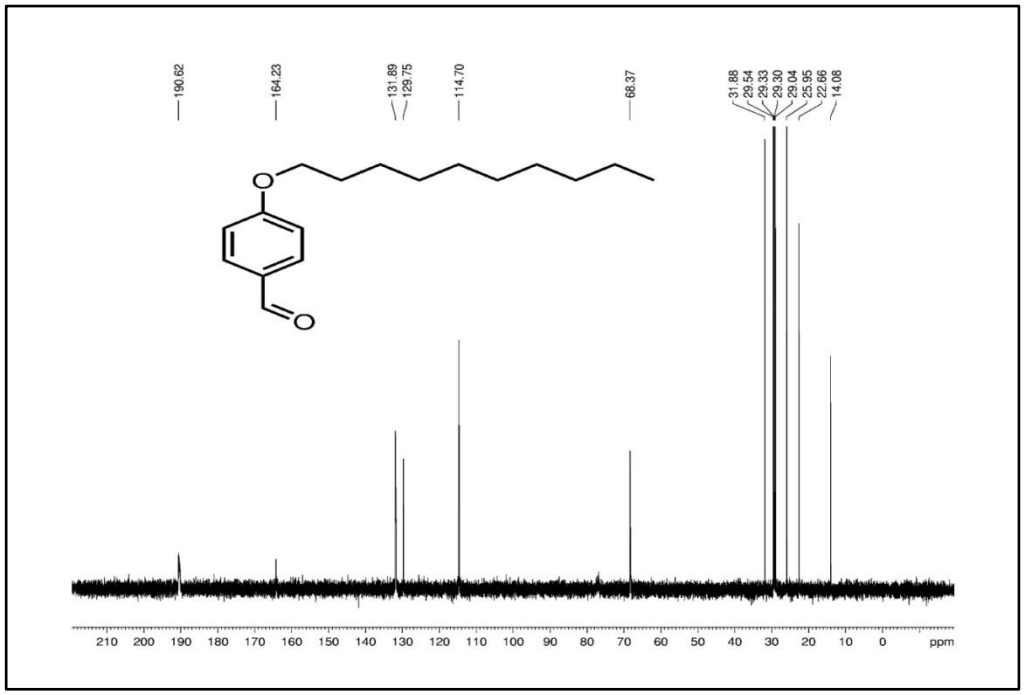

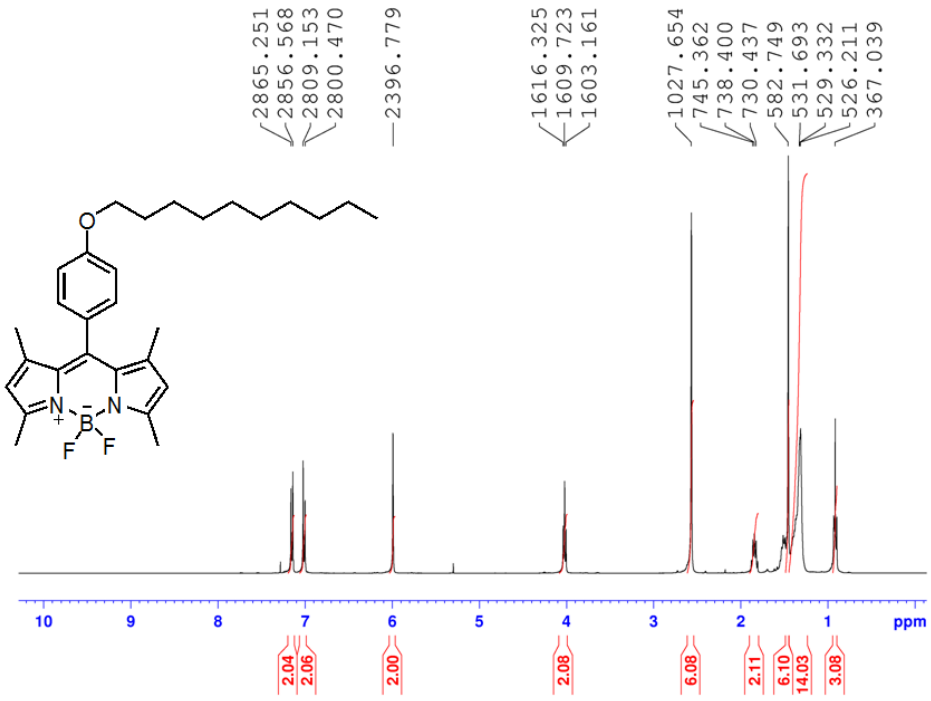
2865.251
2856.568
2809.153
2800.470
2396.779
1616.325
1609.723
1603.161
1027.654
745.362
738.400
730.437
582.749
531.693
529.332
526.211
367.039
O
N
B
F
F
10
9
8
7
6
5
4
3
2
1
ppm
2.04
2.06
2.00
2.08
6.08
2.11
6.10
14.03
3.08

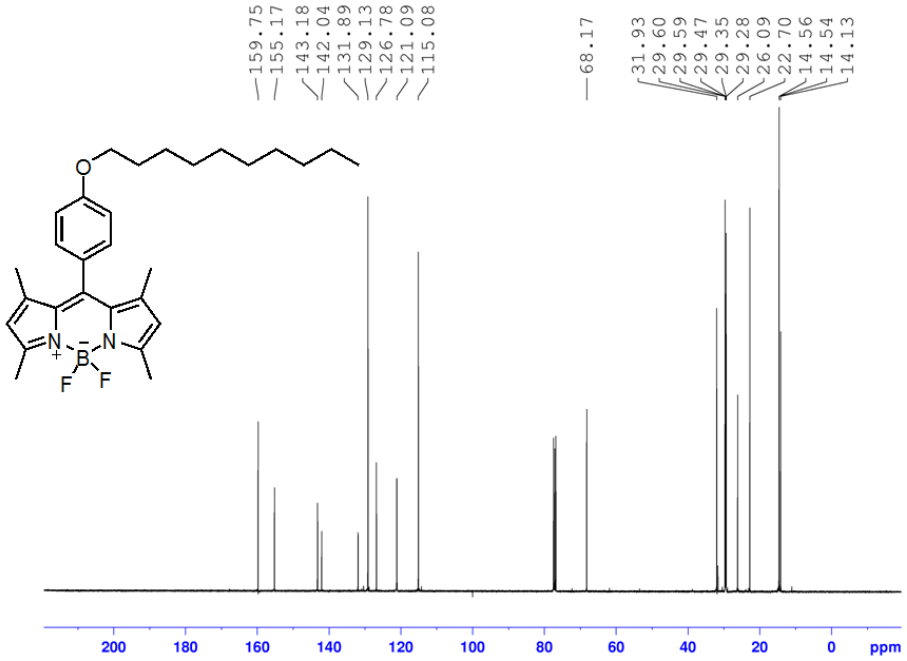
159.75
155.17
143.18
142.04
131.89
129.13
126.78
121.09
115.08
68.17
31.93
29.60
29.59
29.47
29.35
29.28
26.09
22.70
14.56
14.54
14.13
O
N
B
F
F
200
180
160
140
120
100
80
60
40
20
0
ppm

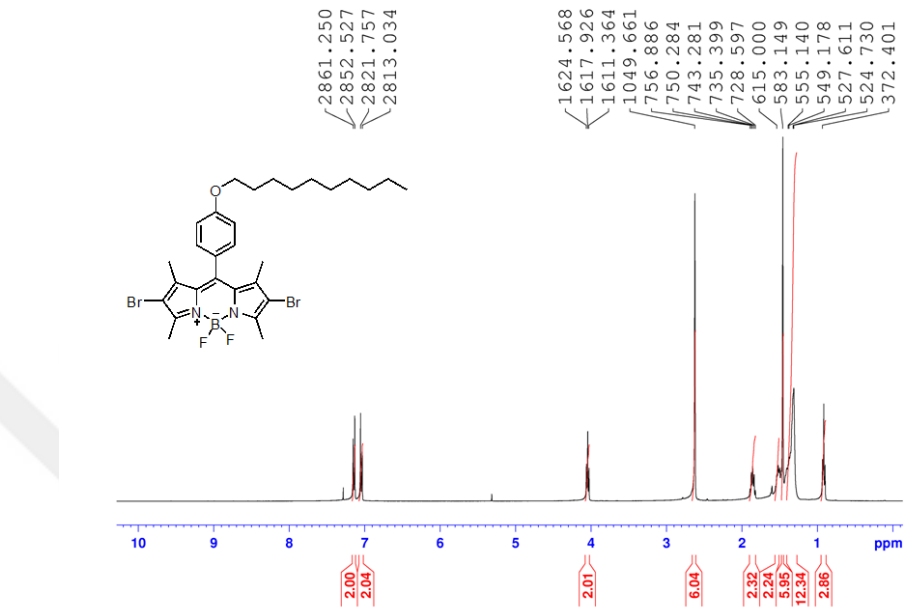
2861.250
2852.527
2821.757
2813.034
1624.568
1617.926
1611.364
1049.661
756.886
750.284
743.281
735.399
728.597
615.000
583.149
555.140
549.178
527.611
524.730
372.401
O
Br
Br
N
B
F
F
10
9
8
7
6
5
4
3
2
1
ppm
2.00
2.04
2.01
6.04
2.32
2.24
5.95
12.34
2.86

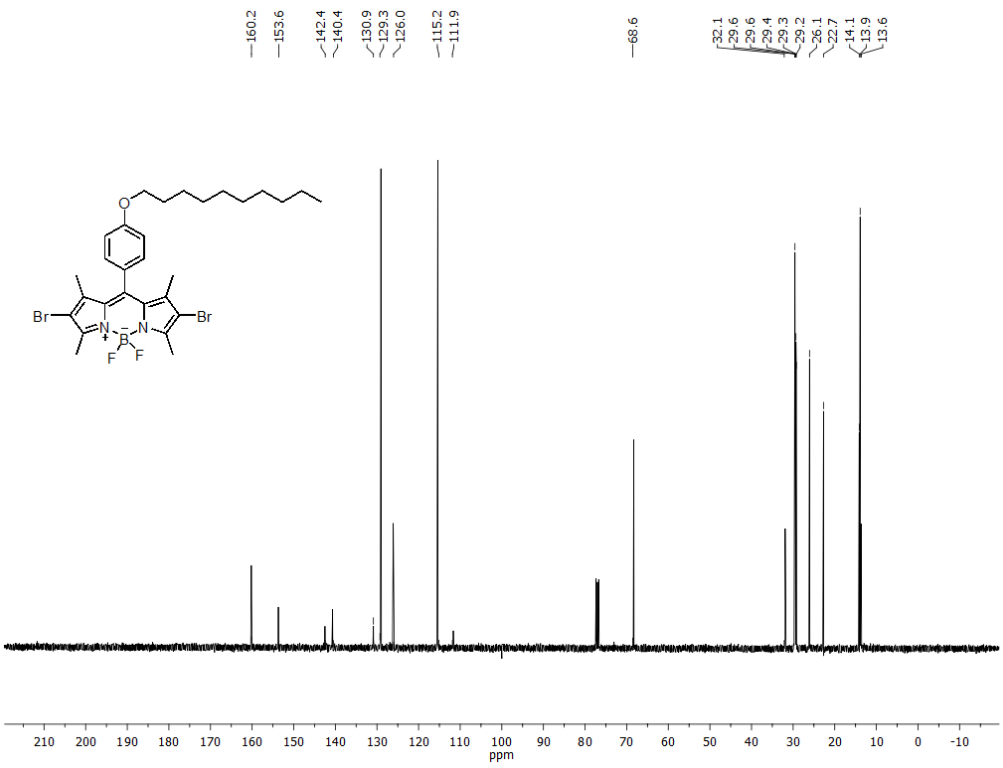
160.2
153.6
142.4
140.4
130.9
129.3
126.0
115.2
111.9
68.6
32.1
29.6
29.6
29.4
29.3
29.2
26.1
22.7
14.1
13.9
13.6
O
Br
Br
N
B
F
F
210
200
190
180
170
160
150
140
130
120
110
100
90
80
70
60
50
40
30
20
10
0
-10
ppm

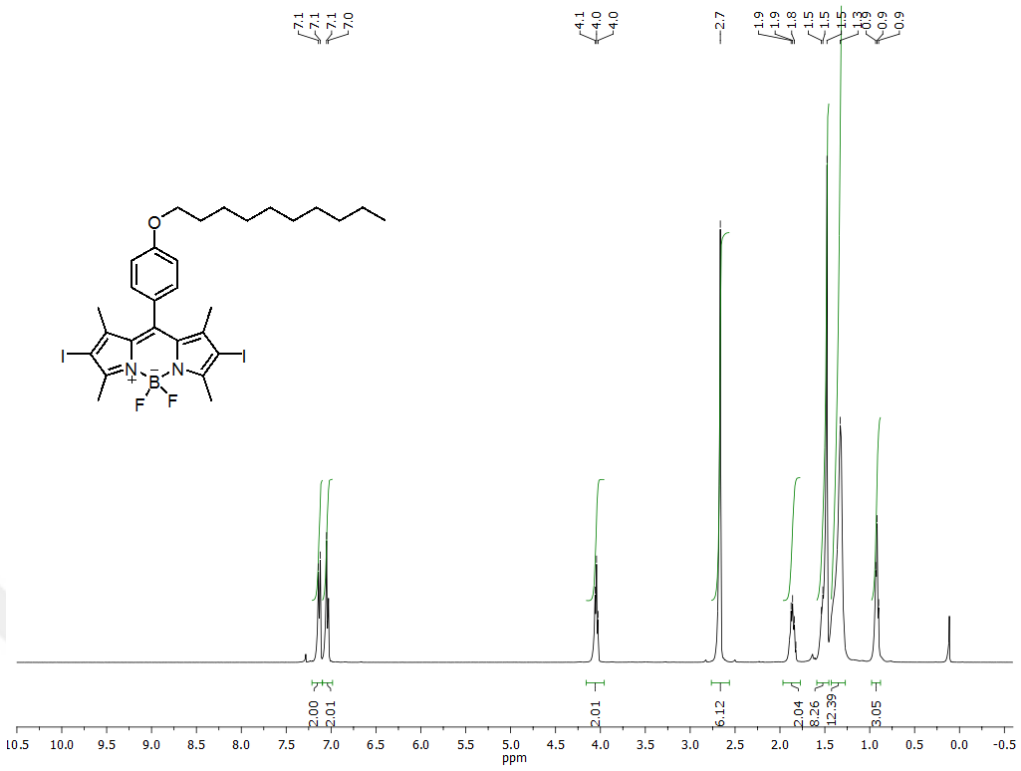
7.1
7.1
7.1
7.0
4.1
4.0
4.0
2.7
1.9
1.9
1.8
1.5
1.5
1.5
1.3
0.9
0.9
O
I
I
N
B
F
F
2.00
2.01
2.01
6.12
2.04
8.26
12.39
3.05
10.5 10.0 9.5 9.0 8.5 8.0 7.5 7.0 6.5 6.0 5.5 5.0 4.5 4.0 3.5 3.0 2.5 2.0 1.5 1.0 0.5 0.0 -0.5
ppm

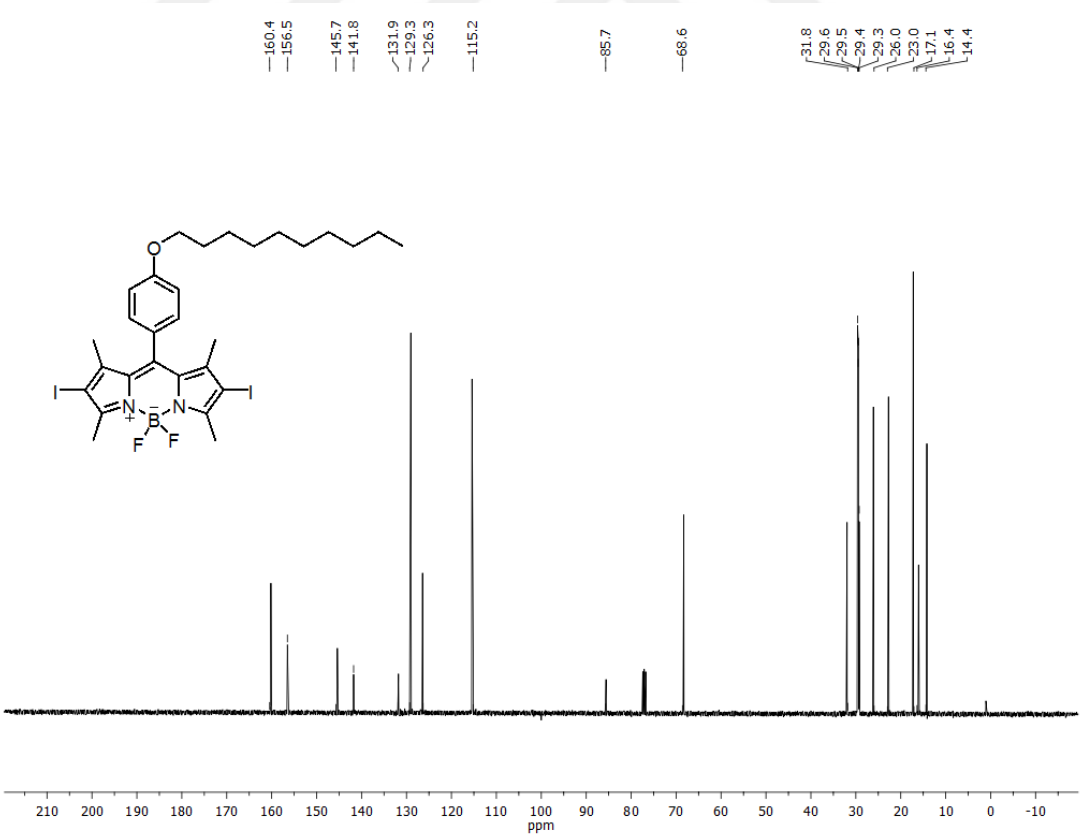
160.4
156.5
145.7
141.8
131.9
129.3
126.3
115.2
85.7
68.6
31.8
29.6
29.5
29.4
29.3
26.0
23.0
17.1
16.4
14.4
O
I
I
N
B
F
F
210 200 190 180 170 160 150 140 130 120 110 100 90 80 70 60 50 40 30 20 10 0 -10
ppm

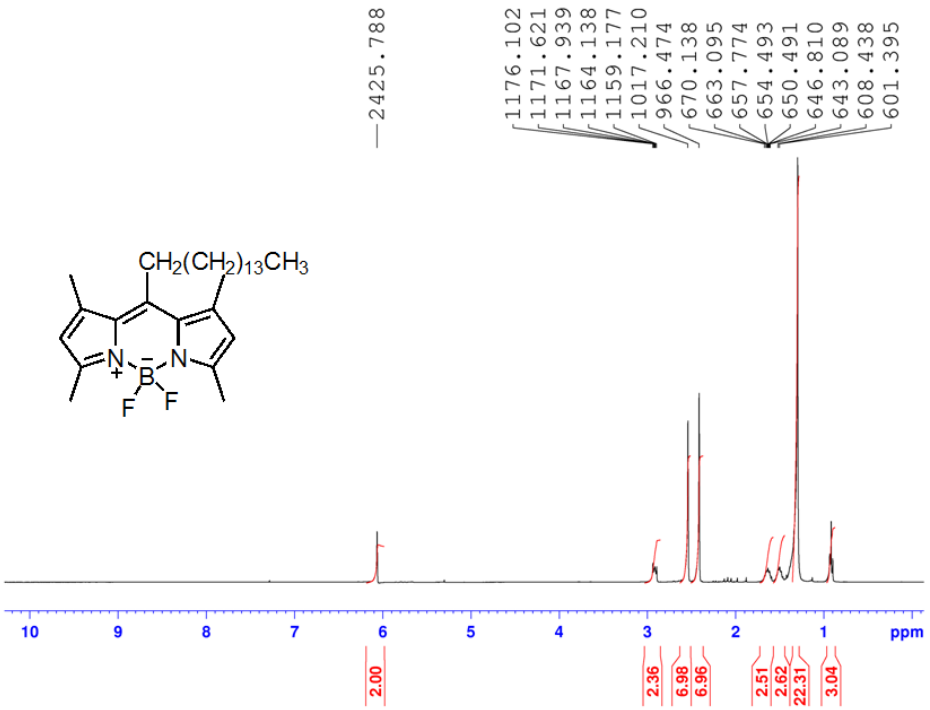
2425.788
1176.102
1171.621
1167.939
1164.138
1159.177
1017.210
966.474
670.138
663.095
657.774
654.493
650.491
646.810
643.089
608.438
601.395
CH2(CH2)13CH3
N
B
F
F
10
9
8
7
6
5
4
3
2
1
ppm
2.00
2.36
6.98
6.96
2.51
2.62
22.31
3.04

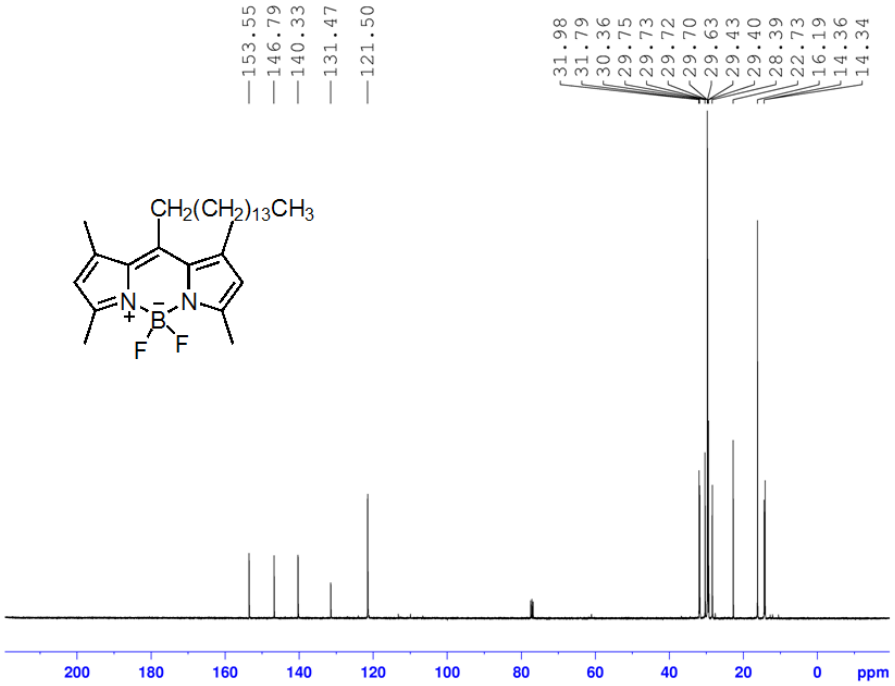
153.55
146.79
140.33
131.47
121.50
31.98
31.79
30.36
29.75
29.73
29.72
29.70
29.63
29.43
29.40
28.39
22.73
16.19
14.36
14.34
CH2(CH2)13CH3
N
B
F
F
200
180
160
140
120
100
80
60
40
20
0
ppm

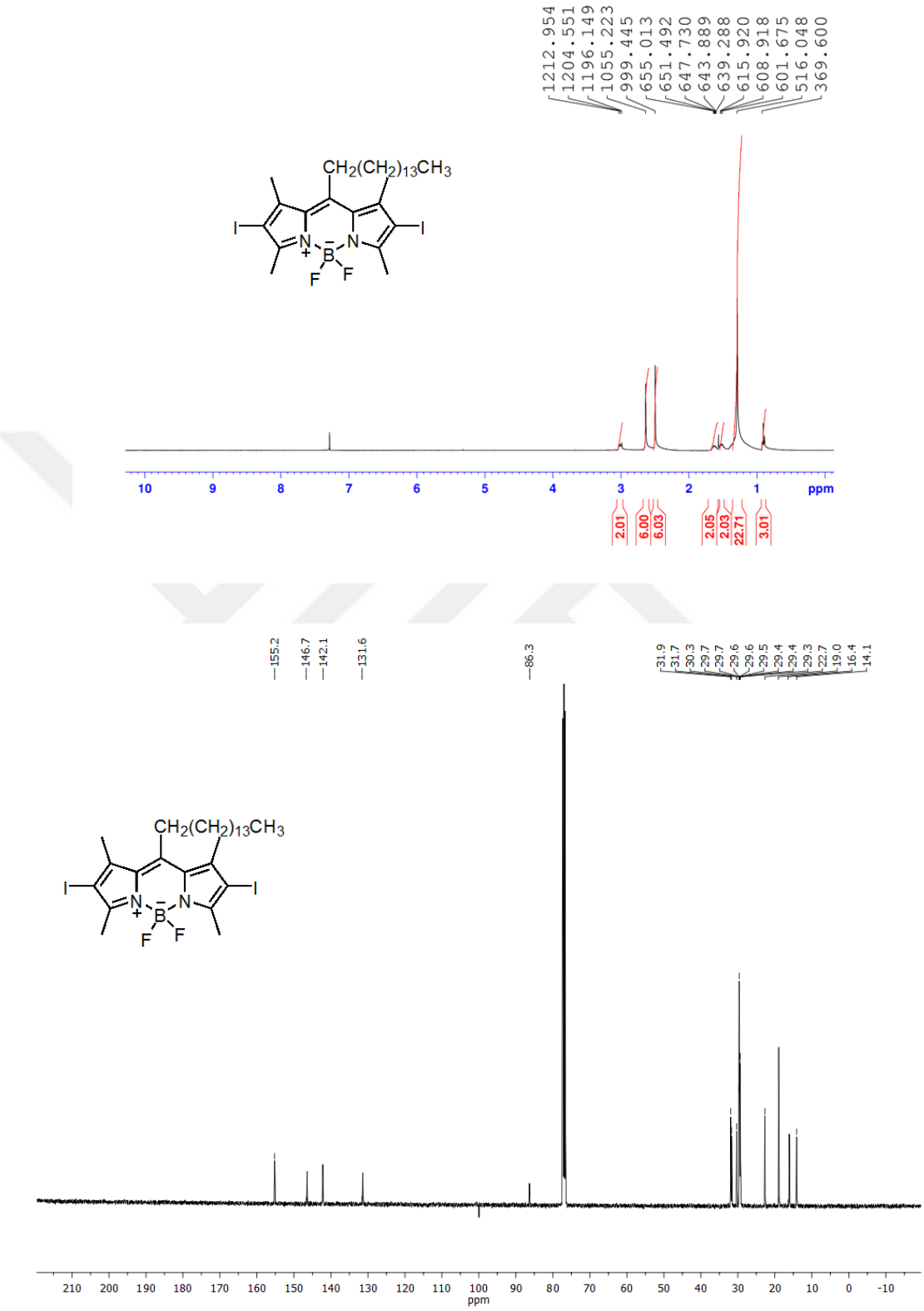
1212.954
1204.551
1196.149
1055.223
999.445
655.013
651.492
647.730
643.889
639.288
615.920
608.918
601.675
516.048
369.600
CH2(CH2)13CH3
I
I
N
B
N
F
F
10
9
8
7
6
5
4
3
2
1
ppm
2.01
6.00
6.03
2.05
2.03
22.71
3.01
155.2
146.7
142.1
131.6
86.3
31.9
31.7
30.3
29.7
29.7
29.6
29.6
29.5
29.4
29.4
29.3
22.7
19.0
16.4
14.1
CH2(CH2)13CH3
I
I
N
B
N
F
F
210
200
190
180
170
160
150
140
130
120
110
100
90
80
70
60
50
40
30
20
10
0
-10
ppm

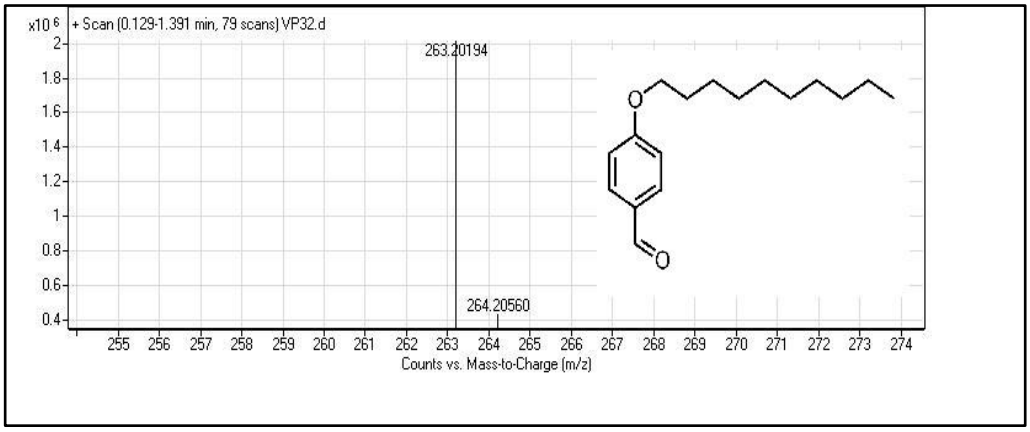
x10 6
+ Scan (0.129-1.391 min, 79 scans) VP32.d
263.20194
264.20560
Counts vs. Mass-to-Charge (m/z)

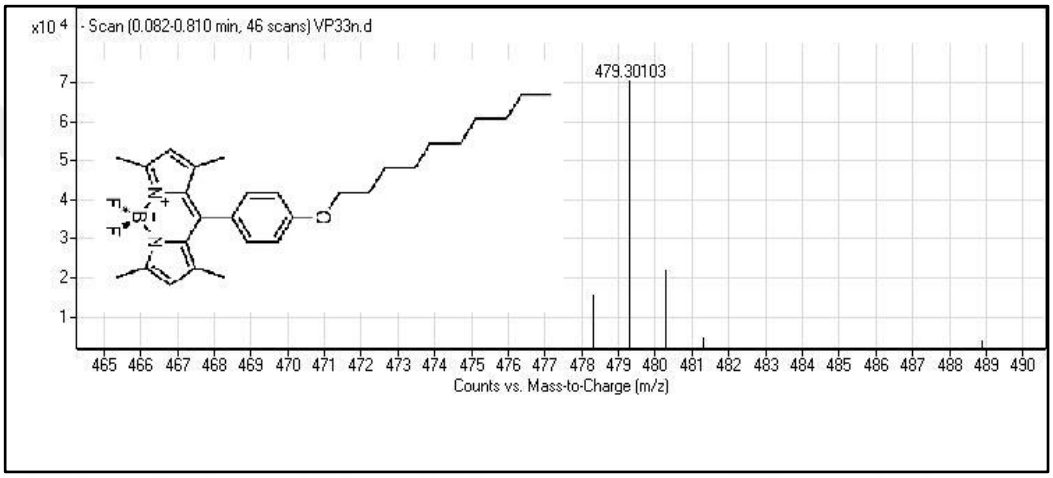
x10 4
- Scan (0.082-0.810 min, 46 scans) VP33n.d
479.30103
Counts vs. Mass-to-Charge (m/z)

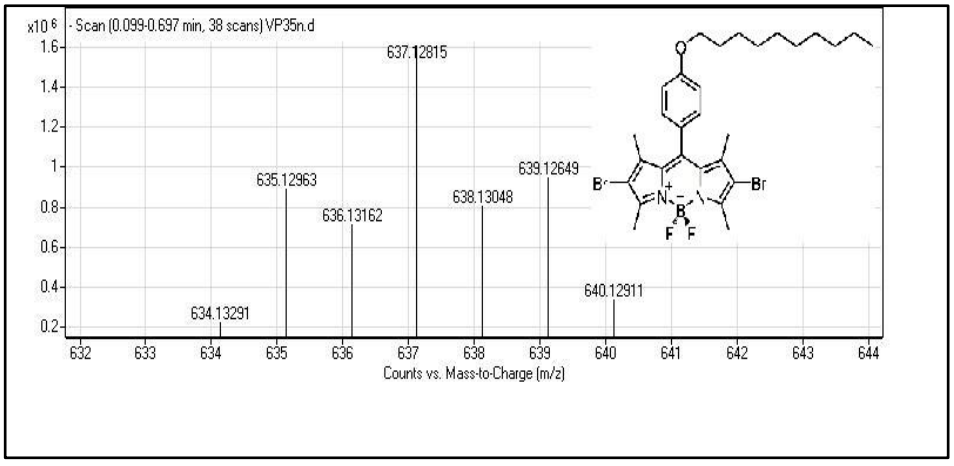
x10 6
- Scan (0.099-0.697 min, 38 scans) VP35n.d
637.12815
635.12963
639.12649
636.13162
638.13048
634.13291
640.12911
Counts vs. Mass-to-Charge (m/z)

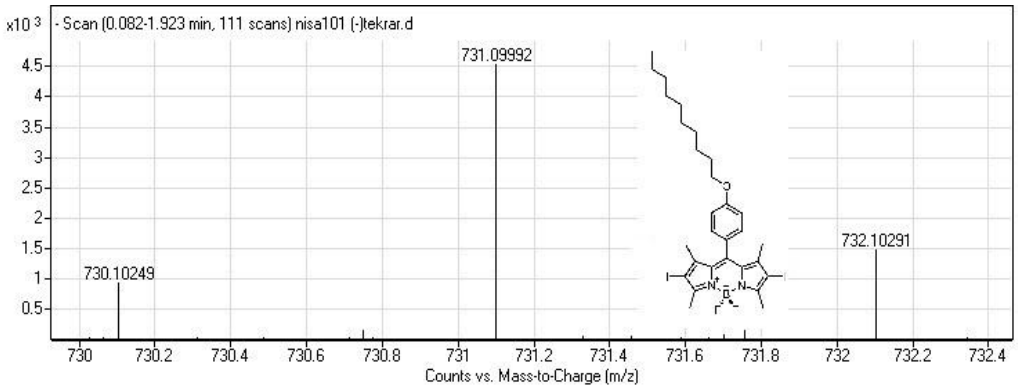
x10 3
- Scan (0.082-1.923 min, 111 scans) nisa101 (-)tekrar.d
731.09992
730.10249
732.10291
Counts vs. Mass-to-Charge (m/z)

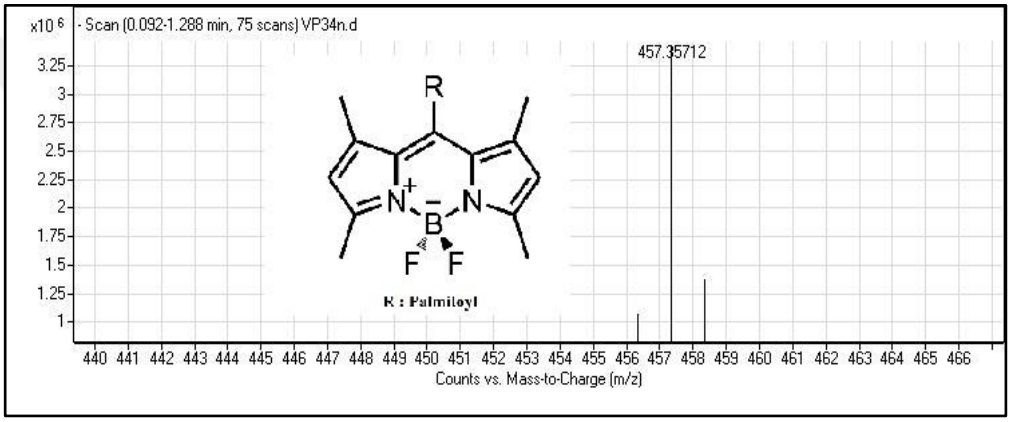
x10 6
- Scan (0.092-1.288 min, 75 scans) VP34n.d
457.35712
R
R : Palmiloyl
Counts vs. Mass-to-Charge (m/z)

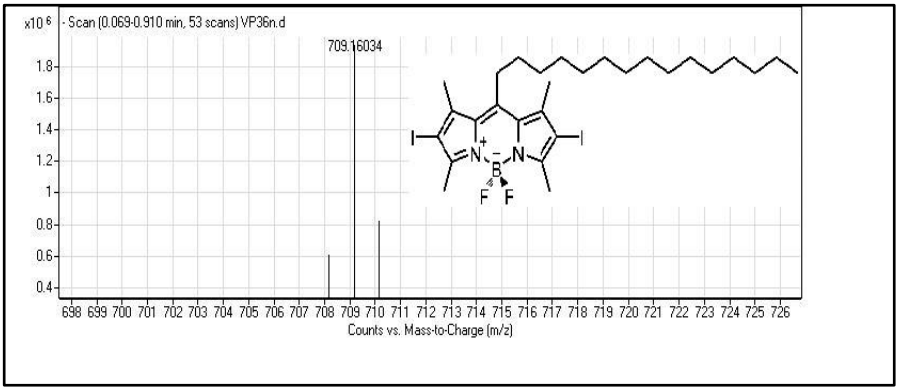
x10 6
- Scan (0.069-0.910 min, 53 scans) VP36n.d
709.16034
Counts vs. Mass-to-Charge (m/z)

Size Distribution Analysis

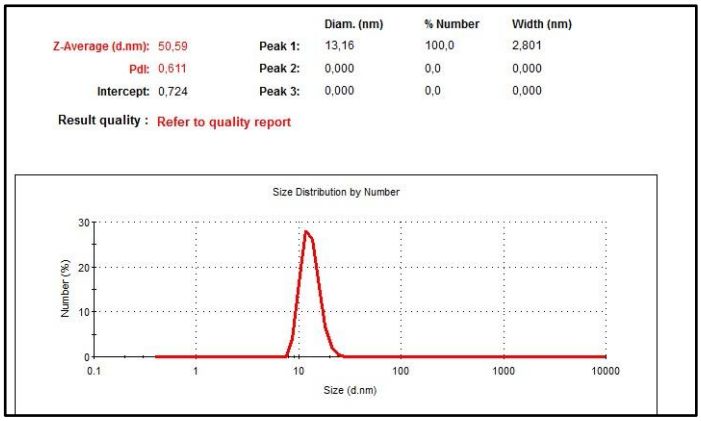

Size distribution of micellar compound **58**. Cremophor EL was used for embedding the dye. Other information related with instrument is given in the Experimental Details.

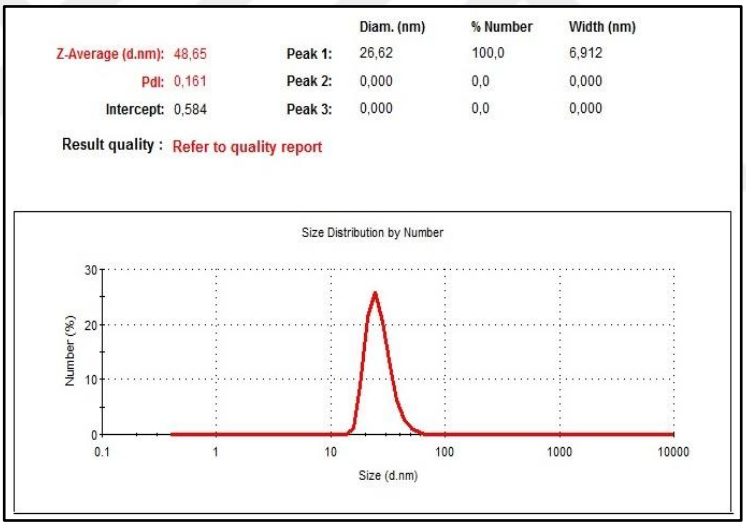

Size distribution of micellar compound **59**. Cremophor EL was used for embedding the dye.Other information related with instrument is given in the Experimental Details.

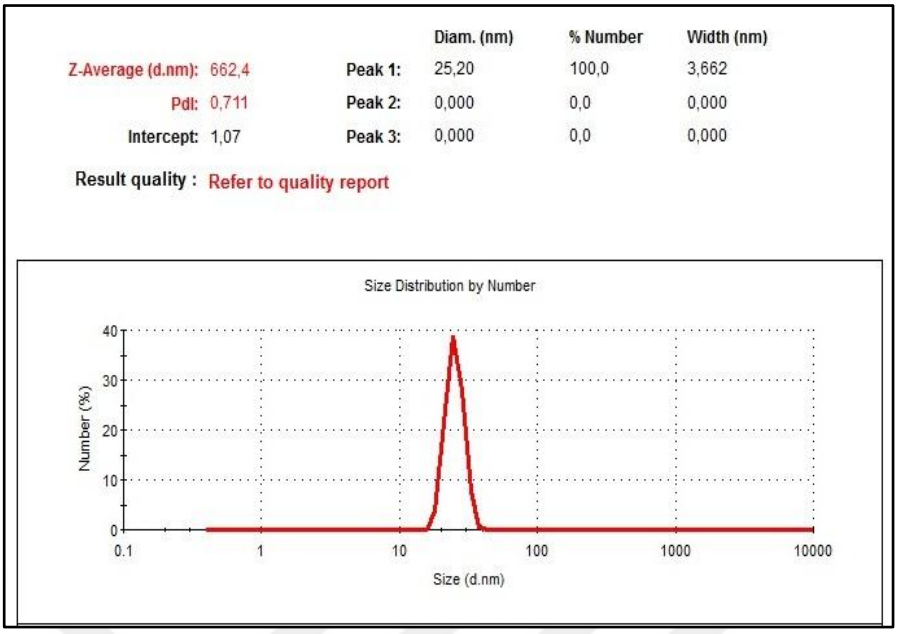

Size distribution of micellar compound **62**. Cremophor EL was used for embedding the dye. Other information related with instrument is given in the Experimental Details.

Zeta Potential Measurements

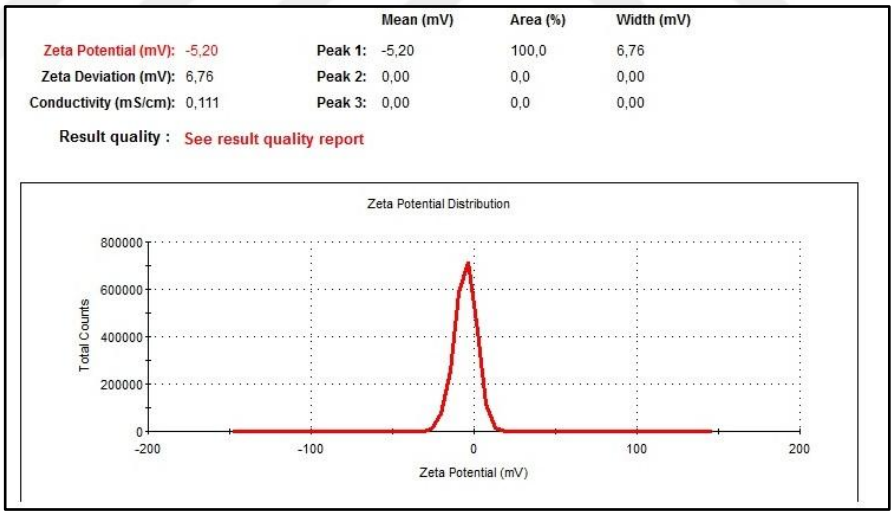

Zeta potential measurement of micellar compound **58**. Cremophor EL was used for embedding the dye.Other information related with instrument is given in the Experimental Details.

		Mean (mV)	Area (%)	Width (mV)
Zeta Potential (mV): -0,741	Peak 1:	9,56	50,8	10,3
Zeta Deviation (mV): 56,3	Peak 2:	-19,3	5,8	4,48
Conductivity (mS/cm): 0,00838	Peak 3:	39,9	3,8	3,45

Result quality : See result quality report

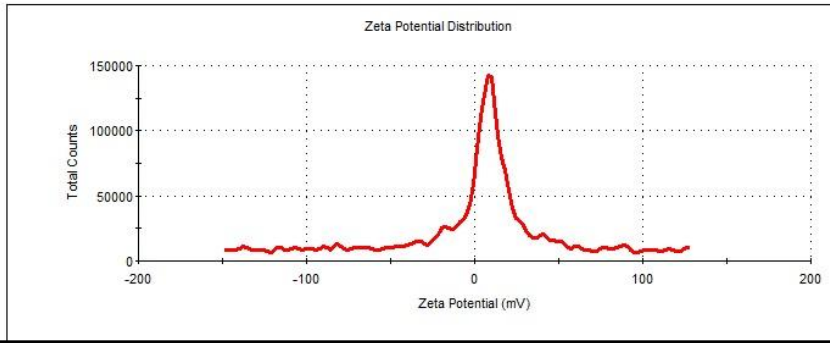

Zeta potential measurement of micellar compound **59.** Cremophor EL was used for embedding the dye.Other information related with instrument is given in the Experimental Details.

A3. A Study on Spectral Changes in tetra-benzocrown Modified BODIPY induced by α, ω-diamino Alkanes. (^{1}H, ^{13}C and Mass Spectra)

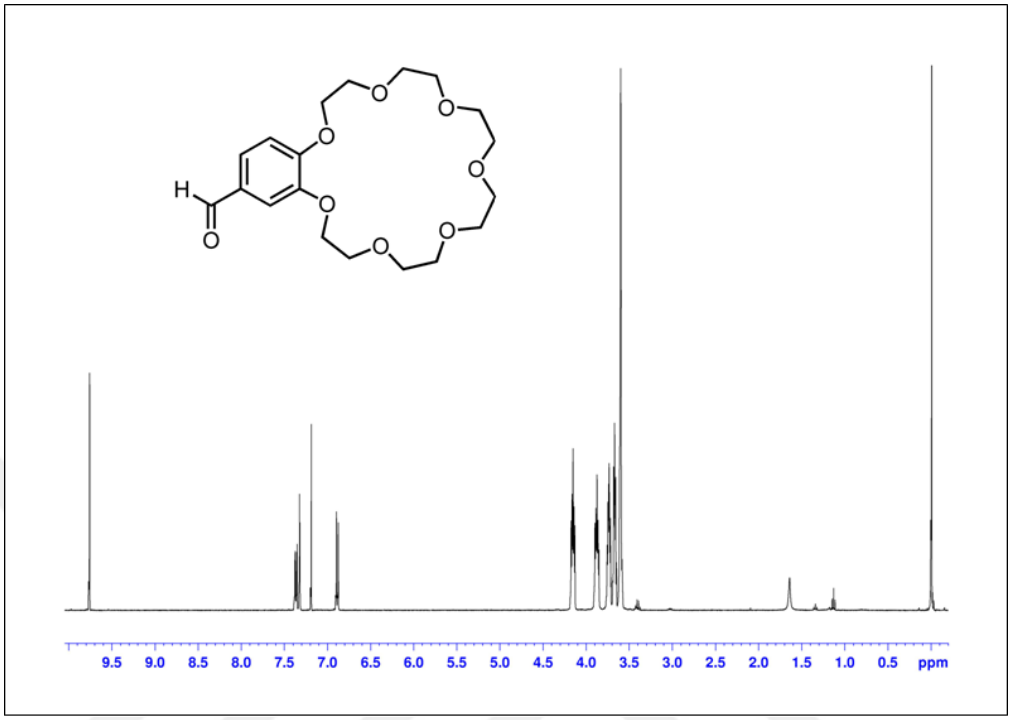

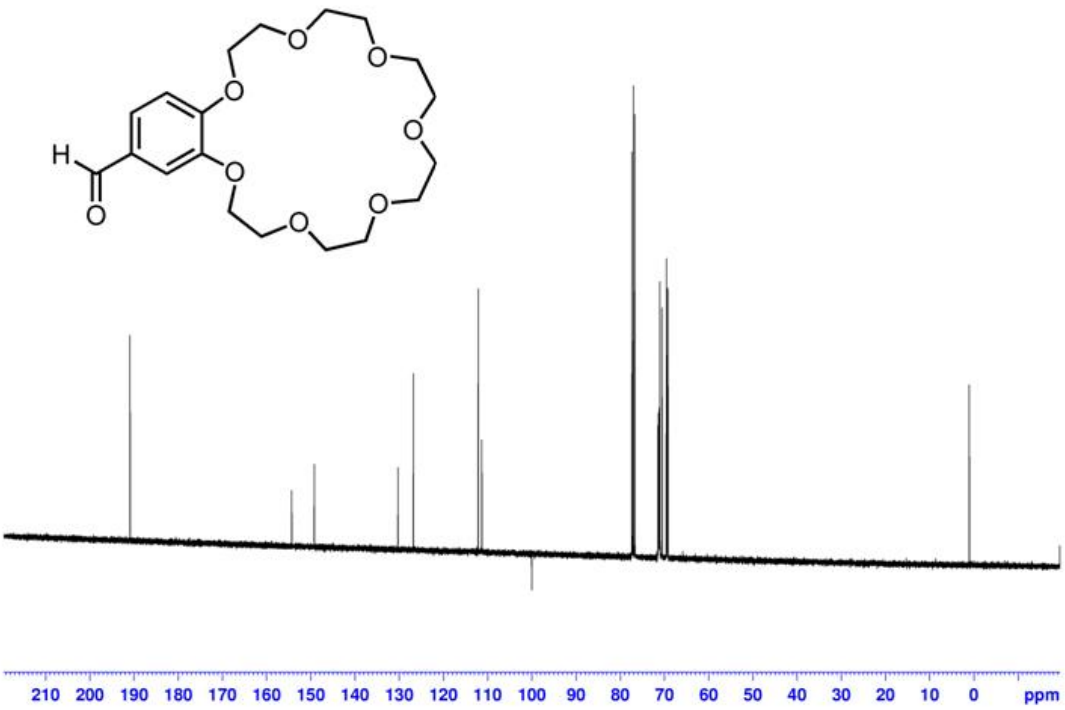

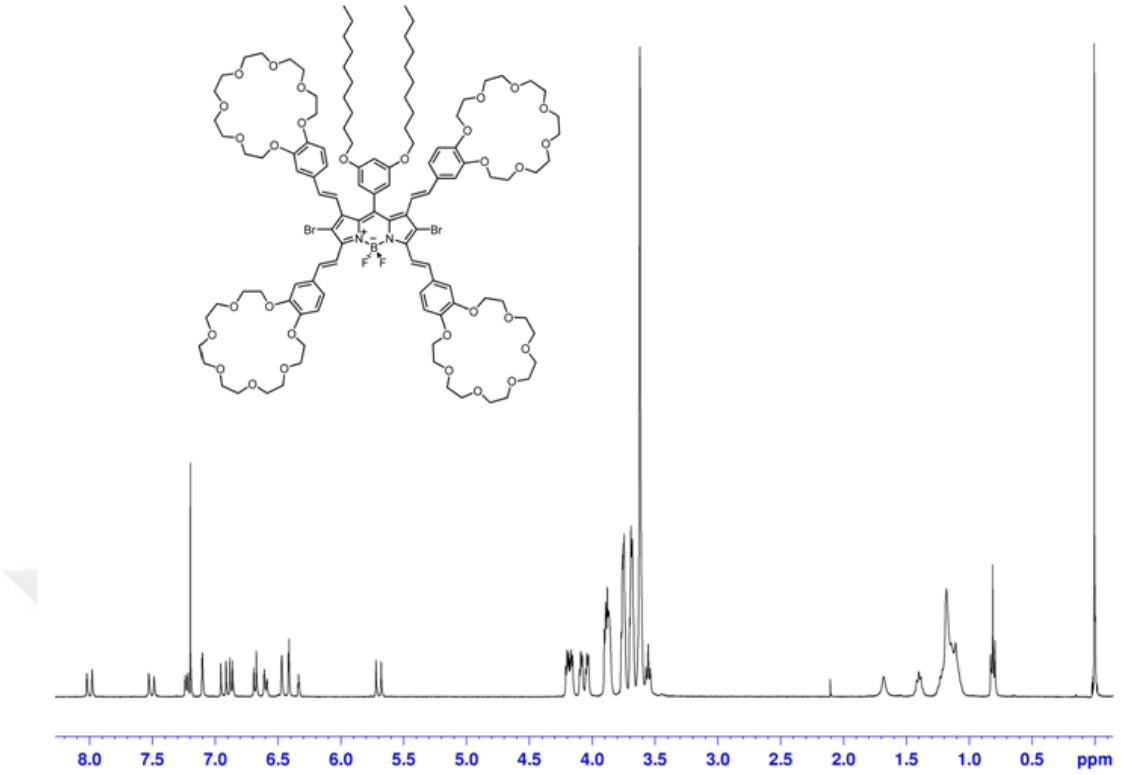
Br
Br
8.0
7.5
7.0
6.5
6.0
5.5
5.0
4.5
4.0
3.5
3.0
2.5
2.0
1.5
1.0
0.5
ppm

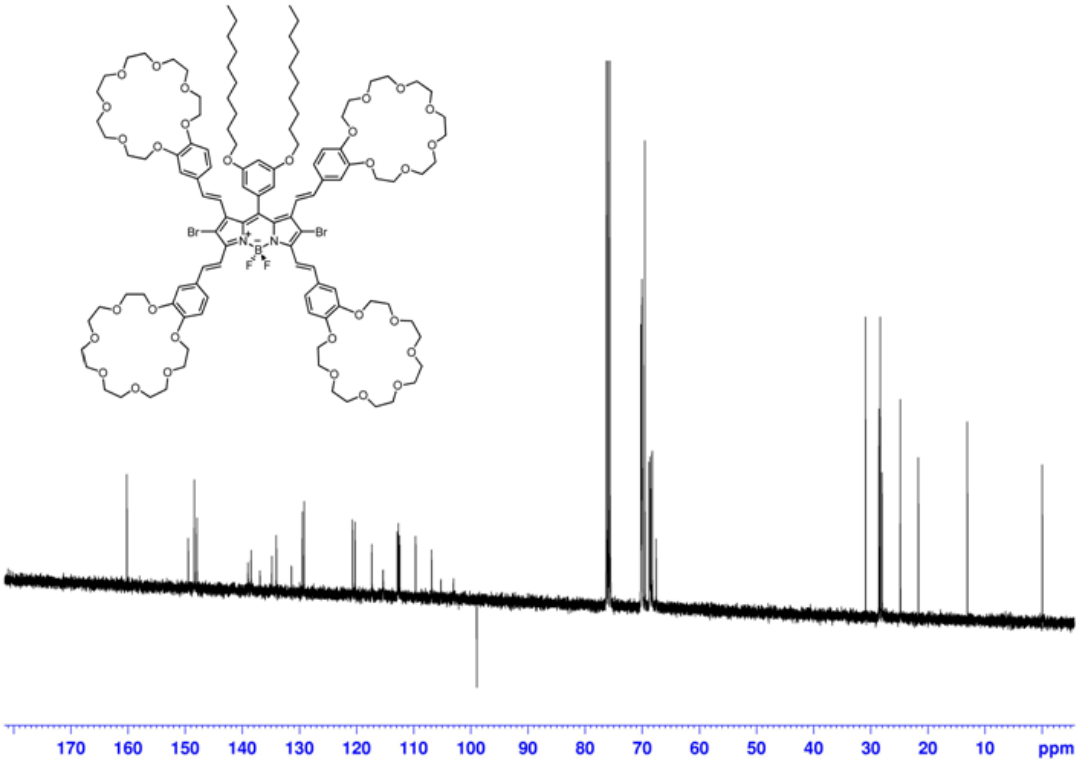
Br
Br
170
160
150
140
130
120
110
100
90
80
70
60
50
40
30
20
10
ppm

A4. Towards A Reaction Based Probe for Reductive Intracellular Conditions. (^{1}H, ^{13}C and Mass Spectra)

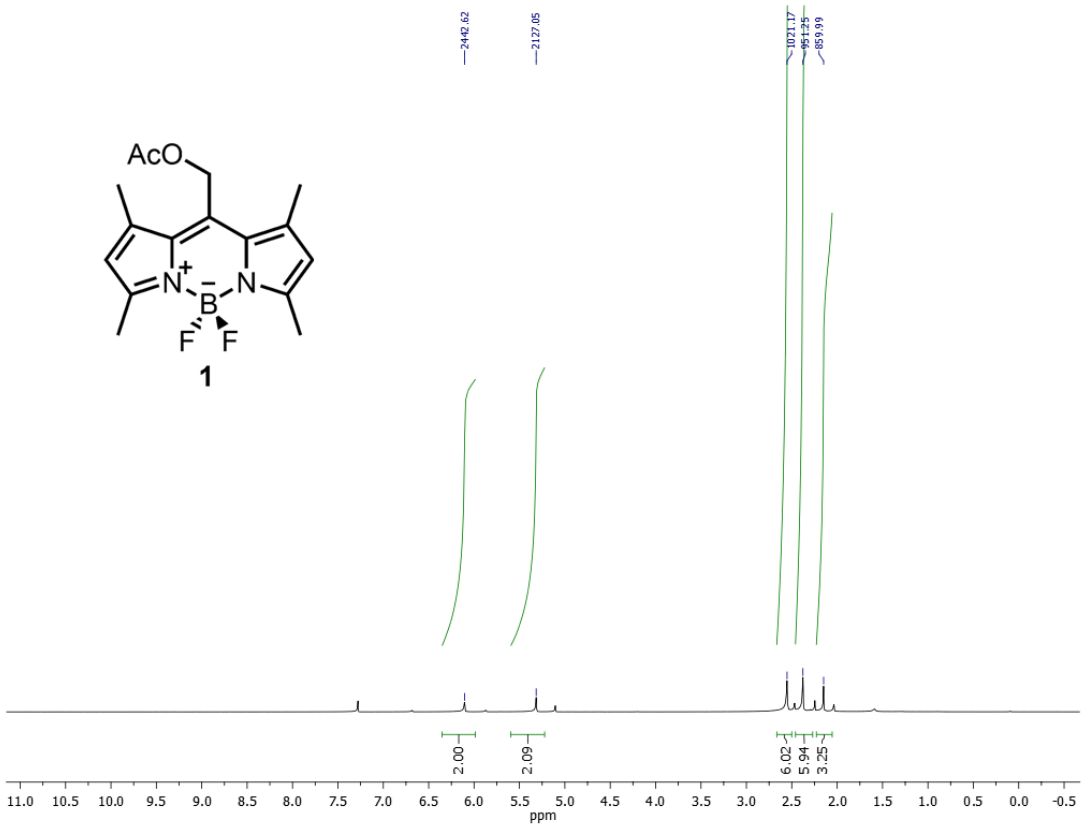

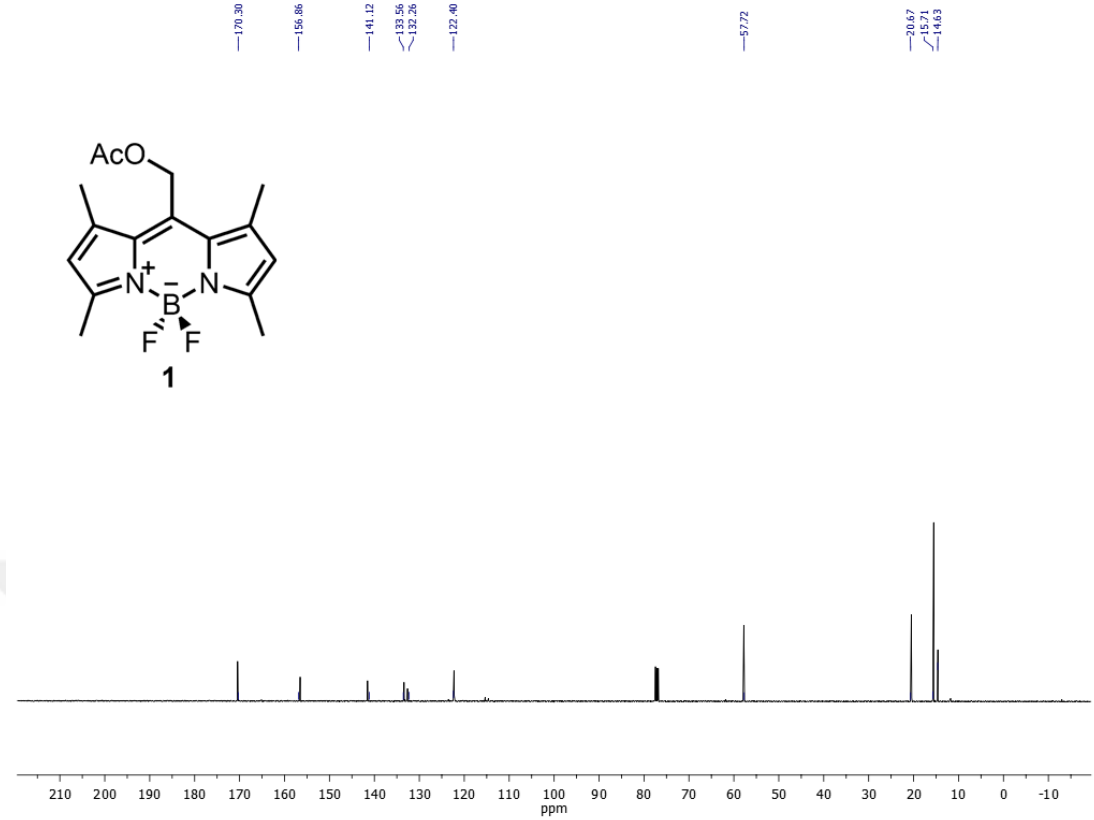
170.30
156.86
141.12
133.56
132.26
122.40
57.72
20.67
15.71
14.63
AcO
N+
B
N
F
F
1
210 200 190 180 170 160 150 140 130 120 110 100 90 80 70 60 50 40 30 20 10 0 -10
ppm

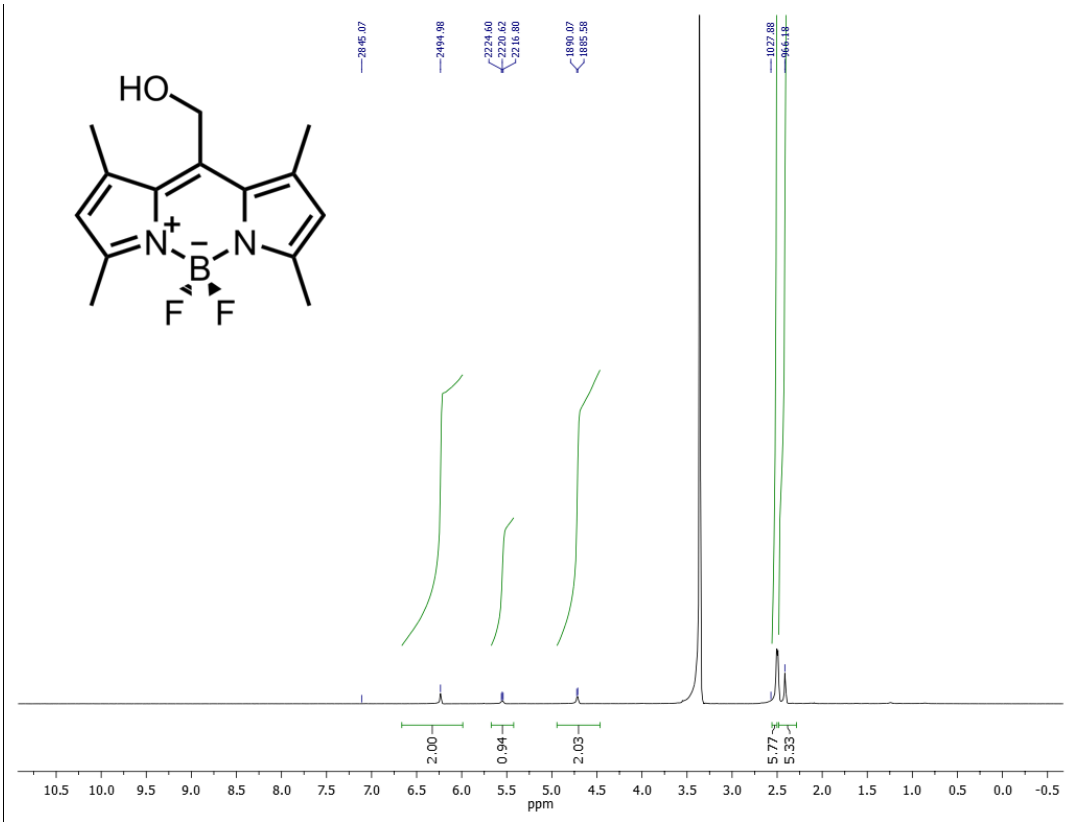
2845.07
2494.98
2224.60
2220.62
2216.80
1890.07
1885.58
1027.88
966.18
HO
N+
B
N
F
F
2.00
0.94
2.03
5.77
5.33
10.5 10.0 9.5 9.0 8.5 8.0 7.5 7.0 6.5 6.0 5.5 5.0 4.5 4.0 3.5 3.0 2.5 2.0 1.5 1.0 0.5 0.0 -0.5
ppm

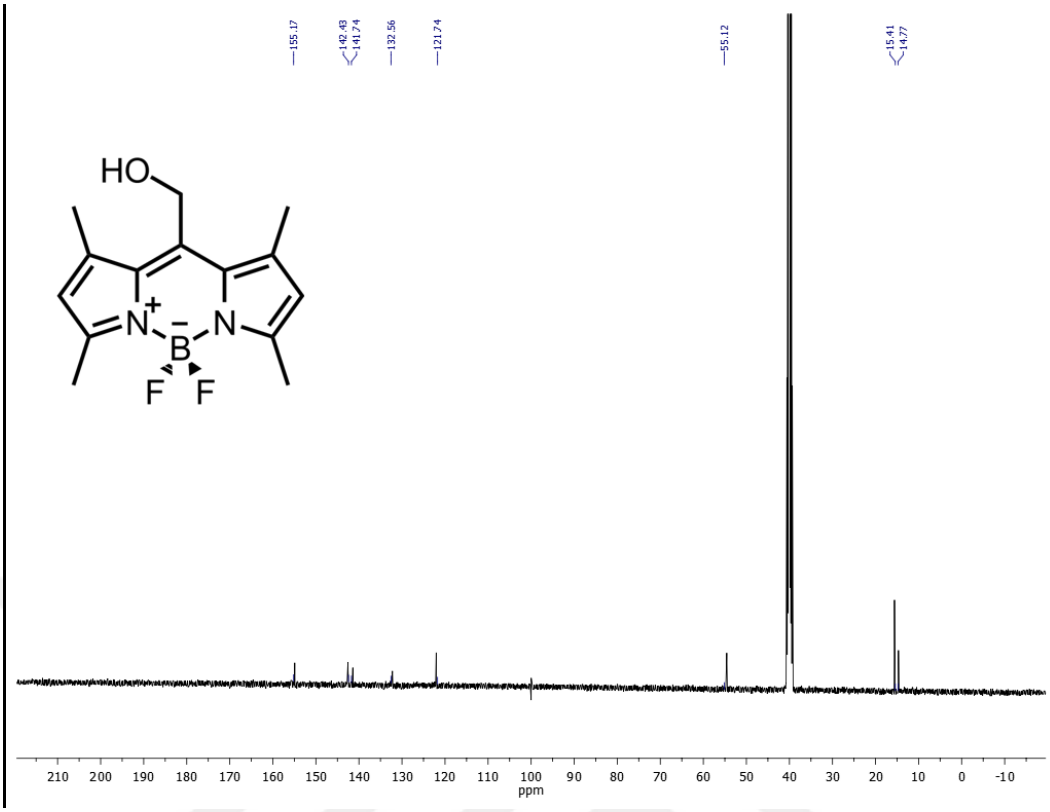
155.17
142.48
141.74
132.56
121.74
55.12
15.41
14.77
HO
N+
B
N
F
F
210 200 190 180 170 160 150 140 130 120 110 100 90 80 70 60 50 40 30 20 10 0 -10
ppm

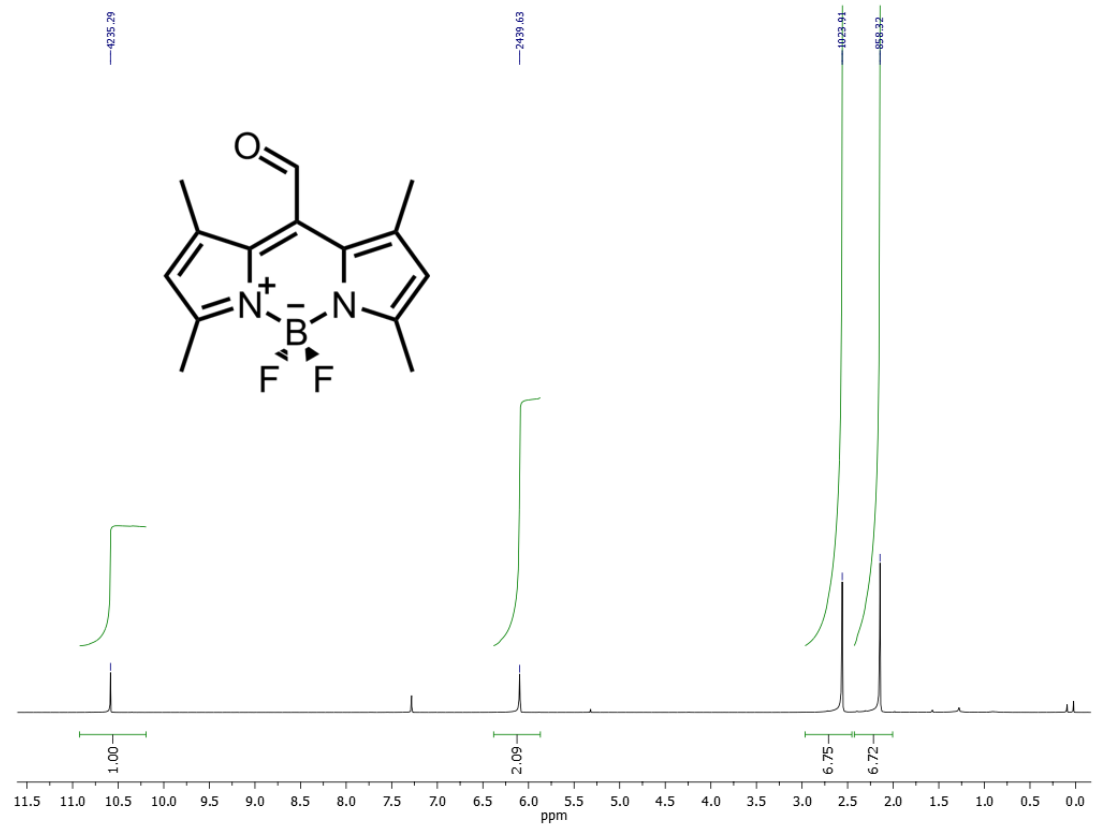
4235.29
2439.63
1023.91
858.32
O
N+
B
N
F
F
1.00
2.09
6.75
6.72
11.5 11.0 10.5 10.0 9.5 9.0 8.5 8.0 7.5 7.0 6.5 6.0 5.5 5.0 4.5 4.0 3.5 3.0 2.5 2.0 1.5 1.0 0.5 0.0
ppm

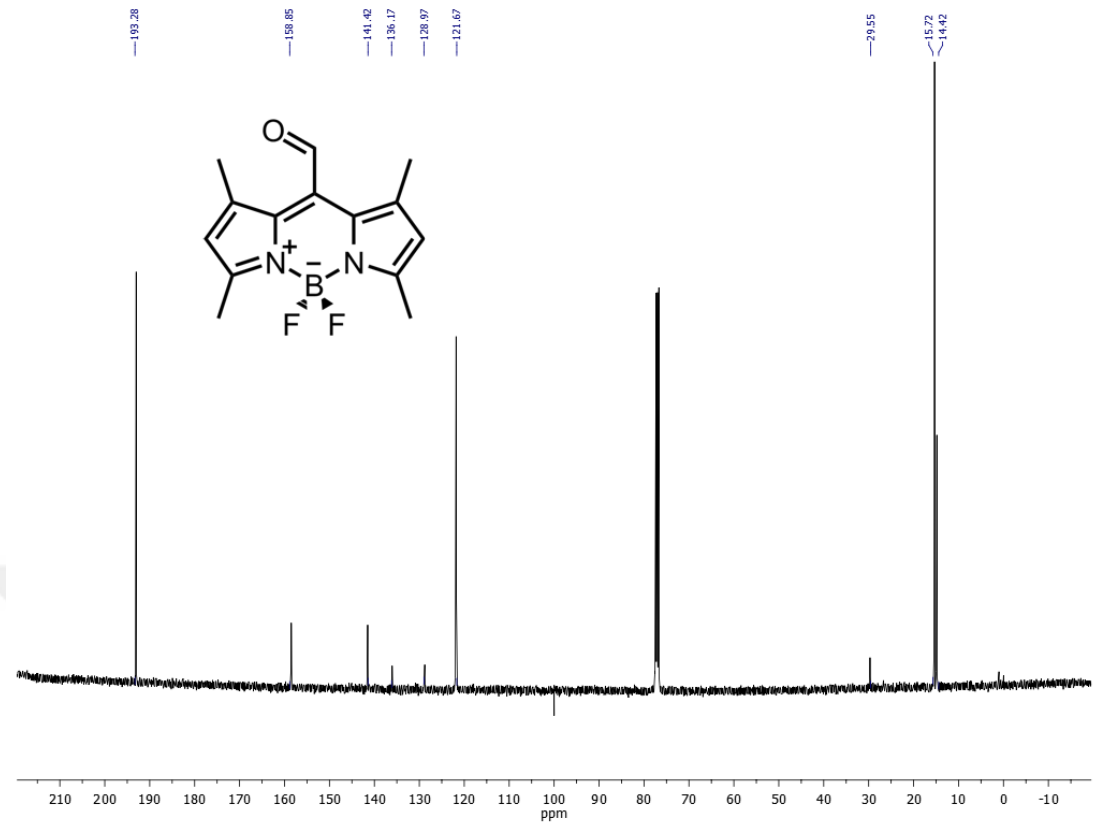
193.28
158.05
141.42
136.17
128.97
121.67
29.55
15.72
14.42
O
N+
B
N
F F
210 200 190 180 170 160 150 140 130 120 110 100 90 80 70 60 50 40 30 20 10 0 -10
ppm

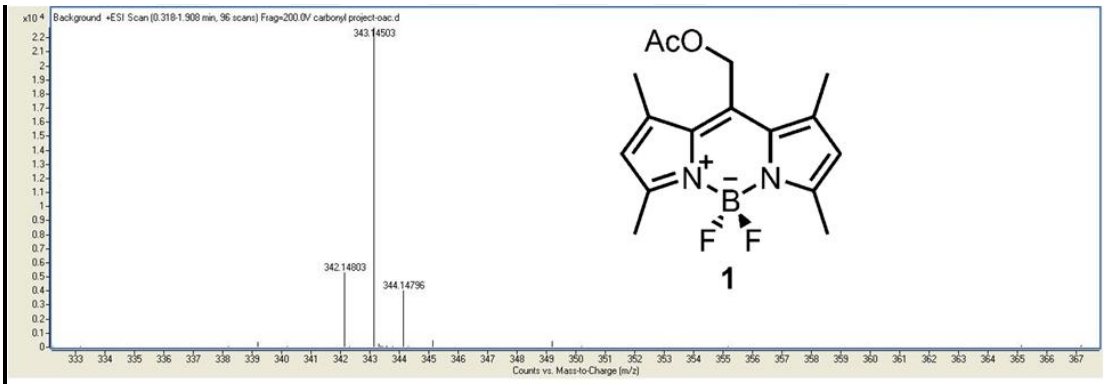
Background +ESI Scan (0.318-1.908 min, 96 scans) Frag=200.0V carbonyl project-oac.d
343.14503
342.14803
344.14796
AcO
N+
B
N
F F
1
Counts vs. Mass-to-Charge (m/z)

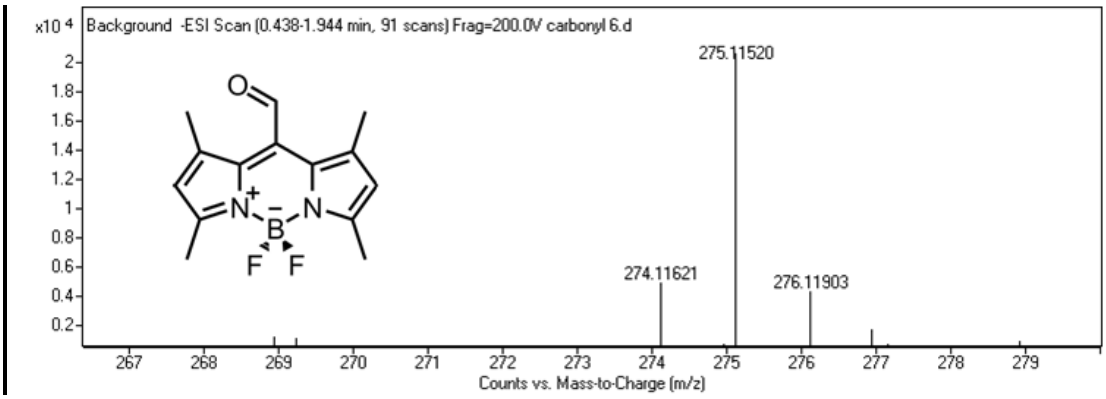
Background -ESI Scan (0.438-1.944 min, 91 scans) Frag=200.0V carbonyl 6.d
275.11520
274.11621
276.11903
O
N+
B
N
F F
Counts vs. Mass-to-Charge (m/z)

A5. Supramolecular Control of Through Space Energy Transfer (^{1}H, ^{13}C and Mass Spectra)

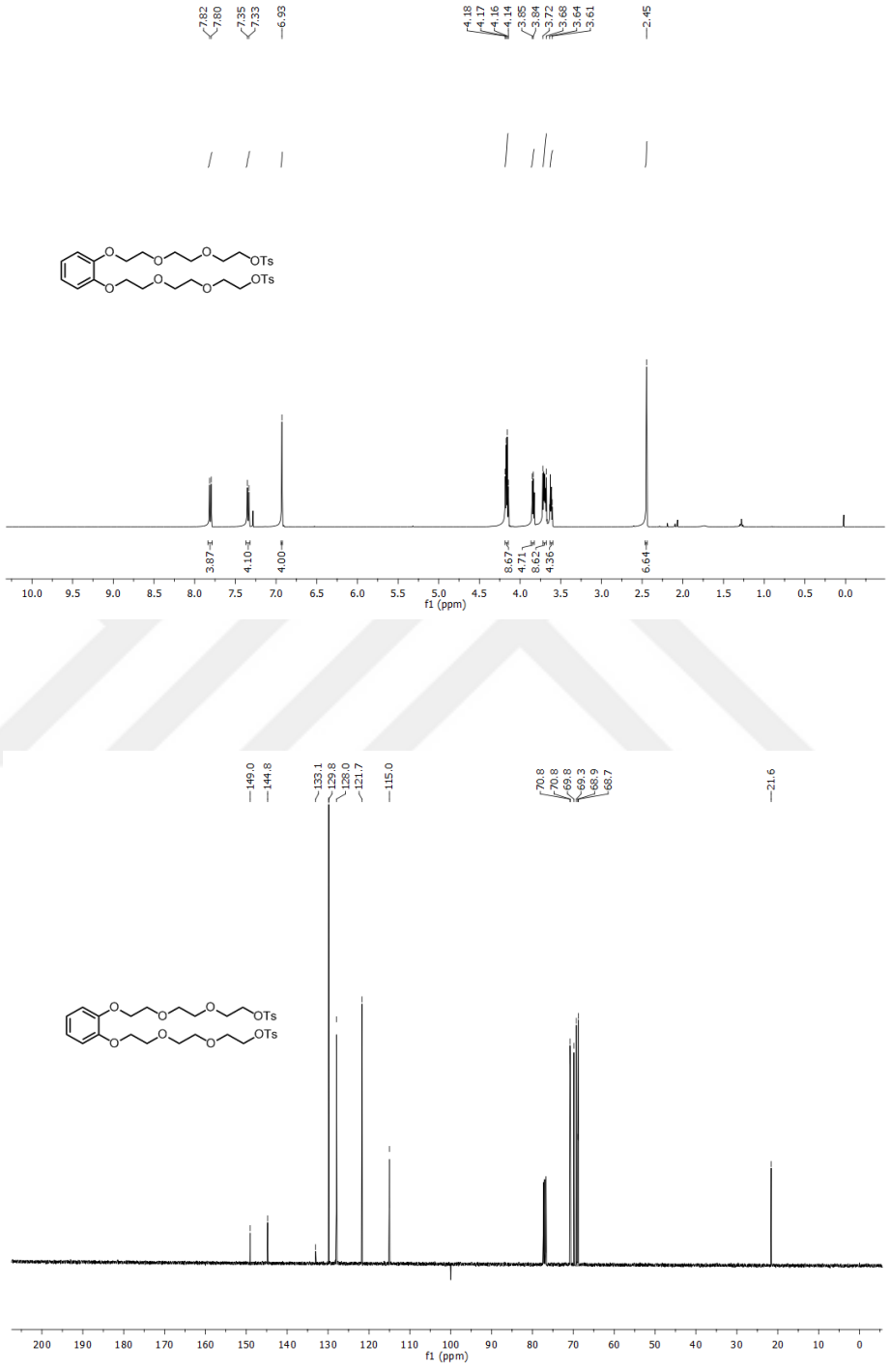

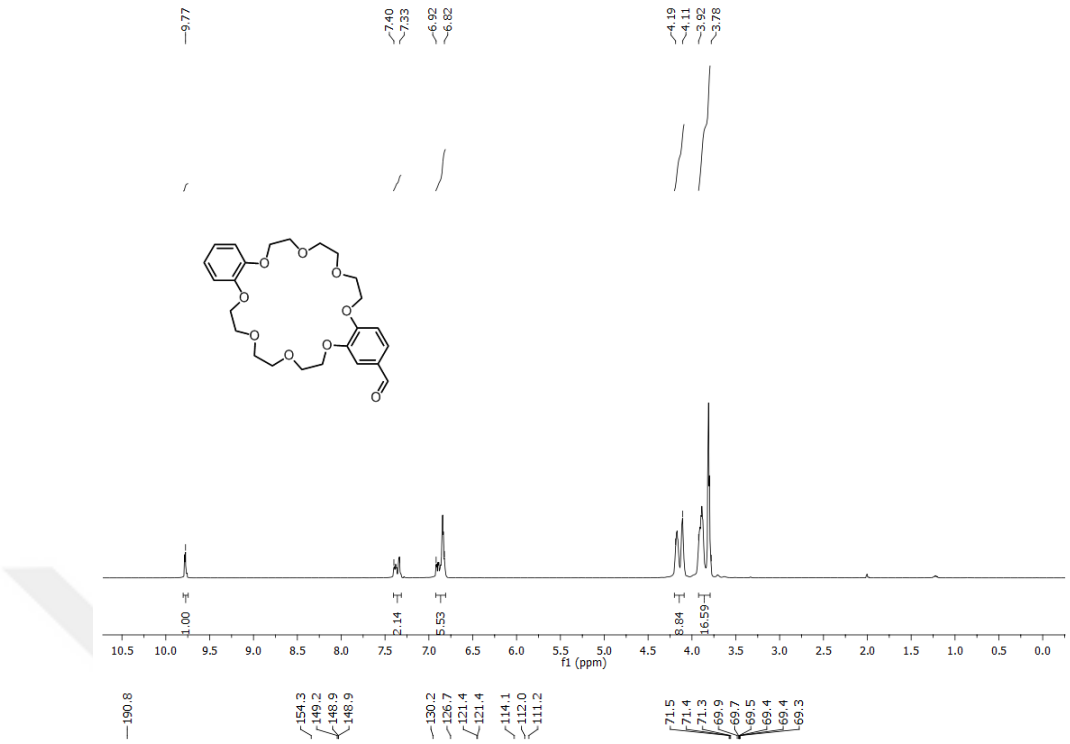
9.77
7.40
7.33
6.92
6.82
4.19
4.11
3.92
3.78
1.00
2.14
5.53
8.84
16.59
f1 (ppm)

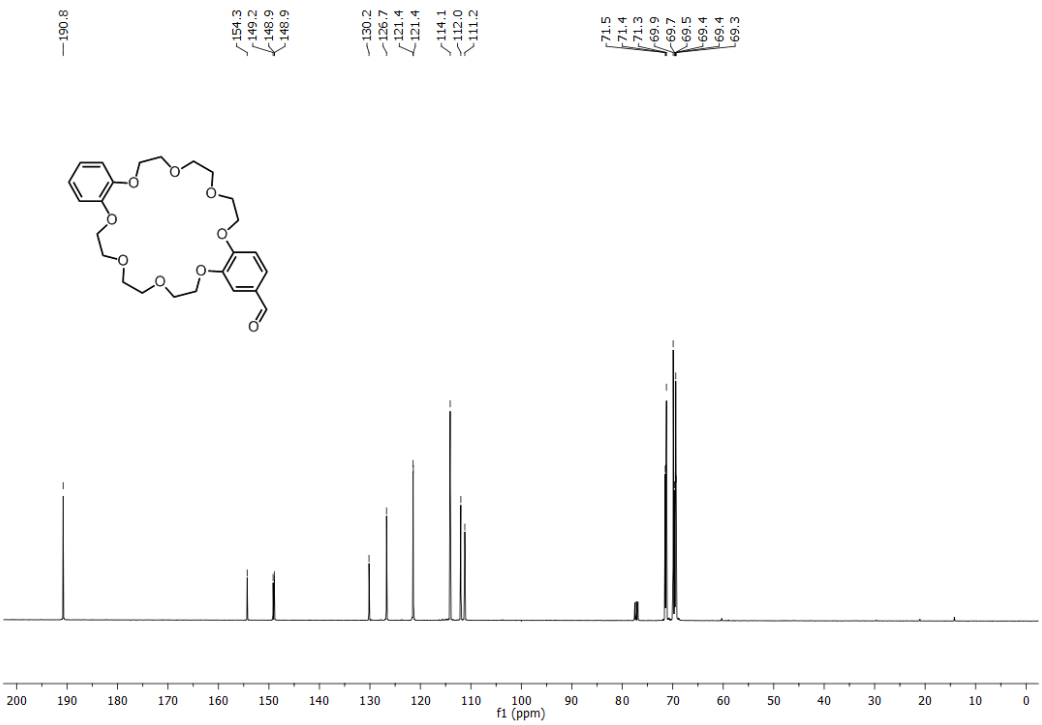
190.8
154.3
149.2
148.9
148.9
130.2
126.7
121.4
121.4
114.1
112.0
111.2
71.5
71.4
71.3
69.9
69.7
69.5
69.4
69.4
69.3
f1 (ppm)

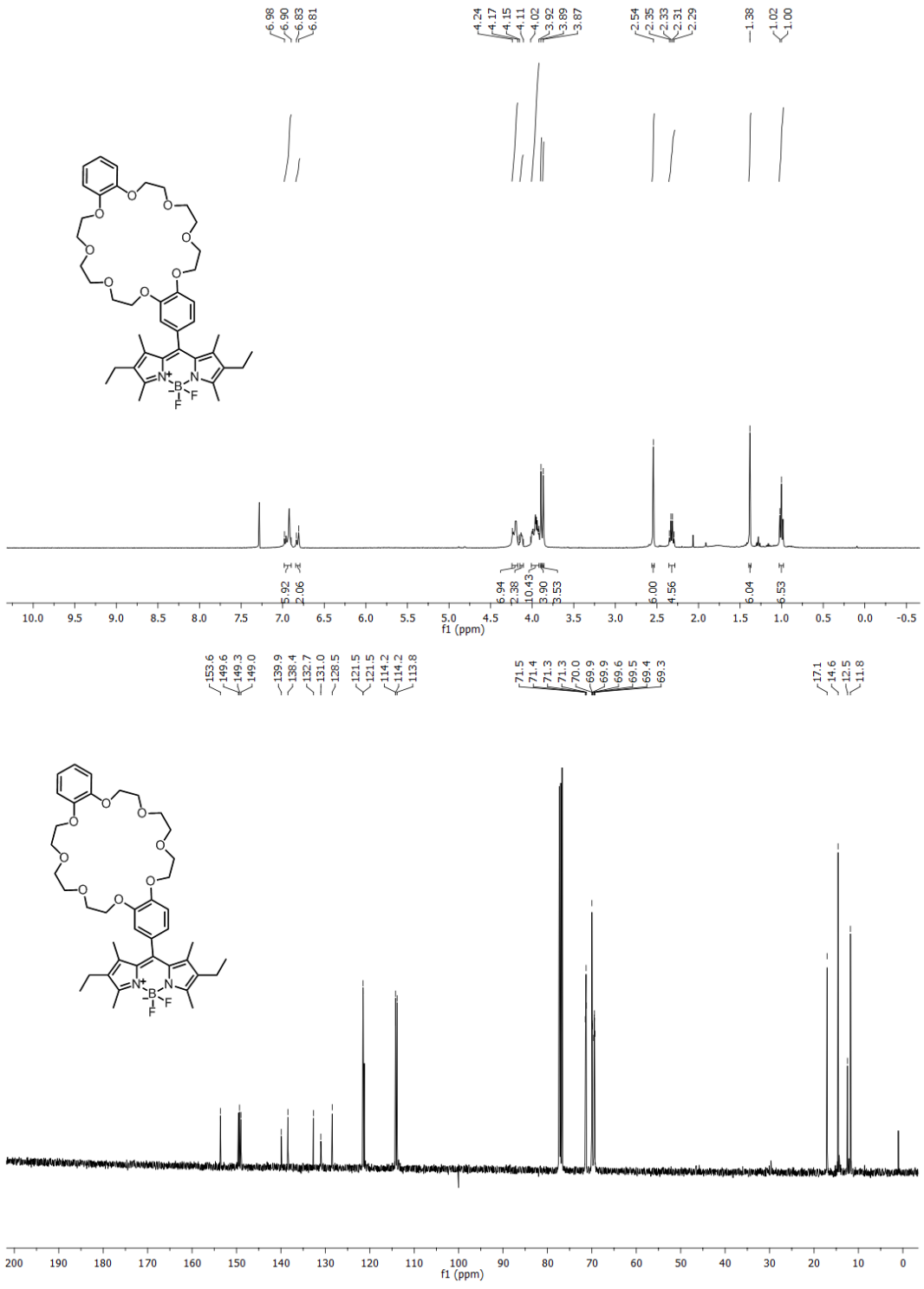
6.98
6.90
6.83
6.81
4.24
4.17
4.15
4.11
4.02
3.92
3.89
3.87
2.54
2.35
2.33
2.31
2.29
1.38
1.02
1.00
5.92
2.06
6.94
2.38
10.43
3.90
3.53
6.00
4.56
6.04
6.53
f1 (ppm)
153.6
149.6
149.3
149.0
139.9
138.4
132.7
131.0
128.5
121.5
121.5
114.2
114.2
113.8
71.5
71.4
71.3
71.3
70.0
69.9
69.9
69.6
69.5
69.4
69.3
17.1
14.6
12.5
11.8
f1 (ppm)

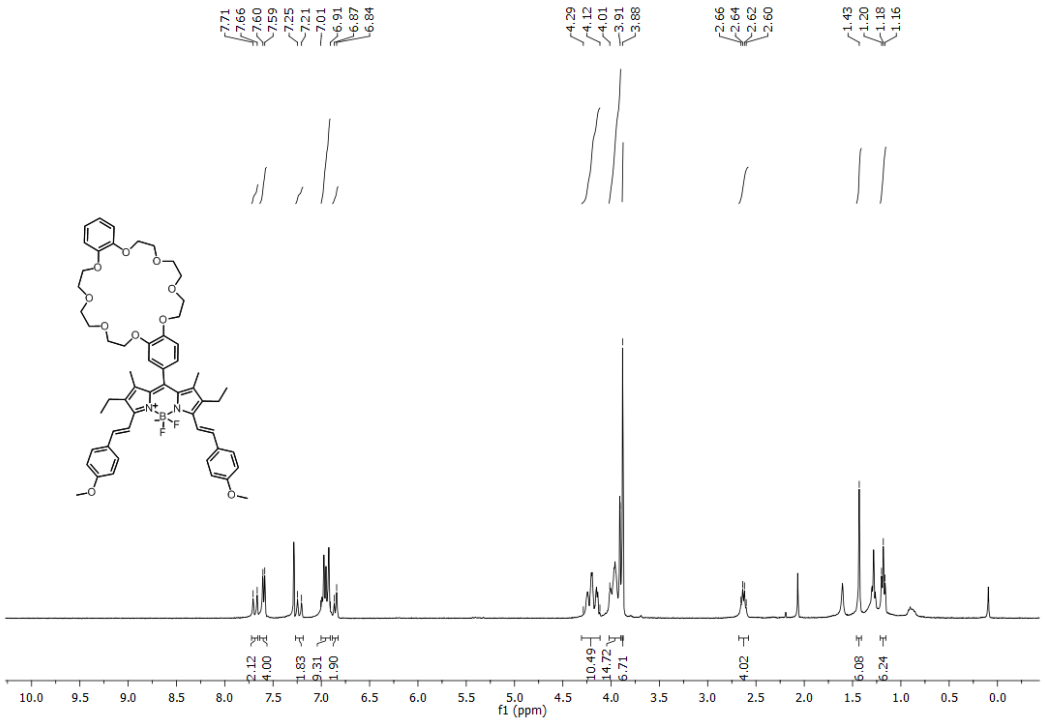
7.71
7.66
7.60
7.59
7.25
7.21
7.01
6.91
6.87
6.84
4.29
4.12
4.01
3.91
3.88
2.66
2.64
2.62
2.60
1.43
1.20
1.18
1.16
2.12
4.00
1.83
9.31
1.90
10.49
14.72
6.71
4.02
6.08
6.24
f1 (ppm)

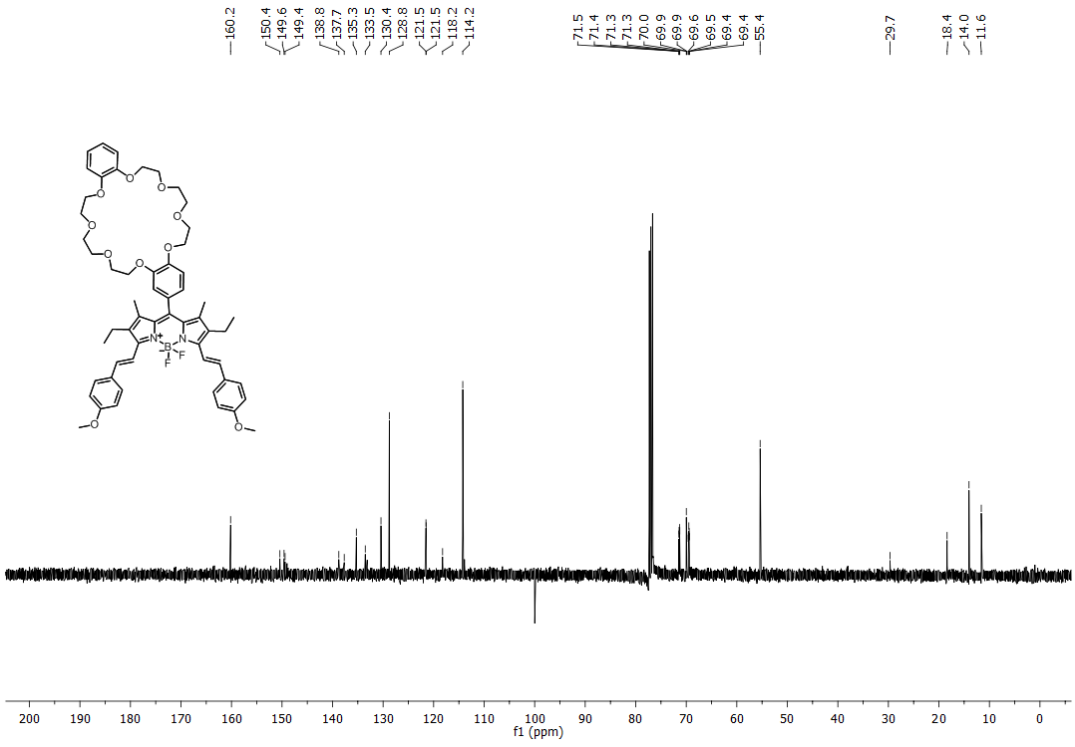
160.2
150.4
149.6
149.4
138.8
137.7
135.3
133.5
130.4
128.8
121.5
121.5
118.2
114.2
71.5
71.4
71.3
71.3
70.0
69.9
69.9
69.6
69.5
69.4
69.4
55.4
29.7
18.4
14.0
11.6
f1 (ppm)

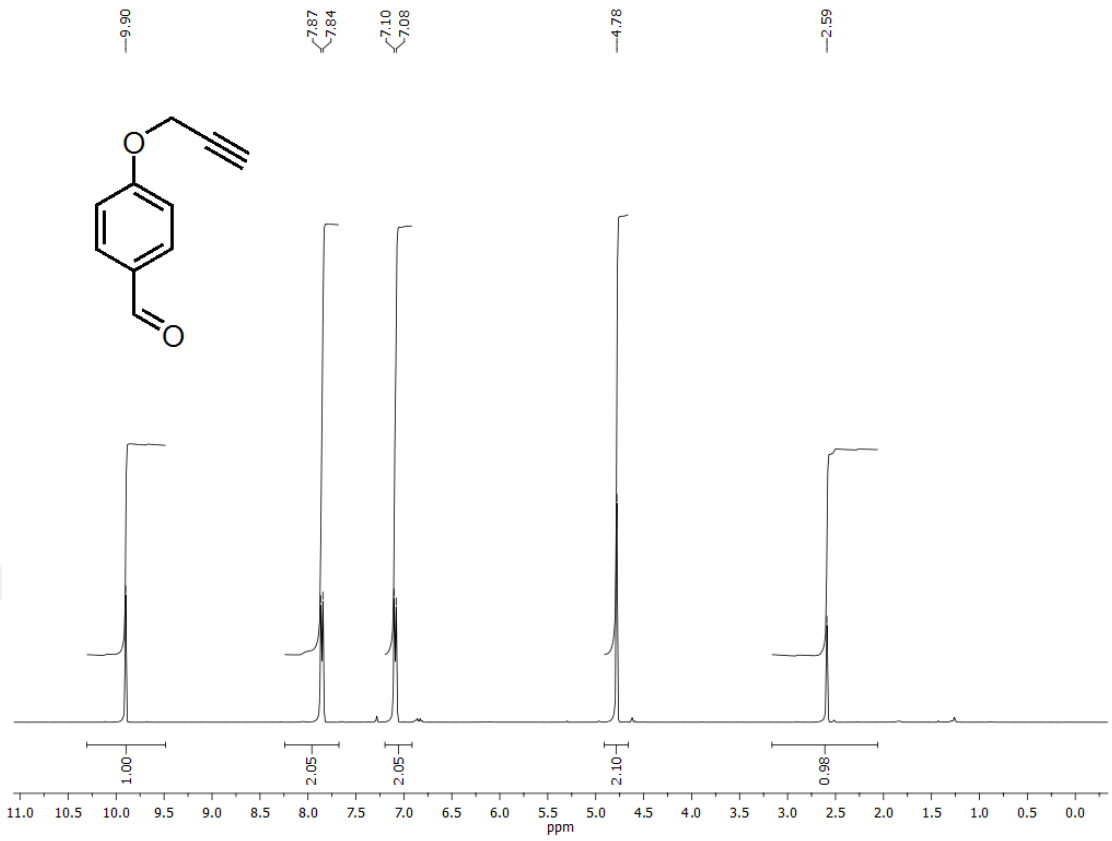
9.90
7.87
7.84
7.10
7.08
4.78
2.59
1.00
2.05
2.05
2.10
0.98
ppm

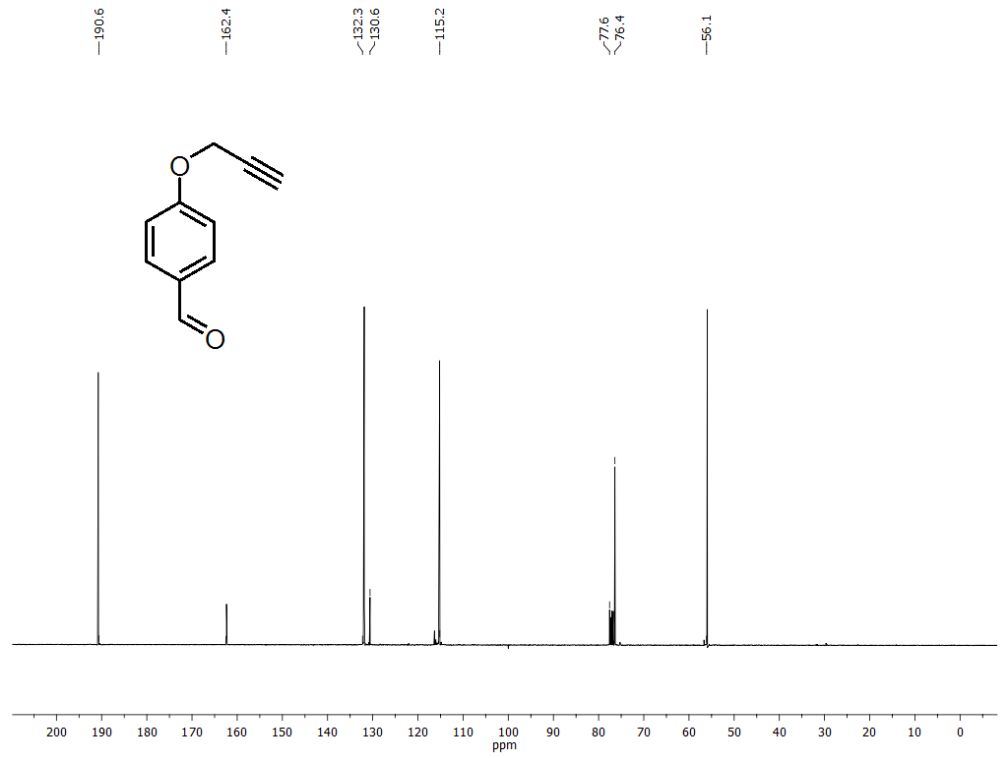
190.6
162.4
132.3
130.6
115.2
77.6
76.4
56.1
ppm

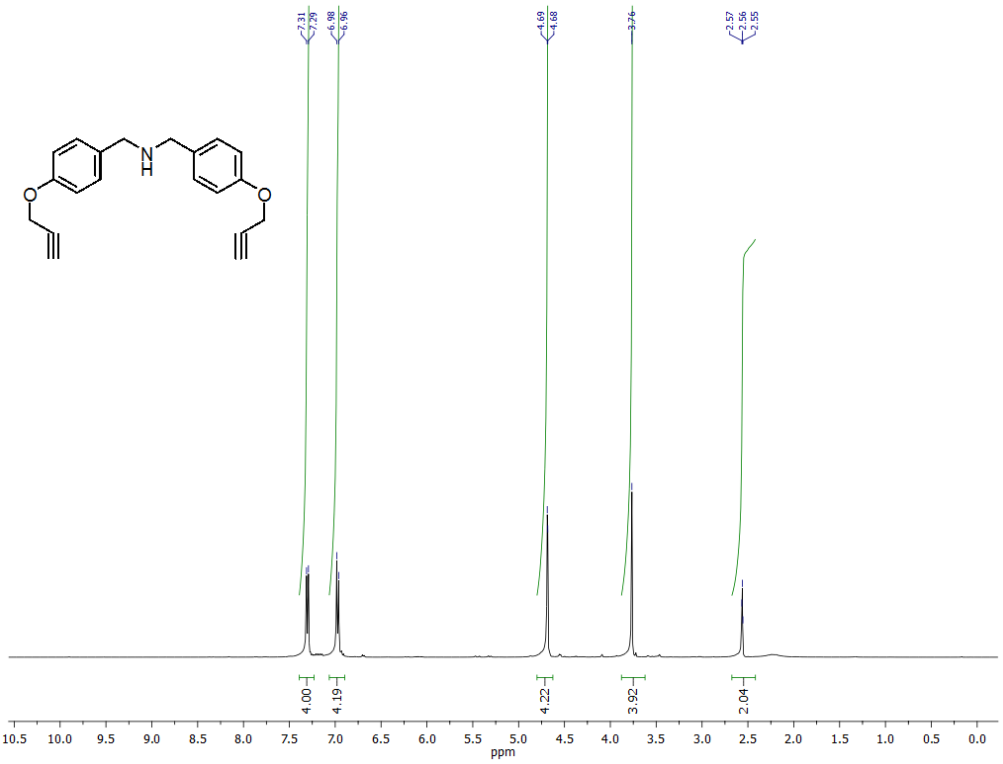
7.31
7.29
6.98
6.96
4.69
4.68
3.76
2.57
2.56
2.55
4.00
4.19
4.22
3.92
2.04
ppm

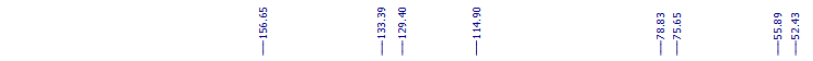
156.65
133.39
129.40
114.90
78.83
75.65
55.89
52.43

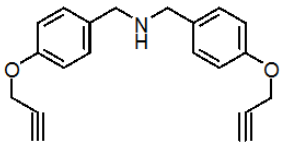

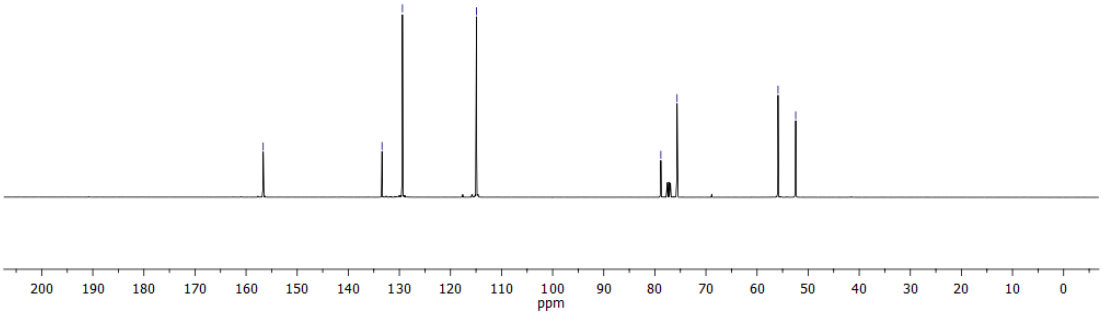
ppm

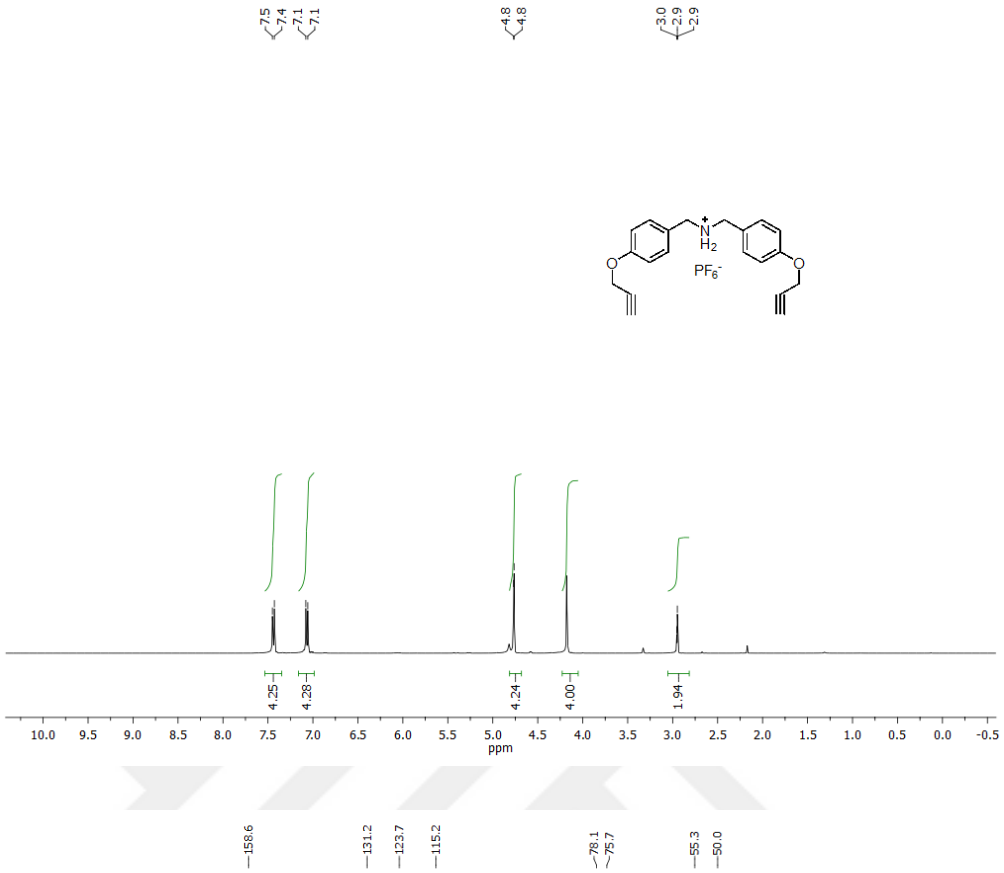
7.5
7.4
7.1
7.1
4.8
4.8
3.0
2.9
2.9
PF6-
4.25
4.28
4.24
4.00
1.94
ppm
158.6
131.2
123.7
115.2
78.1
75.7
55.3
50.0
PF6-
ppm

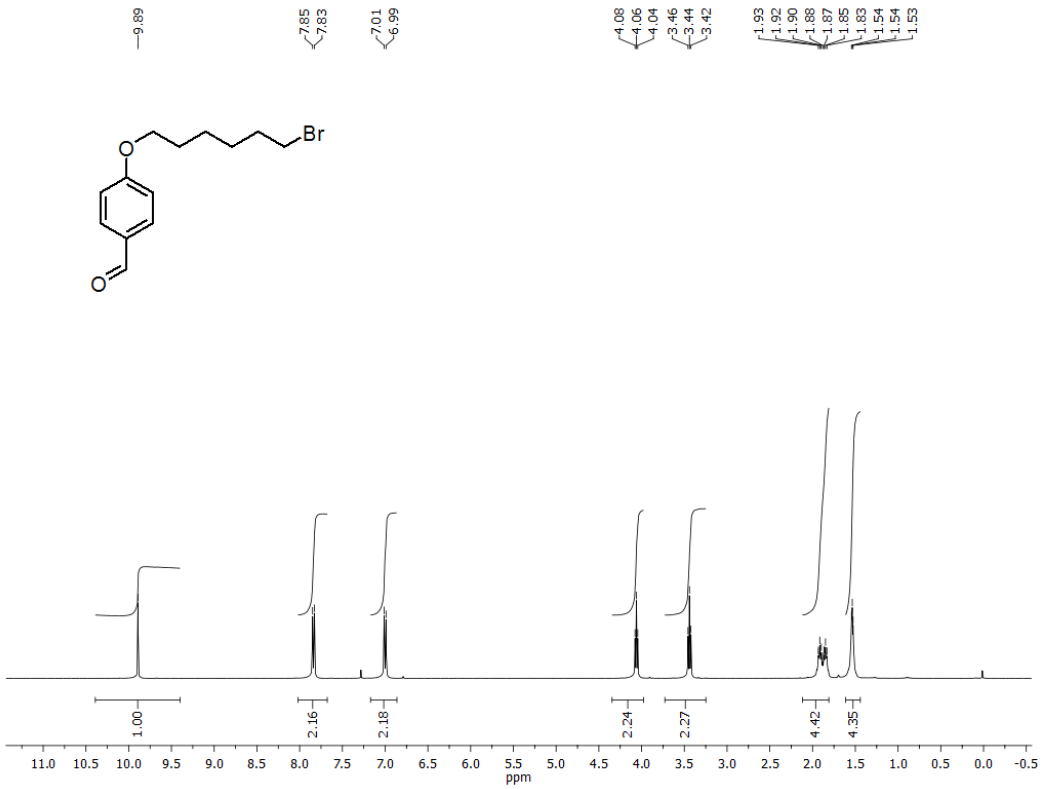
9.89
7.85
7.83
7.01
6.99
4.08
4.06
4.04
3.46
3.44
3.42
1.93
1.92
1.90
1.88
1.87
1.85
1.83
1.54
1.54
1.53
Br
O
O
1.00
2.16
2.18
2.24
2.27
4.42
4.35
11.0 10.5 10.0 9.5 9.0 8.5 8.0 7.5 7.0 6.5 6.0 5.5 5.0 4.5 4.0 3.5 3.0 2.5 2.0 1.5 1.0 0.5 0.0 -0.5
ppm

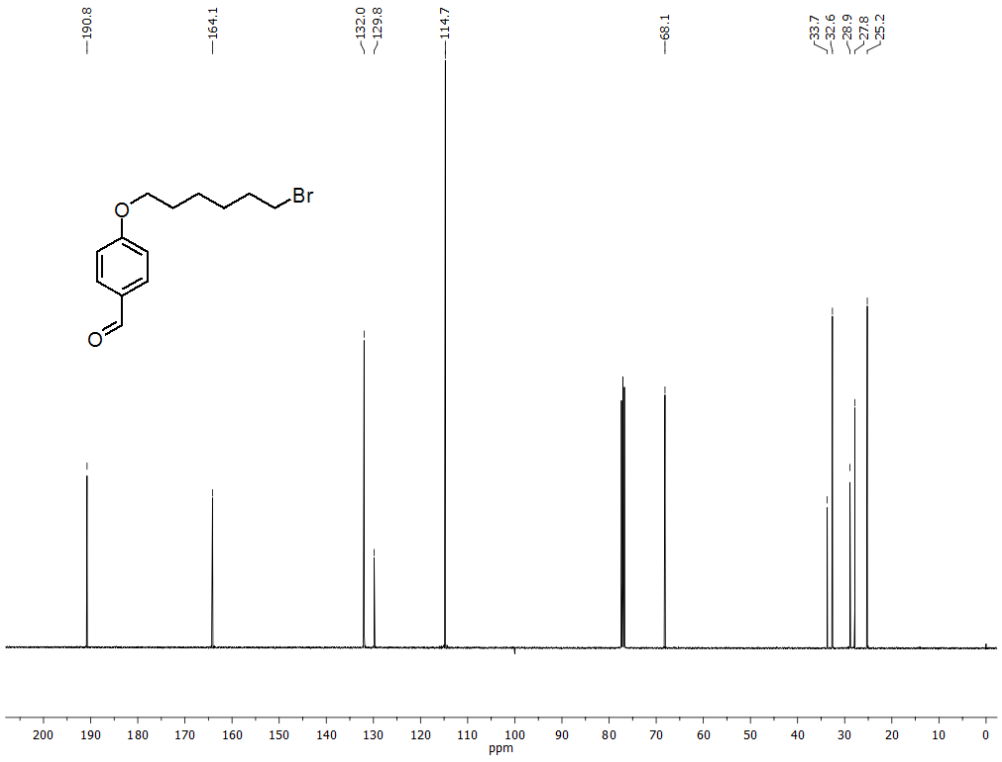
190.8
164.1
132.0
129.8
114.7
68.1
33.7
32.6
28.9
27.8
25.2
Br
O
O
200 190 180 170 160 150 140 130 120 110 100 90 80 70 60 50 40 30 20 10 0
ppm

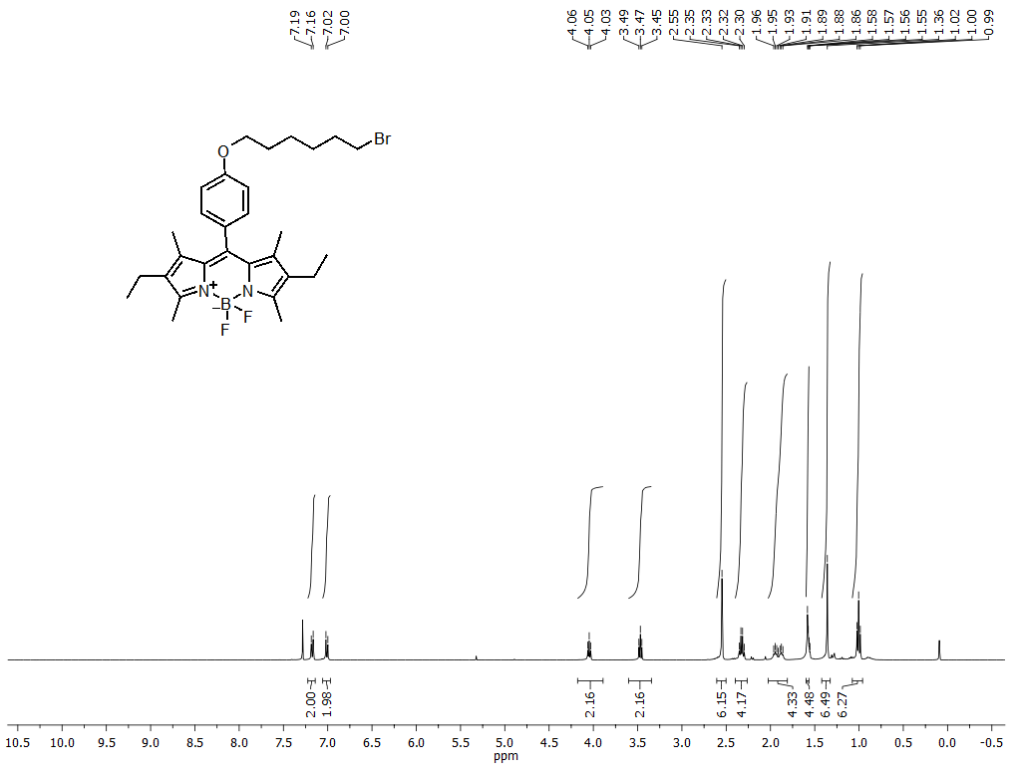
7.19
7.16
7.02
7.00
4.06
4.05
4.03
3.49
3.47
3.45
2.55
2.35
2.33
2.32
2.30
1.96
1.95
1.93
1.91
1.89
1.88
1.86
1.58
1.57
1.56
1.55
1.36
1.02
1.00
0.99
Br
O
N+
N
B
F
F
2.00
1.98
2.16
2.16
6.15
4.17
4.33
4.48
6.49
6.27
10.5 10.0 9.5 9.0 8.5 8.0 7.5 7.0 6.5 6.0 5.5 5.0 4.5 4.0 3.5 3.0 2.5 2.0 1.5 1.0 0.5 0.0 -0.5
ppm

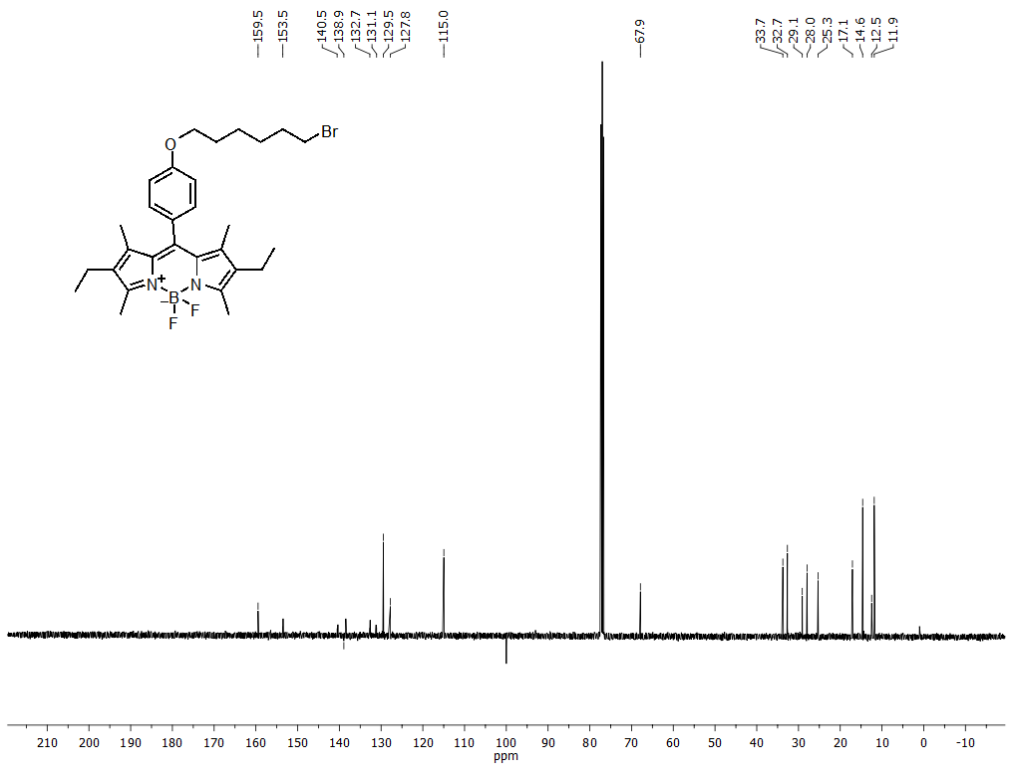
159.5
153.5
140.5
138.9
132.7
131.1
129.5
127.8
115.0
67.9
33.7
32.7
29.1
28.0
25.3
17.1
14.6
12.5
11.9
Br
O
N+
N
B
F
F
210 200 190 180 170 160 150 140 130 120 110 100 90 80 70 60 50 40 30 20 10 0 -10
ppm

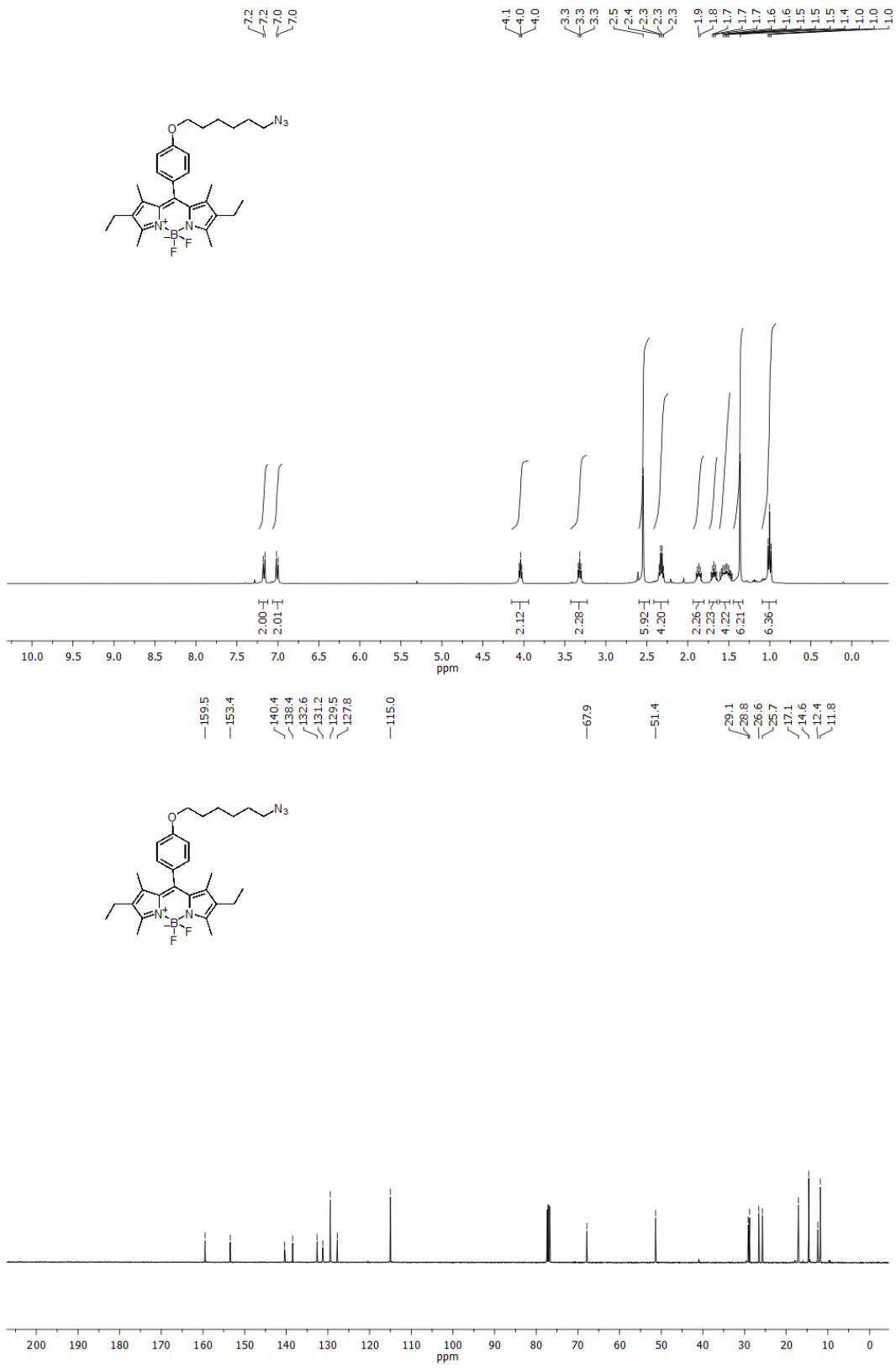
7.2
7.2
7.0
7.0
4.1
4.0
4.0
3.3
3.3
3.3
2.5
2.4
2.3
2.3
2.3
1.9
1.8
1.7
1.7
1.7
1.6
1.6
1.5
1.5
1.5
1.4
1.0
1.0
1.0
N3
O
N+
B
F
F
N
2.00
2.01
2.12
2.28
5.92
4.20
2.26
2.23
4.22
6.21
6.36
10.0 9.5 9.0 8.5 8.0 7.5 7.0 6.5 6.0 5.5 5.0 4.5 4.0 3.5 3.0 2.5 2.0 1.5 1.0 0.5 0.0
ppm
159.5
153.4
140.4
138.4
132.6
131.2
129.5
127.8
115.0
67.9
51.4
29.1
28.8
26.6
25.7
17.1
14.6
12.4
11.8
200 190 180 170 160 150 140 130 120 110 100 90 80 70 60 50 40 30 20 10 0
ppm

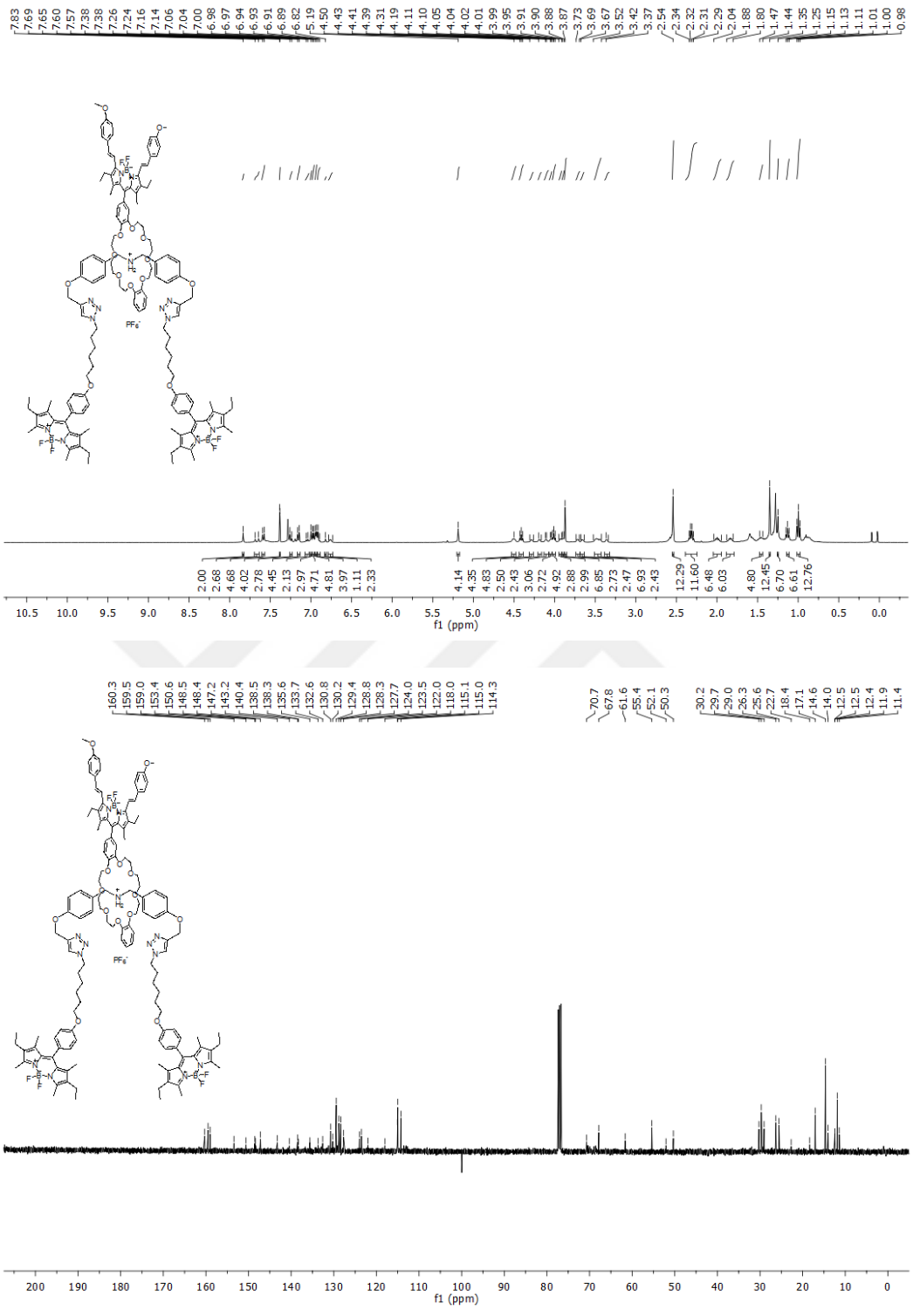

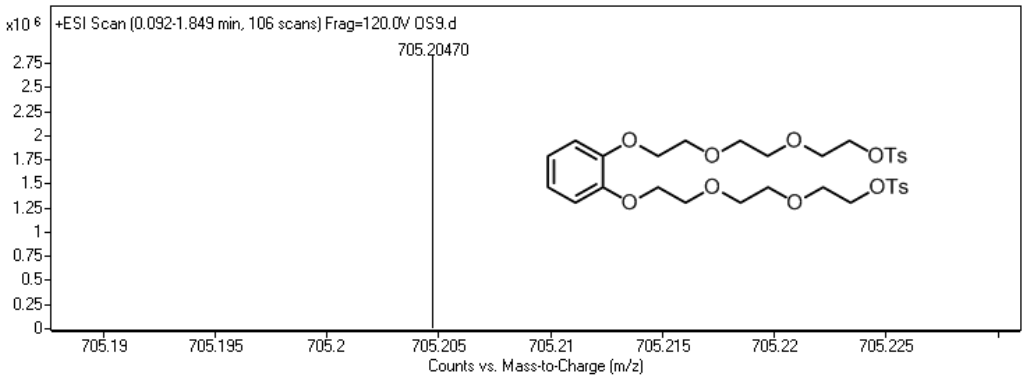
x10 6
+ESI Scan (0.092-1.849 min, 106 scans) Frag=120.0V OS9.d
705.20470
2.75
2.5
2.25
2
1.75
1.5
1.25
1
0.75
0.5
0.25
0
705.19
705.195
705.2
705.205
705.21
705.215
705.22
705.225
Counts vs. Mass-to-Charge (m/z)
OTs
OTs

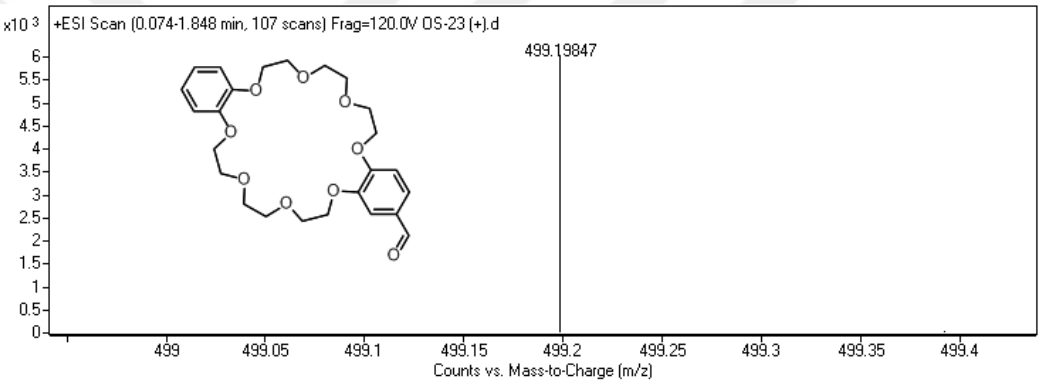
x10 3
+ESI Scan (0.074-1.848 min, 107 scans) Frag=120.0V OS-23 (+).d
499.19847
6
5.5
5
4.5
4
3.5
3
2.5
2
1.5
1
0.5
0
499
499.05
499.1
499.15
499.2
499.25
499.3
499.35
499.4
Counts vs. Mass-to-Charge (m/z)

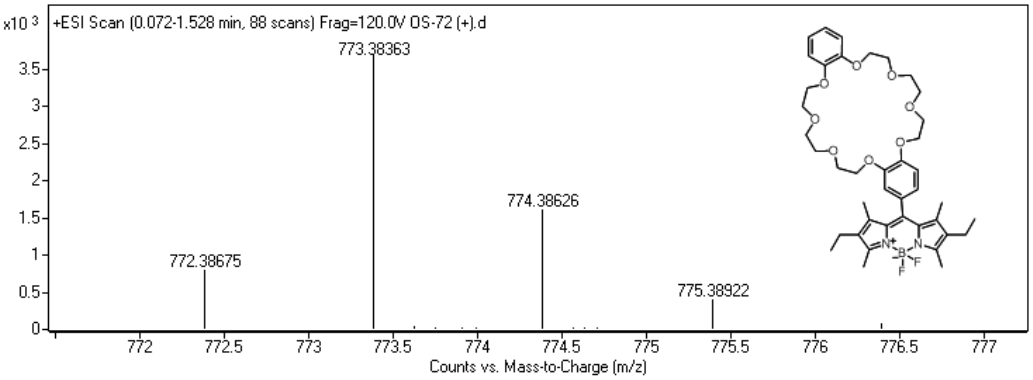
x10 3
+ESI Scan (0.072-1.528 min, 88 scans) Frag=120.0V OS-72 (+).d
773.38363
774.38626
772.38675
775.38922
3.5
3
2.5
2
1.5
1
0.5
0
772
772.5
773
773.5
774
774.5
775
775.5
776
776.5
777
Counts vs. Mass-to-Charge (m/z)

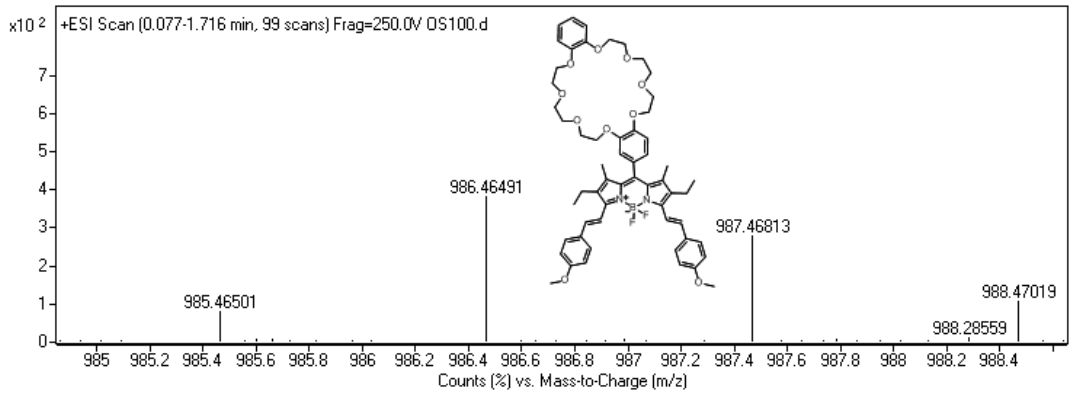
x10 2
+ESI Scan (0.077-1.716 min, 99 scans) Frag=250.0V OS100.d
986.46491
987.46813
985.46501
988.47019
988.28559
Counts (%) vs. Mass-to-Charge (m/z)

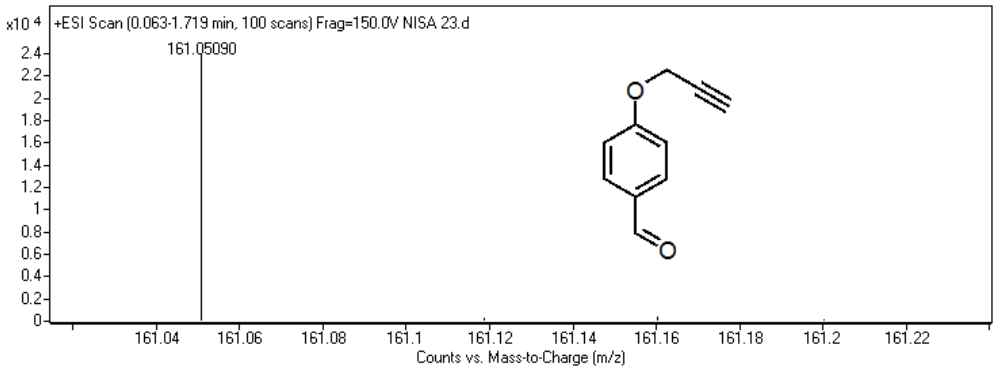
x10 4
+ESI Scan (0.063-1.719 min, 100 scans) Frag=150.0V NISA 23.d
161.05090
Counts vs. Mass-to-Charge (m/z)

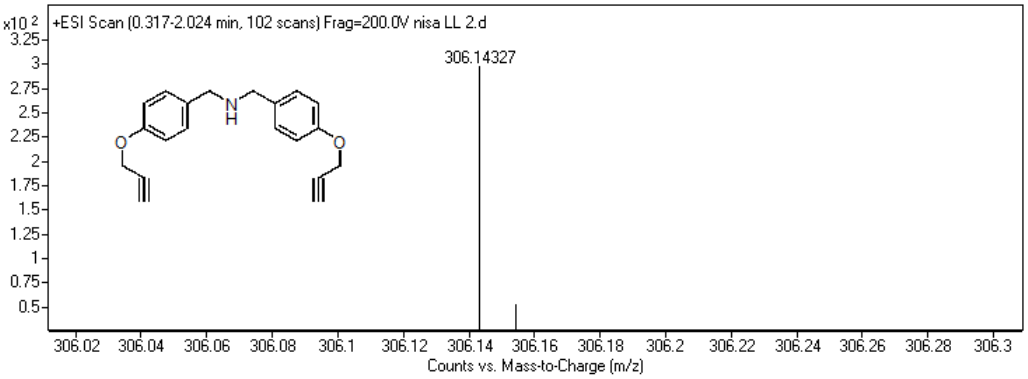
x10 2
+ESI Scan (0.317-2.024 min, 102 scans) Frag=200.0V nisa LL 2.d
306.14327
Counts vs. Mass-to-Charge (m/z)

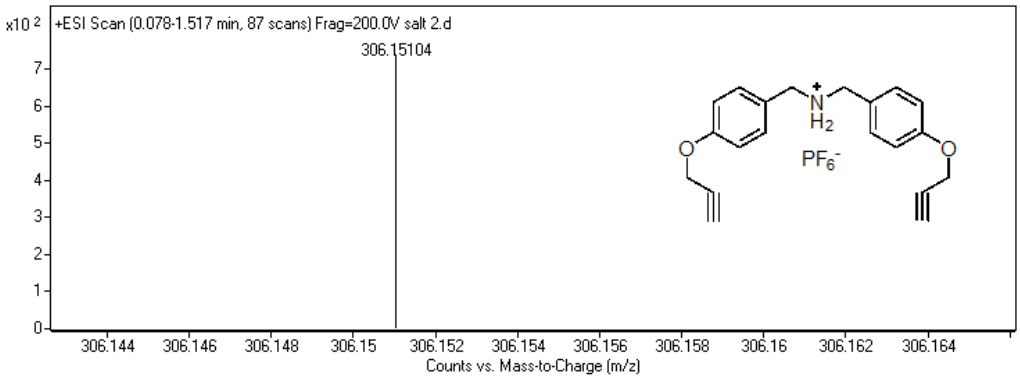
x10 2
+ESI Scan (0.078-1.517 min, 87 scans) Frag=200.0V salt 2.d
306.15104
7
6
5
4
3
2
1
0
306.144
306.146
306.148
306.15
306.152
306.154
306.156
306.158
306.16
306.162
306.164
Counts vs. Mass-to-Charge (m/z)
N
H2
PF6-
O
O

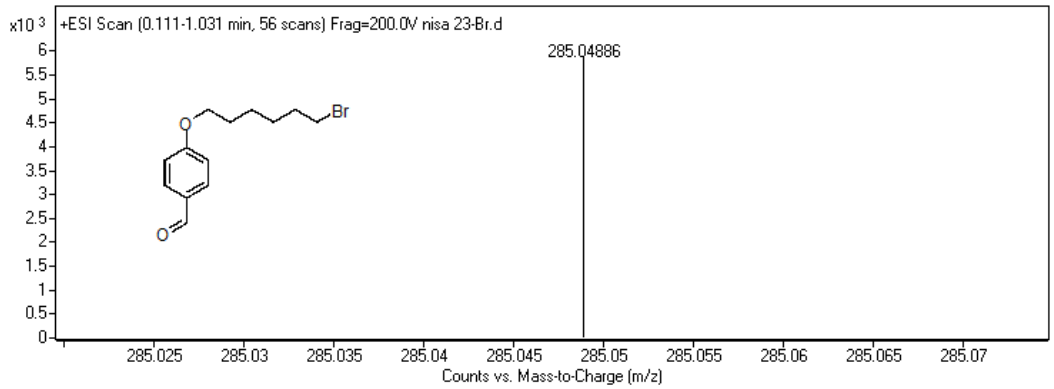
x10 3
+ESI Scan (0.111-1.031 min, 56 scans) Frag=200.0V nisa 23-Br.d
285.04886
6
5.5
5
4.5
4
3.5
3
2.5
2
1.5
1
0.5
0
285.025
285.03
285.035
285.04
285.045
285.05
285.055
285.06
285.065
285.07
Counts vs. Mass-to-Charge (m/z)
Br
O
O

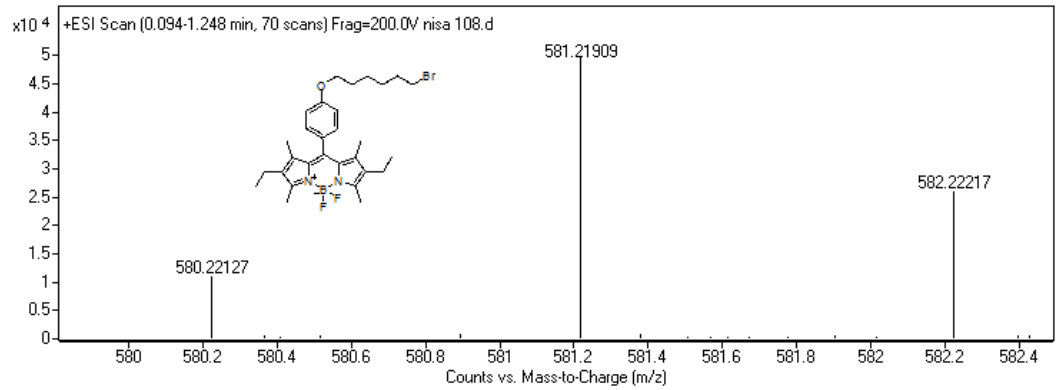
x10 4
+ESI Scan (0.094-1.248 min, 70 scans) Frag=200.0V nisa 108.d
581.21909
582.22217
580.22127
5
4.5
4
3.5
3
2.5
2
1.5
1
0.5
0
580
580.2
580.4
580.6
580.8
581
581.2
581.4
581.6
581.8
582
582.2
582.4
Counts vs. Mass-to-Charge (m/z)
Br
O
N
B
F
F

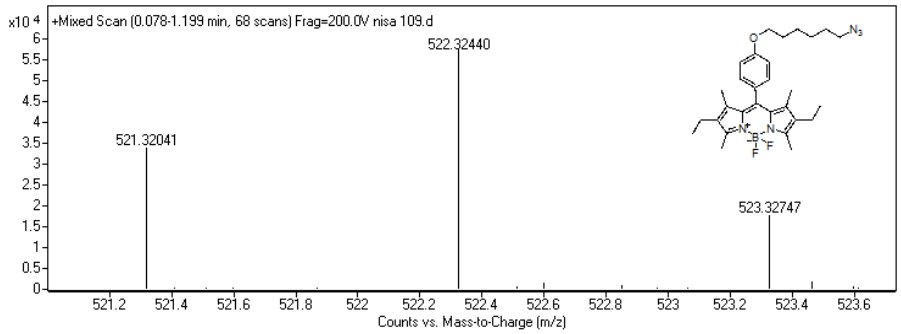
x10 4
+Mixed Scan (0.078-1.199 min, 68 scans) Frag=200.0V nisa 109.d
522.32440
521.32041
523.32747
Counts vs. Mass-to-Charge (m/z)

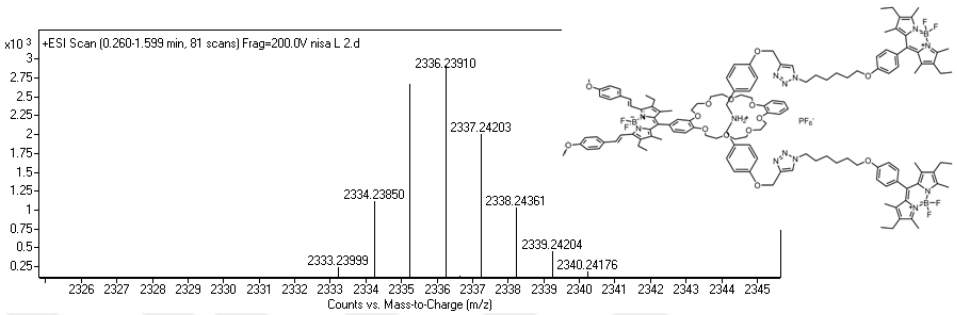
x10 3
+ESI Scan (0.260-1.599 min, 81 scans) Frag=200.0V nisa L 2.d
2336.23910
2337.24203
2334.23850
2338.24361
2339.24204
2333.23999
2340.24176
Counts vs. Mass-to-Charge (m/z)